Wisser, Dominik

Modeling of Irrigation and Reservoirs in Regional and Global Water Cycles

Schriftenreihe Hydrologie/Wasserwirtschaft

Zur Verfügung gestellt in Kooperation mit/Provided in Cooperation with:
Ruhr-Universität Bochum

RUHR-UNIVERSITÄT BOCHUM

RUB

SCHRIFTENREIHE
HYDROLOGIE/WASSERWIRTSCHAFT

Modeling of Irrigation and Reservoirs in Regional and Global Water Cycles

von Dominik Wisser

2010

LEHRSTUHL FÜR HYDROLOGIE,
WASSERWIRTSCHAFT UND UMWELTTECHNIK 26

Die vorliegende Arbeit wurde von der Fakultät
für Bau- und Umweltingenieurwissenschaften als Dissertation angenommen.

Doktorarbeit eingereicht am:	16.06.2009
Tag der mündlichen Prüfung:	10.12.2009

Berichter:

Prof. Dr. rer. nat. habil. Andreas Schumann, Ruhr-Universität Bochum
Prof. Dr. rer. nat. Dr.-Ing. habil. András Bárdossy, Universität Stuttgart
Dr. phil. nat. Bernhard Lehner, McGill University, Montreal, Kanada

Universitätsstraße 150, 44801 Bochum
Tel. +49 (0234) 32 - 24693, Fax. - 14153
ISSN 0949-5975

Herausgeber: Prof. Dr. rer. nat. habil. Andreas Schumann

Kurzfassung

Anthropogene Eingriffe, insbesondere durch die Speicherung und Entnahme von Wasser zur Bewässerungslandwirtschaft haben den natürlichen Wasserkreislauf dramatisch verändert. Jährlich werden dem Wasserkreislauf etwa 3000 km^3 Wasser zu Bewässerungszwecken entnommen. Obwohl diese Menge, verglichen mit 37000 km^3/a Gesamtabfluss, zunächst als relativ gering erscheint, hat die starke Erweiterung bewässerter Flächen nach 1950 und der Bau großer Talsperren mittlerweile einen deutlichen Einfluss auf den hydrologischen Kreislauf in großen Flussgebieten. Dieser Einfluss kann zwar für einzelne Einzugsgebiete quantifiziert werden, die Wirkung auf die globale Wasserbilanz ist jedoch unklar, da anthropogene Eingriffe in der großskaligen Wasserhaushaltsmodellierung bisher wenig Berücksichtigung gefunden haben.

Um die Einflüsse von Talsperren und großflächigen Bewässerungssystemen auf Komponenten des hydrologischen Kreislaufes zu untersuchen, wurde in der vorliegenden Arbeit ein bestehendes, rasterbasiertes, globales Wasserhaushaltsmodell so weiterentwickelt, dass die Wechselwirkungen solcher Eingriffe in den Wasserhaushalt explizit berücksichtigt werden können. Dieses Modell ermittelt sowohl die benötigten Wasserentnahmen als auch die Rückflüsse von bewässerten Flächen in den hydrologischen Kreislauf. Hierdurch können die Wechselwirkungen bewässerter Flächen mit hydrologischen Komponenten untersucht werden. Zur Quantifizierung des Einflusses von Talsperren auf das Abflussregime großer Flusssysteme wurde anhand beobachteter Entnahmedaten von Talsperren ein empirisches Modell entwickelt, das die Abgaben einzelner Talsperren unabhängig von der Nutzung simuliert. Damit kann es auf globaler Ebene angewendet werden, wo detaillierte Angaben zur Betriebsweise und Nutzung in der Regel nicht vorliegen.

Eine Validierung des Modells erfolgte anhand eines Vergleichs der Berechnungs-ergebnisse mit gemessenen Abflussganglinien mehrerer großer Flussgebiete und der Gegenüberstellung mit Angaben zum Bewässerungsbedarf aus nationalen und internationalen Statistiken des landwirtschaftlichen Wasserverbrauches. Diese Validierung wurde für Einzugsgebiete mit einem hohen Anteil bewässerter Flächen und auf globaler Ebene durchgeführt. Insgesamt erwies sich das entwickelte Modell als sehr gut geeignet zur Abschätzung des Bedarfs. Gemessene Abflussdaten können deutlich besser reproduziert werden, wenn die Einflüsse von Bewässerungslandwirtschaft und Talsperren berücksichtigt werden.

Die Anwendung des Modells zur Beurteilung von Flussgebieten mit Wasserknappheit und zur Abschätzung der Folgen des Klimawandels auf hydrologische Verhältnisse wurde beispielhaft für einige Einzugsgebiete gezeigt.

Insgesamt zeigen die Ergebnisse einen signifikanten Einfluss von Bewässerung auf den Abfluss in einzelnen Flussgebieten, der zu einem Austrocknen großer Flüsse führen kann. Auf kontinentaler und globaler Skala ist dieser Einfluss deutlich geringer. Durch den Bau großer Talsperren hingegen wurde das Abflussverhalten großer Flüsse dramatischer verändert, was wiederum eine Reihe physikalischer und biogeochemischer Änderungen zur Folge hat.

Schlagwörter: Grossskalige hydrologische Modellierung, Bewässerung, Talsperren, anthropogene Veränderungen

Abstract

Humans have dramatically altered the natural water cycle by storing and abstracting water. Three thousand km^3 of water per year are extracted globally for irrigation purposes. Although this is small compared to annual runoff (37,000 km^3), irrigated areas have expanded dramatically since the 1950's, and the construction of large reservoirs has additionally altered components of the hydrological cycle in many of the world's river basins. Although these effects have been described at local scales, those alterations have previously been largely overlooked in global scale water balance models.

The purpose of this dissertation is to quantify the impact of irrigation and reservoirs at continental and global scales.

To accomplish this goal, an existing, grid based global water balance model was modified to explicitly account for the feedbacks between irrigation, reservoirs, and the hydrological cycle. Based on globally available data sets from national and international data bases as well as remotely sensed data sets, the model computes irrigation water demand as well as return flows from irrigated areas so that the feedbacks of irrigated areas with the hydrological cycle can be investigated. The model explicitly accounts for variation in water demand for different crops by considering each crop type individually.

To estimate the impact of large reservoirs on the flow regime of large river systems, an empirical reservoir release model was developed using operational data from some 30 reservoirs globally. It estimates release from reservoirs based on inflow, capacity, and storage in the reservoir. Estimates are independent of the reservoir purpose so that the model can be applied at the global scale where such detailed data are not typically available with certainty.

The water balance model was validated using observed discharge and by comparing computed irrigation water withdrawal with reported values in national and international statistics on agricultural water demand. Overall, the model has proven to be capable of estimating irrigation water demand. Observed values of discharge were better reproduced when the effects of irrigation and reservoirs were taken into account.

The application of the model to identify water stressed basins and investigate the impact of climate change on the hydrology was exemplarily shown for some large river basins.

Results indicate that the changes in runoff induced by the development of irrigated areas on the hydrological cycle are highly significant for individual river basins where the abstractions lead to a drying up of major rivers, but over continental and global scales these alternations are small.

The construction of reservoirs, however, has been shown to have significant impacts on the discharge regime of major rivers that, in turn, alter a number of physical and biogeochemical processes.

Keywords: Large scale hydrological modeling, human impact, irrigation, reservoirs.

Acknowledgement

I am highly indebted to many people and institutions that helped make this dissertation possible.

My deepest gratitude goes to Professor Schumann for suggesting a short visit (that later turned out to be a long-term commitment) to the Water Systems Analysis Group (WSAG) of the University of New Hampshire and for his sustained, long distance supervision during my stay.

I am deeply grateful to Charlie Vörösmarty and all members of the WSAG team and the University staff for offering helpful and continuous advice on the research.

I am also indebted to the external reviewers of the dissertation, Professor Bárdossy and Professor Lehner and Professor Scherer for his service on the committee.

Finally, I acknowledge the help and support of friends and family in the completion of this project, without whom this would not have been possible.

Dominik Wisser

Preamble

In many parts of the world the water cycle is strongly affected by human activities. These anthropogenic impacts are often difficult to estimate as data and information about water management activities are rare. At the other side the interest in macroscale hydrology is increasing as the regulating function of the water cycle has to be integrated in Global Circulation Models. Other needs to have a look on large dimensions results from the interactions of regional water activities. Uncoordinated regional water management causes more and more adverse effects as it can be shown at the example of the Aral Sea. Integrated Water Resources Management, which is oriented to the spatial scale of river basins, cannot be implemented for large transboundary rivers if the overlaying impacts of national and regional developments are not combined. This can be ensured by large scale water management models only. In many parts of the world dramatic changes affects water resources. These changes are often caused by an intensification of water uses which are primarily caused by agriculture. Irrigation is the base for national economics in many parts of the globe and indispensable for feeding the world. Reservoirs are often starting points of irrigation systems providing water by temporal redistributions. They fulfill other tasks as well (flood protection, hydropower utilization etc.). In summary irrigation and reservoirs modify the water cycle in different aspects and scales. The consideration of their impacts within global and regional hydrological models is a challenge which was accepted by Dominik Wisser in his PhD-thesis. He started with a fundamental knowledge about irrigation and reservoir management, applied and extended this information to large scale river basins and demonstrated options and limits to describe these anthropogenic impacts at the continental scales. One important result of his work is an overview about the uncertainties of such estimations caused by limited data availability and problems of data assimilation from remote sensing devices. In this way he followed up the tradition of our institute in research activities dedicated to hydrological applications of remote sensing.

The work of Dominik Wisser was not feasible without an integration of the developed simulation tools in a global water balance model. Here the Water System Analysis Group of the University of New Hampshire gave invaluable support and fulfilled all expectations I had when I recommended Dominik Wisser to continue the studies he started in Bochum at the University of New Hampshire. In this sense not only the topic of this dissertation is a global one but also its realization, based on a cooperation of two research institutes which are interested in a common problem.

Bochum, den 05.05.2010 Prof. Dr. Andreas Schumann

Contents

List of Figures

List of Tables

Abbreviations

AOGCM	Atmosphere-Ocean General Circulation Model
AVHRR	Advanced Very High Resolution Radiometer
CCR	Catchment Command Ratio
CLM	Climate version of the Local Model
CRU	Climate Research Unit, University of East Anglia
CWP	Crop Water Productivity
DEM	Digital Elevation Model
DSMW	Digital Soil Map of the World
DWD	Deutscher Wetterdienst
EPA	Environmental Protection Agency
EPIC	Erosion Productivity Impact Calculator
EVI	Enhanced Vegetation Index
FAO	Food and Agricultural Organization
FC	Field Capacity
FrAMES	Framework for Modeling of Aquatic Ecosystems
GAC	Global Area Coverage
GIMA	Global Irrigated Areas Mapping
GIS	Geographical Information System
GLCC	Global Land Cover Characterization
GLUE	Generalised Likelihood Uncertainty Estimation
GMIA	Global Map of Irrigated Areas
GPCC	Global Precipitation Climatology Centre
GPCP	Global Precipitation Climatology Project
GRDC	Global Runoff Data Center
ICOLD	International Commission on Large Dams
IGBP	International Geosphere-Biosphere Program
IPCC	Intergovernmental Panel on Climate Change
IRRI	International Rice Research Institute
IWMI	International Water Management Institute
JRC	Joint Research Center
LAI	Leaf Area Index
LCCS	Land Cover Classification System

LGP ..... Length of Growing Period
LR ..... Leaching Requirement
LSM ..... Land Surface Models
LSWI ..... Land Surface Water Index
LU/LC ..... Land Use/Land Cover
MAE ..... Mean Absolute Error
MBE ..... Mean Bias Error
MHM ..... Macroscale Hydrological Model
MODIS ..... Moderate Resolution Imaging Spectroradiometer
MVC ..... Maximum Value Compositing
NASA ..... National Aeronautics and Space Agency
NASS ..... National Agricultural Statistics Service
NCAR ..... National Center for Atmospheric Research
NCEP ..... National Centers for Environmental Precipitation
NDSI ..... Normalized Difference Snow Index
NDVI ..... Normalized Difference Vegetation Index
NOAA ..... National Ocean and Atmospheric Administration
NSE ..... Nash Sutcliffe Efficiency
PAL ..... Pathfinder AVHRR Land DATA
POES ..... Polar Orbiting Operational Environmental Satellites
PWP ..... Permanent Wilting Point
RCM ..... Regional Climate Model
RMSE ..... Root Mean Square Error
RS ..... Remote Sensing
RU ..... Reflectance Units
SPOT ..... Système Pour l'Observation de la Terre
SRES ..... Special Report on Emission Scenarios of the IPCC
SRTM ..... Shuttle Radar Topography Mission
STN ..... Simulated Topological Network
SVAT ..... Soil-Vegetation Atmosphere Transfer
TRIP ..... Total Runoff Integrated Pathways
UNEP ..... United Nations Environment Programme
USDA ..... United States Department of Agriculture
USGS ..... United States Geological Survey
VE ..... Volume Error
VI ..... Vegetation Index
VIC ..... Variable Infiltration Capacity
VIM ..... Vegetation Monitoring Instrument
WBM ..... Water Balance Model
WEI ..... Water Exploitation Index

WGHM ..... WaterGAP Global Hydrological Model
WMO ..... World Meteorological Organization
WRI ..... World Resources Institute
WTM ..... Water Transport Model

1 Introduction and Objectives

1.1 Problem and Motivation

Irrigation of agricultural areas to secure food production has been applied as early as 6000 B. C. and has facilitated the development and settlement of humans along the Nile, between Euphrates and Tigris, and along the Indus and Ganges river and other regions. The area of irrigated land globally was relatively stable until the 1800's but increased dramatically during the 1970's - the onset of the 'green revolution' - to it's current extent of 275 Mha (*Siebert et al.*, 2005). Despite this increase, irrigated areas constitute a relatively small area of total crop land (17%), yet 40% of the world's food comes from irrigated areas (*FAO-STAT*, 2008). Therefore, providing adequate water to supply the irrigation needed to feed the world's growing population constitutes a major international security concern.

About 70% of the water abstraction globally is used for irrigation, but this rate is much higher in developing countries, reaching 90% (*Shiklomanov and Rodda*, 2003; *Cai and Rosegrant*, 2002). In addition, the abstracted volume is expected to rise in future due to rising population and increasing per-capita demand for food. Water availability may be a serious constraint to achieving future food requirements, and the number of countries unable to sustain adequate water supplies will likely increase (*Postel*, 1998).

Irrigation affects the hydrological cycle through a number of direct and indirect effects, including the alteration of the flow regime of many of the world's major rivers. The abstraction of water for irrigation purposes lowers the volume of water entering river systems (*Haddeland et al.*, 2006a). This has led to the transformation of large, mainstem rivers such as Syr Darya, Huang He, Indus, Yellow River, and Colorado into 'losing streams' with substantial reductions in flow and declining groundwater tables (*Foley et al.*, 2005). The abstraction of irrigation water has also been shown to impact the seasonality of river flow by increasing winter discharge via return flow from irrigated areas (*Kendy and Bredehoeft*, 2006).

Such alterations in the hydrological cycle do not only impact the spatial and temporal distribution of runoff, but have direct and indirect effects on the bio-geophysical state of water and subsequently the sustainable use of water resources. Irrigated areas can also influence atmospheric properties and processes through additional water in the atmosphere (*Douglas et al.*, 2006) and evaporative surface cooling (*Kueppers et al.*, 2007). On a global scale, these anthropogenic changes in global water vapor changes are equivalent to the decrease in evapotranspiration associated with deforestation (*Gordon et al.*, 2005).

Components of the hydrological cycle are not only affected by the abstraction of water but also by the distortion of hydrographs through the storage of water in reservoirs. Today, river

basins are more closely tied to the character of water resources engineering than to the behavior of natural systems (*Vörösmarty et al.*, 2005; *Meybeck*, 2003). Globally, there are more than 45,000 dams over 15 m high, representing an increase in the total number of nearly one order of magnitude since 1950 (*Vörösmarty et al.*, 1997, 2003) with an accumulated storage volume equivalent to about 7% of the global terrestrial discharge. The temporal changes in the flow of water in river systems as a result of those reservoir impoundments greatly affect a number of biogeochemical processes such as the ability of the water to decompose organic matter. Reservoirs impact the sediment retention of major rivers (*Vörösmarty et al.*, 2003), the emission of trace gas emissions (*Soumis et al.*, 2004; *Galy-Lacaux et al.*, 1999; *St.Louis et al.*, 2000) and the cycling of nutrients (*Seitzinger et al.*, 2002). While the impacts of reservoirs and irrigation on components of the hydrological cycle are well documented for single river basins (e.g. *Shibuo et al.* (2007); *Bouwer et al.* (2006); *Haddeland et al.* (2006a)), few studies have explicitly modeled the impact of water abstraction for irrigation in continental and global hydrological models. The analysis of those changes on the global scale using macroscale hydrological models does not only provide valuable information on understanding the water and food nexus that is becoming more important with a growing world population but also offers an opportunity for providing information for the calibration and validation of atmosphere-ocean-general circulation models (AOGCM) that are becoming increasingly realistic in modeling the biosphere-atmosphere interaction and the hydrology of the terrestrial surface.

Unfortunately, quantifying the impacts of irrigation on global and continental water cycles using macroscale hydrological models is constrained by a number of uncertainties. The largest uncertainty arises from the uncertainty in the distribution of irrigated areas, that is typically based on agricultural census data at scales ranging from 10^2 to 10^4 km^2 for district or county level data, to 10^3 - 10^5 km^2 at provincial (state) level to some 10^4 to 10^7 km^2 at national level and is typically not available for every year while the cropping pattern and agricultural practices may change due to market or hydrological conditions faster than the census can document (*Frolking et al.*, 2005). Data sets that entirely rely on national statistics cannot meet the needs of science and policy researchers who require geospatial data at improved temporal and spatial resolutions that is updated regularly (*Xiao et al.*, 2006). The recent advances made in remote sensing instruments, sensors and derived data sets provide an ideal tool for reducing the inherent uncertainties in estimates of irrigation water demand. Remotely sensed data from a variety of sensors at different resolutions, temporal and spatial coverage, in combination with statistical data sets can also provide a means to track changes in the distribution of irrigated areas over time and the potential of such data products has not been fully exploited. The simulation of reservoir operation and their impact on the flow regime of a river is constrained by incomplete registers of reservoirs globally and by the lack of detailed knowledge of reservoir operation rules for individual reservoirs.

1.2 Objectives

This study investigates the role of irrigation water abstractions and the operation of reservoirs on regional and global water cycles and the implications of such alterations on the sustainable use of water resources. To accomplish this, an existing macroscale hydrological model was modified to explicitly account for human interventions in the water cycle at a variety of

spatial domains and at varying resolutions. More in detail, the model represents the interactions of irrigated areas with non-irrigated areas both in terms of water abstraction and as a source for recharge. To model the impact of irrigation water abstractions and reservoir operation on routed streamflow, it is necessary to model the horizontal water flow at the same time step as the vertical water balance calculations. Furthermore, the model is capable of modeling the operation of reservoirs on a global scale with data sets available to date. As uncertainties related to the distribution of irrigated areas can greatly be reduced using remotely sensed data, the model should be flexible enough to accommodate such data at a variety of different spatial and temporal resolutions. To this end, it is essential that the model is implemented in a software modeling framework. Modeling frameworks have been designed to increase the greater inter-operability and portability of software among developers, and to increase the efficiency of software development through a set of shared software systems, standards, and utilities, and the use of such frameworks have recently received considerable attention for hydrological models as well as for more complex Earth system and climate models (*Dickinson et al.*, 2002; *Gattke*, 2006; *Wollheim et al.*, 2008). Model simulated discharge predictions must be validated against observed discharge and the uncertainties related to model parameters and input data must be quantified.

1.3 Methodology and Outline

Following the objectives of this study outlined above, the methodology is described as follows: Chapter 2 introduces some basic principles of irrigation, existing approaches to model irrigation water demand and consumption and the required geospatial data sets. Fundamentals of remote sensing, relevant sensors and instruments and derived data products are described in Chapter 3 followed by a discussion of available statistical data sets related to agriculture with relevance to water balance modeling (Chapter 4). This includes a discussion on the spatial differences between remotely sensed information and data mainly based on agricultural census data. The objective of Chapter 5 is to discuss time varying climate data used as forcing data for the model and auxiliary data that is needed for the validation of the model. An overview of existing implementations of macroscale hydrological models and their limitations with regard to the representation of human interventions in the water cycle is given in Chapter 6. In this context, methods for assessing hydrological models and uncertainty in hydrological models are discussed. Based on these objectives and limitation of existing models, Chapter 7 introduces a newly developed water balance model that is based on the existing WBM model (*Vörösmarty et al.*, 1998) with substantial modifications in the structure and implemented in an existing modeling framework. The irrigation water module of the model and the implications for discharge simulations are validated and assessed with regard to the uncertainty in the model and in data sets for both individual river basins and at continental and global scales. Chapter 9 discusses applications of the model. These include global applications to reconstruct the hydrography of the last century that help understand the role of irrigation and reservoirs as well as assessments of individual river basins that are under stress as a result of irrigation water abstractions, both under contemporary and future climate conditions.

Finally, based on the results presented in the previous chapters, important directions and opportunities for future research needs are discussed.

2 Irrigation Principles

2.1 Introduction

Irrigation is generally understood as 'the application of water to soil for the purpose of supporting plant growth' (*Hargreaves and Merkley*, 1998). A much broader definition is given by *Israelsen and Hansen* (1962) who define irrigation as 'the application of water to the soil for any of the following purposes: (1) to add water to soil to supply the moisture essential for plant growth, (2) to provide crop insurance against short duration drought, (3) to cool the soil and atmosphere, thereby making more favorable environment for plant growth, (4) to wash out or dilute salts in the soil, (5) to reduce the hazard of soil piping, and (6) to soften tillage pans'.
Globally, around one fourth (3.6×10^9 *ha*) of the Earth's land surface are too dry for rainfed agriculture and have to be irrigated to grow crops (*Fischer et al.*, 2002). Irrigation has been applied for millennia to secure adequate food supply and has enabled civilizations to develop residential sites in arid and desert areas. While the irrigated area in 1800 was just about 8 Mha (*Postel*, 1999), it has increased since the beginning of the 'Green revolution' in the 1970's from about 100 Mha to about 270 Mha (*FAOSTAT*, 2008). Figure 2.1 depicts the development of irrigated areas since 1960. As can be seen, the rate of growth is declining since the beginning of the 21st century and reflects the increasing scarcity of suitable areas, rising cost of irrigation investment and losses of irrigated areas due to salinization and land degradation. As most of the increase in irrigated areas will be achieved by converting rainfed agriculture, the net increases in the total cropland area are expected to be marginal in future (*Postel*, 1998, 1999; *Falkenmark et al.*, 1998). As the population is expected to rise further, the irrigated area per person is actually declining since the last two decades (Figure 2.1).

Although irrigated land constitutes only 17% of the global cropland area, 40% of our food are derived from irrigated land (*Postel*, 1999) and providing adequate irrigation water to feed the growing population consitutes therefore one of the major international security concerns in the future (*Vörösmarty et al.*, 2000a). The following section is aimed at briefly summarizing basic principles of irrigation and its implications for estimating and allocating irrigation water demand.

2.2 Water Sources for Irrigation

Of the estimated 3800 km^3 that are diverted from the global hydrological cycle per year, some 70 to 80% are used for irrigated agriculture (*Postel*, 1999; *Shiklomanov and Rodda*, 2003). The water supply for irrigation will have two grow in future for at least two reasons: (1) the increased demand for a growing population and (2) changes in people's diets (towards

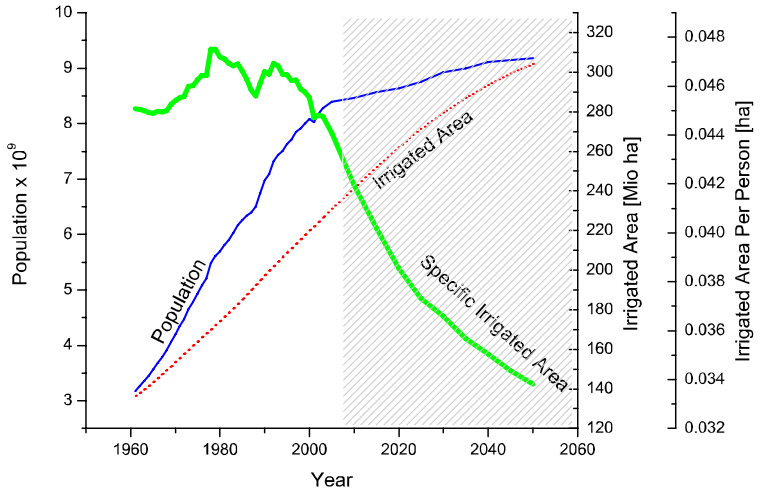

Figure 2.1: Development and forecast of population, irrigated areas and specific irrigated areas 1961-2050. Population forecast from The Population Division of the Department of Economic and Social Affairs of the United Nations Secretariat, World Population Prospects: The 2004 Revision and World Urbanization Prospects, *Medium variant*. Irrigated Area based on FAO data (*AQUASTAT*, 2008)

more meat-rich diets). It is estimated that water abstraction for irrigation will rise by 14% in developing countries from 2000 to 2030 (*World Water Assessment Programme*, 2002) while *Postel* (1999) estimates that an additional 2,000 km^3a^{-1} of water are to be abstracted to meet the required food production levels in 2025.

Water for irrigation use can be abstracted from *surface waters* and *groundwater*. Being the most reliable source of water, groundwater abstractions are particularly important in providing the water needed for irrigation. Irrigated areas based on groundwater produce significantly higher yields than those that rely on surface water (*Moench et al.*, 2003). This is due to the fact that the application efficiency is higher, and that the water is available on demand. Groundwater irrigation has become increasingly popular globally and exceeds surface water irrigation in many parts of the world. Globally, groundwater is believed to supply some 30% of the total water needed for irrigated areas (*Foster and Chilton*, 2003). The dependency of irrigated agriculture on groundwater varies considerably. Groundwater-irrigated areas account for 50% of the irrigated areas in India (*Central Water Comission of India*, 1998), about 50% in China's Henan province, 20% in Spain (*Moench et al.*, 2003) and some 65% of the US irrigated agriculture (*Pimentel et al.*, 2004). A large fraction of irrigation water is obtained from unsustainable use of water resources in general and groundwater resources in particular. Based on documented evidence from India, China, the United States, North Africa and the Arabian Peninsula, *Postel* (1999) estimates that 200 km^3a^{-1} are being abstracted unsustainably from groundwater resources. As this amount is largely used for grain production this estimate suggests that some 10% (about 180 million tons per year) of the global grain harvest are produced by depleting aquifers. Although based on documented evidence and highly uncertain, this first assessment has generated some discussions and has drawn the attention to the importance of groundwater in world food production (*Moench et al.*, 2003).

Vörösmarty et al. (2005) used a geospatial framework of 0.5° to assess what fraction of the demand can be met by locally produced runoff and river corridor discharge (if available). Taking withdrawal values form national statistics, they concluded that the non-sustainable water abstractions could be as high as 400-800 km^3a^{-1}. Some 20% of the irrigated areas in the United States are supplied by groundwater that is abstracted in excess of the natural recharge (*Tilman et al.*, 2002)[1]. The negative aspects and drawbacks of groundwater development are well understood. Typical consequences of groundwater overuse include (*Custodio*, 2002):

- Progressive decrease of groundwater heads
- Decrease in spring discharge, river base flow and surface area of wetlands
- Change in the groundwater flow pattern. This can subsequently lead to seawater intrusion
- Changes in the water quality due to mixing of waters of different depths as a consequence of changing heads
- Decrease in pore pressure. This may lead to land subsistence when sediments are unconsolidated.

Ample examples of groundwater overdraft and declining groundwater levels have been reported for many regions in the world, such as for the North China Plain (*Kendy et al.*, 2003, 2004), the Indo-Gangetic Plains (*Shah et al.*, 2006; *Postel*, 1999) and many others.

Although non-conventional water sources such as *desalinated* water and *reclaimed wastewater* are increasingly being applied, the amount of water abstracted from those source is small on a global scale. The *World Water Assessment Programme* (2002) estimates that some 20 Mha of irrigated land are irrigated with partially diluted or raw wastewater. Although being an important source of water in arid and semi-arid areas (e.g. Cyprus, Israel) with increasing importance, the total area irrigated with waste water in developing countries represents some 10% of the total irrigated area. The use of *desalinated water* for irrigation purposes is only practiced for high value crops, particularly if water prices are subsidized.

Falkenmark et al. (1998) have conceptualized the water in a river basin into two components. *Blue water* is renewable water in liquid form which is the water in rivers, lakes and aquifers and is both accessible and inaccessible to humans. *Green water* is the water in the soil and has two components: a productive part that is required for biomass production in terrestrial ecosystems (transpiration) and a non-productive part that is evaporated (*Falkenmark and Rockström*, 2006). Green water is required to keep natural ecosystems, and plants functioning. The storage medium for green water is the root zone of the soil. The partitioning of blue and green water is therefore strongly affected by land use changes and is shown in Figure 2.2. Out of the estimated 110,000 km^3a^{-1} of precipitation that are reaching the Earth's surface, some 40,000 km^3a^{-1} are converted to runoff and aquifer recharge (blue water) while an estimated 70,000km^3a^{-1} is stored in the soil and eventually returns to the atmosphere through transpiration and evaporation. Rainfed agriculture consumes only green

[1] An extended discussion on sustainable groundwater abstractions will be given in Chapter 9.5.1

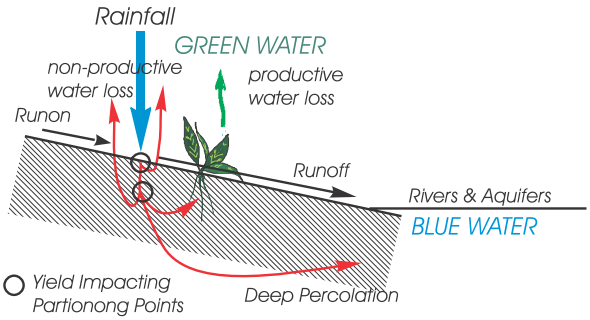

Figure 2.2: Partitioning of precipitation into the vertical green water branch, including the return flow to the atmosphere and unproductive losses (*Falkenmark et al.*, 1998)

water and irrigated agriculture uses blue water to meet the demand that exceeds the amount of available green water.

2.3 Irrigation Infrastructure

Water abstracted from any of the water resources discussed above (surface water, groundwater, re-used water, desalinated water) has to be conveyed into the root zone of the soil. The methods of conveyance can broadly be classified into three main categories: (i) surface irrigation, (ii) sprinkler irrigation and (iii) microirrigation. These methods will be briefly described in the following section.

2.3.1 Surface Irrigation

Surface irrigation is the traditional way of intermittently applying the water to the soil. Depending on the way the water is controlled, surface irrigation may be further subdivided into basin irrigation (confining the water to a given area), furrow irrigation (controlling the water in furrows that are created between row crops) and level-basin irrigation (*Replogle et al.*, 1996). Surface water irrigation is applied on more than 90% of the total global irrigated area (*AQUASTAT*, 2008).

2.3.2 Sprinkler Irrigation

Sprinkler irrigation is the application of water through a network of pipelines and sprinklers. Sprinkler irrigation developed mainly after light-weight aluminum pipes have been introduced after 1950. Sprinklers are most applicable when supplemental[2] irrigation is applied. Depending on whether the sprinkler is moving in the field or is fixed on a permanent structure sprinkler irrigation can be further subdivided into permanent or moving systems. Among the most commonly used moving irrigation systems are center-pivot systems where water is supplied at a central point and a lateral line rotates around this center. The world

[2] Supplementary irrigation refers to a concept 'of providing additional water to stabilize or increase yields under site conditions where a crop can normally be grown under direct rainfall, the additional water being insufficient to produce a crop' (*AQUASTAT*, 2008)

total area irrigated by sprinklers is about 20 Mha (around 8% of the total irrigated area) with the largest areas being found in the USA, Italy, France and other European countries (*Shiklomanov and Rodda*, 2003). Compared to surface irrigation, sprinkler systems have a high energy consumption, high investment cost and require technical support.

2.3.3 Microirrigation

Microirrigation[3] includes drip irrigation, trickle irrigation and subsurface irrigation and is generally considered to be the most efficient irrigation method. Under this method the water is applied directly to the crops' roots through a network of perforated pipelines under the soil or beneath the soil surface. Losses due to evaporation are thereby kept extremely low. Although microirrigation systems have expanded rapidly since the 1970's, the area that is under microirrigation worldwide totals 3 Mha or one per cent of the total area under irrigation (*Postel*, 1999). Compared to other irrigation methods, the requirement with regard to water quality and skilled personell for maintenance as well as the capital cost are higher so that microirrigation is particularly suitable for high-value crops.

2.4 Drainage

The sustainability of irrigated agriculture heavily depends on maintaining an adequate salt balance in the root zone (*Tanji and Kielen*, 2002). Salt is accumulated in the soil root zone through two mechanisms: The salt that is dissolved in the irrigation water remains in the soil after the pure water has evaporated and salt enters the root zone from rising groundwater. The latter occurs if the groundwater recharge induced by irrigation is greater than the natural recharge and causes the water table to rise. The salt that enters the soil with the irrigation water is unavoidable and predictable while waterlogging can be controlled by adequate drainage systems. The amount of salt accumulated depends on (1) the quality of the irrigation water, (2) the volume of the water evaporated and (3) properties of the soil (*Replogle et al.*, 1996). Globally, some 20% of the irrigated land (mostly in arid and semi-arid regions) suffers from a buildup of salt in the soil.

2.5 Irrigation Water Demand

2.5.1 Introduction

Three measurements are typically used to characterize the use of water for agricultural purposes (*Gollehon and Quinby*, 2000): Water *withdrawal* measures the total amount of water diverted from surface water sources and extracted from groundwater aquifers, water *application* refers to the portion of water withdrawn and delivered to the field, excluding conveyance and delivery- system losses and gains. The amount of water that is actually consumed by

[3] sometimes referred to as localized irrigation

evaporation and transpiration is referred to as *consumptive* use or crop water demand[4]. The latter does not include losses to percolation and runoff and is typically estimated based on plant-water-requirement models.

2.5.2 Crop Water Demand

The most commonly applied method for estimating crop water demand is the crop coefficient method according to the procedure recommended in FAO's Irrigation and Drainage Paper 56 (*Allen et al.*, 1998). This method has received a wide acceptance in planning, designing and operation of irrigation schemes as well as for water resources planning. It computes water demand for crops assuming that they are disease free, adequately watered and not affected by any kind of nutrient stress, pest, or water stress. The calculated value, therefore, represents an estimate on the upper end of the actual range of consumptive water use.

The daily values for crop evapotranspiration ET_c [mm] are calculated by multiplying the evapotranspiration ET_0 [mm] from a reference surface[5] by a dimensionless crop coefficient k_c:

$$ET_c = k_c ET_0 \tag{2.1}$$

While ET_0 incorporates various weather conditions and therefore represents an index of climatic demand, k_c varies predominately with the specific crop characteristics (*Allen et al.*, 1998). The method can therefore be applied in different locations and climates. The reference evapotranspiration ET_0 is typically computed using the FAO Penman-Monteith equation (Chapter 7.3) but other evapotranspiration functions may be used if the required data for the Penman-Monteith function are not available. The crop coefficient k_c represents an integrative variable of four characteristics distinguishing crops from reference grass with regard to the evapotranspirative demand (Chapter 5.4) : (1) the crop height which influences the aerodynamic resistance term, (2) the albedo of the crop-soil surface which, in turn influences the net radiation of the surface, (3) the canopy resistance that controls the surface resistance, and (4) the evaporation from the soil. As the crop develops, these characteristics will change and k_c will therefore vary over time. *Allen et al.* (1998) have parameterized the development of the crop coefficient over time using four distinct phases of crop growth: (1) the initial season from planting to about 10% ground cover, (2) the development stage that extents until the crop has reached its full ground cover, (3) the mid-season stage, lasting until the start of maturity, and (4) the late season that runs from the start of maturity until harvest or full senescence. The typical development of the crop coefficient over time and its expected values is given in Figure 2.3. As can be seen, the crop coefficient in the initial stage varies with the frequency of wetting events. A high frequency of wetting events will increase the crop coefficient and hence the crop water demand because evapotranspiration will be dominated

[4] The terms crop water demand and consumptive use are used to describe water that is removed from the environment. Consistent with the terminology used in FAO's manuals, they include crop transpiration and evaporation from the soil that cannot be separated easily. After sowing, evapotranspiration is dominated by evaporation from the soil, while at full crop cover 90% of the evapotranspiration comes from crop transpiration (*Allen et al.*, 1998)

[5] The reference surface is defined as 'a hypothetical reference crop with an assumed crop height of 0.12 m, a fixed surface resistance of 70 sm^{1-}, and an albedo of 0.23' (*Allen et al.*, 1998)

by evapotranspiration from the soil. The crop coefficient is highest in the mid-season, when the crop has reached its full cover and sharply decreases in the late season. The lengths of the individual stages varies with crop type, planting date and climate. Typical values for major crops are given in table A-2 the Appendix.

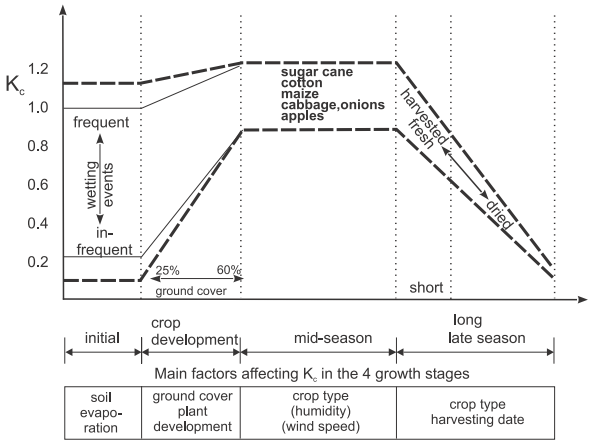

Figure 2.3: Schematized development of the growth stages and typical ranges expected in k_c for the four growth stages (*Allen et al.*, 1998)

2.5.3 Water Application

The crop water demand calculated using Equation 2.1 can be met by rainfall or by applying irrigation water to the soil. The ability of the soil to store water has to be taken into account when planning the timing and application depth of water. The rate of water uptake by crops depends on the rooting density, the soil conductivity, and the difference between average soil water suction and root suction (*Hillen*, 1980). Only a very small fraction of the water absorbed by plants is used in photosynthesis (less than 1%) while the remainder of the water is lost as vapour. The water extraction pattern is not uniform and generally follows the distribution of roots with the greatest extraction near the soil surface. The classical concept used in agronomy to describe the plant activity as a function of available soil moisture is the *soil-water availability concept*. It is based on the assumption that soil water Θ is available to plants only within a defined range of soil wetness and only part of the stored water is available to plants. The upper limit of this range is the Field Capacity (FC), the soil water content when gravitational water has been removed, Θ_{FC}. The lower limit is the Permanent Wilting Point (PWP) and refers to the soil moisture Θ_{PWP} at which plants permanently wilt. The soil hydraulic parameters PWP and FC are dependent on the soil type and can be derived using pedotransfer functions (Chapter 5.6). The concept of soil-water availability has been modified to decrease available water with decreasing soil moisture, or by introducing a 'critical' soil moisture at which crops experience stress because the soil water is more heavily bound to the soil matrix. In practice, a simple soil moisture balance, taking into account precipitation and crop evapotranspiration is typically kept and irrigation water $I_{net}[mm]$ is applied such that the soil water is refilled to its holding capacity whenever the soil moisture drops below a crop-dependent critical threshold.

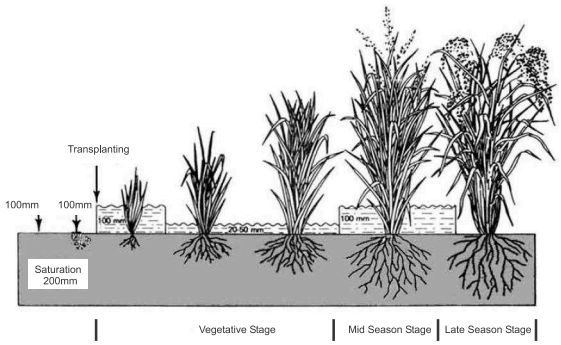

Figure 2.4: Rice growth stages and water application in paddy rice fields (*Brouwer et al.*, 1989)

Paddy Rice Irrigation

Rice (*Orysa sativa L.*) is one the most important crops, supplying 20% of the average per capita human caloric intake (*FAOSTAT*, 2008) and contributing 10% to the total methane emission into the atmosphere (*Xiao et al.*, 2005). Paddy rice fields are also a major water consumer because it is grown on flooded fields in most parts of the world. Paddy rice is usually grown in level basins which are flooded throughout most of the growing season. The following activities are usually carried out for growing paddy rice:

- Preparation of the rice nursery: Usually 5 - 10% of the total area to be planted is used as nursey

- Preparation of the rice fields: To make ploughing easier paddy rice fields are usually flooded about one month before the rice is transplanted

- Transplanting: About one month after sowing the rice seedlings are transplanted into the wet soil. After transplanting a water layer is established. The depth of the the water layer may vary during the growing season and is generally about 100 *mm* during the mid-season stage (*Brouwer et al.*, 1989).

These activities have substantial implications for the hydrology of paddy rice fields and for the water demand of such fields when irrigated. The growth stages of paddy rice and the application of water is illustrated in Figure 2.4.

An additional amount of water needs therefore to be applied to paddy rice fields to maintain the water layer troughout the growing season and for land preparation. The rate of percolation from the flooded rice fields into the soil is controlled by the ponding depth, the depth of the water table and a variety of soil factors such as texture, bulk density and others (*Chen and Liu*, 2002) as well as irrigation management practices (timing and frequency of irrigation) and the condition in the underlying aquifer (*Rushton*, 1997). The percolation rate can greatly be reduced by puddling the soil prior to transplanting (*Chen and Liu*, 2002; *Ting et al.*, 2005; *Tuong and Bhuiyan*, 1999).

Percolation and Leaching

As mentioned in Chapter 2.4, the sustainability of agriculture depends on adequate leaching procedures to control the salt water content in the root zone if the natural drainage is insufficient. The additional fraction of water needed is referred to as the *Leaching Requirement LR* and is commonly expressed as a fraction of the water application. LR can be estimated as a function of salinity of the soil, and depending on the crop type. Typical values for LR range between 1 and 5% of the total demand but can reach 15 to 20% of the total water applied under unfavourable conditons.

2.5.4 Water Withdrawal

The water withdrawal (or gross irrigation water requirement) takes into account losses in the canals, pipelines, and other losses and refers to the amount of water that has actually to be abstracted from the source. The gross irrigation water demand I_{gross} [mm] is obtained by dividing the net irrigation demand with the efficiency of water use E [-].

$$I_{gross} = \frac{I_{net}}{E} \tag{2.2}$$

where E_{eff} is the project efficiency that refers to the volume of water evapotranspired by the crop related to the amount of water that has been abstracted from the source. At project level, this ratio is relatively easy to determine. The concept of efficiency is discussed in more detail below. Estimated values for E for a number of world regions are listed in table A-3 the Appendix.

2.6 Irrigation Performance

Any concept of efficiency is generally a measure of the output obtained from a given input. If the output considered is the amount of yield, the term water productivity is used. Depending on the intended purpose different efficiency concepts are used to describe the 'performance' of irrigation systems. These include physical irrigation efficiency, economic irrigation efficiency, and others. Irrigation efficiency in this study will solely be based on the physical efficiency of water[6]. With regard to the scale under consideration, a distinction can be made between the *project efficiency* of individual irrigation projects and the overall irrigation efficiency within a river basin (*basin efficiency*). The project efficiency is the classical indicator to describe the performance of irrigation systems at project level and has been introduced by *Israelsen and Hansen* (1962). It is generally used to estimate gross water withdrawal (Chapter 7.3.4) as the ratio of the amount of water that is transpired by plants W_u [mm] and the total amount of water abstracted from the hydrological cycle W_d [mm] in the same time period:

$$E = \frac{W_u}{W_d} \tag{2.3}$$

[6] A comprehensive overview of other efficiency concepts is given in *Cai et al.* (2003a)

Based on national statistics on water abstractions, *Faures et al.* (2003) estimated the global overall efficiency in irrigated agriculture to be 38%. Efficiencies vary between 40% in arid and semi-arid regions in North Africa and 25% in South America. Estimated project efficiencies for different world regions are summarized in table A-3 in the Appendix. Frequently, the project efficiency E_p is defined as the product of the conveyance efficiency E_c, the field canal efficiency E_b and the field application efficiency E_a:

$$E_p = E_c \cdot E_b \cdot E_a \tag{2.4}$$

where the single efficiencies are defined as follows:

$$E_c = \frac{Water\,received\,at\,the\,inlet\,to\,fields}{Water\,received\,at\,project\,headworks} \tag{2.5}$$

$$E_b = \frac{Water\,received\,at\,field\,inlet}{Water\,received\,at\,the\,inlet\,to\,fields} \tag{2.6}$$

$$E_a = \frac{Irrigation\,water\,available\,to\,the\,crop}{Water\,received\,at\,field\,inlet} \tag{2.7}$$

While the project based efficiency is a straightforward concept that is relatively easy to measure, efficiency is not entirely independent of scale making it difficult to upscale efficiency to larger scales. It has been argued that the classical approach may be misleading for understanding water resources systems (*Perry*, 1999). *Keller et al.* (1996) showed in their concept of Integrated Water Resource Systems (IWS) that efforts to increase the project efficiency of irrigation systems often lead to reduced irrigation efficiency at the macro level. While losses in an irrigation canal are decreasing the project efficiency, these losses contribute to the recharge of an aquifer and thereby to the efficiency of water in the basin as a whole. An example of an idealized system of irrigation schemes where water is either evapotranspired or lost to drainage is shown in Figure 2.5. In this idealized system, it is assumed that there is no rainfall, the drainage water is salt- and pollution-free and there is no other loss than the evaporation from the crops. The project efficiency in all irrigation sites is 50%, the overall basin efficiency is much larger as drainage 'losses' on one site become sources of water for the subsequent irrigation sites.

To describe the efficiency at the macro (i.e. basin) level, *Keller et al.* (1996) introduced the concept of *effective irrigation efficiency* E_E that measures the amount of beneficially used water W_u over the amount of water consumed during the process of conveying and applying the water W corrected for the net outflow W_d. Formally:

$$E_E = \frac{W_u}{W - W_d} \tag{2.8}$$

In a perfectly closed idealized system such as the system depicted in Figure 2.5, the effective efficiency for all cycles will be 100% and the overall efficiency increases as we go from the micro (project) level to the macro (basin) level. For example, the global efficiency E_c by the end of the second cycle when $(50 + 25)$ of the initial 100 *hm* of water have been evapotranspired, is 75%. Despite very low field efficiencies, the overall efficiency of a real-world irrigation system (such as large systems in Egypt) may reach 80% (*Wallace*, 2000) if this concept of basin efficiency is applied. *Hafeez* (2003) quantified water use efficiency at

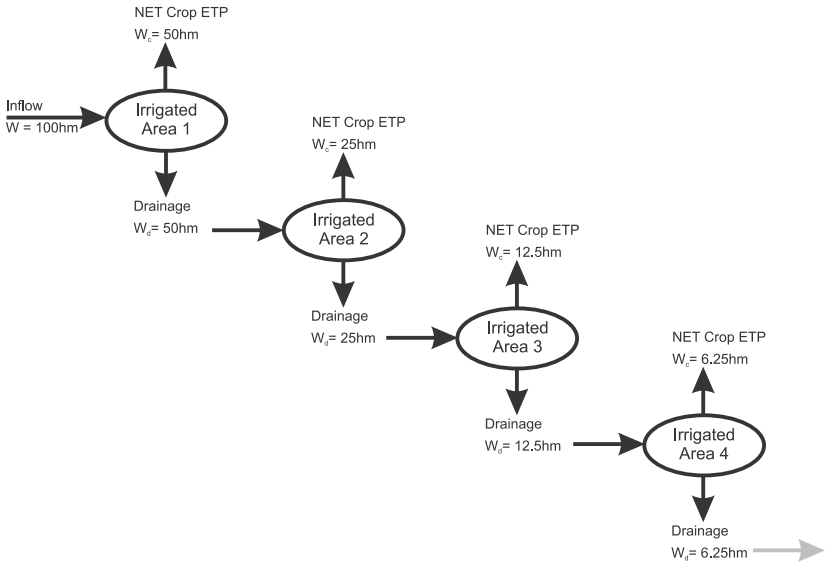

Figure 2.5: Example of an irrigation cycle (idealized) after *Keller et al.* (1996)

10 different spatial scales in an irrigation system in central Philippines and showed that both water productivity and water use efficiency increased at larger scales.

While this is a valuable concept from a pure water quantity point-of view, it fails to address some important aspects. Water quantity cannot be seen independently from water quality and every re-use of the water will require energy to convey the water. The level of pollution of the water will rise by every cycle. The concept neglects costs (especially if pumping is involved) and the fact that 'losses' are always undesirable to those bearing the costs (i.e. the farmers). This is particularly valid if farmers have to spend considerable resources to irrigate the field (*Tuong and Bhuiyan*, 1999). Furthermore, an application of the concept requires a sound understanding of the flows in irrigation systems and in river basins as a whole. For global scale, grid-based applications such knowledge is not available so that estimates of irrigation water withdrawal have to rely on project efficiency estimates.

2.7 Summary and Conclusions

Irrigation water withdrawal represents a significant portion of the global water cycle and therefore needs to be taken into account in continental and global hydrological models. To illustrate the use of water in agriculture from a productivity point of view, a division is frequently made between beneficial and non-beneficial uses. Beneficial use refers to the water that is needed to increase the yield of the crop and includes water used for crop evapotranspiration, leaching, soil preparation, and weed control. Non-beneficial use includes evaporation during storage of water, deep percolation and losses in the conveyance system. From a hydrological balance perspective, the water abstracted may be divided into consumptive and non-consumptive uses. The term consumptive is used in the sense that the water is not immediately available in the hydrological cycle. The two concepts of beneficial and non-beneficial and consumptive and non-consumptive use respectively are illustrated in Figure 2.6. The different components of the irrigation water requirements at the global scale can be estimated using standard methods that have been developed at the project level for which

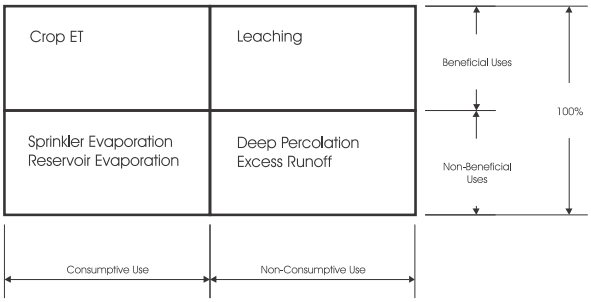

Figure 2.6: Division of irrigation water into beneficial/non-beneficial and consumptive/non-consumptive uses (*Replogle et al.*, 1996)

data is available at the global scale. It is of crucial importance to consider the additional water requirements for paddy rice. Given the low efficiency of irrigation globally, it is also important to account for return flows from irrigated areas that become a source of water downstream. However, the concept of basin efficiency is not applicable at the global scale due to conceptual and data problems. An approach for modeling irrigation water demand in a macroscale hydrological model will be introduced in Chapter 7.

3 Remote Sensing Data

3.1 Introduction

The information needed to estimate irrigation water demand over large geographical domains such as a representation of irrigated areas and crop types can potentially be derived using remote sensing technologies. This chapter will briefly introduce some basic principles of remote sensing as well as relevant sensors for monitoring agricultural areas and derived data sets. Broadly defined, remote sensing is the science and art of obtaining information about an object, area, or phenomenon through the analysis of data acquired by a sensor that is not in direct contact with the target of investigation (*Lillesand et al.*, 2003). In a narrower sense relevant for this study, it is referred to monitoring the surface of the Earth using satellite based systems. Monitoring the environment of the Earth and its temporal variations using remotely sensed data is becoming increasingly important and remote sensing data is today used for a number of operational land-surface applications such as monitoring of droughts, flood and landslide analysis, and monitoring of precipitation. A comprehensive overview and past, current and future observation missions and sensors are given in *Kramer* (2002).

3.2 Principles of Remote Sensing

Remote sensing is generally based on the principle that electromagnetic waves eventually reaching the Earth's surface interact with the surface materials on the Earth in three different ways. The radiation reaching the surface must be reflected, absorbed, or transmitted and proportions of each of those processes depend on the nature of the surface, the wavelength of the electromagnetic energy and the angle of illumination (*Campbell*, 2002). Objects on the Earth's surface have characteristic properties with regard to reflection and absorption at different wavelengths that can principally be used for their identification. A set of such response patterns is sometimes referred to as *spectral signature* or *spectral curves* of an object. A schematic diagram of relative reflectance of some objects is given in Figure 3.1. It must be noted, however, that objects cannot be *uniquely* identified using spectral signatures as the spectra change both over time and over space and depend on a number of other elements (e.g. time of the year, atmospheric conditions, sensor conditions). It is therefore essential to validate such reflectance curves with extensive ground truth data.

3.3 Sensors

Given the objectives of this study (global hydrological modeling and the study of changes in human interventions in the hydrological cycle over time), the sensors that could potentially

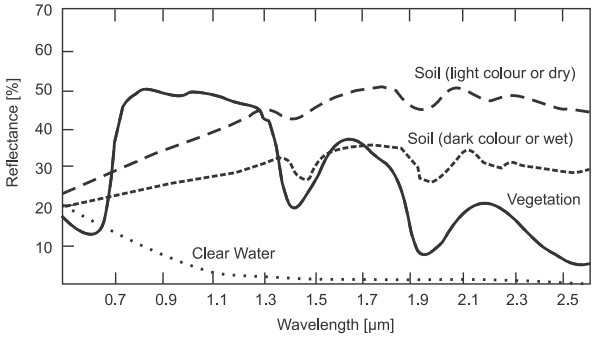

Figure 3.1: Schematic diagram illustrating the relative reflectance of some Earth targets (*Campbell*, 2002)

be used for the present study should provide global coverage and multi-year time series of freely accessible data. Currently, these requirements are met by two sensors: The *Advanced Very High Resolution Radiometer* (AVHRR) and the *Moderate Resolution Imaging Spectroradiometer* (MODIS).

3.3.1 AVHRR

The *Advanced Very High Resolution Radiometer* (AVHRR) is a scanning system that senses the visible, near-infrared, and thermal infrared portions of the electromagnetic spectrum and flies at a nominal altitude of 833 km. The sensor has a spatial resolution of about 1.1 km at local area coverage and a resolution of 4 km for the global area coverage (GAC) product that is formed by on-board sampling. AVHRR acquires global coverage data on a daily basis and has five spectral channels recording the following wavelengths:

- 0.58-0.68 μm (Channel 1): red (R)
- 0.725-1.10 μm (Channel 2): near infrared (NIR)
- 3.55-3.93 μm (Channel 3): mid-infrared (MIR)
- 10.3-11.2 μm (Channel 4): thermal infrared
- 11.5-12.5 μm (Channel 5): thermal infrared

3.3.2 MODIS

The *Moderate Resolution Imaging Spectroradiometer* (MODIS) is a sensor on board the two satellites Terra (launched in 1999) and Aqua (launched in 2002) that fly on a near polar, sun-synchronous orbit at an elevation of 705 km. Unlike the AVHRR, MODIS has been explicitly designed for monitoring land resources and biological and physical processes with a global coverage. The MODIS sensor senses 36 spectral bands, seven of which are designed to study vegetation and land surfaces (*Xiao et al.*, 2005):

- 0.62-0.67 μm (Channel 1): red
- 0.841-0.875 μm (Channel 2): near-infrared (NIR_1)

- 0.459-0.479 μm (Channel 3): blue
- 0.545-0.565 μm (Channel 4): green
- 1.230-1.250 μm (Channel 5): near-infrared (NIR_2)
- 1.628-1.652 μm (Channel 6): shortwave infrared ($SWIR_1$)
- 2.105-2.155 μm (Channel 7): shortwave infrared ($SWIR_2$)

Daily global imagery is provided at 250 m resolution (red and NIR_1) and 500 m (blue, green, NIR_2, $SWIR_1$ and $SWIR_2$).

3.3.3 Data Processing

As the reflectance values sensed by the optical instruments described above cannot penetrate the clouds and are sensitive to atmospheric effects, a considerable fraction of the daily images is 'contaminated' by clouds and atmospheric noise. This problem is usually addressed by a compositing procedure that takes a given value for a period of days assuming that it has been recorded during clear-sky-conditions. A widely applied method is the maximum values compositing (MVC) that computes the composite values by taking the maximum value for a given time period (e.g. 8 days, 16 days). The products contain also quality flags for image artefacts such as clouds and cloud shadow.

3.4 Vegetation Indices (VI)

To use the raw reflectance data measured in different channels described above to map land cover types, the data is typically converted to Vegetation Indices (VI). VI's attempt to measure biomass or vegetative vigor based on digital brightness values from combinations of spectral channels (*Campbell*, 2002). Band ratios are ratios of measurements in separate portions of the spectrum and can generally be effective in revealing latent information from a multispectral image. The most commonly used vegetation indices are described below.

3.4.1 Normalized Difference Vegetation Index (NDVI)

One of the most widely applied VIs it the Normalized Difference Vegetation Index (NDVI) that is calculated as the difference between the reflectance values in the near infrared band ρ_{nir} and the reflectance in the red band ρ_{red} over their sum:

$$NDVI = \frac{\rho_{nir} - \rho_{red}}{\rho_{nir} + \rho_{red}} \tag{3.1}$$

and hence ranges between +1 and -1. Growing and healthy vegetation has usually NDVI values between 0.3 and 0.8 while negative values indicate no vegetation or snow, ice, and clouds. Numerous studies have shown that the NDVI is proportional to several vegetation properties such as the fraction of absorbed photosythetically active radiation (%fPAR), leaf area index (LAI), vegetation fraction and net primary production (e.g. *Maselli and Rembold* (2001)).

Despite its wide acceptance, NDVI is limited by the fact that it tends to saturate under closed canopy and its sensitivity due to atmospheric conditions and soil background (*Xiao et al.*, 2006).

3.4.2 Other Vegetation Indices

Although the NDVI has been the most widely used vegetation index since it was developed in 1973, its application is severely constrained by a number of non-vegetation artefacts such as atmospheric conditions (water vapour and aerosols), cloud contamination, soil and background reflection, and others. Partly to correct for such factors and partly to take advantage of additional bands in more recent sensor systems, a number of different indices have bee proposed; The *Land Surface Water Index* (LSWI) is a vegetation index that is sensitive to equivalent water thickness in the plant tissue. It is defined as (*Xiao et al.*, 2006):

$$LSWI = \frac{\rho_{nir} - \rho_{swir}}{\rho_{nir} + \rho_{swir}} \tag{3.2}$$

The *Enhanced Vegetation Index* (EVI) uses the blue band that is sensitive to cloud cover to correct for atmospheric contamination and adjusts the reflectance in the red band depending on the reflection in the blue band. It thereby accounts for residual atmospheric contamination as well as variable soil and background reflectance (*Xiao et al.*, 2006). Furthermore, some of the influences of a mixed soil vegetation reflectance signal are also reduced (*Fensholt*, 2004). The EVI is given by

$$EVI = 2.5 \times \frac{\rho_{nir} - \rho_{red}}{\rho_{nir} + 6\rho_{red} - 7.5\rho_{blue} + 1} \tag{3.3}$$

The *Normalized Difference Snow Index* (NDSI) is not a vegetation index but has been designed to mask areas that are covered with snow and ice. It takes advantage of the fact that snow and ice have high reflectance in the blue, green, and red band, but very low relflectance in the mid-infrared band. It is defined as

$$NDSI = \frac{\rho_{green} - \rho_{nir}}{\rho_{green} + \rho_{nir}} \tag{3.4}$$

3.5 RS-Based Data sets

3.5.1 Phenology Data

Based on time series of vegetation indices, a number of products have been developed that depict the phenology of vegetation. Such products typically determine phenological events (onset of vegetation growth, maturity, and senescence) based on the curvature of observed time series of vegetation indices or fitted functions to those time series. An example is the MODIS Global Phenology Product (MOD12Q2)[1] that is based on 2 years of input data (*Zhang et al.*, 2003).

[1] NASA Data Set Name: MODIS/Terra Land Cover Dynamics Yearly L3 Global 1km SIN Grid; Detailed description available at http://lpdaac.usgs.gov/modis/

3.5.2 Land Cover Products

Classification of land cover[2] has been one of the earliest and most important applications of remote sensing. Early attempts to produce global land cover maps include the products developed by *DeFries and Townshend* (1994) and *Loveland and Belaward* (1997) and others who used metrics of AVHRR derived vegetation indices to map land cover globally at a resolution of 1°.
Using the same set of vegetation indices, land cover products can be largely different as a number of land cover classification schemes have been proposed, and there is no generally accepted global-scale classification system that has been recognized as an international standard. The classification systems differ in purpose, resolution, number of classes, class attributes and many others. *Hansen et al.* (2000) provide a comprehensive overview of the differences between classification systems. Among the most commonly used classification schemes are the FAO Land Cover Classification System (LCCS (*Gregorio and Jansen*, 2000; *Georgiou et al.*, 2006)), the University of Maryland classification (UMD (*DeFries and Townshend*, 1994)), and the International Geosphere-Biosphere Program (IGBP (*Loveland and Belaward*, 1997)). Both, the UMD and the IGBP represent the most widely used classification schemes during the early to mid 1990's (*Cardille et al.*, 2002). All of those land cover classification systems have one or more category for cropland or cultivated land. However, none has a distinct class for irrigated areas that could be used for estimating irrigation water demand. It is also important to note that the differences in the classification system and the source data may lead to large discrepancies in land cover classification. Areas defined as cropland in one product may not be classified as cropland in another product. This is particularly true for non-homogeneous pixels that represent a number of land cover classes. Figure 3.2 shows exemplary a comparison of land areas classified as 'cropland' in the GLC 2000[3] land cover product and the MODIS MOD12Q1 standard land cover product at 1 km spatial resolution for the Indian subcontinent for the year 2000. Despite an agreement in the overall pattern, there are significant differences between two land cover products.

3.5.3 Global Irrigated Area Mapping Project (GIAM)

As seen above, *global* attempts to map areas related to agriculture in general were limited to generic classification systems and a consistent definition of land cover types in the agricultural category with regard to irrigated areas is missing. The most recent effort to systematically map irrigated areas globally has been made by the International Water Management Institute (IWMI) in Colombo, Sri Lanka. The Global Irrigated Areas Mapping (GIAM (*Thenkabail et al.*, 2006)) project was aimed at producing a suite of remotely sensed products of irrigated areas at the end of the last century at various spatial resolutions. It is based on a variety of time series of remote sensing data as well as auxiliary data (such as global climate

[2] Although land cover is often used as a synonym to land use, they describe different concepts; Land use describes the human activities carried out on land resources while land cover refers to the biogeophysical cover of the Earth's surface. Remote sensing provides land cover information rather than land use information.

[3] GLC 2000 is based on data from the VEGETATION sensor on board the SPOT 4 satellite with a nominal resolution of 1km and global coverage. For details see *Hartley et al.* (2006)

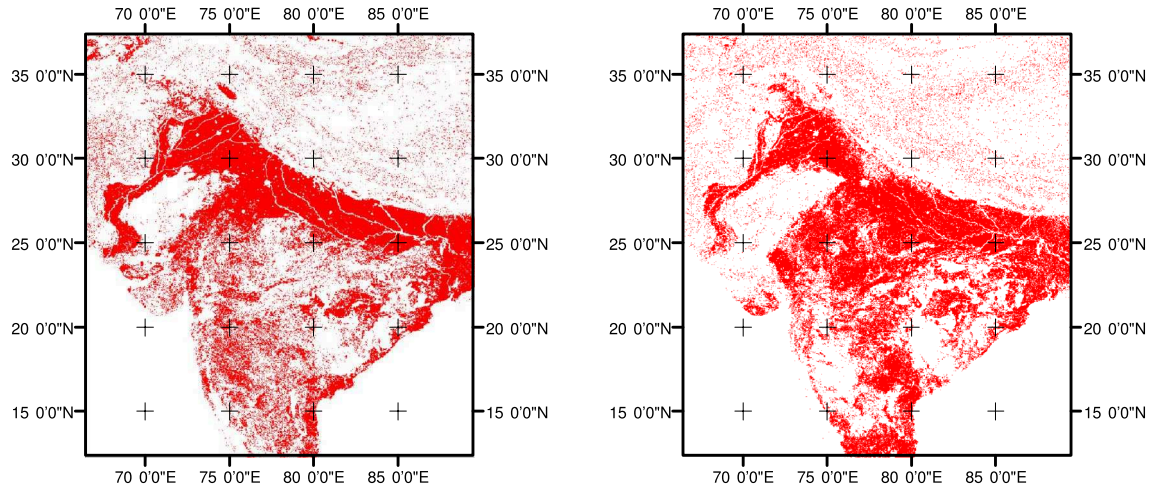

(a) GLC 2000 (b) MOD12Q1

Figure 3.2: Comparison of the areas classified as 'cropland' using two different global land cover data sets at 1 km resolution for the Indian subcontinent. MODIS land cover (left) and GLC 2000 (right)

data sets). The basic algorithm that has been used is unsupervised classification and decision trees (details are given in *Thenkabail et al.* (2005)). Version 2 of this product[4] reports areas for a total of 28 crop-rotation and water use classes and for each growing season (growing season 1, growing season 2, or continuous cropping) separately. The product has a nominal resolution of 1 km.

3.5.4 Paddy Rice Maps

Using a combination of the MODIS derived indices NDVI, LSWI and EVI, *Xiao et al.* (2005) developed an algorithm to map paddy rice and applied it to Southern China and later to South East Asia (*Xiao et al.*, 2006). The algorithm is based on a unique feature of paddy rice agriculture that distinguishes flooded rice from other types of vegetation. As described in Chapter 2.5.3, during the flooding and transplanting period, the paddy fields are characterized by a mixture of water and vegetation. This leads to a temporarly inversion of the vegetation indices: the LSWI is higher than the NDVI or the EVI. When adequate thresholds for the vegetation indices and their temporal relationship over paddy rice fields are defined, these unique characteristics in the reflectance of paddy rice fields can be used to identify them using RS data.

[4] released in May 2007, available at http://www.iwmigiam.org

3.6 Conclusions and Selection of Appropriate Data Sets

Remote sensing and classification of land use and land cover offers a unique set of advantages over conventional techniques of land cover and land use mapping. Such advantages include the repeatability of classification algorithms for data from different points in time that can help track the development of land use over time, and the objectivity of the approach that removes biases arising from user errors. Furthermore, remote sensing products can provide a consistent classification of land use and land cover at a global coverage that is independent of different definitions of land use within administrative boundaries.

Distinguishing irrigated from non-irrigated areas based on plant physiological parameters is a challenging task that only recently has received increased attention. Most attempts focus on the temporal characteristics of a vegetation index rather than the magnitude of the vegetation index itself. In a recent study, *Suyker and Verma* (2009) found no differences in biomass production, water use efficiency or transpiration efficiency between rainfed and irrigated crops. Determining whether the cause for variability in biomass production (that is seen by spectral indices such as the NDVI or the EVI) is rainfed plant growth or irrigation is therefore difficult, particularly in areas with high rainfall and vigorous natural vegetation (*Ozdogan and Gutman*, 2008). Approaches based on the temporal pattern of vegetation indices assume that the greenness in rainfed areas is closely linked to the availability of soil moisture (and hence the timing of precipitation) while the greenness in irrigated areas is more or less independent of rainfall. Despite the simplicity of this approach, there is enormous challenges in mapping irrigated areas over large scales owing to the wide range of irrigated areas with regard to timing of plant growth, vigor of vegetation, crop types and others. *Ozdogan and Gutman* (2008) have recently presented a classification scheme that first determines the potential for irrigation as a function of climate conditions and then combines this index with a supervised classification of MODIS spectral indices. Their approach resulted in irrigated area maps that agreed reasonably well with the reported overall pattern of irrigated areas in the USA but showed significant discrepancies between reported and classified in some areas. Furthermore, the approach focuses on dryland areas only and global applicability is a major concern since most of the irrigated areas in Asia are paddy rice fields.

Remotely sensed data on rice paddies in Asia could potentially be used to supplement existing maps of dryland irrigation but are not yet available at the global scale so that IWMI's GIAM data set is the only approach that explicitly and consistently maps irrigated areas on a global scale based on remotely sensed data. The advantage of this product over other efforts to map irrigated areas, is that it has been validated using a large set of some 2000 ground truth data points from missions in India, Central Asia, and Southern Africa. The product will therefore be used to estimate irrigation water demand on a global scale and to compare those estimates with country based water use statistics. The differences of the remotely sensed product GIAM with national statistics will be discussed in Chapter 4.7.1.

With regard to tracking the development of irrigated areas over time, the classification scheme based on remotely sensed data could potentially provide time series of irrigated areas but is limited to the availability of satellite data of a reasonable quality. Despite being available since 1978 AVHRR derived data does not meet those requirements due to the quality of the sensor, geometric and atmospheric correction, and spatial resolution. MODIS derived

data is only available for the period since 2002 so that long-term trajectories in irrigation development cannot be tracked based on remotely sensed data. Spatially explicit time series data for irrigated areas will therefore have to rely on a combination of national statistics and auxiliary spatial information. The availability of such data sets in national and international statistical databases related to agricultural water use will be discussed in the next chapter.

4 Agronomy Data

4.1 Introduction

This chapter is aimed at introducing statistical data sets related to agriculture and data specifically required to assess irrigation water demand and its impacts using large scale hydrological modeling and to validate the developed model. It is important to note that some of those data sets are derived from modeling approaches similar to the one presented in this study so that a validation of model results using truly independent data can be sometimes challenging. National and international statistics and agricultural census data typically hold aggregated data for some administrative unit such as counties, provinces or countries. The scale at which agricultural census data is usually reported at is generally coarse, ranging from 10^2 to 10^4 km^2 for district or county level data, to 10^3 - 10^5 km^2 at provincial (state) level to some 10^4 to 10^7 km^2 at national level (*Frolking et al.*, 2005). Furthermore, detailed census data is typically not available for every year while the cropping pattern and agricultural practices may change due to market or hydrological conditions faster than the census can document (*Frolking et al.*, 2005). It is important to note that data sets that entirely rely on national statistics cannot meet the needs of science and policy researchers who require geospatial data at improved temporal and spatial resolutions that is updated regularly (*Xiao et al.*, 2006). Also, statistics supplied by different agencies or countries may not be strictly compared due to nomenclature problems, different methods of gathering data and others. Such problems are even evident at the sub-national level. Census data sometimes does not report an actual condition but rather a potential use. For example, fertilizer use is usually determined from fertilizer sales rather than from records on the actual application of fertilizer in the field. Care must therefore be taken when comparing agricultural census data from different agencies and when merging such data.

4.2 FAOSTAT

FAOSTAT, the database of the Food and Agricultural Organization (FAO) contains some 3 million time series of data related to food production, nutrition, prices, consumption, resources, population, land use data and related data sets on a country level for some 200 countries (*FAOSTAT*, 2008). Although some data is related to irrigation, it does not specifically provide information for agricultural water management.

4.3 AQUASTAT

The AQUASTAT program of the FAO has been launched in 1993 to provide a comprehensive and reliable inventory of data on water resources with a global and regional perspective and with a focus on developing countries and countries in transition. For each country, the database contains some 50 variables grouped into different categories. The variables that are most relevant to this study are (1) the irrigated areas per country, (2) irrigation efficiency, (3), cropping intensity, and (4) water withdrawal per country. Irrigated areas refer to the 'areas equipped for irrigation' rather than the actually irrigated areas for most countries but the definition is not used consistently in all countries[1] and is also constrained by nomenclature problems within countries. *Nickum* (2003) illustrates such problems by analyzing the statistics for irrigated areas in China. Irrigation efficiency describes the (project) irrigation efficiency (Eq. 2.2 and Eq. 7.9) based on water balance calculations and reported values. Cropping intensity in agriculture (both irrigated and rainfed) is defined as the total area of harvested crops (where double or triple croppings are counted twice or three times) over the total cropland area (land in use plus fallow). For example, if two crops are grown per year on the same field, the cropping intensity is 200%. An intensity of 120% implies 20% of the area has two irrigated cropping seasons per year, and 80% has one. Cropping intensity may vary from sporadic cropping (once in a few years) to intensive cultivation of rice where it can reach 300%. On a global basis, average cropping intensity for seasonal crops is about 80% for both irrigated and rainfed agriculture but varies greatly in different regions (*Wood et al.*, 2000). From a water resources point of view, the distribution and extent of cropping intensities over irrigated areas is of utmost importance as it directly affects the amount of water that has to be diverted from the hydrological cycle to meet the requirements of the crops planted. Furthermore, multi-cropped fields generally receive higher fertilizer input and multicropping may therefore have significant impacts on the biogeochemical cycling of carbon and nitrogen in agro-ecosystems (*Froking et al.*, 2002; *Xiao et al.*, 2005). Water withdrawal for agriculture refers the quantity of water withdrawn for agricultural purposes, including livestock. For some countries, the latter category is sometimes included in the statistics for domestic water withdrawals. The information in AQUASTAT is primarily based on national water resources and irrigation master plans, national statistics and yearbooks, reports from FAO or other surveys and results from surveys made by national or international research centers (*AQUASTAT*, 2008). While AQUASTAT provides the most comprehensive global inventory of water use related to agriculture, and the figures have been critically reviewed and checked for consistency, the accuracy and reliability varies greatly between regions and categories of information, and the information is sometimes outdated (*Gleick*, 2003). Inherent uncertainties in the data are not only related to the accuracy of values for a given country but also related to inconsistent definition of variables in different countries, and different time of reporting and nomenclature problems.

[1] Irrigated Area in the AQUASTAT database is defined as *Area equipped to provide water to crops. It includes areas equipped for full and partial control irrigation, and equipped lowlands (wetlands and inland swamp bottoms) and is sometimes reported as the area actually irrigated and sometimes as the area equipped for irrigation which is usually bigger. It does not include other cultivated wetland and inland valley bottoms or flood recession cropping areas* (*AQUASTAT*, 2008)

4.4 Agricultural Census, USDA

Arguably on of the most comprehensive surveys of agriculture is conducted once every five years by the National Agricultural Statistics Service (NASS) of the United States Department of Agriculture (USDA). The Census of Agriculture provides data on acreage, yield and production of individual crops and livestock as well as data on economical and demographic information related to agriculture on county level. The most recent census available is for 2002[2]. Data and their definitions supplied by the census and relevant for this study are the irrigated areas, harvested cropland, and water withdrawal. Although the data is not explicitly given as geospatial data, the small average county size allows a fairly good representation of the spatial distribution within the US.

4.5 FAO AgroMAPS

The Mapping of Agricultural Production Systems[3] initiative was launched in 2002 by FAO, the International Food Policy Research Institute (IFPRI) and the Center for Sustainability and the Global Environment (SAGE). Its goal it to provide a database that holds national and subnational statistics and agricultural land use data for selected countries. The data is compiled from a variety of sources, including national agricultural statistics, data from international agencies and others. The subnational data is checked for consistency with the country data supplied by FAOSTAT. Although AgroMAPS does not specifically provide geospatial data, the small size of administrative units in some countries make the data a quasi-geospatial data set that may be appropriate for various macroscale modeling applications.

4.6 Atlas of Rice (IRRI)

The Atlas of Rice provided by the International Rice Research Institute[4](IRRI) illustrates rice area by type of culture for South, Southeast, and East Asia and provides information about the different rice ecosystems and relevant statistics of rice production. Non-spatial time series related to rice are routinely collected in the World rice statistics (WRS) published at IRRI. The primary source is the FAOSTAT database (Chapter 4.2), although for China and India data is based on state and provincial level respectively. A web-based geographical data set showing the rice areas by type of culture is available for South, Southeast an East Asia.

4.7 Global Map of Irrigated Areas (GMIA)

The Global Map of Irrigated Areas (GMIA) has been the first attempt to systematically map irrigated areas on a global scale (*Döll and Siebert*, 2000). It shows the areal fraction of each grid cell (5 min resolution (about 10 x 10 km at the equator)) that was 'equipped for irrigation in the 1990s. The most recent version (Version 4.01[5]) has been released in 2008. The map

[2] http://www.nass.usda.gov/census/
[3] Agro-MAPS; available online at http://www.fao.org/landandwater/agll/agromaps/
[4] http:www.irri.org
[5] available at http://www.fao.org/nr/water/aquastat

was basically developed by combining two data sets: (1) national or subnational statistics on irrigated areas provided by national statistics, statistics from FAO and other international organizations (such as those described above), and (2) geospatial information showing the location and extent of irrigated areas. Statistics on irrigated areas for some 10,000 administrative units have been combined with a number of digitized regional or local maps showing the spatial information of irrigated areas. The methodology distributes the area as reported by countries or smaller administrative units over the geospatial data on irrigated areas. Details of the algorithm are described elsewhere (*Döll and Siebert*, 2000; *Siebert et al.*, 2005) and only a concise overview will be given here. The irrigation density in a grid cell (i.e. a cell mapped as irrigated) is determined by comparing the sum of the areas of all irrigated cells within a country (or other administrative units) to the total area reported for that unit so that the total sum of all irrigated cells is equal to the reported irrigated area for the same unit. As the map depends on the data supplied by countries its quality differs strongly between countries and regions. Systematic uncertainties include the inherent inconsistencies in the underlying statistical data (see above). *Siebert et al.* (2005) compared the GMIA with areas classified as cropland in remotely sensed global land cover data that have been discussed in Chapter 3 and concluded that the overall accuracy of the GMIA is good and can generally be recommended as input data for large-scale modeling and assessment of irrigated areas, although large discrepancies have been found using a pixel by pixel comparison. The discrepancies are believed to originate from the subpixel problem in remotely sensed data and the inability of classification methods to classify cells as irrigated if the fraction within a sensored cell is less than a predefined threshold. On the other hand, as GMIA is based on national statistics it will most likely underestimate the extent of irrigated areas in regions where small-scale, informal irrigation is practiced (*Siebert and Döll*, 2007). Conversely, GMIA overestimates the actual irrigated areas, especially in regions where large infrastructure projects exist that are no longer used due to market constraints, dysfunctional infrastructure or water resources concerns. Despite these weaknesses and uncertainties, the GMIA is generally accepted and widely used for regional and global studies on irrigation water demand (*Döll and Siebert*, 2002; *de Rosnay et al.*, 2003; *Alcamo et al.*, 2000; *Haddeland et al.*, 2006a) and crop productivity (*Tan and Shibasaki*, 2003), in part because it has been the only available map of irrigated areas on a global scale until recently.

4.7.1 Comparison of GMIA and GIAM

Besides the remotely sensed irrigated area map GIAM (Chapter 3.5.3), GMIA is the only global geospatial data set of irrigated areas today. As GIAM reports the irrigated areas for each season separately while GMIA only reports the areas that could be irrigated regardless of the number of times a crop is grown, a reasonable comparison of the two data sets must be based on the *harvested irrigated area*. The harvested area in the GIAM product is given as the sum of the area in season one and two and the harvested area in the GMIA can be computed by multiplying the area equipped for irrigation with the cropping intensity in irrigated areas reported by *AQUASTAT* (2008) (Chapter 4.3). Assuming a cropping intensity of one for countries that do not report cropping intensities, the total harvested area in irrigated areas for GMIA is 322 Mha, whereas GIAMs estimate is around 438 Mha, representing a difference of 36%.

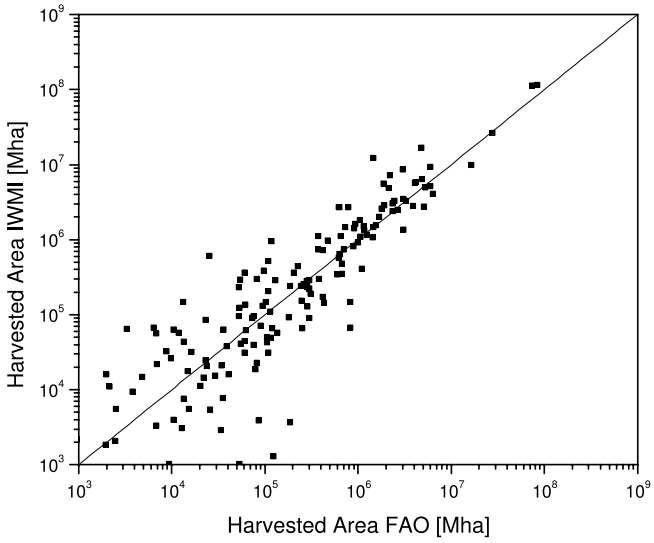

Figure 4.1: Comparison of harvested area based on FAO's GMIA and IWMI's GIAM for all countries that have reported irrigated areas to AQUASTAT

While GIAM and GMIA agree in the total irrigated areas for North America (both have been validated using USDA county statistics (Chapter 4.4)), considerable relative differences exist for South America (GIAM area is 1.8 times larger), Australia (1.9), and Europe (0.78). The largest absolute difference is found in Asia where GIAM reports 321 Mha versus 239 Mha reported by GMIA (Table 4.1). This difference can largely be explained by the irrigated areas for India and China alone. The GIAM numbers for China and India are 36% and 54% higher than those derived from GMIA and this large deviation can partly be attributed by an underreporting of areas in national statistics on which GMIA is based on (see above). On the other hand, the sub pixel problem (the non-uniformity of pixels) in remote sensing may lead to an overestimation of irrigated areas in the GIAM product. The irrigated area of a remote sensing product can vary depending on the threshold that is used to classify a pixel as irrigated.

Figure 4.1 shows a comparison of harvested irrigated area on a country-by country basis. For countries with smaller areas, the spread in FAO harvested area is generally greater than for IMWI harvested area data. This can be explained with uncertainties in the cropping intensity that is only available for large regions and are even more uncertain for countries with smaller areas. The implications of those spatial differences for estimating irrigation water demand on the global scale will be discussed in Chapter 8.2.4

4.7.2 Time Series of Irrigated Areas

As the irrigated areas globally have grown by an order of magnitude over the last century (Chapter 2), a time varying geospatial representation of those areas is essential to track the impact of irrigation water abstraction on the water cycle over time. As such a geospatial data set is presently not available, a scaling approach was used in this study to generate annual

Table 4.1: Comparison of harvested irrigated areas reported by GMIA and GIAM for all continents in Mha

Continent	GMIA	GIAM Season 1	GIAM Season 2	GIAM Total
Asia	239.9	180.4	140.8	321.3
North America	35.2	25.8	9.8	35.6
Europe	22.1	28.5	11.0	39.5
Africa	12.9	5.9	4.1	10.1
South America	8.1	13.5	8.9	22.3
Oceania	0.8	0.1	0.1	0.1
Australia	3.0	6.7	2.0	8.7
Total	322	261	177	438

geospatial time series of irrigated areas. Using the time series of irrigated areas per country recently compiled from national statistics by *Freydank and Siebert* (2008), the fraction of irrigated area A in each grid cell g for year y was rescaled using the total irrigated area in a country, as

$$A_{g,y} = \frac{A_{c,y}}{A_{c,2000}} A_{g,2000} \tag{4.1}$$

where $A_{g,2000}$ is fraction of irrigated area per grid cell taken from GMIA. Irrigated area expanded from just over 53 Mha in 1901 to 285 Mha in today. Figure 4.2 shows the aggregated irrigated areas per continent after applying the scaling approach. With the exception of Europe, irrigated areas have been growing monotonically over the last century but the rate of growth has slowed down at the end of the century. Globally, about two thirds of the irrigated areas are found in Asia.

4.8 Blended Data Sets

While data products derived from remotely sensed data are generally able to delineate important patterns of agricultural land cover, they are usually unable to distinguish the most important features of agricultural cropping systems that are critically needed for understanding the consequences of agricultural production on global cycles of matter (*Leff et al.*, 2004). Such critical information include crop varieties, agricultural inputs (irrigation, machinery, fertilizer) and outputs (such as yield and production). The spectral and spatial resolution of the sensors may not be adequate to identify agricultural areas, in particular if the individual field sizes are small compared to the sensor resolution. National and subnational statistical data, on the other hand do not provide adequate geographic information to be used in modeling efforts (*Xiao et al.*, 2006). One possible solution to this problem is to take the advantages of both, statistical data and remotely sensed data to derive an improved mapping and assessment by merging both data sets. The technique to merge satellite-based data with administrative unit-level inventory data is sometimes referred to as fusion technique. It implicitly assumes that there exists a statistical relationship between the census data and the satellite derived data that can be used to 'blend' the two data sources. The two data

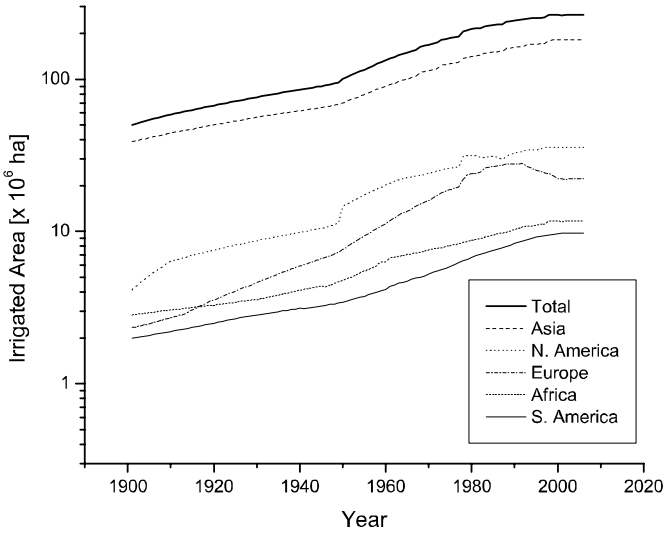

Figure 4.2: Time series of irrigated areas per continent after scaling the irrigated area map for the year 2000 based on national statistics from *Freydank and Siebert* (2008)

sets described below will illustrate the method of deriving geospatial data sets from merging statistical and remotely sensed data.

4.8.1 Global Cropland Data Layer

Ramankutty and Foley (1998) have combined satellite data with land cover data from a variety of national and sub-national inventory data to create a global map showing the distribution of cropland in the early 1990s. They used remotely sensed land use data and statistical data form FAO, USDA and supplemented it with more detailed statistical information from individual countries (where available). The statistical relationship between statistical data and the RS based land cover map was explored using a simple linear regression. The map has a spatial resolution of 5 min ($\sim$ 10 km at the equator) and shows the fractional land cover (i.e. the fraction of total area within one gridcell covered by cropland related to the total area of the gridcell) in the yearly 1990s. An update of the data has recently been prepared by *Ramankutty et al.* (2008).

4.8.2 Distribution of Major Crops

Physiologic characteristics of different crops may have drastic impacts on their water requirements, nitrate export, and methane emissions. For understanding the environmental consequences of cultivated ecosystems as well es for large scale models of matter (such as carbon, nitrogen, water) it is therefore important to have geospatial information on the extent and distribution of crops. Although the national statistical databases discussed above may provide time series of harvested areas for a number of crops, they do not supply geospatial information on the distribution and extent of those crops. *Leff et al.* (2004) used a fusion

technique to produce a global data set of the distribution of major crops across the world. Organizing crop categories by biogeochemical, food resource, and other characteristics, they classified all crops into 17 major crop categories (barley, cassava, cotton, groundnuts or peanuts, maize, millet, oil palm fruit, potatoes, rapeseed or canola, rice, rye, sorghum, soybeans, sugar cane, sugar beets, sunflower and wheat), one major crop group category (pulses and beans, and peas) and 10 other minor crop categories (fibers, vegetables, and spices, and others). The final product shows the average fractional cover of those crops at a spatial resolution of 5 min for the period 1990 to 1995. The algorithm is similar to the method used for creating the global cropland data layer and is based on two data sources: (1) average census data for the period 1992 to 1995 from various census organizations and (2) the global cropland distribution data set by *Ramankutty and Foley* (1998) that shows the fraction of cropland in each 5 min cell roughly around 1992 (Chapter 4.8.1). Building on the methodology described above, *Monfreda et al.* (2008) have recently compiled a global data set depicting the harvested area of 175 distinct crops in the year 2000 at a spatial resolution of 5 minutes based on an updated global data set of croplands (*Ramankutty et al.*, 2008).

4.9 Conclusion and Selection of Appropriate Data

Two products mapping the contemporary extent of irrigated areas at the global scale are available. FAO's GMIA has received a wide acceptance and has become a *de facto* standard product of present-day global irrigated areas (*Ozdogan and Gutman*, 2008). IWMI's recently release GIAM product is based on a different approach and therefore shows significant differences to the GMIA. Those differences have implications for irrigation water demand that are discussed using a modeling approach (Chapter 8.2.4). Geospatial data sets showing the distribution of crops are essential for estimating irrigation water demand. The differences in water demand for rice and non-rice crops make explicit maps of individual crops or crop groups a necessity. The blended data sets showing the distribution of major crops meet the requirements from an irrigation water modeling perspective and have recently been updated to reflect data for a period consistent with the irrigated area maps. Geospatially explicit data sets showing the development of irrigated areas are currently not available. The yearly data sets that were created by scaling the grid cell values in the GMIA for the period 1901-2002 may not be accurate in detail but adequately reflect the dynamics of irrigated areas on continental and global scales and can therefore be used to estimate the impact of the expansion of irrigated areas on large scale water cycles.

Country based statistics on agricultural water use that could be used to validate modeling results are available with a varying quality for 159 countries from FAO AQUASTAT and for US counties from USDA.

5 Physical Data Sets

5.1 Introduction

Spatially interpolated physical data sets covering the Earth are required for a number of applications in Earth systems modeling and there has been considerable progress in recent years in compiling such data sets. This chapter will briefly discuss the global data sets needed for modeling components of the hydrological cycle and its distortions induced by the abstraction of water for irrigation and the construction of reservoirs. It is organized in three sections. The first section will discuss commonly used global precipitation data sets and their spatial differences. The second section focuses on the data available from the Climate Research Unit (CRU) of the University of East Anglia (UK) for the description of other climate data and methods to derive fields of reference evaporation from those data sets. The last section will present data sets relevant to the application and validation of macroscale models taking into account the operation of large reservoirs.

5.2 Precipitation Data Sets

Since precipitation is the ultimate source of water for the land surface water budget, it is one of the most important climate variables for determing accurate water balance calculations (*Fekete et al.*, 2004). During the last two decades considerable progress has been made in compiling global precipitation data sets based on various sources (satellite estimates, ground observations, and climate model simulations). The methods and data sources used for deriving such fields will be discussed below for a set of four commonly used global precipitation data sets[1].

5.2.1 CRU Precipitation

Version TS 2.1 of the CRU data set (*Mitchell and Jones*, 2005) covers the period 1901-2002 and includes a number of climate variables, including precipitation at a spatial resolution of 0.5°. The time series of monthly gridded precipitation have been created by applying a two step procedure. First, a climatology of mean monthly precipitation from some 27,000 stations globally has been created for the period 1961-1990 (*New et al.*, 2002). Based on this climatology, the anomalies for each station reporting time series have been computed and

[1] Precipitation data from the Tropical Rainfall Monitoring Mission (TRMM) mission that was specifically designed to monitor tropical rainfall between 35°N and 35°S is not part of this study as it does not provide global coverage. Details are available at http://trmm.gsfc.nasa.gov/

those anomalies have been interpolated using an angular distance weighting procedure to interpolate monthly anomalies. The correlation decay distance (i.e. the distance at which the correlation of annual values for neighboring stations is no longer significant) for precipitation was assumed to be 450 km. The advantage of this method is that the number of stations that provide climatological values (normals) is far greater than the number of stations that report time series, so that the long-term mean values are applied in cases where no time series data from neighboring stations is available[2]. While this is a practical approach because it minimizes the impact of the fluctuations in network station density, it may lead to unreasonable results when the time series for data-poor regions is analyzed. The average number of stations that inform the value in a given grid cell (i.e. the number of stations in the 450 km range) gradually increased from 1901 to 1980 and declined after that. The average number of stations for the CRU TS 2.1 data product is depicted in Figure 5.1. The highest number of stations are found in North America, Europe, South Africa, and Australia. South America, North and Eastern Africa, and regions in the high latitudes are generally poorly observed. It is important to note that the CRU precipitation fields have not been corrected for gauge biases, the most significant of which is undercatch of solid precipitation in colder areas (*New et al.*, 2000; *Adam et al.*, 2006; *Tian et al.*, 2007). Correcting the observed precipitation data sets for those effects could increase the terrestrial precipitation by almost 12% (*Adam et al.*, 2006).

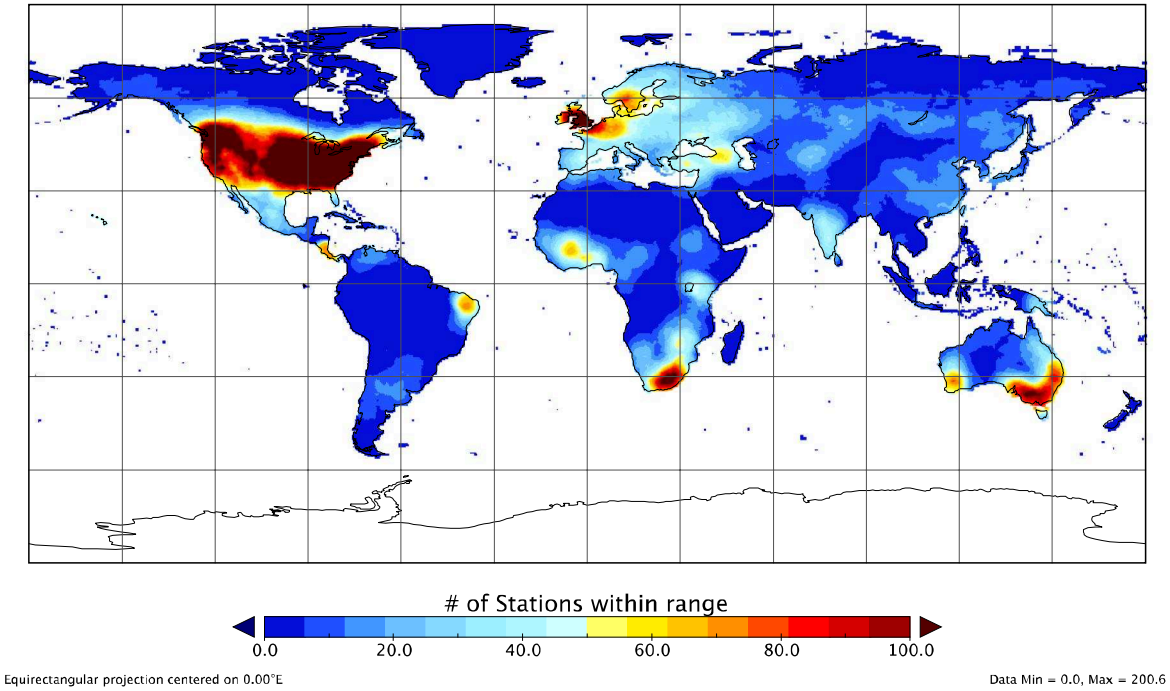

Figure 5.1: Average number of stations in the correlation decay range used to interpolate precipitation at each 30 min grid cell for the period 1901-2002 (*Mitchell and Jones*, 2005)

[2] This method is referred to as *relaxation to the climatology*

5.2.2 GPCC Precipitation

The Global Precipitation Climatology Centre (GPCC)[3] at the German Weather Service (Deutscher Wetterdienst (DWD)) provides free access to a suite of monthly gridded precipitation data sets for climate monitoring and related applications. A *Monitoring product* based on quality-controlled gauging station data from 7,000 stations is available at spatial resolutions of 1.0° and 2.5° and covers the period 1986 to present with a delay of 2 months after observation. The *Full Data Product* (*Rudolf et al.*, 1994) is based on a larger number of stations (up to 43,000) with irregular coverage and covers the period 1951 to 2004 at a spatial resolution of 1.0° and 2.5°. Other products include the *First Guess* product of precipitation anomaly (based on 6,000 stations) that is available 5 days after observation, and the *50-year Climatology* for the period 1951 to 2000, based on 9,343 stations. GPCC gridded precipitation data is not corrected for systematic biases arising from undercatch of solid precipitation, wind-related errors and others. However, GPCC provides estimates of that error and the station density used to interpolate data at any given month that can be used to assess the quality of the data and to correct for systematic biases.

5.2.3 GPCP Precipitation

The Global Precipitation Climatology Project (GPCP) has developed monthly time series of rainfall for the period 1979 to present at a spatial resolution of 2.5°. Unlike the purely gauge-based CRU and GPCC products, GPCP's approach has been to combine precipitation data sets from a number of different sources, including satellite based estimates and gauging station data. Version 2 combines gauge-corrected GPCC data with precipitation estimates from microwave (Special Sensor Microwave Imager (SSM/I), infrared sensors, and other satellite data. The primary products are the *One-Degree Daily Precipitation Data Set* (1DD) (*Huffman et al.*, 2001) that provides daily, global precipitation fields at one degree resolution from 1997 to present, the combined *Satellite-Gauge* (SG) product (*Adler et al.*, 2003), that provides monthly gridded fields at 2.5° resolution from 1979 to present and the *Pentad product* (*Xie et al.*, 2003) that has a temporal resolution of 5 days and is a companion of the SG data set. Since it is based on satellite data, the product covers the globe (i.e. not only the terrestrial surface of the Earth). Figure 5.2 shows precipitation totals for the year 2007 based on the SG product.

5.2.4 NCEP Precipitation

The NCEP/NCAR reanalysis project (*Kalnay et al.*, 1996) uses a frozen state of the art global data assimilation system to produce climate variables at high temporal resolutions. This reanalysis product uses a data assimilation system that incorporates a number of measured data and is unchanged for the entire simulation period. While the temperature data in the NCEP/NCAR reanalysis product are influenced by the observations, the produced fields of precipitation are not influenced by observations and represent modeled fields. NCEP/NCAR

[3] available at http://gpcc.dwd.de

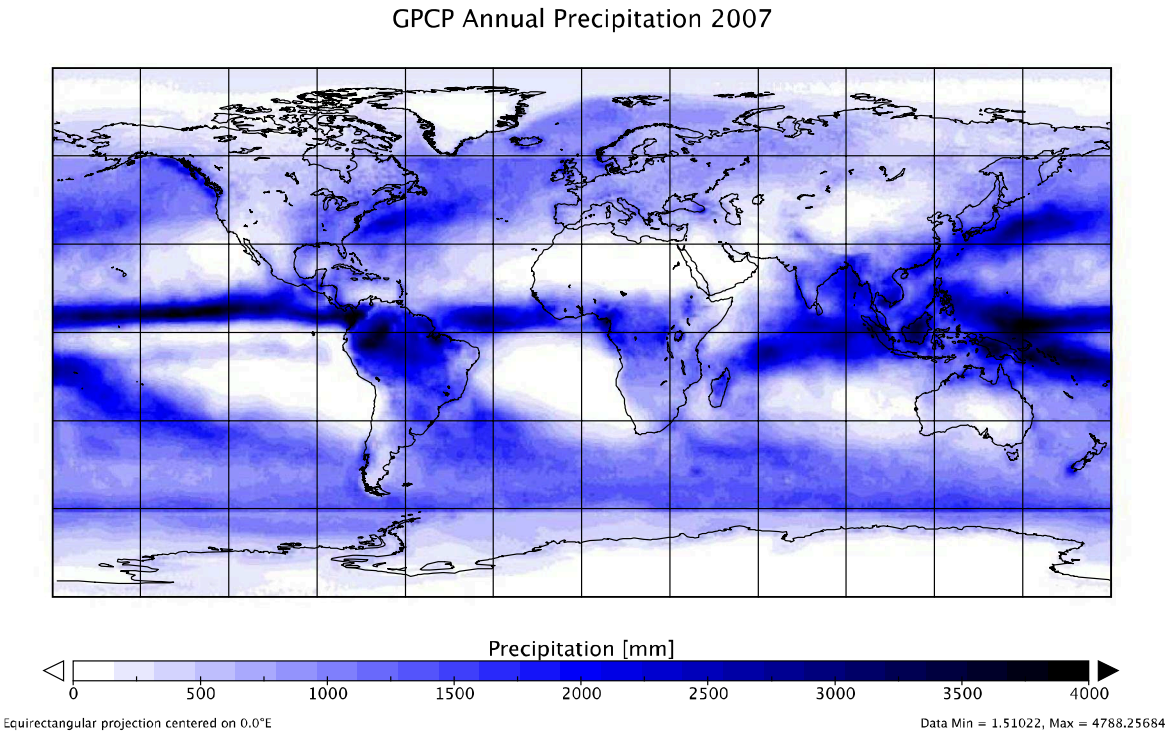

Figure 5.2: Precipitation totals in 2007 from GPCP data [mm]

data has a horizontal resolution of about 210 km and provides 6-hour integrals of the variables.

5.2.5 Temporal and Spatial Differences

The different data sources and methodologies used for the development of the data sets described above lead to significant differences in the spatial distribution of precipitation on the surface of the Earth. While the GPCP and CRU data largely agree in the low latitudes, there are considerable differences in higher latitudes that can be attributed to the gauge undercatch bias in the CRU data described above. The NCEP precipitation is generally higher (mean annual precipitation over the terrestrial surface is 918 mma^{-1}) than both GPCP (793 mma^{-1}) and CRU (785 mma^{-1}). The uncertainties related to the seasonal partitioning of precipitation is generally higher in dry regions where the relative differences in the mean annual precipitation are highest (*Fekete et al.*, 2004). The implications of those differences for simulations of irrigation water demand and global runoff will be discussed in Chapter 8.2.4.

5.3 CRU Climate Data

Besides precipitation, the CRU TS 2.1. data product contains monthly gridded values for the period 1901-2002 at 0.5°x 0.5° for the variables mean temperature, diurnal temperature range, wet-day frequency, vapor pressure, cloud cover, and ground frost frequency. Temperature and the diurnal temperature range are primary variables that are directly based on observed station data. Vapor pressure, the frequency of wet days, cloud cover, and frost day

frequency are secondary variables, for which the station data was augmented with synthetic estimates from temperature and precipitation (*Mitchell and Jones*, 2005). For interpolating the monthly fields of climate data, the same method that has been applied for creating precipitation fields has been applied.

5.3.1 Air Temperature

As the station density required to capture the monthly variability of temperature is lower than the density required for precipitation, the correlation decay distance for temperature was assumed to be 1200 km.

5.3.2 Number of Wet Days per Month

The threshold above which a day is defined *wet* varies between 0.1 $mm\ day^{-1}$ and 1 $mm\ day^{-1}$ depending on the weather service providing the data. As the 0.1 $mm\ day^{-1}$ threshold is typically applied to define a wet day, wet day frequencies that have been reported for a greater threshold have been converted using an empirical relationship. The number of wet days per month WD for the time series of precipitation was synthetically derived from a conceptual relationship between monthly precipitation in cases where no station data is available in the correlation decay distance (assumed to be 450 km) as (*Mitchell and Jones*, 2005):

$$WD = (a \cdot PRE)^x \tag{5.1}$$

where

$$a = \frac{WD_n^{1/x}}{PRE_n} \tag{5.2}$$

where $x = 0.45$ and WD_n and PRE_n denote the mean monthly wet frequency and mean monthly precipitation for the period 1961-1990.

5.3.3 Vapor Pressure

The spatial extent of vapor pressure e_a fields was extended by converting fields of monthly relative humidity RH[-] to vapor pressure at saturation that was derived from mean air temperature T using the Shuttleworth relationship (*New et al.*, 2000):

$$e_s = 6.108 \exp\left(\frac{17.27T}{237.3+T}\right) \tag{5.3}$$

and

$$e_a = RH\ e_s \tag{5.4}$$

where e_s and $e_a[hPa]$ are the saturated vapor pressure and actual vapor pressure, and T[°C] is the mean air temperature.

5.3.4 Cloud Cover

Cloud cover observations were only available for a few regions outside of Europe, Asia, and North America. Moreover, there have been difficulties with cloud cover data for the period before 1950, so that the majority of monthly cloud cover data was derived by merging observed data for sunshine duration and cloud cover using an algorithm by *New et al.* (1999).

5.3.5 Wind Speed

Wind speed is the least monitored climate variable globally and has been interpolated from around 4,000 stations globally. Wind speed is generally measured between 2 and 20 m above the ground surface with the majority of the stations measuring at 10 m height. Wind speed interpolated in the CRU data therefore assumes the wind field at that height. Wind speed is not part of the CRU TS data set but only given as a mean monthly value for the 1961-1990 period at a spatial resolution of 10' (*New et al.*, 2002). Windspeed measured at a given height can be converted to the wind speed measured at 2 m (which is needed for some evapotranspiration functions) using the following relationship (*Allen et al.*, 1998):

$$u_2 = u_z \frac{4.87}{\ln(67.8z - 5.42)} \tag{5.5}$$

where u_z represents the windspeed at z in meters.

5.4 Potential Evapotranspiration

5.4.1 Introduction

Evaporation represents more than 60% of the precipitation input of the terrestrial water cycle (*Baumgartner and Reichel*, 1975; *Vörösmarty et al.*, 1998) and thereby conveys an important constraint on water availability, that in turn controls the distribution of plant communities (*Vörösmarty et al.*, 1998). The rate of evaporation is controlled by the availability of energy and by the ease with which water vapour can diffuse into the atmosphere (*Shuttleworth*, 1992). Potential evapotranspiration is a concept that characterizes the environmental demand for evapotranspiration and is a representation of the flux of vapor from a stand of plants when the soil water supply is not limiting. Methods for determining potential evapotranspiration range from simple temperature dependent equations to physically-based approaches and can also be classified into methods that are dependent on the land cover and those that are independent of land cover. The following section exemplifies the use of the climate data described above for estimating fields of potential evapotranspiration using the Penman-Monteith equation recommended by FAO, and for a simple temperature-dependent function. An intercomparison of methods for calculating potential evaporation and the implications for regional and global water balance models is given in *Federer et al.* (1996) and in *Oudin et al.* (2005).

5.4.2 Penman-Monteith

Penman-Monteith Combination equation

The Penman-Monteith method to compute evapotranspiration is based on both an energy balance of the surface and empirical relationships describing the diffusion of energy from the surface. It is therefore known as a combination equation which is given by (*Allen et al.*, 1998):

$$\lambda ET = \frac{\Delta (R_n - G) + \rho_a c_p \frac{e_s - e_a}{r_a}}{\Delta + \gamma \left(1 + \frac{r_s}{r_a}\right)} \tag{5.6}$$

where

ET	$[mmd^{-1}]$	=	potential evapotranspiration
λ	$[MJkg^{-1}]$	=	latent heat of vaporization = 2.45
R_n	$[MJm^{-2}d^{-1}]$	=	net radiation, Eq. A-15
G	$[MJm^{-2}d^{-1}]$	=	soil heat flux density, A-16
e_s	$[kPa]$	=	saturation vapor pressure, Eq. A-18
e_a	$[kPa]$	=	actual vapor pressure
$e_s - e_a$	$[kPa]$	=	saturation vapor pressure deficit
ρ_a	$[Mgm^{-3}]$	=	mean air density at constant pressure
c_p	$[Jkg^{-1}K^{-1}]$	=	heat capacity of the air = 1005
Δ	$[kPa°C^{-1}]$	=	slope of the vapor pressure curve, Eq. A-8
γ	$[kPa°C^{-1}]$	=	psychrometric constant , Eq. A-6
r_s	$[sm^{-1}]$	=	surface or canopy resistance, Eq. A-3
r_a	$[sm^{-1}]$	=	aerodynamic resistance, Eq. A-2

A detailed description of the method and the variables is given in the appendix. Table 5.1 summarizes how global climate data sets such as the CRU data set can be used to compute various terms in Eq. 5.6.

5.4.3 Hamon Evapotranspiration

The Hamon function (*Hamon*, 1963) to estimate potential values of evapotranspiration PET $[mmd^{-1}]$ is based on an empirical relationship and is given as (*Federer et al.*, 1996):

$$PET = \frac{715.5 \Lambda \; e_s \; T_m}{T_m + 273.2} \tag{5.7}$$

where T_m [°C] is the mean daily air temperature and Λ is the daylength [-], computed as the fraction of daylight hours N (Eq. A-13) in a 24 hours period, and e_s is the vapor pressure at saturation, computed as a function of air temperature (Eq. A-17). For global application, mean air temperature can be taken from gridded temperature data sets such as CRU or NCEP (see above). Although the function is basically a function of latitude, day of the year, and air temperature alone, it has been shown to give reasonable estimates of evapotranspiration

Table 5.1: Overview of climate and radiation related variables and globally available data sets for the Penman-Monteith equation

Variable	Meaning	Data required
e_s	saturation vapour pressure	max/min air temperature
R_a	extraterrestrial radiation	day of year, latitude
Δ	slope of the vapour pressure curve	max/min air temperature
R_n	net radiation	vapour pressure, e_s, sunshine duration[a], R_a
P	atmospheric pressure	elevation
u_z	windspeed at height z	wind speed, transfer function[b]
R_s	solar radiation	sunshine duration

[a] sunshine duration can be derived from cloud cover, for example using Eq. A-20
[b] maybe required to convert windspeed measured at different heights, for example Eq. 5.5

when used in a water balance model. *Vörösmarty et al.* (1998) used 11 commonly used evapotranspiration functions for a water balance model applied to the conterminous US and found that discharge estimates produced using the Hamon function had the lowest bias of all tested reference evapotranspiration functions when compared to observed values. Similar findings have been reported by *Oudin et al.* (2005) who tested a set of 27 evapotranspiration functions over a large set of catchments around the globe and concluded that simple temperature dependent functions produce the best results with regard to model efficiency and found no advantage in using more complex methods. The mean air temperature required in Eq. 5.7 can be taken directly from the air temperature provided by CRU or any other globally available data sets of air temperature.

5.5 Climate-Based Phenology

Modeling the phenology of crops is of utmost importance for assessing the water demand as the timing of the growing season will largely influence the evapotranspirative crop water demand and the fraction of that demand that can be met by precipitation. Whereas the development of plant growth in high latitudes is usually limited by temperature, their development in arid and semi-arid regions depends solely on soil moisture conditions. Linking available soil moisture and temperature to phenological events of crop development has led to the concept of Length of Growing Period (LGP) that is simply defined as the period in which both temperature and soil moisture are conducive for crop growth (*Fischer et al.*, 2002). A number of different thresholds have been defined to determine the onset of the growing season[4] based on those criteria. In regions where the growing season is constrained by temperature, the temperature threshold is typically set between 0 and 10°C (*Chmielewski*, 2003; *Fischer et al.*, 2002). In the present study, a temperature threshold of 5°C was used. In areas where crop growth is not limited by temperature constraints, the onset of the growing season has been determined based on the monthly values of the rainfall record and assuming that the growing season starts one month before the month with the maximum rainfall in a given

[4] A survey of different criteria for soil moisture and temperature is given in *Groten and Ocatre* (2002)

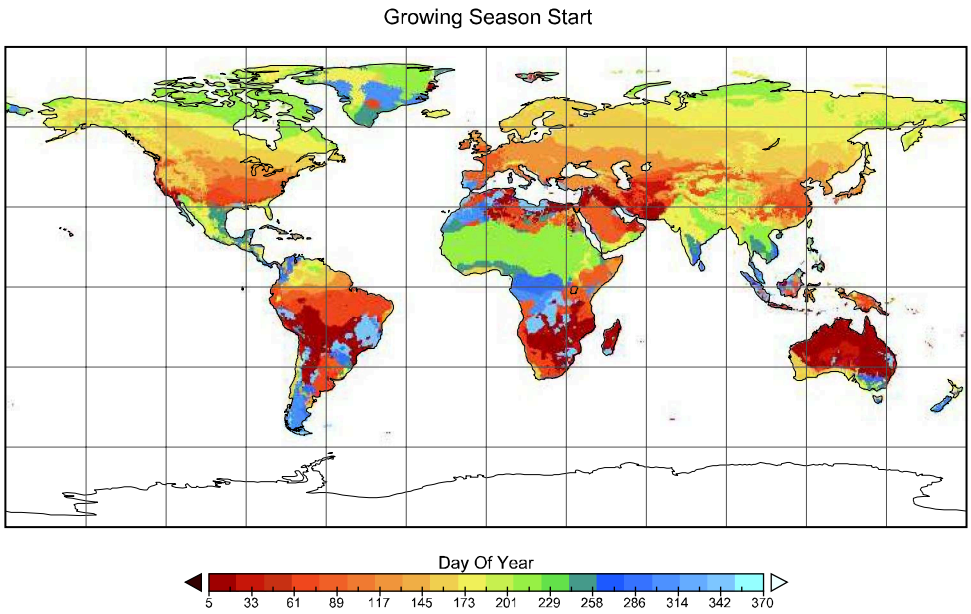

Figure 5.3: Computed onset of the first growing season 2002 based on CRU data

year. If multiple cropping is possible, the second season is assumed to start 180 days after the start of the first season. Figure 5.3 shows the computed onset of the first growing season for the year 2002 based on the CRU climate data set.

5.6 Soil Hydraulic Properties

To calculate the amount of water that can be hold in the soil in irrigated as well as non-irrigated soils, the soil hydraulic parameters field capacity, wilting point, and the root depth are required. A global data set of soil properties was compiled by *FAO* (2003) in the Digital Soil Map of the world (DSMW). Version 3.6 of this product is based on the soil map of the world published in 1974 but has been complemented with supplementary information and more details since then and is available at a spatial resolution of 5 minutes. Hydraulic soil parameters can be derived using pedotransfer functions that are mathematical relationships between one or more soil parameters. If properties of the soil are based on modal characteristics of soil units, the transfer function is often referred to as taxotransfer function. Based on a set of more than 4,300 soil samples, *Batjes* (2002) has developed such functions for a number of soil parameters, including hydraulic properties that control water retention globally at a resolution of 30 minutes[5]. The root depth controls the amount of water that can actually be extracted from the soil by the vegetation cover. Estimated root depths for different land cover types are given in table A-1 in the Appendix.

[5] Data sets are available online at http://www.daac.ornl.gov

5.7 Global Hydrography Data

5.7.1 River Networks and Basins

Gridded river networks are needed to represent the horizontal linkages of the continental land mass to the oceans and are typically derived from high resolution elevation data at various resolutions and determine the flow direction in each grid cell relative to one of its eight neighbors[6].

As river networks are typically derived from high resolution digital elevation data at a much finer resolution than macroscale hydrological models and AOGCM's are usually operated, scaling procedures are necessary to transform the river networks into coarser resolution (network upscaling) while preserving the topology and key geomorphic properties of the network (*Fekete et al.*, 2001). Examples of such network upscaling algorithms are given in *Olivera et al.* (2002), *Fekete et al.* (2001), and *Döll and Lehner* (2002).

STN River Networks

One of the earliest attempts to derive such networks globally has been the Simulated Topological Network (STN (*Vörösmarty et al.*, 2000a,b)) that is based on an aggregated digital elevation model (DEM) at 30' resolution and manual editing of the resulting flow directions. Drainage basins and sub-basins have subsequently been defined based on the Strahler stream order[7]. In this way, 6,152 river basins have been identified with sizes ranging from a few hundred km^2 to $5.8 \times 10^6 km^2$. Out of these, 1,123 river basins have a catchment area of more than 5 cells ($10,000 km^2$) which is considered the minimum size that can be represented by a 30 min network (*Fekete et al.*, 2001). The 522 basins with areas larger than $25,000 km^3$ drain 82% of the land mass (*Vörösmarty et al.*, 2000c). Recently, a 6 min version of the STN was prepared using the same input data and manually editing the derived flow directions.

DDM30

The Global Drainage Direction Map (DDM30 (*Döll and Lehner*, 2002)) is a global drainage direction map at 30 min resolution that has been derived by network upscaling of existing river networks and manual corrections using vectorized maps of rivers, wetlands, and comparison of discharge station attribute data.

HydroSHEDS

The Hydrological Data and Maps Based on Shuttle Elevation Derivatives (HydroSHEDS) product (*Lehner et al.*, 2008) is a suite of hydrography data with a level of quality and accuracy that was previously unachieved. It is primarily based on elevation data obtained from NASA's Shuttle Radar Topography Mission (SRTM) in February 2000 with a coverage

[6] This method is commonly referred to as the D8 algorithm (*O'Callaghan and Mark*, 1984)
[7] A hierarchical ordering of streams based on their degree of branching

from 56°S to 60°N and contains both raster and vector data of topography, watersheds, and drainage networks of the Earth's terrestrial surface that have been generated by applying a set of standard procedures (including sink filling, stream burning, and deriving flow directions). Details of the algorithm are given in *Lehner et al.* (2006a). Regions outside the SRTM coverage have been filled by using existing global elevation data (HYDRO1K[8]). HydroSHEDS is available at resolutions of 3, 15, and 30 arcseconds (approximately 90, 500, and 1000 meters at the equator).

5.7.2 Selection of a river network

The recently released HydroSHEDS data sets represent a significant improvement over STN and DDM 30 with regard to draingage basin delineation, flow directions, and the representation of lakes and wetlands. Using the algorithms described above, the data could be upscaled to the 30min resolution at which contemporary global models typically operate. However, as most GRDC gauging stations and data on reservoirs (Chapter 5.7.4) has already been registered to the STN 30 river network, the simulations carried out in this study were based on STN data.

5.7.3 Discharge Data

Discharge data provides the most accurate information about the terrestrial water cycle and provides an integrated measure of all hydrological processes. The Global Runoff Data Center (GRDC)[9] is the digital world-wide repository of discharge data to which member states of the World Meteorological Organization (WMO) contribute voluntarily. As of January 2008, GRDC holds daily and monthly data for some 7,000 stations, some of which are regularly updated. The temporal distribution of station data has a peak in 1980, partly because the database was complemented with a UNESCO river discharge collection and partly because the initial request to provide data has been very successful. Since the mid-1980s, however, the number of stations reporting data is declining steadily (Figure 5.4). While this decline is caused by a number of reasons (including legal considerations regarding the restriction of data, privatization of services and others) and does not necessarily correspond to a decline in the hydrological networks as such, it makes large scale assessments of water resources more difficult. Since the network of gauging stations are the mainstay of monitoring and assessing water resources, this lack of data continues to challenge water science (*Vörösmarty et al.*, 2005).

For the present study, a set of global gauging stations has been selected based on interstation area, length of record, and quality of data. This selection has been used by *Fekete et al.* (2002) and contains 663 stations. The selected stations monitor 52% of the continental land mass (excluding Antarctica) and 70% of the continental discharge to oceans (*Fekete et al.*,

[8] A suite of topographically derived data sets including, streams,networks, and ancillary data at 30 arcseconds. Available from the United States Geological Survey (USGS)

[9] available at http://grdc.bafg.de

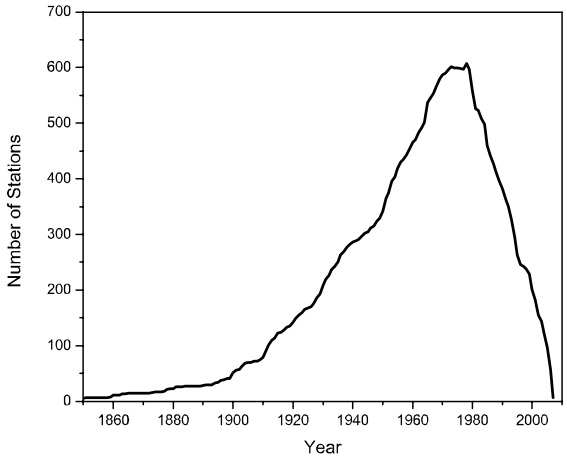

Figure 5.4: Time Series of Holdings in the GRDC database. Monthly data, based on the GRDC station catalogue, version 2008-01-07. Data is available from 1850 to 2007

2002). The period of observation varies greatly between stations with a peak in data availability in the 1980's. The number of observation months for the final selection of 663 stations ranges from 120 to 1224 (mean 541, median 477) months.

5.7.4 Dams and Reservoirs

Globally, some 40,000 reservoirs with a dam height of more than 15 m are currently in operation (*ICOLD*, 2003). The contemporary aggregate storage of those reservoirs listed in the dam register of the International Commission on Large Dams (ICOLD) is about 6,700 km^3 (*ICOLD*, 2003). The ICOLD register provides a number of attributes for each dam but does not give the geographic coordinates, mean inflow to the reservoir, or detailed information on the operation rules of those reservoirs. Based on a series of dam registers published by ICOLD, *Vörösmarty et al.* (1997) have compiled and geo-referenced a time-varying global database of 668 large impoundments with a a nominal storage capacity greater than 0.5 km^3 and registered the locations to the STN-30 river network (see above), ensuring the dams are located on the right tributaries. The residence time[10] for more than 75% of the reservoirs is under one year, with a median of 0.4 years (*Vörösmarty et al.*, 1997). The combined contemporary maximum capacity for those reservoirs is 4,653 km^3 and represents 70% of impoundments formed by dams over 15 meters.

The construction of large reservoirs has peaked in the 1970s and is declining since then. Figure 5.5 shows the accumulated storage capacity of the 668 reservoirs since the beginning of the last century. The ICOLD database also provides some information on the purpose(s) of the reservoir. While large-volume reservoirs are usually designed for multipurpose needs, smaller reservoirs typically serve one purpose (*Nagy et al.*, 2002). More than 70% of the

[10] computed as reservoir capacity over mean annual inflow, computed from *Fekete et al.* (2002) and assuming an utilization factor of 0.67. An extended discussion of the residence time of registered reservoirs will be given in Chapter 7.4.2

referenced dams in the ICOLD database are classified as 'single purpose' reservoirs of which nearly 50% are exclusively used for irrigation, 17% for hydropower, 13% for water supply, 10% for flood control, and the remainder for recreation, navigation, and other uses (*ICOLD*, 2003). The *primary* use of multi purpose reservoirs is 25% for irrigation, 19% for hydropwer, 16% for water supply, 18% for flood control, 12 % for recreation and the remainder for navigation and others (*ICOLD*, 2003).

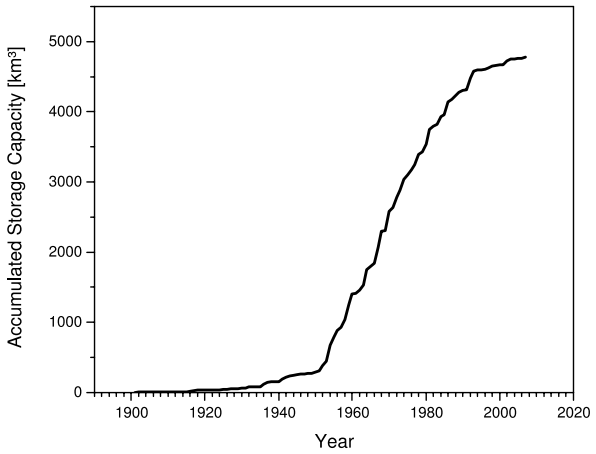

Figure 5.5: Time series of accumulated reservoir storage using the data set of registered impoundments with a storage capacity larger than 0.5 km^3 based on *Vörösmarty et al.* (1997)

5.8 Conclusions and Selection of Appropriate Data

Out of the global precipitation data sets described above, the CRU data set has certainly received the widest acceptance. Furthermore, it has the longest record of all global precipitation data sets which makes it the obvious choice to track impacts of reservoirs and irrigation over time. The spatial and temporal differences in precipitation data sets have implications for components of the hydrological cycle, including the use of irrigation water that are explored in a modeling context (Chapter 8.2.1).

The validation of continental and global scale hydrological models is severely limited by the globally available discharge data. Both data availability and data quality tends to be lower in regions with high irrigation water abstractions making it more difficult to validate the models this study is concerned with. Similarly, the repository of registered reservoirs is incomplete and covers only reservoirs with a capacity larger than 0.5 km^3. However, those reservoirs represent an estimated 70% of the global storage capacity so that the data can be used to estimate the impact of reservoirs on continental and global water cycles.

6 Macroscale Hydrological Modeling

6.1 Introduction

This chapter will review some basic concepts of macroscale hydrological models. After defining macroscale hydrological models and its interfaces and linkages to Atmosphere-Ocean General Circulation Models (AOGCM), four macroscale hydrological models will be introduced to exemplarily show the wide range of approaches for modeling vertical and lateral components of the hydrological cycle at continental and global scales. Given the objective of this study, the description will focus on approaches to account for human interventions in those models and their limitations. Finally, some commonly used measures for assessing the performance of hydrological models, the causes for uncertainty in hydrological models and approaches to quantify the uncertainty will be discussed.

6.2 Macroscale Hydrological Modeling

The definition of different scales in Earth Science in general is far from uniform and varies greatly with different disciplines. In atmospheric sciences, for example, a clear definition of different scales exists with interfaces at 2 km and 2,000 km and subdivisions for large, medium and small sub-scales, denoted γ, β, and α. Scales in hydrology are typically subdivided into the microscale, mesoscale, and the macroscale. *Microscale* is the scale at which very localized processes such as pore-water processes take place and typically extends over a few meters. The *Mesoscale* is typically attributed to more or less uniform landscapes or catchments, and the *Macroscale* covers catchment areas larger than 100 km^2. The definitions of scale in hydrology and atmospheric sciences are depicted in Figure 6.1.

While the development in hydrological science has long been on the classic problems of engineering works for supply and natural hazard reduction (*Eagleson*, 1986), there has been a growing interest in the large scale hydrological *and* atmospheric processes starting in the 1980s that has resulted in the developed and application of Macroscale Hydrological Models (MHM) or Land Surface Schemes (LSM). There is no universally accepted definition of MHMs and they may simply be defined as the application of hydrological models over a large spatial domain (*Xu*, 1999). *Vörösmarty* (1991) defines MHMs as hydrological models that simulate water fluxes in two or three dimensions, discretize the spatial domain at length scales varying from 10 to 50 km and typically use a monthly time step. Vertically, the water fluxes are simulated through precipitation, evapotranspiration and recharge to subsurface storage, while the horizontal water flux is simulated using simulated network topologies that route surface water and groundwater. The organizing concept for addressing hydrological issues is the watershed (*Vörösmarty*, 1991) and the scale of application ranges from those

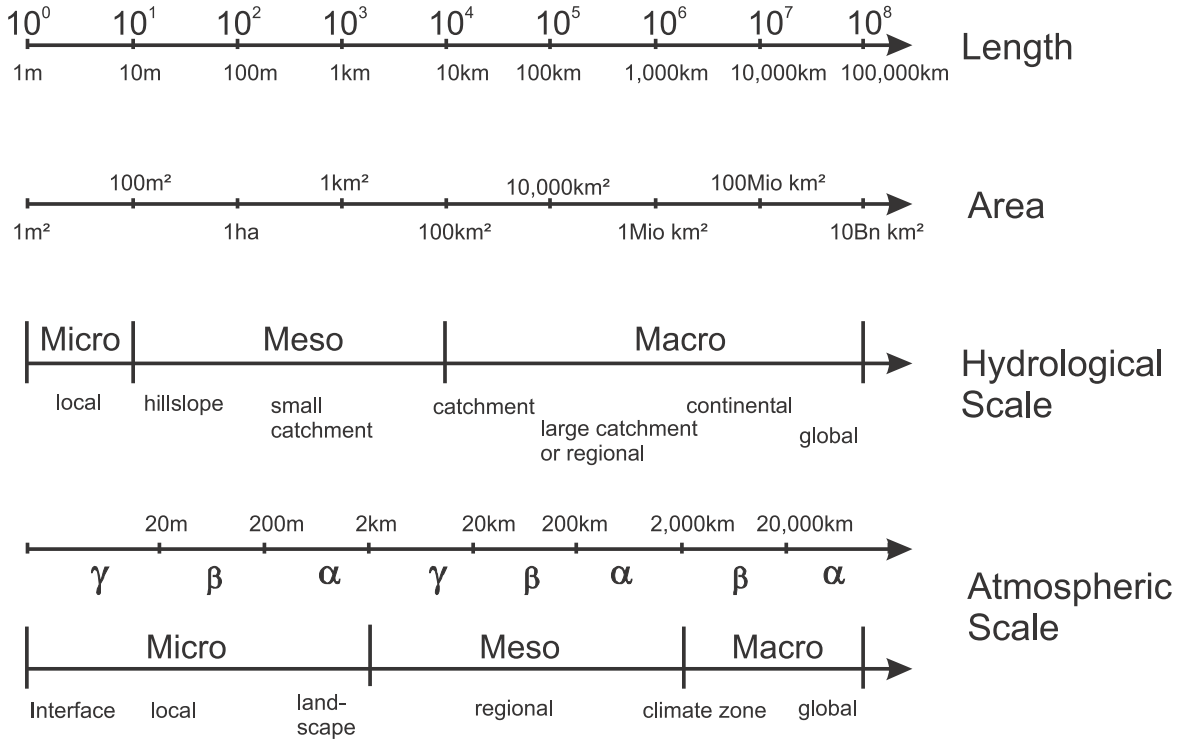

Figure 6.1: The terminology of spatial scales in hydrology and climatology and their relationships to actual spatial lengths or areas (*Bronstert et al.*, 2005)

watersheds to continents and the globe. The basin allows a closure of the terrestrial mass balances and permits spatially aggregated observations of fluxes, such as runoff, sediments, and river-borne biogeochemicals (*Wood et al.*, 1997). Present-day global water balance models typically simulate components of the hydrological cycle at a spatial resolution of 0.5 x 0.5° latitude-longitude. Macroscale hydrological modeling was motivated by the need to answer two main questions: (*Wood et al.*, 1997; *Xu*, 1999):

1. What are the impacts of human activities on water resources, hydrology and biogeochemical cycles and how are these systems affected by a potential climate change ?
2. How can improved representations of the land surface hydrology contribute to improve the performance of climate models that use the terrestrial surface and its water fluxes as a lower boundary condition ?

While the first question will be at the focus of this study and the discussion the the subsequent chapters, it is worth mentioning the interactions and linkages of MHMs with AOGCMs that are increasingly coupled with MHMs. AOGCMs numerically solve the fundamental equations governing the dynamics of fluid motion in the atmosphere and are typically run at a fine temporal resolution, ranging from minutes to some hours while the spatial resolution is generally coarse (~200 km) with a vertical discretization of the atmosphere through a set of layers (typically 10 to 20). AOGCMs consist of several components (atmospheric, land, ocean, and sea ice) that are interlinked to each other. While the atmospheric component of AOGCM an is typically very sophisticated, the land-phase parameterizations do not agree with most hydrological variables (*Xu*, 1999) and the representation of the terrestrial surface fluxes and the link to the lower boundary has historically been the weakest part of AOGCMs

(*Feddes*, 1995). Early implementations of AOGCMs treated the land surface as a passive and weak participant and parameterized the hydrological process as a prescribed soil moisture state (*Eagleson*, 1986).

The land surface component of climate models is a key component because it controls the partitioning of water into evapotranspiration and runoff, and the fluxes of energy (*Pitman*, 2003). Runoff modeling, the traditional realm of hydrological models, is connected to AOGCM simulations at two points (*Bazzaz and Sombroek*, 1996): (1) At the boundary between atmosphere and land surface where the rainfall is partitioned into surface runoff and evapotranspiration and (2) at the boundary between land and ocean where the simulated hydrographs provide the input for the ocean model. A better representation of the water cycle in AOGCMs can thus facilitate the calibration and validation of such models (*Vörösmarty*, 1991; *Arora and Boer*, 2001) with regard to the water and energy balance. *Kite* (1995) has formulated the following requirements to be met by macroscale hydrological models to be integrated into AOGCMs:

1. MHMs must be applicable to large scales and different regions without recalibration,
2. they must be able to operate at a variety of different time scales,
3. they must include the effects of topography, land cover and meteorological variations, and
4. the spatial coverage must range from the smallest hydrological element to the grid size used in AOGCMs.

To accomplish these requirements, the model should be physically based, distributed, and have some mechanism for aggregation and disaggregation of data. Furthermore, the model should not be too detailed because the data needed is not available at a macroscale and microscale physics will not be applicable (*Kite*, 1995). Finally, it is necessary to adequately consider the effects of human interventions in the water cycle in MHMs. Among the most important impacts of such interventions are the impacts of irrigation activities on the energy and water budget and the distortion of hydrographs due to the storage of water in impoundments. To represent the water cycle in AOGCMs using MHMs, both models can be coupled. A fundamental problem in coupling hydrological models and AOGCMs is that spatial and temporal scales are very different. Typical AOGCMs use short temporal scales (minutes to hours) while hydrological models (MHMs in particular) are usually run at daily, weekly or monthly time steps. The 'standard' spatial resolution found in most contemporary hydrological models is 0.5° which is 25 to 100 times finer than the resolution typically found in AOGCMs were a latitude-longitude element ranges from $2.5° \times 2.5°$ to $5° \times 5°$ (*Harvey*, 2000). These temporal and spatial mismatches require scaling techniques for which various methodologies have been developed[1].

6.3 Existing Models

MHMs generally differ in the representation of hydrological processes, the level of detail, the required input data, and their spatial and temporal resolution. The following section will

[1] An overview of coupling methods is given in *Mölders* (2005)

briefly summarize the main characteristics and process representation of four macroscale hydrological models that have received a wide attention for regional, continental, and global applications. The main characteristics and differences of the four models are summarized in Table 6.1.

The core of the vertical water balance that is computed by MHMs is given by the water balance equation that can be written as

$$R = P - E - \frac{\partial W}{\partial t} \tag{6.1}$$

where $R[mm]$ is the runoff, $P[mm]$ is the precipitation, $E[mm]$ is the actual evapotranspiration and $\frac{\partial W}{\partial t}[mm]$ is the change in storage. The soil moisture model in any MHM is the most critical component with regard to long-term water balances. The soil-atmosphere interactions are typically based on physical principles where actual evapotranspiration E is modeled as a function of actual soil water storage and potential evapotranspiration. The runoff formation process is usually represented using a conceptual model with parameters that may be used for calibration. The horizontal transport of computed runoff to the outlet of a river basin (routing) is modeled using one of the river networks described in Chapter 5.7.1. Routing methods differ in the parameterization of the delay in lakes, reservoirs, and river stretches. Routing is usually done in the post processing of model simulations; vertical components are computed for each time step and the runoff (corrected for water withdrawals in some models) is routed through a river network.

The Water-Global Assessment and Prognosis Model (**WaterGAP** (*Alcamo et al.*, 2003a; *Döll et al.*, 2003; *Kaspar*, 2004)) is an integrated global water model that was one of the first models explicitly accounting for the use of water and its impacts on runoff and has been applied in a wide range of applications (e.g. *Döll and Siebert* (2002); *Alcamo et al.* (2003b, 2000)). Runoff from land within one grid cell is modeled following the HBV[2] approach as a function of precipitation and actual soil moisture. The computed runoff is corrected for the consumptive use of water before routing. Whereas irrigation water use is modeled, domestic and industrial water use are disaggregated from national statistics.

The Variable Infiltration Capacity model (**VIC** (*Liang et al.*, 1994, 1996; *Haddeland et al.*, 2006a)) is a grid-based MHM that has been developed at the University of Washington and the University of Princeton. It has been applied at spatial scales ranging from $1/8°$ to $2°$ and it stands out among most hydrological models because it also solves the energy balance at the land surface. The VIC model parameterizes the spatial subgrid variability of the soil properties by a variable infiltration capacity and represents the subsurface by multiple (usually three) layers, the upper layer representing the dynamic behavior of the soil to rainfall events and the lower layers representing the slowly-varying behavior of the soil between storm events. The lateral transport of the runoff computed for each cell is modeled by accumulating the grid-based runoff using the river network taking into account some simple assumptions with regard to travel distance and velocity, after convolving the grid based runoff with a unit impulse response function (*Nijssen et al.*, 1997).

[2] The HBV-model (*Bergström*, 1995) is a conceptual water balance model named after the abbreviation of Hydrologiska Byråns Vattenbalansavdelning (Hydrological Bureau Waterbalance-section of the Swedish Meteorological and Hydrological Institute)

Table 6.1: Overview of the main characteristics of of contemporary MHMs

Model	**WaterGAP**	**VIC**	**TRIP**	**WBM/WTM**
Time step	daily	varying (hourly to daily)	monthly	monthly/pseudo-daily
Spatial resolution (degree)	0.5; irrigated/non-irrigated	varying (1/8 to 2);mosaic approach	1	0.5
Evapotranspiration	$E = f(W)$	subgrid variability of soil properties: variable infiltration	-	$E = f(W)$
Runoff formation	HBV-approach; surface runoff and subsurface runoff	3 soil layers	input from LSM	Fast/slow components
Groundwater	linear reservoir	non-linear reservoir from deepest soil layer	linear reservoir	linear reservoir
Lakes	linear reservoir	-	-	-
Routing	linear reservoir; constant velocity; post process	linearized Saint-Venant equation	linear reservoir; constant velocity;post process	linear reservoir;post process
River network	DDM30	various	1° TRIP network	STN 30, STN 6
Water withdrawal	Irrigation (modeled), domestic and industry from statistical data	Irrigation (modeled)	Irrigation (modeled), domestic and industry from statistical data	-
Calibration	1-2 tuning parameters, multiple regression for regionalization; river basin	(river basin)	-	-

Total Runoff Integrating Pathways (**TRIP** (*Oki and Sud*, 1998; *Oki et al.*, 2001)) is not a hydrological model itself but a method to estimate water availability by using offline data from different Land Surface Models (LSMs). Computed runoff is routed through a river network with a horizontal resolution of $1° \times 1°$ where the river bed parametrization uses empirical discharge to width relationships. It has recently been modified to account for the effects of irrigation water use on the vertical components (*Hanasaki et al.*, 2008) and has implemented a reservoir operation scheme in the routing module (*Hanasaki et al.*, 2006).

The Water Balance Model (**WBM** (*Vörösmarty*, 1991; *Vörösmarty et al.*, 1998)) is a physically based, one-dimensional model that has been developed at the University of New Hampshire and has been used for a number of studies on the terrestrial water cycle (*Syvitski et al.*, 2005; *Green et al.*, 2004; *Fekete et al.*, 2002; *Vörösmarty et al.*, 2000a,d; *Sharma et al.*, 2000). A modified version that models the distribution of permafrost and its dynamics has been developed by *Rawlins et al.* (2002) for application in the pan-Arctic domain. The daily soil moisture budget is given by

$$dW_s/dt = \begin{cases} -g(W_s)(E_p - P_a) & \text{for } P_a \leq E_p \\ P_a - E_p & \text{for } E_p < P_a \leq D_{ws} \\ D_{ws} - E_p & \text{for } D_{ws} < P_a \end{cases} \tag{6.2}$$

where

W_s	$[mm]$	=	soil moisture
E_p	$[mm\ d^{-1}]$	=	potential evaporation
P_a	$[mm\ d^{-1}]$	=	precipitation available for soil moisture recharge (rainfall P_r plus snowmelt M_s
D_{ws}	$[mm\ d^{-1}]$	=	soil moisture deficit to fill soil to its capacity and satisfy E_p
$g(W_s)$	$[-]$	=	soil drying function (Eq. 6.3)

The unitless drying function of the soil is expressed as a function of the soil water as

$$g(W_s) = \frac{1 - e^{\left(-\alpha \frac{W_S}{W_c}\right)}}{1 - e^{-\alpha}} \tag{6.3}$$

where α is an empirical constant (set to 5.0) and W_c $[mm]$ is the soil and vegetation-dependent available water capacity. Estimated actual evapotranspiration $E_s[mm]$ is given by

$$E_s = \begin{cases} P_a - dW_s/dt & \text{for } P_a < E_p \\ E_p & \text{for } E_p \leq P_a \end{cases} \tag{6.4}$$

The rainfall excess $X_r[mm]$ that is available for runoff after the soil moisture deficit has been filled is given by

$$X_r = \begin{cases} 0 & \text{for } P_a < D_{ws} \\ P_r - D_{ws} & \text{for } D_{ws} < P_a \end{cases} \tag{6.5}$$

where P_r is the precipitation available for soil recharge as rainfall. Excess snowmelt $X_s[mm]$ is given by

$$X_s = \begin{cases} 0 & \text{for } M_s < D_{ws} \\ P_r - D_{ws} & \text{for } D_{ws} < M_s \end{cases} \tag{6.6}$$

where $M_s[mm]$ is the snowmelt excess. Whenever rainfall exceeds the field capacity it will augment the rainfall-derived runoff pool and generate runoff:

$$\frac{dD_r}{dt} = (1-\gamma)X_r - \beta D_r \tag{6.7}$$

$$R_r = \gamma X_r + \beta D_r \tag{6.8}$$

where $D_r[mm]$ is the rainfall runoff detention pool, $R_r[mmd^{-1}]$ is the rainfall-derived runoff from the grid cell, β is an empirical parameter that controls the outflow from the runoff pool and γ determines the fraction of excess rainfall that fills the pools or becomes runoff instantaneously. The parameter β has units of $1/T$ and has been set to 0.5 for monthly time steps and 0.0167 for daily timesteps and α is 0.5 for both daily and monthly time steps. Snowmelt is modeled as a function of elevation and temperature. At elevations below 500 m, the snow dynamics are described by

$$\frac{dK_s}{dt} = \begin{cases} P_s - E_p & \text{for } T < -1.0°C \\ -M_s - E_p & \text{for } T \geq -1.0°C \end{cases} \tag{6.9}$$

where $K_s[mm]$ is the snowpack that accumulates at monthly temperatures below -1.0°C, $P_s[mm]$ is the daily snowfall. Snowmelt at elevations below 500 m is assumed to be equal to K_s in the first month when $T \geq -1.0°C$. Above 500 m, snowmelt proceeds over two months with one-half of K_s lost within each month. Runoff derived from snowmelt is added to the rainfall derived runoff R_r to form the total runoff on one grid cell. Similar to rainfall derived runoff, a detention pool $D_s[mmd^{-1}]$ is tracked to generate runoff from snow $R_s[mmd^{-1}]$:

$$\frac{dD_s}{dt} = X_s - R_s \tag{6.10}$$

For elevations below 500 m, R_s is given as 0.1 D_s in the first month when $T \geq -1.0°C$ and 0.5 D_s thereafter. Above 500 m, the runoff is assumed to be 0.1 D_s in the first month when $T \geq -1.0°C$, 0.25 D_s in the second and 0.5 D_s thereafter.

Water Transport Model

The Water Transport Model (**WTM** (*Vörösmarty*, 1991)) is a dynamic model that computes the horizontal transport of runoff computed using the WBM. It uses the STN river network (Chapter 5.7.1) to route the runoff until it reaches the outlet of the basin. Channel flow is represented by a linear reservoir model. The resulting flow and continuity equations for one grid cell are

$$\frac{dS_c}{dt} = \left(\sum_1^n Q_u\right) - Q_d + Q_g + Q_f \tag{6.11}$$

$$\frac{dS_f}{dt} = -Q_f \tag{6.12}$$

$$Q_d = KS_c \tag{6.13}$$

$$Q_g = A(X_r + X_s)/1000 \tag{6.14}$$

$$Q_f = \begin{cases} 0 & \text{for } Qd < c_f Q_{dma} \\ -r_f \left[\left(\sum_1^n Q_u \right) - Q_d + Q_g \right] & \text{for } Q_d \geq c_f Q_{dma} \end{cases} \tag{6.15}$$

where

S_c	$[m^3]$	=	Channel storage in a grid cell
S_f	$[m^3]$	=	Floodplain storage in a grid cell
K	$[month^{-1}]$	=	Downstream transfer coefficient
A	$[m^2]$	=	Area of the grid
Q_u	$[m^3 month^{-1}]$	=	Monthly upriver input
Q_d	$[m^3 month^{-1}]$	=	Discharge from cell exported downriver
Q_g	$[m^3 month^{-1}]$	=	Input from runoff generated within the cell
Q_f	$[m^3 month^{-1}]$	=	Exchange between channel and floodplain
Q_{dma}	$[m^3 month^{-1}]$	=	Mean annual downstream recharge
c_f	$[-]$	=	Flood initiation parameter (0..1) defining the proportion of long-term mean annual flow required to invoke floodplain exchanges
r_f	$[-]$	=	Fraction of potential volume change assigned to flooplain storage (0..1)
n	$[-]$	=	number of donor grid cells

6.4 Irrigation and Reservoirs in MHM's

As mentioned above, irrigation and reservoirs have previously been overlooked in MHM and only a few attempts have been recently made to represent such human interventions in the hydrological cycle in MHMs. Although the amount of water withdrawn for agriculture represents a small fraction of the global runoff, the regional impacts can be dramatic and have been transforming rivers into 'loosing streams' (e.g. Nile, Indus, Yellow river). As 83% of the global runoff are affected by the operation of dams (*Nilsson et al.*, 2005) it is equally important to model the effect of reservoirs on the routed discharge. The following section summarizes existing implementations of reservoir and irrigation schemes in WaterGAP, VIC, and the TRIP model.

6.4.1 Irrigation

The implementation of agricultural water demand modules in WaterGAP, VIC, and TRIP is based on the partitioning of the grid cell into an irrigated part and into a non-irrigated part. WaterGAP and TRIP further subdivide the irrigated part into rice and non-rice crops for

which the water demand is computed differently. Irrigation water demand for crops in the VIC model is estimated using the FAO-56 approach[3]. VIC uses a soil moisture accounting to determine irrigation water required to fill up the soil to its capacity whenever the soil moisture drops below a given threshold. WaterGAP uses the same approach to determine the evapotranspirative crop water demand but does not take into account the storage capacity of the soil. Instead, the dampening effect of the soil water storage is taken into account by averaging the (generated) daily precipitation over a period of 3 days (for rice growing regions in Asia) or 10 days (for other regions). *Hanasaki et al.* (2008) determined water demand for irrigation in the TRIP model as the volume of water required to maintain soil moisture at 75% of field capacity throughout the growing season and starting 30 days prior to the planting data. The water requirement for rice paddies is conceptualized by assuming that soil moisture is kept at saturation level throughout the growing season. Additional amounts needed for land preparation and percolation in rice paddies are not taken into account. All models use climate drivers to determine the onset of the growing season and national statistics to model the number of growing seasons in a grid cell.

As those schemes are implemented in MHMs, the linking of the irrigation water demand with the non-irrigated part of the cell is of crucial importance as it determines how irrigation water abstractions and return flows impact the vertical water balance in the grid cell and the horizontal flow of water through that cell. Water demand is met from the locally produced runoff (i.e. from the storage components in groundwater or from surface water) in all models and additionally from lakes present in the same grid cell in the WaterGAP model. All models only withdraw the consumptive crop water demand and do not explicitly account for return flows from irrigated areas. To assess the impact of irrigation water abstractions on the hydrological cycle it is also important to adequately represent the supply of water in periods of scarcity. Clearly, an estimated demand can exceed the amount of water that is available in the same grid cell and may reflect the mining of fossil groundwater for irrigation purposes, in which case the amount of water available in a river basin would be larger than the amount that would be available under natural conditions. *Döll et al.* (2003) have addressed this problem by delaying the reduction in local runoff caused by consumptive irrigation water use by up to one year and by abstracting water from neighboring grid cells. The VIC model supplies water from pre-defined points in the river basin and can optionally limit the irrigation water needs to renewable sources so that irrigation water is only applied if it is available from local runoff or transfer from other grid cells in the basin.

6.4.2 Reservoirs

The approaches implemented in MHMs calculate the distortion of the discharge routing through the river network for single reservoirs and do not consider the simultaneous operation of reservoirs in a river basin. *Hanasaki et al.* (2006) have recently modified the TRIP routing scheme to model the impact of large storage reservoirs on discharge by parameterizing the operation of reservoirs based on the main purposes of the reservoir, the storage capacity of the reservoir, and the demand that needs to be supplied from a given reservoir. They used the geo-referenced database by *Vörösmarty et al.* (1997) (see Chapter 5.7.4) and

[3] This approach is described in Chapter 2.5.2

modeled reservoirs as irrigation and non-irrigation reservoirs at a monthly time step. The monthly release $r'_{m,y}[m^3/s]$ from a non-irrigation reservoir is assumed to be constant and equal to the long-term mean inflow $i_{mean}[m^3s^{-1}]$ of the reservoir, i.e. $r'_{m,y} = i_{mean}$. The release of reservoirs for irrigation shows a highly seasonal pattern and is parameterized as follows:

$$r'_{m,y} = \begin{cases} \frac{i_{mean}}{2}\left(1 + \frac{\sum_{area}\left\{k_{alc}\times\left(d_{irg,m,y}+d_{ind}+d_{dom}\right)\right\}}{d_{mean}}\right) & d_{mean} \geqslant 0.5 \times i_{mean} \\ i_{mean} + \sum_{area}\left\{k_{alc} \times \left(d_{irg,m,y} + d_{ind} + d_{dom}\right)\right\} - d_{mean} & d_{mean} < 0.5 \times i_{mean} \end{cases} \tag{6.16}$$

where $d_{m,y}$ $[m^3s^{-1}]$ is the monthly demand from this reservoir and the subscripts *irg*, *ind*, and *dom* indicate irrigation and industrial and domestic demand (assumed constant). The allocation coefficient k_{alc} is determined based on the number of reservoirs upstream of the current reservoir and set to 1 if there is only one reservoir. d_{mean} is the mean annual total water demand for the reservoir $[m^3s^{-1}]$ which is determined by adding the demand for all sectors downstream of the reservoir:

$$d_{mean} = \sum_{area}\left\{k_{alc} \times \left(d_{irg,mean} + d_{ind} + d_{dom}\right)\right\} \tag{6.17}$$

and Σ_{area} indicates the integration over all areas downstream of the reservoir (i.e. down to the next reservoir, the river mouth, or a maximum distance for 10 grid cells[4]). The monthly release is then calculated as

$$r_{m,y} = \begin{cases} k_{rls,y} \times r'_{m,y} & c \geq 0.5 \\ \left(\frac{c}{0.5}\right)^2 k_{rls,y} \times r'_{m,y} + \left\{1 - \left(\frac{c}{0.5}\right)^2\right\} i_{m,y} & 0 \leq c < 0.5 \end{cases} \tag{6.18}$$

where c is the storage capacity $C[m^3]$ related to mean annual runoff volume ($c = C/i_{mean}$) and $k_{rls,y}$ is a storage release coefficient that reflects water storage at the beginning the operational year:

$$k_{rls,y} = \frac{S_{first,y}}{\alpha\, C} \tag{6.19}$$

where $S_{first,y}[m^3]$ is the storage at the beginning of the year and α is set to 0.85. The storage volume at month m of year $y[m^3/s]$ is calculated using the water balance equation:

$$S_{m,y} = S_{m-1,y} + \left(i_{m,y} - r_{m,y}\right) dt \tag{6.20}$$

where $i_{m,y}$ and $S_{m,y}$ $[m^3]$ and denote the reservoir storage and inflow in year y and month m, subject to:

$$0 \leq S_{m,y} \leq C \tag{6.21}$$

The parameter α was developed and tested using the operational data for some 20 reservoirs globally.

The reservoir operation in the VIC model (*Haddeland et al.*, 2006a,b) calculates the release from individual reservoirs using an optimization algorithm based on the SCEM-UA[5] algorithm. Based on the purpose of the reservoir (taken from the ICOLD database, see Chapter

[4] Around 1100 km at the equator for the TRIP river network

[5] Shuffled Complex Evolution Metropolis (*Vrugt et al.*, 2003)

5.7.4), an objective function that defines an economic value depending on release from the reservoir, is optimized. To define the topological relationships of irrigated areas for which a demand has been computed and the reservoir that could supply this demand, it is assumed that the dam can supply all areas downstream of the reservoir up to a distance of around 250 km. The model is retrospective, i.e. it assumes a complete knowledge of the future reservoir inflows and determines reservoir releases based on these future inflows for one year.

The approach implemented in WaterGAP does not consider the operation of reservoirs but computes the release of water from both reservoirs and lakes in the river network as

$$Q_{out} = k_r S_r \left(\frac{S_r}{S_{r\,\max}} \right)^{1.5} \tag{6.22}$$

where $S_{rmax}[m^3]$ is the storage capacity (simply calculated as $A_{lake} \times h$), and k_r is an outflow coefficient that is set to 0.01 $1/d$ globally. S_r is the actual storage of the reservoir or lake and $h[m]$ is the maximum storage depth that is set to 5 and 2.5 for lakes and wetlands, globally.

6.5 Limitations of Macroscale Hydrological Models

With regard to a representation of the entire terrestrial water cycle, the main shortcoming of contemporary MHMs is the inadequate representation of horizontal groundwater flow (*Lettenmaier*, 2001). This has practical implications for the soil moisture storage and the routed discharge as the groundwater storage can dominate the soil moisture storage and groundwater can be recharged by river flow. Furthermore, most MHMs do not contain a physically based description of glaciers and permafrost (*Kite*, 1995) which constrains the application of such models in high latitude regions, although some attempts have been made to explicitly model the dynamics of permafrost and its impacts on hydrological processes (e.g. *Rawlins et al.* (2002)).

Although originally developed to estimate irrigation water *demand* at field scale, the approach to estimate irrigation water use implemented in WaterGAP and VIC (Chapter 2.5.2) is generally independent of scale as it computes water demand per unit area and can therefore be applied at larger scales if the extend of irrigated areas and the distribution of crops is known. The approaches to represent the interactions of irrigated areas with the hydrological cycle discussed above lack a representation of return flows in storage components that have been shown to substantially impact river flows (Chapter 2.5.3), in particular during low flow periods. Given the large water demand for paddy rice and the high percolation rate in flooded fields (Chapter 2.5.3) it is also important to geospatially represent rice paddies and parameterize the water demand and the percolation adequately. Furthermore, the capacity of the soil to store water available to plants needs to be accounted for.

The implementation of reservoir operating schemes in the MHMs described above are based on topological relationships of demand sites for each reservoir. This information is derived from digital elevation models, but global applicability is a major concern as the actual relationship between reservoir location and irrigation demand site might be constrained by a number of other local circumstances. In addition, they model reservoir release as a function

of *one* purpose of the reservoir, taken from the ICOLD database (Chapter 5.7.4) although reservoirs serve several purposes.

It has been argued that MHMs should be applied over large geographic domains without calibration at the catchment level since a substantial part of the world is ungauged and calibration is questionable when the model is used for climate change studies (*Hanasaki et al.*, 2008; *Arnell*, 1999; *Kite*, 1995). However, it is clearly impossible to reproduce observed discharge within a reasonable margin of error for all river basins globally using the global data sets that are available today and with one single model without calibration of the model parameters. *Döll et al.* (2003) have addressed this problem by 'tuning' the WaterGAP model in a way that the model reproduces the long-term average discharge measured at 724 discharge gauging stations globally. The 'tuning' is done by changing a parameter in the runoff formation module for each basin. *Döll et al.* (2003) found that the process of changing could reproduce the long term discharge in 385 out of the 724 basins and that most of the deviations in basins where the long-term discharge could not be reproduced are snow-dominated basins. *Fekete et al.* (2002) used a set of 663 river gauging stations from the GRDC data set (Chapter 5.7.3) and corrected modeled discharge from the WBM model based on long-term monthly climate forcings to create composite runoff fields that reflect the accuracy of measured discharge and preserve the spatial and temporal distribution of simulated runoff. While both approaches may lead to similar results, the approach used by *Fekete et al.* (2002) implicitly acknowledges the imperfections of MHM simulations arising from inadequate process representation and uncertainties in input data. It is important to note that the model performance of MHMs does not necessarily increase with an increasing model complexity (*Demaria et al.*, 2007; *Huang and Liang*, 2006; *Perrin et al.*, 2001) and that more parsimonious approaches may lead to similar results but better identifiable models.

6.6 Assessing Hydrological Models

MHMs, like hydrological models in general are usually validated by comparing the observed values of interest O_i and simulated values P_i at time step i. Most commonly, they are validated against observed discharge, that can be measured more accurately than any other component of the land water cycle and is routinely measured at a number of points. One of the most important criteria for assessing the performance of hydrological models is a visual comparison of both observed and simulated time series but a number of quantitative and objective criteria for assessing the performance of those models have been developed, partly to assist automatic calibration procedures. A comprehensive overview of such criteria is given in *Krause et al.* (2005). Most commonly, the error $e_i = P_i - O_i$ is statistically summarized for the modeled time series. Generally, the model-estimation error can be written as (*Willmott and Matsuura*, 2005):

$$\overline{e_\gamma} = \left[\sum_{i=1}^{n} w_i \left| e_i \right|^\gamma \frac{1}{\sum_{i=1}^{n} w_i} \right]^{\frac{1}{\gamma}} \tag{6.23}$$

where $\gamma \geq 1.0$ and w_i is a scaling factor assigned to each absolute value of the individual error $|e_i|^\gamma$. The scaling factor w_i reflects unequal time intervals in the time series and is

most commonly set to 1.0. Setting $\gamma = 1$ and $w_i = 1$ for all values, Equation 6.23 becomes the equation for Mean Absolute Error (MAE) that measures the magnitude of the deviations between O_i and P_i:

$$MAE = \frac{1}{n}\sum_{i=1}^{n}|e_i| = \frac{1}{n}\sum_{i=1}^{n}|P_i - O_i| \tag{6.24}$$

When the mean absolute error is computed with the signs of the error not removed, the average error becomes the Mean Bias Error (MBE), or 'bias' that is usually computed to assess the over- or under-prediction of a model compared to the observed values and to indicate systematic biases (*Willmott and Matsuura*, 2005):

$$MBE = \frac{1}{n}\sum_{i=1}^{n}e_i = \overline{P} - \overline{O} \tag{6.25}$$

where $\overline{P}$ and $\overline{O}$ indicate the predicted and observed means respectively. With $\gamma = 2$ and $w_i = 1$ for all values, Equation 6.23 gives the Root Mean Square Error RMSE:

$$RMSE = \left[\frac{1}{n}\sum_{i=1}^{n}|e_i|^2\right]^{0.5} \tag{6.26}$$

that removes the sign of the errors and is a frequently used indicator of model performance in hydrological modeling. However, it has some disadvantages over the MAE and is therefore not generally recommended as an unbiased error estimate[6]. The measures MAE, MBE, and $RMSE$ are 'dimensioned' errors that are in the units of the variable of interest (e.g. discharge) and are zero for a model that perfectly reproduces the observed values. However, as under-predictions and over-predictions can cancel out in the calculation, these error measures alone are not sufficient to assess the model performance. A commonly used *relative* measure of error is the relative volume error VE that measures the difference of observed and simulated discharge O_i and P_i as a fraction of observed volume:

$$VE = \frac{\sum_{i=1}^{n}P_i - \sum_{i=1}^{n}O_i}{\sum_{i=1}^{n}O_i} \tag{6.27}$$

The volume error has a value of zero for an ideal model but since it ignores the temporal dynamics of the time series, the limitations described above apply. One of the most frequently applied criterion to assess the performance of hydrological models is the model efficiency criterion R^2 proposed by *Nash and Sutcliffe* (1970). It is a dimensionless transformation of the sum of squared errors and is defined as

$$R^2 = 1 - \frac{\sum_{i=1}^{n}(O_i - P_i)^2}{\sum_{i=1}^{n}\left(O_i - \overline{O}\right)^2} \tag{6.28}$$

[6] *Willmott and Matsuura* (2005) show that RMSE tends to become increasingly larger than MAE as the distribution of error magnitudes becomes more variable, and that it grows larger than MAE with $n^{1/2}$ and therefore generally discourages the use of this measure.

where $\overline{O}$ is the mean value of observed values. R^2 has a value of 1.0 if modeled and observed values totally agree and has a value of zero if the model does not perform better than the mean value $\overline{O}$ of the observed values. Theoretically, R^2 ranges from $-\infty$ to 1.0 and is a relative index that can be used to assess models over different temporal and spatial domains. As it implicitly compares the model performance against the simplest model (i.e. one that uses the constant mean value of the observation), a value of 0.0 indicates that the model is as good as using the mean value as a prediction and values below 0.0 indicate questionable model results altogether. *Willmott* (1981) proposed the Index of Agreement or d-statistics as an additional relative index:

$$d_j = 1 - \frac{\sum_{i=1}^{n} |O_i - P_i|^j}{\sum_{i=1}^{n} \left(|P_i - \overline{O}| + |O_i - \overline{O}|\right)^2} \tag{6.29}$$

where j represents an arbitrary positive integer value (typically j=2) and d_j ranges from zero (poor model) to 1.0 (perfect model). This criterion is considered an improved model evaluation tool over R^2 because it takes into account differences in observed and modeled means (biases) and variances, as well as correlation.

6.7 Uncertainty And Sensitivity Analysis

Uncertainty is an integral part of any hydrological modeling exercise. It is therefore important to analyze the sources of uncertainty and their effects on the model predictions. Uncertainties in hydrological modeling are due to the following (*Uhlenbrock*, 2005; *Gattke*, 2006):

1. Errors are due to measurement errors in the input data. For global scale applications, the most important error of this kind is related to gauge undercatch in measuring precipitation values (Chapter 5.2).
2. Errors are due to uncertainties in the spatial interpolation of the input data. Input climate data is typically measured at point locations and has to be spatially interpolated. This is particularly significant if data from a sparse network of stations was interpolated over large spatial domains.
3. Errors can arise from uncertainties in the model structure that simplify the underlying processes and do not adequately represent the relevant processes at the modeling scale.
4. Errors are due to the uncertainties related to the model parameters. Parameters typically refer to a collection of aggregated processes that cannot be represented separately (*Wagener et al.*, 2003) and cannot be determined based on observations. A large number of parameters in a model and interactions between those parameters can lead to similar model predictions for different sets of parameter values.

The uncertainty in model predictions is therefore a combined result of the uncertainty related to the input data and the process representation of the model. The assessment of model uncertainty and the assessment of model parameters has received an increased interest in the

last decade (*Mantovan and Todini*, 2006) and a number of formalized approaches to quantify the uncertainty and its propagation through the modeling process have been developed. While sensitivity analysis is aimed at determing crucial model inputs (*Christiaens and Feyen*, 2002), uncertainty analysis tries to quantify the uncertainty in the model outputs. The following section will discuss commonly used methods for quantifying both the sensitivity of models to input data and uncertainty related to model predictions. The selection of an appropriate method to perform uncertainty and sensitivity analysis depends on the output variable that is evaluated, and the time and space scale of the output variable (*Christiaens and Feyen*, 2002).

6.7.1 One Dimensional Sensitivity Analysis

Sensitivity analysis is an essential tool that is aimed at understanding the importance of variables and their effect on the computed outputs, specifically, how outputs respond to perturbations in inputs (*Carrera and Bastidas*, 2005). Secondly, the analysis can highlight the importance of several variables in the model that may only be apparent when performing a sensitivity analysis (*Carrera and Bastidas*, 2005). Sensitivity analysis can therefore be used to determine the direction of data collection activities that could help improving the model results. Formally, the sensitivity of the model can be expressed using a Taylor series expansion of the explicit function (*McCuen*, 2003):

$$O = f(F_1, F_2, ...F_n) \tag{6.30}$$

where O is the model output and F_i are the factors that influence O. The sensitivity S is derived from the incremental change in O:

$$S = \frac{\partial O}{\partial F_i} \tag{6.31}$$

Given the complexity of hydrologic models, Equation 6.31 is most commonly solved by factor perturbation by incrementing F_i by ΔF_i and computing the resulting change in the solution O. Formally, the sensitivity S is given by

$$S = \frac{\Delta O_0}{\Delta F_i} = \frac{f\left(F_i + \Delta F_i, F_{j|j\neq i}\right) - f(F_1, F_2, ..., F_n)}{\Delta F_i} \tag{6.32}$$

Despite being a simple and direct method, this individual parameter (or one dimensional) sensitivity analysis has the disadvantage of being calculation intensive if a number of different input data sets are varied. Furthermore, it ignores the interactions among model input data and parameters.

6.7.2 Uncertainty Analysis

A number of approaches to assess the uncertainty of a model and to assign likelihood values to model predictions have been developed. Most commonly, these methods are based on Monte Carlo techniques that are based on randomly sampling the parameter space and

a comparison of observed and predicted values. The Generalized Likelihood Uncertainty Estimation (GLUE) is the most popular of those methods[7] (*Wagener et al.*, 2004) and will be briefly described here.

Based on the observation that there is no unique set of parameters and several models can lead to equally acceptable representations of observed natural processes, *Beven and Binley* (1992) have introduced the concept of equifinality and proposed a formalized method to quantify uncertainties in hydrological predictions. The GLUE procedure is based on making a large number of model simulations with different sets of randomly chosen parameter values (assuming that lower and upper limits for each parameter can be specified) and assigns a likelihood for each parameter set being a simulator of the system based on the comparison of simulated and observed data. The likelihood is quantitatively described by goodness-of-fit measures such as the criteria described in Chapter 6.6, as long as they monotonically increase with model performance. The likelihood values are rescaled such that the sum of all likelihood values equals unity. The likelihood measure is then used to confine the parameter space such that acceptable sets of model predictions can be evaluated at each time step. Prediction bounds can then be computed by calculating the weighted cumulative distribution function of a predicted value.

The result is is an evaluation of the model results for each time step and a likelihood for each simulated value that reflects the uncertainties in the model as well as the uncertainties in the input data sets.

[7] An overview of other methods is given in *Gattke* (2006)

7 A Macroscale Model Accounting for Human Interventions

7.1 Introduction

Based on the objectives for a macroscale hydrological model outlined in Chapter 1.2, this chapter describes a model that explicitly accounts for human interventions in the water cycle. The model is implemented in the recently developed modeling Framework for Modeling of Aquatic Systems (FrAMES; *Wollheim et al.* (2008)), which was designed to enable the application of coupled hydrological/biogeochemical models at scales ranging from regional (grid cell size in the range of a few hundred meters) to global (grid cell size ranging from 6 min to 30 min), operating at a daily time step. It is built around the existing WBM (Chapter 6.3) with some substantial modifications and will be referred to as WBM_{plus}. The main modifications encompass two modules: (1) An irrigation water module that models the interactions of irrigated areas with non-renewable and renewable water resources (Chapter 7.3), and (2) a module that simulates the alterations of the hydrological cycle induced by reservoirs, including small reservoirs that are used to store water for irrigation purposes (Chapter 7.4). Furthermore, the model integrates a newly developed flow routing scheme (Chapter 7.5) that replaces the Water Transport Model (WTM) in previous versions. As the model is run at a daily time step with most global variables having a temporal resolution of one month, a temporal downscaling of precipitation data was implemented in the modeling framework (Chapter 7.7). The modules for irrigation, large reservoirs, small reservoirs, and the temporal disaggregation of precipitation data were developed as part of this study whereas the horizontal water transport functionality is provided by the software framework FrAMES. A validation of the model and an assessment of its uncertainties will be given in Chapter 8, while applications of the model will be discussed in Chapter 9.

The water balance calculations representing the vertical water exchange between the atmosphere and the land surface are performed for rain-fed and irrigated areas separately. Each grid cell is partitioned into irrigated and non-irrigated parts, and the water budget over the whole cell is computed as the area weighted average of the two parts. A schematic overview of the vertical water flows in the model is given in Figure 7.1. The irrigated part of the cell can be made up of any number of crops each having its own characteristics with regard to crop physiology, cropping patterns and hence water requirements. Water demand is computed individually for each crop type, and a soil moisture balance is calculated for each crop. The total irrigation water demand is obtained by summing the demand over all crops. This mosaic approach allows for a flexible integration of data sets on irrigated areas and different crops from a variety of sources into the existing grid cell framework.

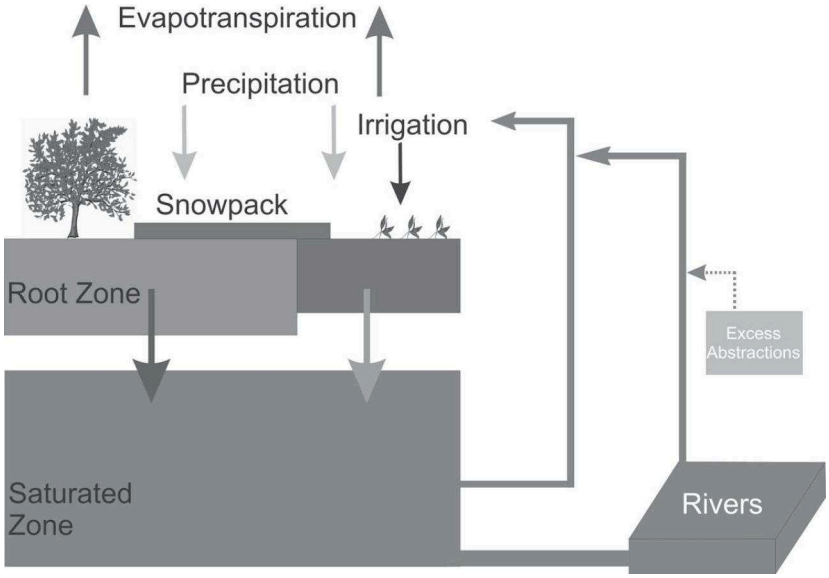

Figure 7.1: Schematic diagram of the vertical flows in the WBM_{plus} model showing the partitioning of grid cells into an irrigated and a non-irrigated part. Water for irrigation can be abstracted from local runoff storage components, rivers in the same grid cell or non-renewable resources.

7.2 Rainfed Water Balance

The soil water budget in the non-irrigated fraction of the cells is not changed compared to the original version of the WBM model. It is fully described by Equation 6.2, explained in the previous chapter.

7.2.1 Snowpack

WBM_{plus} implements an improved snowpack simulation over the previous version. The snowpack is calculated uniformly over irrigated and non-irrigated areas. Precipitation is considered snow if the daily mean air temperature is below a snowfall threshold SF [$^{\circ}C$] and rain above that threshold. The snow accumulates during the snowing period without allowing sublimation. During the melting periods when snow is on the ground and the temperature is above freezing, the snowmelt $SM[mm]$ is computed as function of mean daily temperature T_m [$^{\circ}C$] and daily rainfall P [mm] (*Willmott et al.*, 1985):

$$SM = 2.63 + 2.55\ T_m + 0.0912\ T_m\ P \tag{7.1}$$

7.3 Irrigation Water Demand

7.3.1 Introduction

As described in Chapter 2.5, irrigation water demand shows a considerable variability over time as a result of crop growth and senescence. Furthermore, different crop physiological properties, cropping patterns, and growing season length for different crops can significantly

vary, and those characteristics need to be considered when modeling irrigation water abstractions. Instead of assuming a constant crop water demand throughout the growing season (*Hanasaki et al.*, 2008), the approach implemented here takes into account time varying demand and computes crop (evaporative) water demand for each crop separately depending on the crop's physiological characteristics and the growing season length. Before the method for estimating crop water demand for individual crops is described, the following section summarizes the partitioning of the irrigated part of the grid cell and the onset of the growing season.

7.3.2 Modeling the Cropping Pattern

The distribution of crops in the irrigated part of the cell is based on globally available data sets showing the spatial distribution of crops such as the data sets discussed in Chapter 4.8.2. A simple scaling procedure is applied to each irrigated grid cell to determine the fraction of a given crop CF_i in the grid cell

$$CF_i = \frac{CR_i}{\sum CR_i} \tag{7.2}$$

where CR_i is the fraction of the crop related to the cropland layer. As the cropland data layers and the global irrigated area maps are derived from entirely different data sources, cases may occur where a grid cell is designated as irrigated but no cropland is reported in the cropland data set. For example, when the crop distribution maps by *Monfreda et al.* (2008) are used in combination with the GMIA irrigated area map, this affects 10% of the grid cells. Six per cent of the grid cells designated as irrigated in the GIAM data set do not have any cropland according to the cropland data layer. In those cases, it is assumed that a seasonal cereal crop is grown. The cropping intensity (i.e. the number of cropping seasons) is taken from country statistics (Chapter 4.3) if a static irrigated area maps such as the GMIA is used and implicitly given if GIAM is used, as GIAM reports areas for each cropping season separately (Chapter 4).

To determine the onset of the growing seasons, two approaches are generally possible. The onset of the growing season can be taken from remotely sensed products (Chapter 3) or can be derived from climate data sets as presented in Chapter 5.5. Phenology data products based on remotely sensed data are available for a number of sensors and platforms and generally have the advantage of high spatial resolution compared to approaches based on agro-climatic data sets. On the other hand, climate based approaches have the advantage of global coverage, and sensitivity to variations in the climate data. The latter is particularly significant for simulations with future climate data where changes in the phenology that have already been observed in the last century are likely to magnify (*Penuelas and Filella*, 2001).

7.3.3 Irrigation Water Demand

With regard to the total water demand for a given crop it is important to explicitly take into account the additional water required for the cropping of rice as a result of the growing practices for paddy rice described in Chapter 2.5. To model the irrigation water demand for each crop, the approach recommended by FAO for designing irrigation water demand

known as the FAO-56 method (*Allen et al.*, 1998) was implemented. Daily values of crop evapotranspiration ET_c $[mm]$ are calculated by multiplying the evapotranspiration ET_0 $[mm]$ from a reference surface by a dimensionless crop coefficient k_c:

$$ET_c = k_c ET_0 \tag{7.3}$$

Evaporative crop water demand is computed for each crop separately and the total demand is computed as the area weighted sum for all crops.

The capacity of the soil to retain water is parametrized as the total available water TAW $[mm]$ that is defined as the water that can be held against the gravitational forces and the point below which it cannot be extracted by crops, multiplied by the rooting depth Z_r $[m]$:

$$TAW = (\Theta_{FC} - \Theta_{PWP}) Z_r \tag{7.4}$$

where Θ_{FC} and Θ_{PWP} represent the soil water content at field capacity FC and permanent wilting point PWP and are given in m^3/m^3 and TAW is the total available water in meters. Although water is theoretically available until Θ_{PWP} is reached, the crop will experience difficulties in quickly enough extracting the water to meet the evaporative demand. To avoid water stress, irrigation water must therefore be applied before TAW is depleted. The fraction of TAW that can be extracted without suffering water stress is the readily available water RAW and is given by (*Allen et al.*, 1998):

$$RAW = p\,TAW \tag{7.5}$$

The dimensionless depletion factor p is a function of the evaporation power of the atmosphere and differs from one crop to another. Values for p range between 0.3 and 0.7 and are given, for example in *Allen et al.* (1998). Expressed as depletion, the daily soil water balance in the irrigated part of a grid cell on day i is given by

$$D_{r,i} = D_{r,i-1} - (P - RO)_i - I_{net,i} - CR_i + ET_{c,i} + DP_i \tag{7.6}$$

where

$D_{r,i}$	$[mm]$ =	root zone depletion at the end of the day
$D_{r,i-1}$	$[mm]$ =	root zone depletion at the previous day
P_i	$[mm]$ =	Precipitation
RO_i	$[mm]$ =	Surface runoff
I_{net}	$[mm]$ =	Net irrigation depth that infiltrates the soil
CR_i	$[mm]$ =	Capillary rise from the groundwater
$ET_{c,i}$	$[mm]$ =	Crop evapotranspiration
DP_i	$[mm]$ =	deep percolation

Neglecting RO, CR_i and DP_i, Equation 7.6 is simplified to

$$D_{r,i} = D_{r,i-1} - P - I_{net,i} + ET_{c,i} \tag{7.7}$$

where $I_{net,i}$ $[mm]$ is the net amount of applied irrigation water. Irrigation is required when $D_{r,i} \geq RAW$ and the net irrigation depth should be smaller than or equal to the root zone depletion to avoid deep percolation losses ($I_i \leq D_{r,i}$), so that the depletion following an irrigation event is zero. Figure 7.2 illustrates the soil water balance and the development of the root zone depletion after precipitation or irrigation events.

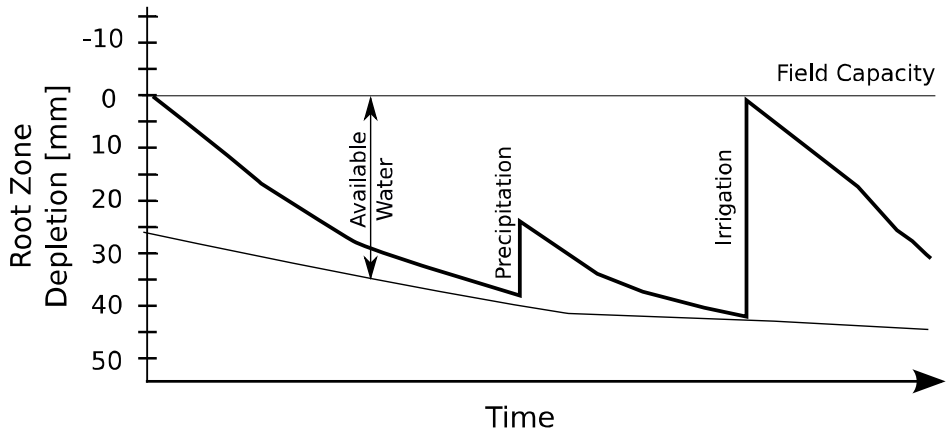

Figure 7.2: Development of the soil moisture (expressed as depletion) after precipitation and irrigation events after *Allen et al.* (1998)

Water Abstractions for Paddy Rice

The crop coefficient method described above is generally appropriate for estimating the crop water requirements of all non-rice crops. The agricultural practices carried out when growing rice outlined in Chapter 2.5.3, however, require an additional amount of water for irrigated paddy rice. The variables that control this additional water demand are the depth of the water layer WL [mm] and the daily rates of percolation DP [mm], seepage S [mm], and the preparation of the land SAT [mm]. Preparation of the land starts one month before sowing and usually involves flooding of the fields to make ploughing easier and varies greatly among regions. The total water demand for rice crops is therefore given by (*Brouwer et al.*, 1989)

$$I_{net} = ET_c + SAT + S + DP + WL - P \tag{7.8}$$

where ET_c [mm] is the crop water requirement for rice computed using the method described above. Evapotranspiration for paddy rice in the initial stage is equal to the evaporation from standing water. *Allen et al.* (1998) recommends k_c values ranging from 1.0 to 1.2 depending on local climate. Percolation refers to the flow of water below the root zone while seepage is the lateral flow of water under the soil surface. Because both loss terms are difficult to measure in the field, they are often considered as one loss term SP (*Tabbla et al.*, 2002). Both, WL and SP vary greatly with climatic region, agricultural management practices, and soil type. *Simmers* (1997) notes that typical recharge water losses in flooded rice irrigation are 10 to 15 $mm\ d^{-1}$, of which 2 mm per day are typically lost as vertical flow through the plough layer and the remainder through the bunds. Typical values for SP in Asia range from $1-5\ mm\ d^{-1}$ in heavy clay soils to $25-30\ mm\ d^{-1}$ in sandy and sandy loam soil (*Tabbla et al.*, 2002). *Brouwer et al.* (1989) recommend values between 2 $mm\ d^{-1}$ for heavy soils, 8 $mm\ d^{-1}$ for light soils and 5 $mm\ d^{-1}$ on average. However, even values of more than 20 $mm\ d^{-1}$ may be reached under unfavorable conditions (*Tuong and Bhuiyan*, 1999). *Frolking et al.* (2006) used the sand:clay ratio derived from FAO's soil map of the world to model percolation rates in India. They assumed a daily percolation rate of 20 $mm\ d^{-1}$ for the highest ratio (8.9) and and rate of 1 $mm\ d^{-1}$ for the lowest ratio (0.1) and used a country-wide mean value of 4.7 $mm\ day^{-1}$. For the present study, percolation rates for paddy rice were estimated by assigning percolation rates between 2 and 8 $mm\ d^{-1}$ to soil drainage classes in

FAO's soil map (Chapter 5.6) and computing a rice-area weighted average percolation rate for each grid cell (Table 7.1).

Table 7.1: Estimated daily percolation rates for different soil drainage classes

Soil Drainage Class	Daily Percolation [mm]
excessively drained	8
extremely drained	7
well drained	6
moderately well drained	5
imperfectly drained	4
poorly drained	3
very poorly drained	2

The water layer WL is typically maintained around 50 to 100 mm and is kept until terminal drainage (1-2 weeks before harvesting). Rice grown under traditional practices in medium to heavy textured soil in Asia requires about 150 to 200 mm for land preparation and 50 mm for growing the rice seedlings in the nursery (*Guera et al.*, 1998; *Brouwer et al.*, 1989). In this study, a water layer of 50 mm was assumed for the length of the growing season until terminal drainage two weeks before harvesting.

7.3.4 Water Withdrawal and Return Flows

The amount of water that needs to be abstracted from groundwater and surface water sources needs to be higher than the net irrigation water demand to account for losses in the irrigation system. Such losses include evaporation and percolation from canals, pipelines, over-irrigation (percolation out of the root zone), and other losses. The gross irrigation water demand I_{gross} $[mm]$ is obtained by dividing the net irrigation demand with the efficiency of water use E [-].

$$I_{gross} = \frac{I_{net,i}}{E} \tag{7.9}$$

where E_{eff} is the project efficiency (Chapter 2.6) for which global estimates are available on the country scale. Estimated values for E_{eff} for a number of world regions are listed in table A-3 in the Appendix. While it is sufficient when computing irrigation water requirements to just consider those losses by a single efficiency factor, it is important to consider the 'sink' for those losses in a water balance model as they partly return from irrigated areas as return flow and are available for irrigation downstream. The low efficiencies found in irrigation projects around the globe are typically a result of evaporation and percolation losses in canals, ponds, diversions etc. In paddy rice fields, a considerable amount of water percolates into the root zone and results in aquifer recharge. However, as the quality of the recharging water is deteriorated, this simultaneously provides a resource benefit and a pollution hazard (*Foster and Chilton*, 2003) that needs to be adequately addressed when modeling water demand for irrigation and the interactions to available water. The amount of water that is returned from the cultivated area to the abstracted areas depends on a number of different factors including

type of irrigation system, crops types, soil conditions, and many others. The coefficient of return flow can vary from 50% for rice crops to close to 0% when higly efficient drip irrigation is used. Based on field data and soil charactereistics, *Dewandel et al.* (2007) found return flow coefficients varying at the watershed scale from 51% in the rainy season and 24% for summer vegetables while *Kim et al.* (2009) found 25% of the water from irrigated rice fields returning to streams, canals, and groundwater. Using a modelling approach with regression trees, *Vijayalakshmib* (2009) found return flow coefficients varying between 3% and 45% depending on soil conditions for rice cropping systems in India. Clearly, the return flow coefficients are controlled by the fraction of rice area from which the percolation rates are relatively well known. In this study, it was assumed that 10% of the total losses (i.e. the difference between gross and net water demand) returns to the groundwater pool in addition to the amount of water that percolates from rice areas at a constant rate. This value reflects the lower return flow rate for non-rice crops and the percolation from rice areas that are explicitely accounted for by the daily percolation rates.

7.4 Reservoirs

7.4.1 Introduction

The implementation of reservoir operations in WBM_{plus} distinguishes two kinds of impoundments: (a) *large* reservoirs for river flow control that directly alter the discharge in river channels (typically with a capacity of 0.5 km^3 or larger[1] and (b) *small* reservoirs for local water management that act as an additional storage pool providing water resources for irrigation. Large river flow control reservoirs are represented explicitly by their position in the simulated river network, and their impact on discharge is expressed via flow regulation functions that calculate the outflow at the reservoir location as a function of inflow and reservoir storage. Small water management reservoirs are expressed as lumped storage within grid cells that withhold some of the runoff generated on the non-irrigated portion and release it later to satisfy irrigation water demand.

7.4.2 Large Reservoirs

Storage reservoirs provide one of the most effective tools to minimize discrepancies of supply and demand over space and time. The purposes that reservoirs serve range from hydropower generation, water supply, irrigation water supply, recreational uses, to flood control. Each of such reservoir purposes imposes some constraints on the operation policy of the reservoir. Mathematically, the basic problem of reservoir operation under deficiency conditions is to find a relationship between storage S, demand D, and the reliability of the reservoir R (*Nagy et al.*, 2002):

$$S = f_s(D,R) \tag{7.10}$$

that is dependent on the reservoir inflow I and the operation policy of the reservoir. The reservoir storage equation 7.10 can be solved using deterministic, stochastic and hybrid methods. Model parameters are usually derived from historical streamflow records, as a function of

[1] The threshold of 0.5 km^3 is based on the data set of geo-registerd large reservoirs describded in Chapter 5.7.4

the reservoir purpose and can also be derived for multiple reservoirs simultaneously (*Brass and Schumann*, 2003). This subchapter is aimed at introducing a simple reservoir operation model that is based on reservoir capacity, and inflow to the reservoir. Its parameters were determined based on time series of operational data for a subset of 29 of the geo-registered reservoirs described in Chapter 5.7.4. Before the development of this model is discussed, it is necessary to discuss the characteristics of the subset of reservoirs with regard to the total population of registered reservoirs.

Reservoir Characteristics

Monthly time series of reservoir release, inflow, and storage was available for 29 reservoirs globally[2], with an average length of recording of 290 months and a median length of 359 months. A list of available records for those reservoirs is given in table A-4 in the Appendix. The maximum reservoir capacity for the selected reservoirs ranges from 0.017 km^3 to 150 km^3 and is 14.42 km^3 on average (median 4.36), compared with a range of 0.5 km^3 to 204 km^3 (mean 7.28 km^3, median 1.92 km^3) for the 661 reservoirs in the ICOLD data set. These differences in the capacity of both reservoir distributions lead to differences in the residence time distributions.

Figure 7.3 shows the distribution of residence time values for the 29 reservoirs and the data set of all registered reservoirs. Whereas the mean value of the 29 reservoirs (1.1) is much smaller than the mean value for all reservoirs (2.09), general distribution of residence time is similar for both data sets[3].

The larger mean values for the entire data set can largely be explained with biases arising from registered reservoirs with a multi-year capacity such as the Lazaro Cardenas (El Palmito) in Mexico with a residence time of more than 50 years, and the Marimbondo in Brazil with a residence time of 23 years[4]. The distribution of residence time values, with a majority of values below one year shows that most reservoirs were built to change the seasonal pattern of river flow within a year rather than to balance multi-year flow patterns by carrying over stored water from one year to another. With regard to the main reservoir purposes, the reservoir set represents a wide range of purposes (9 reservoirs are mainly operated for hydropower purposes; 10 for irrigation; 8 for flood control; 1 for water supply, and 1 for recreational purposes) that is comparable with the range of reported reservoir purposes in the registered set of reservoirs (Chapter 5.7.4).

[2] Out of these reservoirs 26 are located in North America, 2 in Thailand, and 1 in Ghana (Table A-4 in the Appendix)

[3] To formally test if both data sets come from the same population, a nonparametric, one-sided Mann and Withney test was performed and the null hypothesis H_0 that both populations have the same reservoir residence time was accepted. The test statistics were U' = 8573 and z = 0.9629

[4] This calculation is based on the storage capacity reported by ICOLD and does not consider dead storage capacity which is not reported in this database

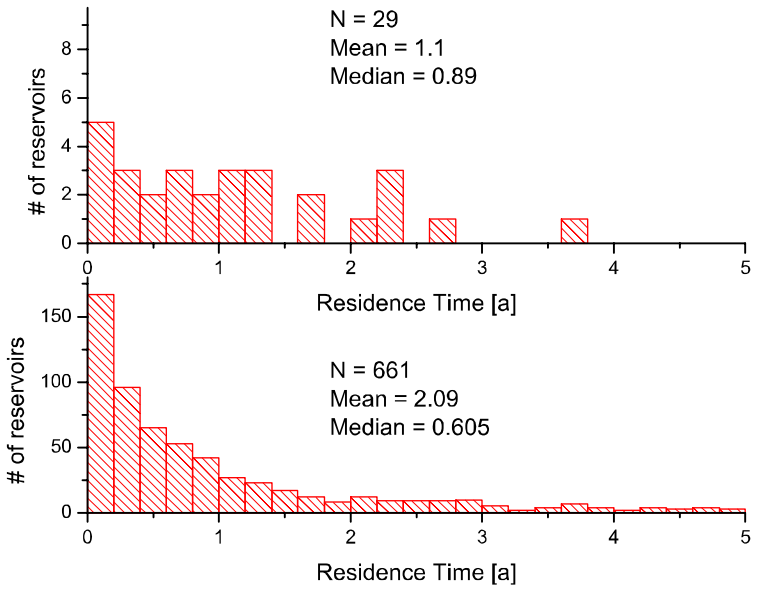

Figure 7.3: Distribution of residence time (computed as reservoir capacity over mean annual inflow for the period 1998-2002) for the subset of reservoirs with operational data and the entire set of geo-registered reservoirs

Observed Reservoir Operation

The observed monthly flow and release patterns were analyzed with respect to the wet season (defined as periods where inflow is greater than long-term mean inflow) and the dry season (defined as periods where inflow is less than mean annual inflow) and release coefficients relating reservoir release to inflow and mean annual inflow were computed. Averaged over all 29 reservoirs, the dry season period is 253 days in one year whereas the inflow is greater than long-term mean inflow on 112 days (Figure 7.4). The operation of reservoirs lowers wet season flow from 159% to 117% of the long term mean and increases dry season flow from 68% of long-term mean inflow to 83% compared to the flow under natural conditions.

As the long-term release approaches the long-term inflow for most reservoirs, the inter-annual variations in reservoir storage are small. Table 7.2 summarizes the reservoir release with respect to inflow and long term mean inflow for all reservoirs and shows descriptive statistics of those relationships. Despite a relatively low inter quartile range of release coefficients for all reservoirs, there is a considerable variation of release coefficients reflecting the wide range of reservoir purposes, reservoir capacity, climate condition, and other factors affecting the operation policy.

It can be assumed that the variations in reservoir release with respect to inflow in dry and wet seasons are partly dependent on the residence time of the reservoir. Reservoirs with residence times greater than one year carry over water from one year to another and will tend to release less water during the wet season. Conversely, reservoirs with a larger residence time can release more water during the dry season in a given year. To test the assumed relationship between release, inflow and residence time of the reservoir, release coefficients

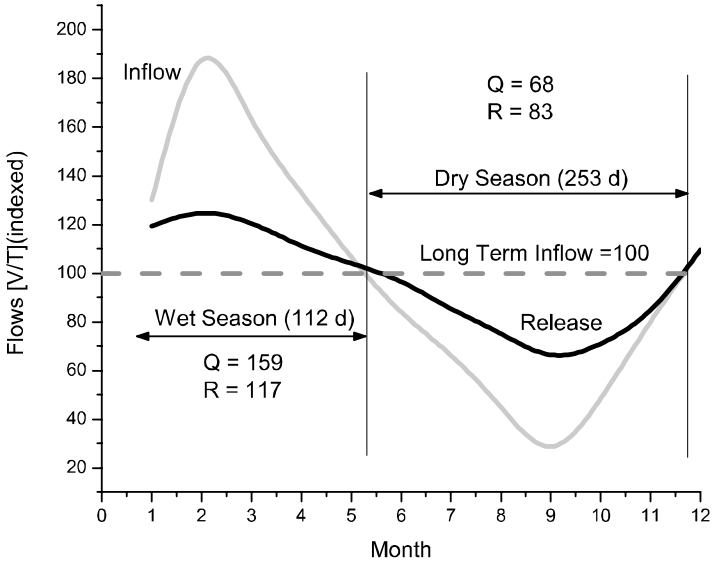

Figure 7.4: Long-term inflow (grey line) and release (black line) for all 29 reservoirs during wet and dry seasons, and long-term season average flows, indexed to the long-term mean inflow (100). Q = Inflow in the reservoir, R = observed reservoir release

Table 7.2: Selected statistics of reservoir release coefficients for wet and dry season flows based on operational reservoir data for 29 reservoirs. R = Release, Q = Inflow, wet and dry denote periods where inflow is below and above long-term mean inflow

	R_{dry}/Q_{dry}	R_{wet}/Q_{wet}	Q_{dry}/Q_m	Q_{wet}/Q_m
Average	1.59	0.68	0.83	1.17
Std Dev	0.72	0.23	0.13	0.29
Minimum	0.98	0.19	0.61	0.46
1st Quartile	1.13	0.55	0.73	1.08
Median	1.37	0.68	0.83	1.20
3rd Quartile	1.68	0.85	0.92	1.32
Maximum	3.46	1.00	1.11	1.89

were plotted as a function of residence time. The results of this analysis are shown in Figure 7.5. Simple linear models that predict seasonal reservoir release are highly significant and

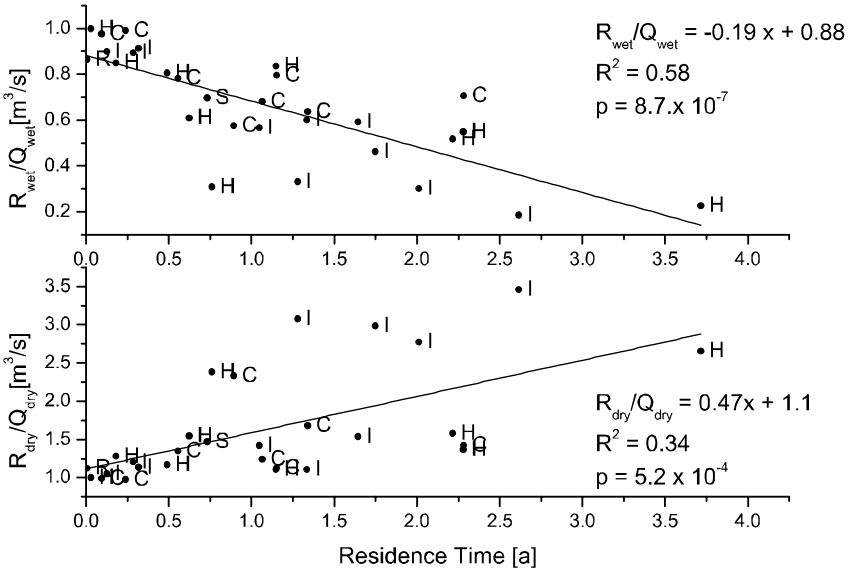

Figure 7.5: Observed relationship between residence time and release coefficients during wet and dry periods and results of a linear regression model to predict those coefficients. Main purpose from ICOLD database; I = Irrigation, H = Hydropower, C = Flood Control, S = Water Supply

show a moderate correlation (Figure 7.5). A linear model that predicts wet season release as a function of residence time explains 58% of the variation in observed release. The linear relationship between residence time and dry season release explains 34% of the variation in relative dry season release. Although the plots in Figure 7.5 may suggest a different relationship for reservoirs that primarily serve irrigation purposes, the number of available data sets is too small to derive robust relationships that would take into account different reservoir purposes.

Reservoir Operation Model

To develop a simple model that predicts release from a reservoir, the observed reservoir operation patterns were parameterized so that the model predicts reservoir outflow independent of the purpose based on inflow/capacity relationships for wet and dry season flows separately. Formally, the model predicts release from a reservoir R_t $[m^3 s^{-1}]$ as:

$$R_t = \begin{cases} \kappa Q_t & Q_t > Q_m \\ \lambda Q_t & Q_t \leq Q_m \end{cases} \tag{7.11}$$

where the parameters $\lambda[-]$ and $\kappa[-]$ are release coefficients and Q_t $[m^3 s^{-1}]$ is the time varying inflow to the reservoir. Q_m $[m^3 s^{-1}]$ is the long-term mean inflow.

Two approaches are generally possible to determine the release coefficients λ and κ based on the observed reservoir operation. They can be static and based on observed release patterns, such as the statistical values reported in Table 7.2. Release coefficients can also be based on the significant relationship between reservoir capacity and reservoir release described above. In this case, the reservoir release (Equation 7.11) is written as

$$R_t = \begin{cases} (-0.19B + 0.88)Q_t & Q_t > Q_m \\ (0.47B + 1.12)Q_t & Q_t \leq Q_m \end{cases} \tag{7.12}$$

where B [a] is the residence time of the reservoir. To test this reservoir release model, predicted reservoir release was compared with the observed release, and the performance measures discussed in Chapter 6.6 were used to assess the model performance. If Equation 7.12 is used to predict reservoir release for all reservoirs, the d-statistics vary between 0.29 and 0.97 and are 0.68 on average. The Nash-Sutcliffe efficiency ranges from -1.2 to 0.87 and is less than zero for 12 of the reservoirs and ranges between 0.04 to 0.87 with an average of 0.49 for the remaining reservoirs. Figure 7.6 shows modeled and observed time series for selected reservoirs with a wide range of model performance ranges and residence times. Despite the low performance of the model when compared to observed daily values of reservoir release, the model captures the seasonal release from reservoir reasonably well (Figure 7.7).

Sensitivity and Validation

As the parameters used to determine the release function (Equation 7.12) are based on a limited number of observed reservoir operation, the predicted release will depend on the reservoir data sets that were used to determine the empirical relationships. To investigate how the sample reservoir data affects the results, the parameters λ and κ were determined on a set of 15 reservoir data sets, randomly selected from the 29 observed reservoir data sets. Such an approach can be considered a split sample test in context of testing hydrological models following the notion of *Klêmes* (1986). The static parameters for this randomly selected subset are λ = 1.56 and κ = 0.63 and are very similar to the results (1.59 and 0.67, Table 7.2). When the release coefficients are computed as function of residence time, the linear regression for wet and dry season release is weaker but still significant. The equations are:

$$R_{t,wet} = (-0.22B + 0.96)Q_t \ (R^2 = 0.76,\ p = 0.00003) \tag{7.13}$$

and

$$R_{t,dry} = (-0.0106B + 1.89)Q_t \ (R^2 = 0.24,\ p = 0.04) \tag{7.14}$$

When the reservoir release model based on the parameters computed using these release coefficients to model the release from the remaining 15 reservoirs, the d-statistics is slightly lower (0.65) but the seasonal release pattern compares with the observed pattern sufficiently well (Figure 7.8).

Summary and Conclusions

Based on observed operational data from a set of 29 reservoirs, which was representative of the global data set of registered reservoirs with regard to the distribution of residence times,

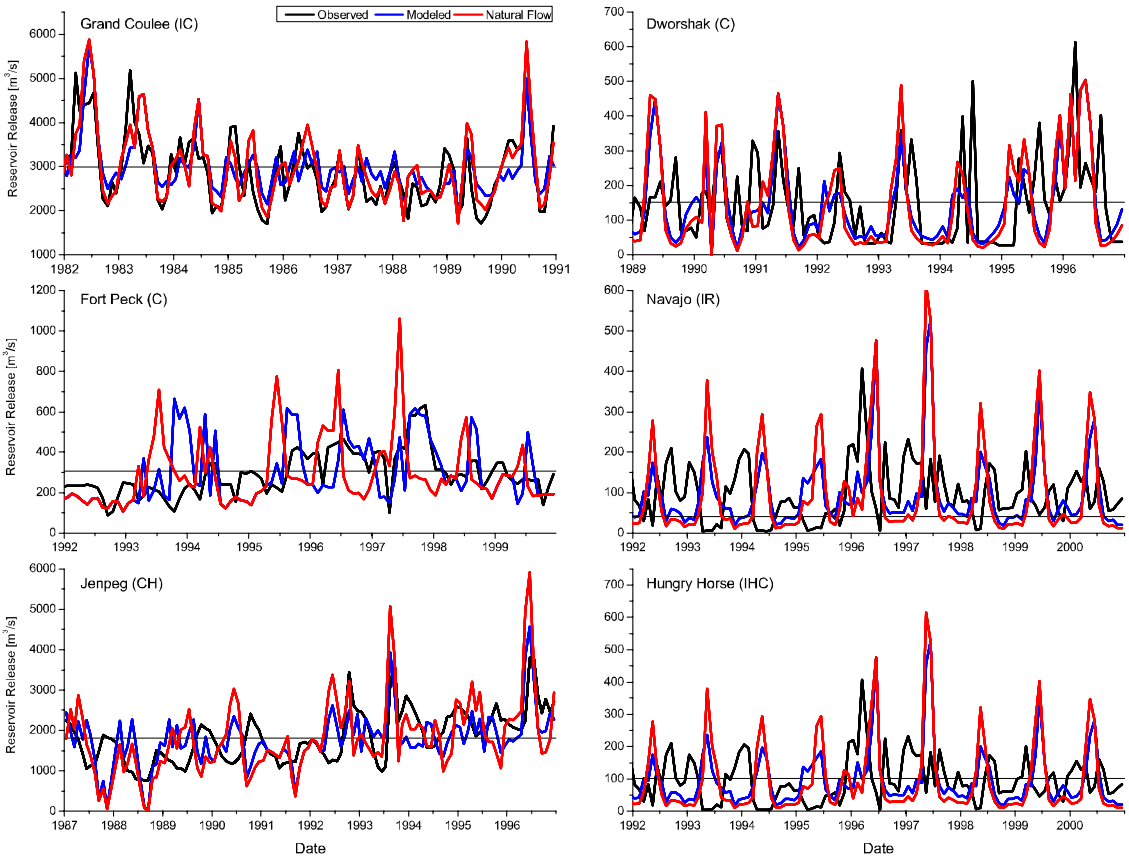

Figure 7.6: Observed and modeled release from selected reservoirs using the empirical model with adjustment for residence time. Mean annual inflow is indicated by the straight lines, inflow to the reservoir by the red line

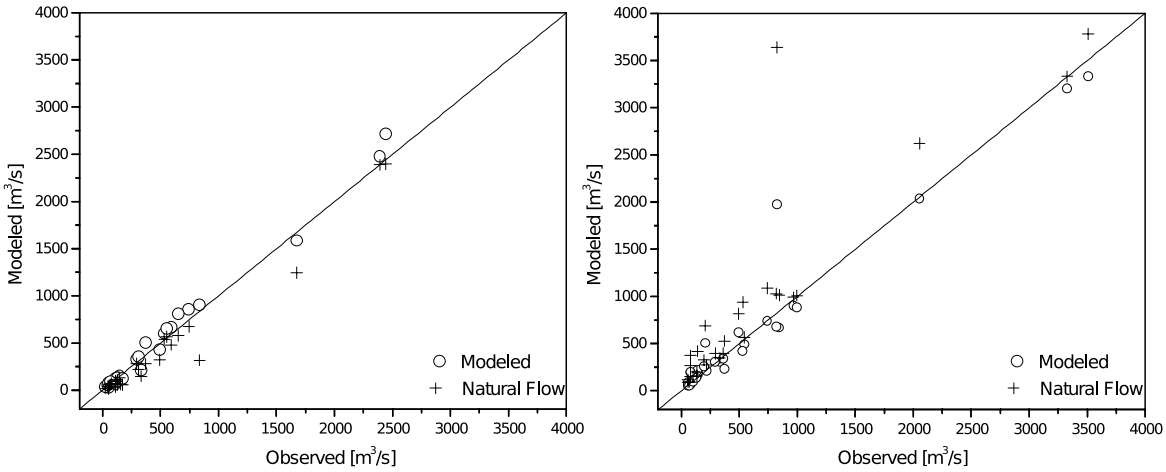

Figure 7.7: Modeled and observed release from reservoirs compared to the inflow to the reservoir (natural flow) for dry season (left) and the wet season (right)

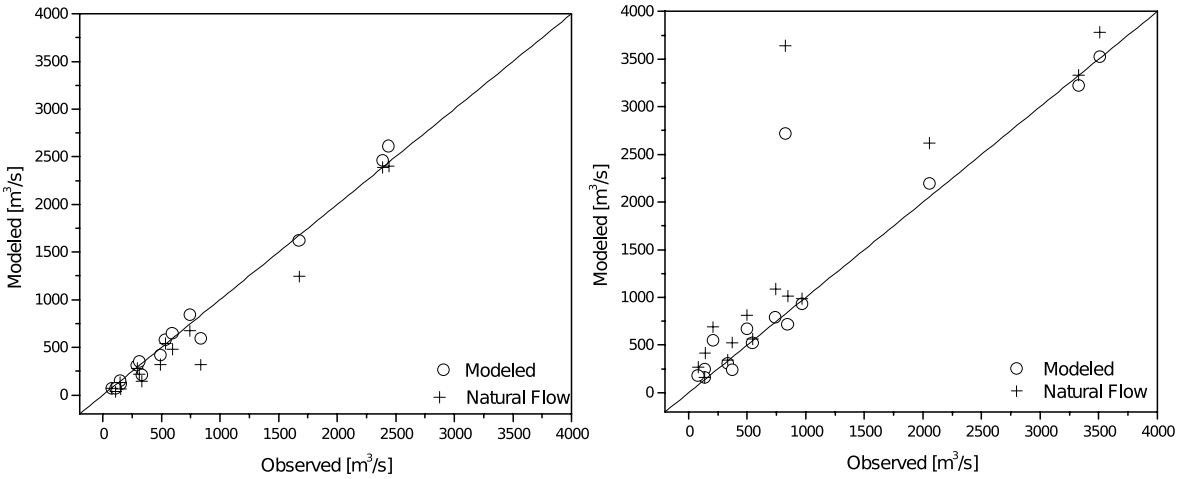

Figure 7.8: Modeled and observed release from reservoirs compared to the inflow to the reservoir (natural flow) for wet season (left) and the dry season(right) based on the split sample test

a simple reservoir operation model was developed to predict reservoir release for wet and dry seasons. The model parameterizes observed reservoir operation independent of reservoir purpose and only is based on inflow and reservoir capacity. Compared to observed reservoir releases the model is capable of predicting the seasonal flows, although the model performance of monthly predicted values for some reservoirs are lower than what is typically expected for hydrological models. The split sample test indicated that the seasonal predictions are robust with regard to the reservoir data. As the model does not require additional data on individual reservoirs, it can be applied to reservoir operation in global models without modifications.

7.4.3 Small Reservoirs

Local 'water harvesting'[5] methods are aimed at collecting rainwater when it is available in abundance to supply irrigated areas during low-rainfall periods. Those methods have long been recognized as a means to increase water productivity and to reduce the risk of crop failure by storing runoff in small farms ponds, cisterns, and other microstorage facilities. With growing population numbers and limited land resources, those facilities are growing in importance, particularly in arid and semi-arid regions. *Downing et al.* (2006) compiled a number of statistical data sets and reported annual growth rates of those reservoirs varying from 1-2% in the agricultural areas in the United States to more than 60% in parts of India. Small farm tanks supply an estimated 37% of the irrigated area in the semi-arid regions of India (*Anbumozhi et al.*, 2001), and are of utmost importance in many arid and semi-arid regions in the world. The number, distribution, and storage capacity of such storage facilities is unknown on a global scale, and only some estimates exist. By extrapolating data from India, Great Britain, and the U.S., *Downing et al.* (2006) estimated the total surface area of farm

[5] The term refers to a number of different methods to store water including collecting water from rooftops, floodwater storage, and others. *Bruins et al.* (1986) therefore suggested using 'runoff farming' referring to the storage of runoff for agricultural purposes

ponds to be around 80,000 km^2. Assuming an individual area of 0.001 km^2, the total number could be as high as 80 million. The total storage volume (assuming a depth of 2 m) would be about 154 km^3, representing 3% of the storage volume of the registered large reservoirs (Chapter 5.7). Although the total storage volume is insignificant at the global scale, given their importance in regional water management, they need to be accounted for in hydrological models as they provide an essential tool to secure water availability for food production. A simple model was therefore implemented to account for the storage and release from small reservoirs. Small reservoirs (SR's) in WBM_{plus} are assumed to collect part of the estimated surface runoff from the non-irrigated part of the grid cell and partially supply the estimated irrigation water requirement I_{gr} in the irrigated fraction of the grid cell.

The amount of surface water that can actually be collected depends on a number of local conditions including soil texture, land use, and topography, as well as socio-economic factors (*Kahinda et al.*, 2008; *Qadir et al.*, 2007) and those criteria are mostly site specific (*Rockström*, 1999). In accord with how runoff harvesting systems are typically designed in the field (*Srivastava*, 2001), the accumulated capacity of small reservoirs in each grid cell was constrained by the the fraction of surface runoff that can be collected and the total amount of irrigation water needed in each grid cell in a typical year:

$$C_{sr} = \min\left(\sum \mu\gamma X_r, \sum I_{gross}\right) \tag{7.15}$$

where $I_{gross}[mm]$ is the estimated irrigation water demand (Equation 7.9) and μ is an efficiency factor that describes the fraction of the non-irrigated part of the grid cell from which runoff can actually be collected. The parameter γ controls the amount of excess water X_r $[mm]$ that runs off on the surface (and can be collected) and is globally set to 0.5 (see Equation 6.8). The most appropriate design parameter to determine μ is the relationship between the catchment area for a reservoir at which runoff is collected and the cultivated area supplied by an individual reservoir. This parameter is commonly referred to as the catchment command area ratio (CCR) (*Critchley et al.*, 1991). The design objective for small reservoirs is to minimize CCR, as higher values lead to high evaporation and percolation losses that render small reservoirs less effective and less economical. This ratio strongly depends on the seasonal variability of rainfall and storage capacities. Values for CCR between 1.0 and 5.0 are generally considered appropriate but values ranging between 17 and 30 with an average of 20 have been reported (*Boers and Benasher*, 1982). As the factors controlling the design value μ are unknown at the local scale, the model simulations are carried out for different values of CCR that are set constant globally and are varied between zero (no small reservoirs) and 20. Implications of those variations will be discussed in 8.2.5. Evaporation $[mmd^{-1}]$ from small reservoirs will depend on the actual type of reservoir used to store the water (closed tanks, open surface reservoirs, covered reservoirs, etc.) and is computed (*Martinez-Alvarez et al.*, 2008) as as $ET = \eta\ ET_0$ where η is set to 0.6 (*Arnold and Stockle*, 1991). The depth of small reservoirs is assumed to be 2 m globally which is a typical depth of small reservoirs, for example in the semi-arid regions of India (*Gunnel and Krishnamurthy*, 2003; *Mialhe et al.*, 2008).

7.5 Horizontal Water Transport

The horizontal water transport in WBM_{plus} is allowed only through river systems. For the present study, the monthly routing system in the previous model version has been replaced by a routing scheme that uses a Muskingum type scheme and estimates the necessary parameters based on river bed geometry. FrAMES offers the basic skeleton for flow routing along gridded river networks (*Döll and Lehner*, 2002; *Oki and Sud*, 1998; *Vörösmarty et al.*, 2000c) that propagates water downstream where the actual flow simulation can be carried out by different methods. For the present study, a Muskingum type solution (*McCarthy*, 1938) of the Saint-Venant flow equations was implemented that estimates the outflow $Q_{j+1}^{t+1}[m^3 s^{-1}]$ as a linear combination of the inflow Q_j^t and the outflow from the previous time step and the inflow in grid cell j of the current time step t:

$$Q_{j+1}^{t+1} = C_0 Q_j^{t+1} + C_1 Q_{j+1}^t + C_2 Q_j^t \tag{7.16}$$

The sum of the unit-less coefficients C_0, C_1, and C_2 equals one, reflecting the conservation of volume in the river routing system. As opposed to the traditional Muskingum flow routing where model parameters have to be calibrated using inflow and outflow hydrograph data, the method implemented in WBM_{plus} determines parameters from channel characteristic features, expressed as the cell Courant number C and cell Reynolds number D (*Ponce and Yevjevich*, 1978):

$$C_0 = \frac{-1 + C + D}{1 + C + D} \tag{7.17}$$

$$C_1 = \frac{1 + C - D}{1 + C + D} \tag{7.18}$$

$$C_2 = \frac{1 - C + D}{1 + C + D} \tag{7.19}$$

which are calculated as:

$$C = U_w \frac{\Delta t}{\Delta l} \tag{7.20}$$

and

$$D = \frac{Q_{mean}}{W_{mean} S_0 U_w \Delta l} \tag{7.21}$$

where U_w $[m^3/s]$ is the characteristic speed of the flood wave propagation, $\Delta l[m]$ is the river cell length, $\Delta t[s]$ is the time step length, S_0 [-] is the riverbed slope, Q_{mean} $[m^3/s]$ and $W_{mean}[m]$ are mean annual discharge and the corresponding flow width. Considering the Manning or the Chezy flow equation and approximating the riverbed shape with the power-function

$$Y = aW^b \tag{7.22}$$

where Y and W are channel depth and width$[m]$, α is a shape coefficient and β is a shape exponent, one can demonstrate that the flood wave velocity $U_w[m^3/s]$ is strictly a function of the flow velocity $U[m^3/s]$ and the shape exponent b[-]:

$$U_w = \xi U = \left(1 + \frac{bp}{b+1}\right) U \tag{7.23}$$

where p is the exponent of the hydraulic radius according to the Chezy or Manning equations ($1/2$ or $2/3$ respectively). The power function approximation for the riverbed geometry is consistent with empirical at-a-site discharge-depth, and discharge-width relationships (*Dingman*, 2007). The reference width W_{mean} and depth Y_{mean} at mean discharge are calculated by empirical equations:

$$W_{mean} = \tau Q_{mean}^{\phi} \tag{7.24}$$

and

$$Y_{mean} = \eta Q_{mean}^{\nu} \tag{7.25}$$

where η, τ, ν, and ϕ are empirical constants (set to 0.25, 0.40, 8.0, and 0.58 respectively (*Knighton*, 1998).

7.6 Model Integration and Water Sources for Irrigation

The irrigated and the non-irrigated part of the grid cell interact in two ways; irrigation water applied in the irrigated part lowers the stocks in the non-irrigated part and water returning from irrigated areas as return flows increase the runoff detention pool in the non-irrigated fraction of the grid cell.

The estimated water requirement for irrigation calculated using the method described in Chapter 7.3 is met by withdrawing water from the non-irrigated part of the grid cell, as depicted in Figure 7.1. The water sources for irrigation are determined by abstracting the computed demand from the stocks in the non-irrigated part in a given order until the demand is met. Conceptually, the water is first withdrawn from locally stored water resources (small reservoirs), and if those resources are not available or depleted, from groundwater resources (D_r in Eq. 6.8). If the required amount of water is greater than those sources, water is withdrawn from river discharge flowing in the same grid cell (Chapter 7.5). In cases where both surface water resources and renewable groundwater resources are depleted, irrigation water is still applied assuming that it is coming from the mining of groundwater resources (Chapter 6.4.1) that are not connected to the hydrological cycle. Figure 7.9 depicts the priorities of water abstraction from different sources to meet the estimated water demand in one grid cell.

7.7 Temporal Downscaling of Climate Data

Most globally available precipitation data sets (see Chapter 5) have a temporal resolution of one month. However, the non-linearities in system behavior in hydrological processes are particularly relevant with respect to precipitation and make daily precipitation data a necessity for ecosystem modeling (*Friend*, 1998). Two approaches to generate daily precipitation data sets have been used in this study. The first approach is to distribute the monthly values using a daily precipitation fraction derived from global daily precipitation data sets such

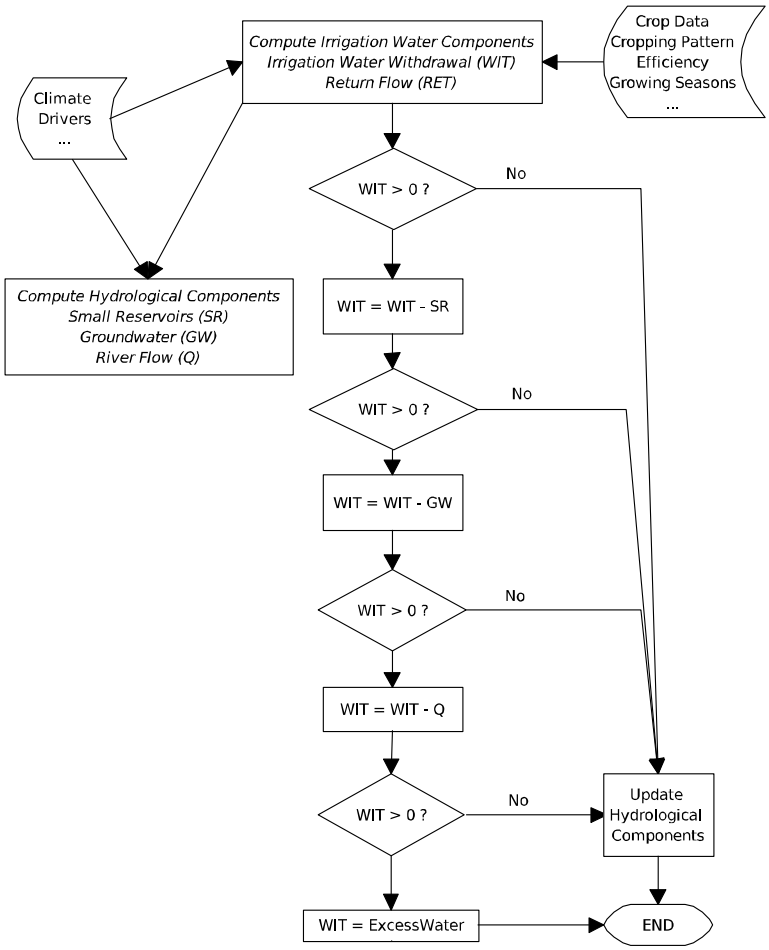

Figure 7.9: Flowchart showing the withdrawal of the modeled water requirement from different sources in one grid cell

as the one degree daily (1DD) precipitation product from GPCP (Chapter 5.2.3). This approach maintains the spatial covariance of precipitation while applying monthly totals from observed data with a longer observation period than the satellite record of GPCP.

The second approach is to stochastically generate daily precipitation data using a weather generator procedure for individual grid cells and thereby loosing any spatial covariance in daily precipitation of neighboring grid cells. The most commonly used models for generating daily precipitation are two-part models that first model the occurrence of wet and dry days and then assign an amount of precipitation to a wet day (*Castellvi et al.*, 2004). Traditionally, Markov Chains are incorporated to model the sequence of wet and dry days. Although higher order Markov chains have been used to model the wet and dry day sequence, first order Markov chains are generally considered to be adequate for most locations although higher order models may be required at specific climate conditions (*Srikanthan and McMahon*, 2001). The procedure implemented in WBM_{plus} is described in detail in *Castellvi et al.* (2004) and is based on the WGEN weather generator. The WGEN weather generator (*Richardson*, 1981)[6] uses a two-state, first-order Markov model and describes the probability of a wet day on day i given that the day $i-1$ was wet, and the probability of a wet day i given

[6]The method described here is sometimes referred to as the 'short method' of the WGEN weather generator

a dry day on day $i-1$:

$$P_i(D/W) = 1 - P_i(W/W) \tag{7.26}$$

$$P_i(D/D) = 1 - P_i(W/D) \tag{7.27}$$

where $P_i(D/W)$ and $P(D/D)$ are the probabilities of a dry day given a wet day on day $i-1$, and the probability of a dry day on day i given a dry day on day $i-1$. As the transitional probabilities are conditional, the following expression holds (*Castellvi et al.*, 2004):

$$f_{wet} = P(W/D)(1 - f_{wet}) + P(W/W) f_{wet} \tag{7.28}$$

where f_{wet} is the fraction of wet days within the modeling period. Once the estimates of the transitional probabilities $P(W/W)$ and $P(W/D)$ are determined, the occurance of a rainy day is simulated by comparing a uniform random deviate u in the interval [0,1] with the transitional probabilities. A day is classified a dry day if u is less than or equal to $P(W/W)$ or $P(W/D)$ (whichever is appropriate); otherwise the day is defined a wet day (*Geng et al.*, 1986). To determine the transition probabilities, a historic record of daily rainfall measurements is required. However, by analyzing rainfall data from various locations around the world, *Geng et al.* (1986) found that the transitional probabilities of a wet day followed by a wet day tends to be greater but parallel to the transitional probabilities of a dry day followed by a wet day. This relationship leads to a linear relationship between the transitional probabilities and the fraction of wet days within a month. *Geng et al.* (1986) proposed the following simple equations to estimate the transitional probabilities:

$$P_i(W/D) = 0.75 f_{wet} \tag{7.29}$$

Using the marginal probability equation (Eq. 7.28), $P(W/W)$ can be estimated as

$$P_i(W/W) = 0.25 + P_i(W/D) \tag{7.30}$$

This simple relationship explains more than 96% of the total variation among transitional probabilities in time and space (*Geng et al.*, 1986) and greatly simplifies the process of estimating transitional probabilites without long daily time series of precipitation. The second part of the model is the implementation of a suitable distribution function for the simulation of precipitation on days that have been defined wet. Commonly used distribution functions for the distribution of precipitation include the exponential function, the Weibull distribution, and others. *Richardson* (1981) found that the gamma distribution generally fits well to observed daily precipitation amounts. The probability density function of the two-parameter Gamma distribution is given by :

$$f(p) = \frac{p^{\alpha-1} e^{-p/\beta}}{\beta^{\alpha} \Gamma(\alpha)} \tag{7.31}$$

where p is a random variable of daily rainfall and α and β denote the shape and scale parameters of the Gamma distribution. Parameter α is dimensionless and usually less than one while parameter β has units of precipitation with a wide range of possible values. The value of β determines to what extent extreme values of precipitation can occur while α influences the proportion of small amounts of precipitation (*Geng et al.*, 1986). Since the rainfall distribution is usually positively skewed, the parameter β of the density function is

closely related to the amount of rainfall per wet day, P_{wet}. *Geng et al.* (1986) found that the simple linear relationships

$$\beta = -2.16 + 1.83 P_{wet} \tag{7.32}$$

and

$$\alpha = P_{wet} / \beta \tag{7.33}$$

explain more than 96% of the total variation of precipitation in time and space for a wide range of climate conditions. Daily rainfall values can thus be generated using only four parameters (two transitional probabilities and two gamma distribution parameters) that are estimated from the amount of rainfall per month and the fraction of wet days per month. Both rainfall amount and fraction of wet days are available globally for a number of years in databases such as CRU (Chapter 5.3). Despite its simplicity, the method described above has been widely used in larges-scale hydrological modeling (*Li et al.*, 2005) as well as regional crop modeling (*Hartkamp et al.*, 2004).

Stochastically generated rainfall using the method described above does not necessarily reproduce the monthly totals of recorded precipitation R_M. Many simulations may therefore be required to reproduce the monthly target value within an acceptable range of accuracy. It may be necessary to constrain the generation such that the sum of the generated daily values R'_M exactly matches the recorded values R_M. *Hansen and Ines* (2005) suggested an iterative procedure that repeatedly generates a time series of rainfall for a given month until R_M deviates less than a threshold T of R'_M. The generated time series of daily values is then rescaled to exactly match the target value. Since the sum of the generated values is not known in advance, only a constant multiplier can rescale the generated values to match the target value. The rescaling is done by multiplying each generated value by R_M / R'_M. This iterative procedure avoids large discontinuities due to the rescaling process while maintaining the statistical properties of the observed rainfall time series.

8 Validation and Uncertainty

8.1 Introduction

Validation is generally understood as an assessment of accuracy or validity of a model using independent, reliable data. *Klêmes* (1986) proposed a hierarchical approach for testing hydrological models using four basic schemes (split-sample, proxy-basin, differential split-sample, and proxy-basin differential split sample). While such a procedure is very valuable for validating hydrological models at individual river basins, the restrictions with regard to observed discharge data at a global scale (Chapter 5.7.3) limit the application of such a formalized procedure for continental and global water balance models.

The validation of the newly developed WBM_{plus} model involves a validation of the irrigation water simulations and simulated discharge against observed data and is performed both for individual river basins and globally. These assessments are made for model simulations with the irrigation and reservoir module turned on ('disturbed' conditions) and for model predictions ignoring irrigation and reservoir operation ('natural' or 'pristine' conditions). The uncertainty related to model parameters and input data sets is assessed by sensitivity studies of model predictions with regard to input data and Monte Carlo simulations of model parameters.

The results of the model simulations described in the following section were performed using the CRU TS data (Chapter 5.3) and the Hamon function (Chapter 5.4.3) to compute potential evapotranspiration. Geospatial data sets of irrigation efficiency and irrigation intensity were derived from national statistical data provided by *AQUASTAT* (2008) (Chapter 4.3). The distribution of crops in irrigated areas was modeled using the cropland data layer compiled by *Monfreda et al.* (2008) (Chapter 4.8.2). The 175 crops in this data set were aggregated into four crop groups: seasonal, (paddy) rice, vegetables, and perennials, and average k_c values for those crop groups were computed from *Allen et al.* (1998). This data was aggregated to 30-min resolution and crop areas were distributed proportionally over the irrigated areas. If grid cells were designated as irrigated but had no cropland area, the area was assigned a 'seasonal crop' (the lowest water requirement). The onset of the growing season was estimated using the climatological method described in Chapter 5.5.

8.2 Irrigation Water Use and Withdrawal

8.2.1 Global, Long-term Withdrawal

Very few attempts have been made to model irrigation water demand on a global scale. Among the few studies is the WaterGAP model (*Döll and Siebert*, 2002), that has been described in Chapter 6.3. *Haddeland et al.* (2006b) have made some regional assessments for Asia and the USA by applying a modified version of the VIC model (see Chapter 6.3), and *Hanasaki et al.* (2008) have used a simple irrigation water module to model irrigation water demand and withdrawal globally at a spatial resolution of 1°. The WaterGAP calculations are based on climatological drivers for the period 1961 to 1999 (CRU data), while VIC was run with daily atmospheric data for the period 1980 to 1999. Both studies relied on the GMIA as the irrigation base map. The estimated values are aggregated per country and are also compared to independent data from statistical databases such as AQUASTAT and the USDA agricultural statistics (Chapter 4.1). To compare modeled irrigation water withdrawal with these data sets, the mean annual irrigation water withdrawal was computed for the period 1963-2002 using the CRU data, assuming constant irrigated areas and constant distribution of crops. Since irrigation area expanded significantly during this period (*Postel*, 1997; *AQUASTAT*, 2008) this analysis was not an estimate of historical irrigation water use, but rather an estimate of the mean irrigation water withdrawal during that period. The modeled long-term annual withdrawal is shown in Figure 8.1.

The total irrigation water withdrawal was estimated to be 3,135 km^3a^{-1} (Table 8.1). This contemporary withdrawal is slightly higher than previous, global-scale estimates that range from 2,200 to 2,900 km^3a^{-1} (*Döll and Siebert*, 2002; *Hanasaki et al.*, 2008; *Siebert and Döll*, 2007; *Vörösmarty et al.*, 2005). By continents, most of the withdrawal is estimated for Asia ($\sim$83%), home to most of the world's rice paddies and multiple cropping (*Maclean et al.*, 2002). To compare the modeled values with reported values in databases provided by USDA and AQUASTAT the grid based values were spatially aggregated and the results of this comparison are shown in Figure 8.2 and in Table 8.1.

Despite significant differences for individual countries, the modeled data agrees reasonably well with country based statistics.

The estimated net irrigation water demand (1,118 km^3a^{-1}) that is used for crop evapotranspiration (I_{net}) is remarkably close to the estimates from *Döll and Siebert* (2002) and *AQUASTAT* (2008). The largest differences between WBM_{plus} estimated irrigation water withdrawal occur in areas with a large fraction of rice where the different assumptions regarding the additional water demand (Chapter 2.5) significantly increase the total water withdrawal. For example, the net irrigation water requirement estimated for India is similar to the value reported by *AQUASTAT* (2008) but the additional water for rice leads to an estimated water withdrawal that exceeds the reported value by nearly 52% (Table 8.1).

The values of irrigation water withdrawal estimated by *Döll and Siebert* (2002) are generally in better agreement with the reported values of FAO AQUASTAT then those calculated using WBM_{plus}. Besides the differences in the parameterization of the water demand for rice paddies, these deviations can be explained with the differences in the model structure with regard to the calculation of soil water storage, temporal disaggregation of precipitation, and

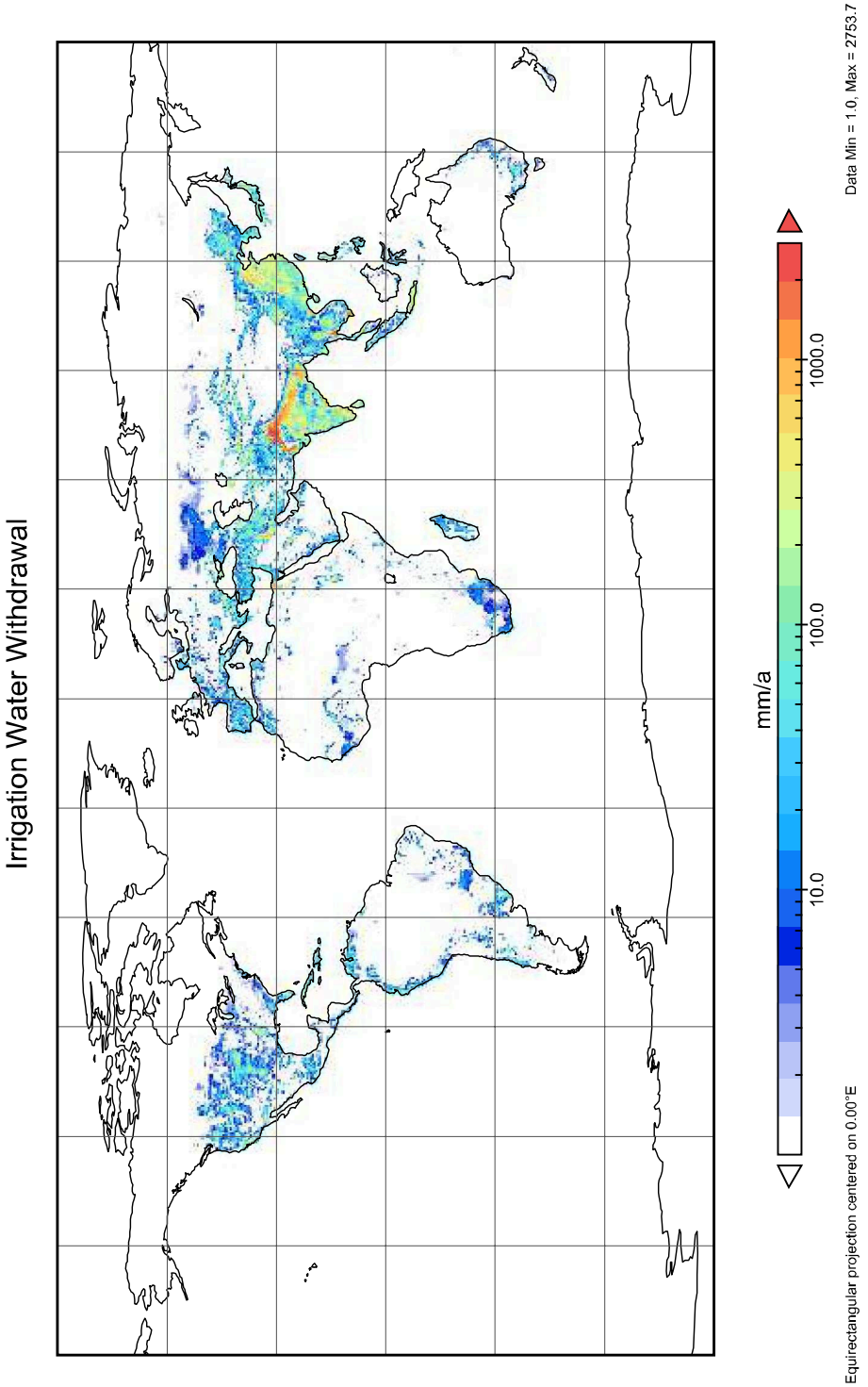

Figure 8.1: Modeled long term irrigation water withdrawal for the period 1963-2002 based on GMIA irrigation data

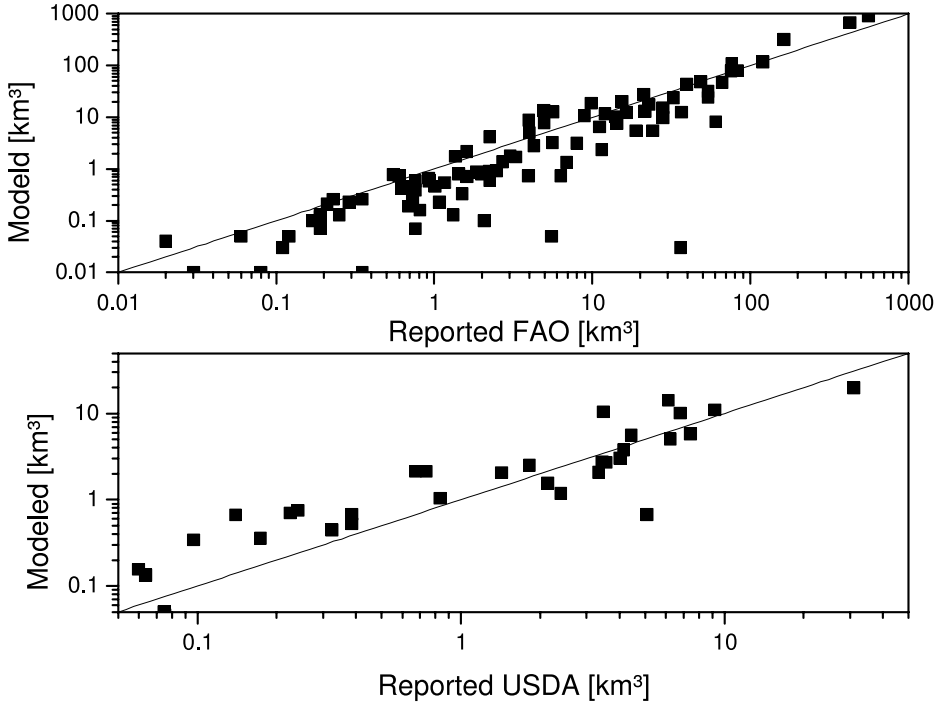

Figure 8.2: Comparison of the estimated water withdrawal with reported values: Data aggregated for 159 countries and compared with data in FAO AQUASTAT (top) and data aggregated for US States and compared with USDA statistical data

different crop coefficients used in both models. Furthermore, the *Döll and Siebert* (2002) estimates are based on an earlier version of the Global Map of Irrigated Areas (GMIA) that reported a total area of 254 million ha; this value is 8% lower than the sum of irrigated areas in the version 3 of GMIA (275 million ha). It is important to note, however, that values on the actual water withdrawal for irrigation in FAO AQUASTAT are known with a reasonable accuracy only for a few world regions (*Döll and Siebert*, 2002) and some of those national estimates are incomplete or grossly outdated (*Gleick*, 2003). It is likely that many national totals reported to AQUASTAT are based on water use modeling (methodologically similar to the analysis used here) and not on actual water use statistics.

8.2.2 Inter-Annual Variability

From a water resources point of view, it is not only important to quantify the amount of water that needs to be withdrawn from aquifers and rivers on average but also to look at the inter-annual variations of required water withdrawal in a dry year and water required in a wet year. As dry years are generally likely to be years with reduced water supply (lower flows in rivers, lower levels in reservoirs), this variability has implications for regional water management. Figure 8.3 shows the variability of WBM_{plus} modeled water withdrawal per unit area, expressed as the coefficient of variation of annual values for the period 1963-2002, for all grid cells with irrigation (computed using the same input data as described above) and affirms the

Table 8.1: Comparison of global estimates of net and gross irrigation water demand from national statistics and other models [km^3a^{-1}]. Reported values for the USA are taken from *USDA* (2002), FAO from *AQUASTAT* (2008), WaterGAP from values from *Döll and Siebert* (2002), VIC from *Haddeland et al.* (2007). Values are reported to four significant figures

Country	WaterGAP		FAO(reported)		VIC		This study	
	I_{net}	I_{gross}	I_{net}	I_{gross}	I_{net}	I_{gross}	I_{net}	I_{gross}
India	223	655	303	558			306	845
China	120	352	153	426			277	606
Egypt	42	60	29	54			21	38
USA	112	186		120	80	191	69	141
Global	1,092	2,452	1,100	2,305			1,118	3,135

Table 8.2: Mean values, 20% and 80% percentiles, and extremal values of modeled annual water withdrawal [km^3a^{-1}] using CRU data, 1963-2002 and assuming static irrigated areas for selected countries

Country	Mean	20-80%	Min-Max
India	845	820-866	801-910
China	606	583-632	540-684
Egypt	38	37-39	36-41
USA	141	133-148	125-142
Global	3,135	3,085-3,182	3,037-3,351

finding of *Haddeland et al.* (2006a) for the Mekong and Colorado basins. The climate-driven variability in estimated water withdrawal is highest in areas where rainfall typically provides a significant fraction of crop water demand. In areas where crop growth depends almost entirely on irrigation (e.g., Egypt), variability in estimated withdrawal is mainly a function of evapotranspiration (and thus temperature) alone; this variability is generally small (Table 8.2). Globally, the estimated irrigation water withdrawal for the simulation period ranges between 3,037 and 3,351 km^3a^{-1}, representing variations of around 5% but can be significantly higher for countries where the demand is generally lower and rainfall supplmenents irrigation water needs. It is important to note that these caluclations do not consider limitations in water supply.

8.2.3 Uncertainty of Irrigation Parameters (Krishna Basin)

To test the impact of variations in model parameters in the irrigation model on irrigation water abstractions, return flow, and subsequently on discharge, river basins with a considerable fraction of their catchment area under irrigation and a complete record of recent observed data should ideally be selected. As the model parameters related to the parameterization of

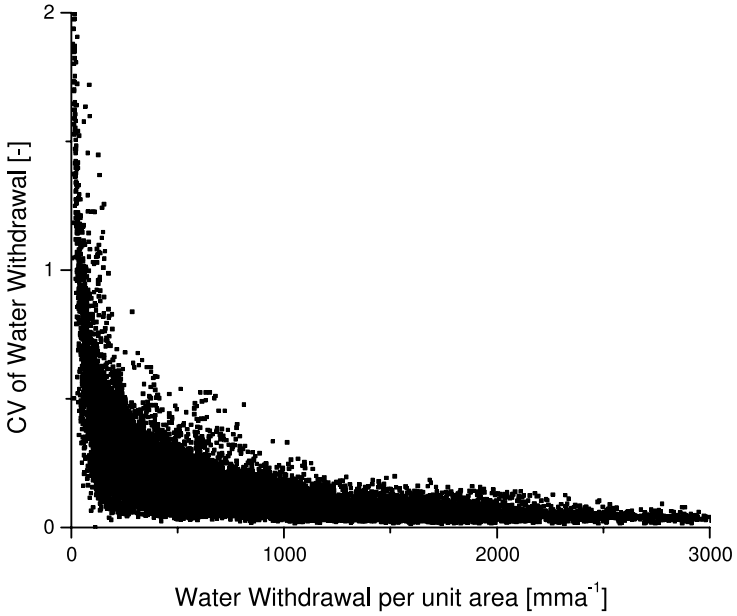

Figure 8.3: Variability of estimated annual water withdrawal per unit irrigated area based on CRU climate data (1963-2002) and assuming constant irrigated areas for 24,817 grid cells

paddy rice fields are of particular importance, a considerable fraction of the irrigated area should be under paddy rice irrigation. However, this selection is constrained by the lack of observed discharge in most heavily irrigated river basins (see Chapter 5.7). For this study, the Krishna river basin was selected to validate the irrigation parameters against observations of discharge and reported irrigation water withdrawal.

The Krishna basin has 16% of its area under irrigation, so that variations in irrigation parameters are likely to translate to variations in modeled discharge. The irrigated area consists of 12% rice, 14% vegetables, 9% perennials, and 65% other seasonal crops. The irrigation efficiency and irrigation intensity (based on the country values for India) for the basin are 34 and 130%. Irrigation water withdrawal and discharge predictions were tested for their sensitivity to the irrigation model parameters irrigation efficiency, rice ponding depth, rice percolation, and irrigation intensity. All of these parameters are only available at the country scale and therefore have a considerable degree of uncertainty. These values have randomly been chosen in a range around the global mean values; irrigation efficiency from 10 to 66%, the rice ponding depth between 10 and 90 mm, daily rice percolation between 0.5 and 3 mm, and irrigation intensity between 100 and 200%. 5,000 simulations were run with varying parameters and the predicted irrigation water demand and the impact on discharge simulations were analyzed for the period 1995-1999. Using the country data (irrigation efficiency = 40%, irrigation intensity= 130%) for the basin, the estimated withdrawal for irrigation water is 47 km^3a^{-1}, consistent with the 31 km^3a^{-1} consumptive water use that was estimated by *Bouwer et al.* (2006) and an estimated water use for all sectors in the basin of 47 km^3a^{-1} in 1989 (*Central Water Comission of India*, 1998). As expected, predictions of irrigation water withdrawal are most sensitive to variations in irrigation efficiency and irrigation inten-

sity (Figure 8.4). Lowering efficiency by 50%, can lead to a more than two-fold increase in irrigation water withdrawal. Similarily, an increase in irrigation intensity leads to a proportional increase in irrigation water withdrawal. The sensitivity of irrigation water withdrawal to parameters controlling the water demand for rice is generally weaker as only 12% of the irrigated area are under paddy rice irrigation.

These variations in irrigation water withdrawal have implications for estimates of discharge for which observed monthly values were available for contemporary conditions. Observed monthly discharge data is available for the station Vijayawada (A = 251,355 km^2) near the mouth of the river. Under pristine conditions, the modeled discharge is constantly overestimated (mean annual flows are 148% higher than observed), particularly during low flow periods (Figure 8.5). Including the effects of irrigation and reservoirs leads to considerably lower discharge predictions during those periods and therefore a better fit to observations. The mean annual discharge under disturbed conditions (averaged over all simulations) is 603 m^3s^{-1}, compared to 1,320 m^3s^{-1} under pristine conditions and 531 m^3s^{-1} for the observed values during the period 1995-1999. To estimate the likelihood of irrigation parameters being a predictor of the system, the GLUE method (Chapter 6.7) was used. Figure 8.6 shows the d-statistics of model simulations as a function of parameter values. Despite large differences in modeled irrigation water withdrawal, the impact of variations in irrigation parameters on modeled discharge is generally low. Model parameters are identifiable if the likelihood shows a distinct maximum as a function of the parameter value. Parameters that do not show a distinct pattern with regard to model performance are therefore poorly identifiable. As can be seen, model simulations are most sensitive to variations in irrigation efficiency and intensity but the impact of variations on discharge is small. The scatterplots of parameters against model performance suggest that d-statistics values are well constrained for efficiency values of 25 to 30% and irrigation intensities around 130%, values slightly lower than the country values used as default values for the simulation.

To investigate the uncertainties in the predictions of discharge arising from the parameter variations discussed above, the GLUE method was applied to estimate the 0.05 and 0.95 percentiles of the likelihood weighted discharge values (based on the d-Statistics) at each time step (Chapter 6.7.2). Figure 8.5 shows the GLUE estimated uncertainty in discharge simulations based on the 1,000 best of the 5,000 simulations, measured by the d-statistics. The 90% confidence range of the simulated discharge can be interpreted as the uncertainty in the predictions related to variations in the model parameters. It is not related to one particular simulation result but to the likelihood weighted discharge values that could represent a different parameter set at each time step. It is also important to note that the range does not represent the percentiles of the discharge itself but of the likelihood weights and the corresponding discharge. The irrigation related uncertainty is highest during the rainy season (starting in June) when irrigation supplements rainfall in many regions. The impact of irrigation on discharge during low flow periods is generally a reduction of flows; the absolute uncertainty during those periods is low.

The return flow in the Krishna basin is primarily controlled by the efficiency value. The rate of water returning to the sources varies from 15% for high efficiency values of 65% to 87% assuming an efficiency of only 10%. Using the country based values, 41% of the

irrigation water abstracted returns to the hydrological cycle, which is consistent with the reported literature values mentioned in Chapter 7.3.4.

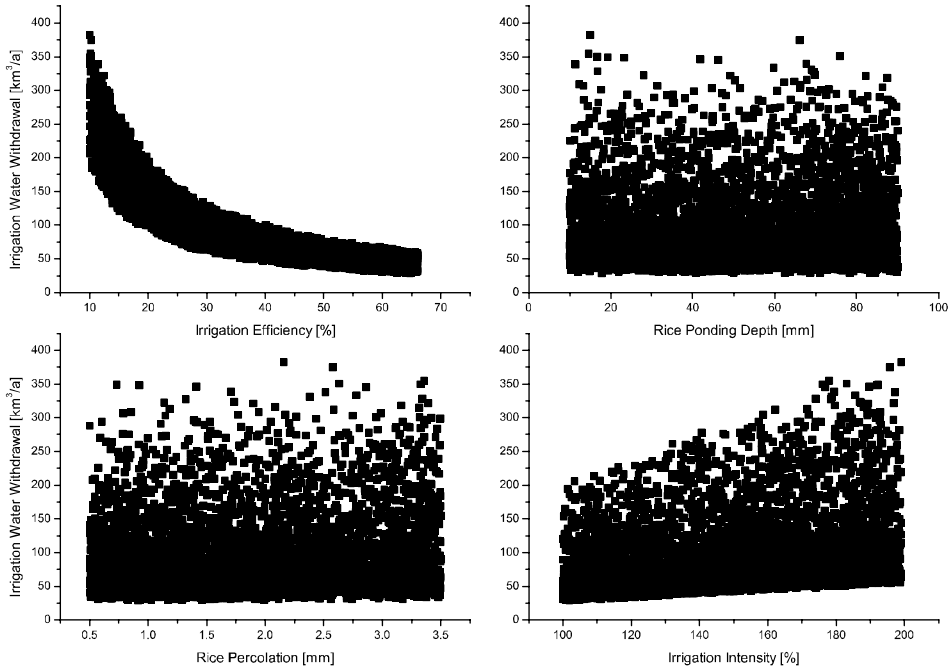

Figure 8.4: Scatterplot showing the sensitivity of irrigation water withdrawal estimates to variations in parameters related to the irrigation water module for 5000 simulations

8.2.4 Global Data Uncertainty

To assess the uncertainties related to the simulated irrigation water withdrawal at the global scale, a simple sensitivity analysis (Chapter 6.7.1) was performed. As the magnitude of the uncertainties in irrigation water withdrawal at large scales will be dominated by variations in the distribution of irrigated areas and climate drivers, simulations were done by combining two different sets of climate drivers and two different geospatial data sets showing the distribution of irrigated areas. To further assess the effect of variations in the agricultural data sets on irrigation water withdrawal, other model input data was varied. The water holding capacity and the daily percolation rate for paddy rice was varied by $\pm 50\%$ and the impact of the crop distribution was assessed by assuming that one non-rice crop is grown everywhere. The climate-driven variability was tested using the monthly CRU TS data set (Chapter 5.2.1) and the daily NCEP/NCAR reanalysis product (Chapter 5.2.4) for precipitation and air temperature. CRU precipitation data was stochastically downscaled to daily values using the method described in Chapter 7.7. The distribution of crops and the onset of the growing season was modeled as described in Chapter 8.1. The geospatial distribution of irrigated areas was taken from the GMIA (Chapter 4.7) that is based on national and sub-national statistics and the GIAM (Chapter 3.5.3) that is a remotely sensed product based on a variety of sensors and

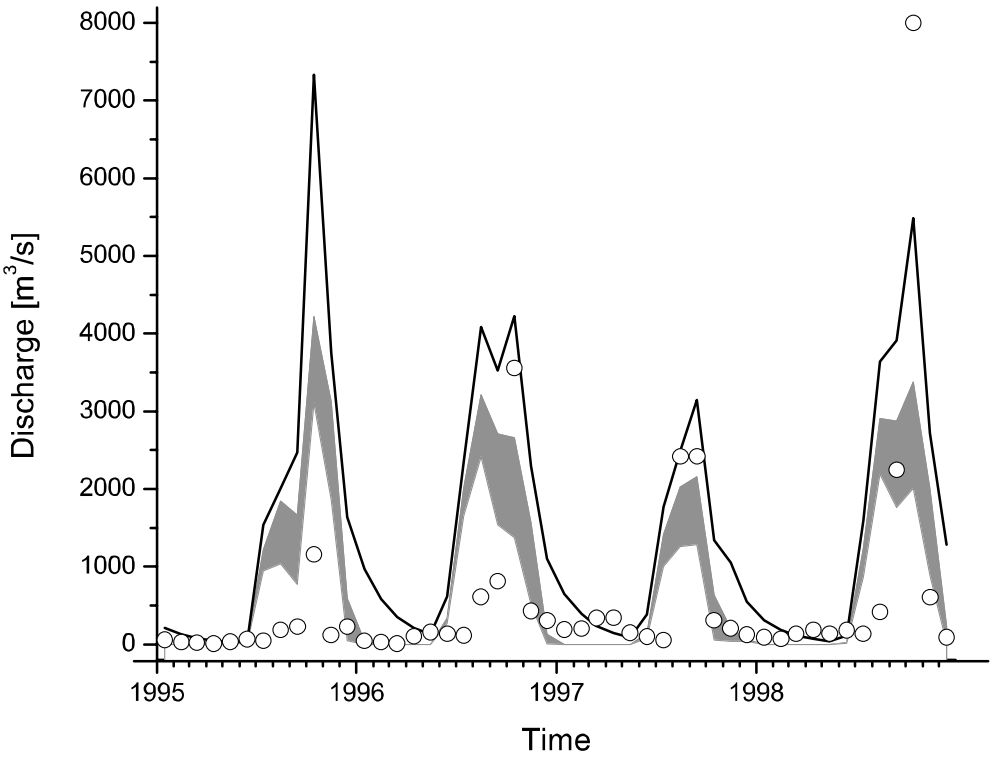

Figure 8.5: GLUE estimated uncertainty for the predicted discharge for the Krishna basins, for 1000 out of 5000 simulations (grey), observed values (circles) and model simulations under pristine conditions (black line)

auxiliary data sets. Figure 8.7 shows the zonal averages over 0.5° latitude bins of the four data sets. Spatial differences in the precipitation data sets and the two maps of irrigated areas have been discussed in Chapter 5.2 and Chapter 4.7.1 respectively. Using both CRU and NCEP weather data, the mean annual irrigation water withdrawal for the period 1963-2002 for both the GMIA and GIAM irrigation area maps, assuming constant irrigated area over time was computed.

Results and Discussion

The combination of the two irrigation data sets and the two climate reconstruction data sets showed substantial differences in the mean annual water withdrawal. Using the GMIA data set, the 40-yr mean irrigation water withdrawal is 3,135 km^3a^{-1} (see Chapter 8.2.1). If the same map is used with NCEP climate data, the estimated irrigation water withdrawal reduces to 2,159 km^3a^{-1} (Table 8.3). Both values fall in the range of previously reported values using the GMIA data set (*WRI*, 1998; *Hanasaki et al.*, 2008; *Döll and Siebert*, 2002; *Siebert and Döll*, 2007; *Vörösmarty et al.*, 2005).

When the GIAM data set is used, the computed withdrawal based on CRU and NCEP data

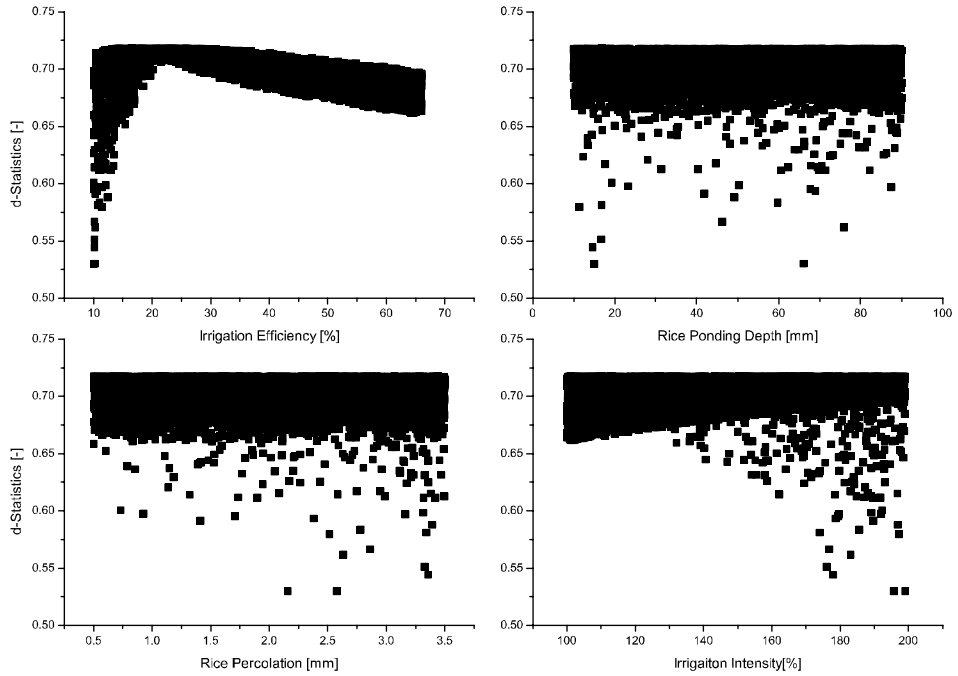

Figure 8.6: Scatterplot showing the sensitivity of discharge predictions to variations in parameters related to the irrigation water module for 5000 simulations

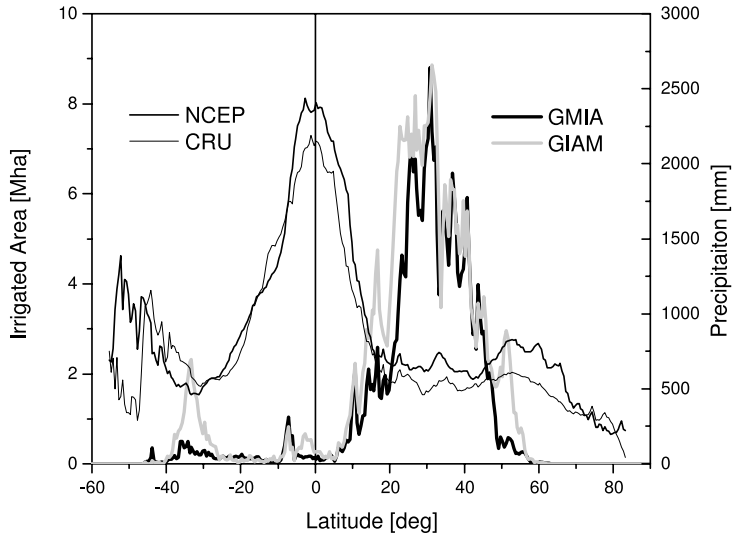

Figure 8.7: Latitude profiles (0.5°bins) of irrigated area, using GIAM and GMIA data sets, and mean annual precipitation over all land (1963-2002) for the CRU and NCEP precipitation data

Table 8.3: Mean values of annual estimated irrigation water withdrawal globally [km^3a^{-1}] and for selected countries based on combinations of climate drivers and irrigated area data sets

Climate	CRU	CRU	NCEP	NCEP
Irrigation Area	GMIA	GIAM	GMIA	GIAM
Global	3,135	3,847	2,159	2,724
India	845	1,696	511	1,281
China	606	755	351	423
Egypt	38	19	35	17
USA	141	122	117	96

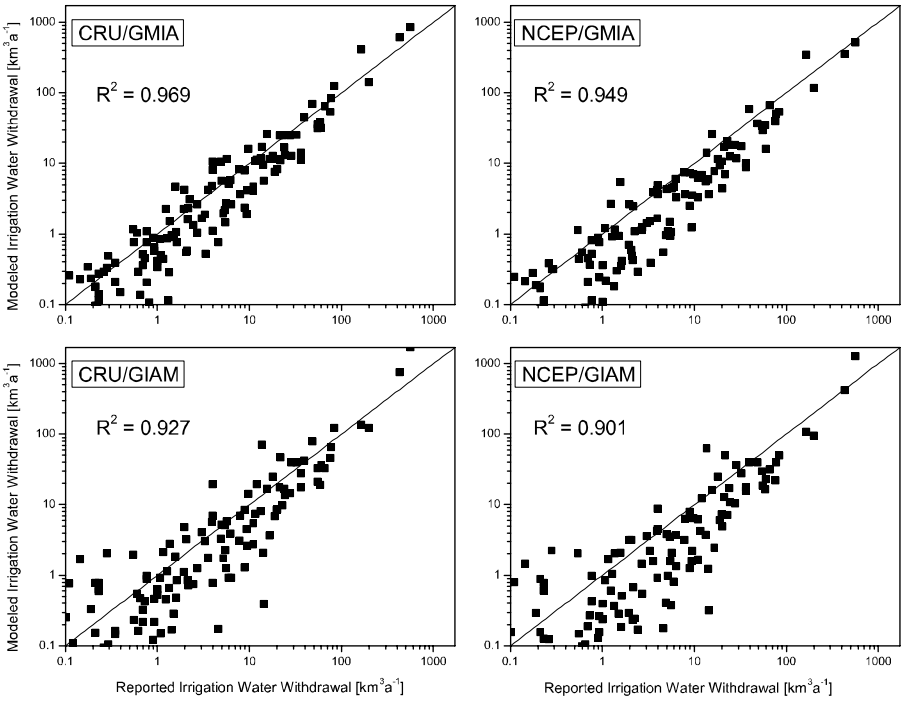

Figure 8.8: Modeled irrigation water withdrawal per country for different irrigated area and weather data configurations compared with reported irrigation water withdrawal from *AQUASTAT* (2008) for 159 countries. 1:1 lines added to each panel

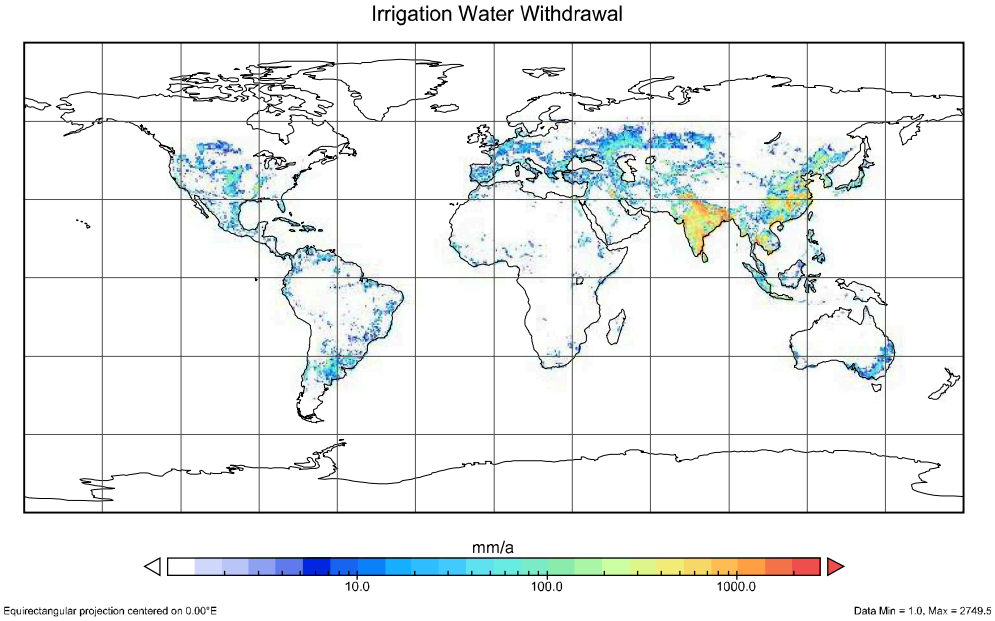

Figure 8.9: Modeled long term irrigation water withdrawal for the period 1963-2002 based on GIAM irrigation data and CRU climate data

is 3,847 km^3a^{-1} and 2,724 km^3a^{-1}, respectively, a ~30% increase over the GMIA results. For a given irrigation base map, the computed global withdrawal is ~30% lower when forced with NCEP data than CRU data (Table 8.3), as NCEP precipitation is higher over most irrigated areas (Figure 8.7) and precipitation supplements irrigation water demand. The highest estimate, using the combination of GIAM and CRU, is about 54% higher than what has previously been reported for global irrigation water use (2,452 km^3a^{-1} (*Döll and Siebert*, 2002)) while the lowest value, using GMIA data and NCEP climate drivers, is about 15% lower. Simulated mean annual irrigation water use, aggregated by country, correlates with national statistics reported by *AQUASTAT* (2008), though for many countries the simulation results are biased low (Figure 8.8), indicating an underestimation of irrigation water withdrawal. Not surprisingly, the bias is lowest for the combination of GMIA data with the CRU data set that was probably used to estimate national water use in many countries where actual water use statistics were not available. Following the spatial differences in both irrigated area maps discussed in Chapter 4.7.1, the largest absolute differences in irrigation water withdrawal are calculated for India and China where the withdrawal based on the GIAM map is 100% and 22% higher than the estimate based on GMIA data. Figure 8.9 shows the modeled irrigation water withdrawal using the CRU data set and the GIAM irrigated area map.

The impact of variations in the model parameters rice area, percolation rate for paddy rice and distribution of rice have been found to be much smaller than the uncertainties in irrigated area maps and climate drivers. Generally, model results were very sensitive to factors related to paddy rice, and much less sensitive to other factors. Changing the percolation rate for paddy rice by ±50% caused a ±10% change in global irrigation water use, implying that, in these simulations, 20% of global irrigation water percolates from flooded fields. These calculations are based on continuous flooding; paddy water management in some regions is changing to intermittent drainage (e.g., *Li et al.* (2002)), reducing total irrigation water requirements. Neglecting cropping information by assuming that only one, namely non-rice

crop is grown on all irrigated land reduced irrigation demand by 50%, again highlighting the importance of paddy rice. Sensitivities to changes in soil water holding capacity and the timing of the growing season were very low and changed the global estimate of irrigation water withdrawal by ~1%.

It is important to note that the estimated water withdrawal could be affected by further sources of uncertainties that have not been investigated here due to the lack of sufficient data. For example, the choice of a different reference evapotranspiration function ET_0 could change the estimated demand by ~40% (*Weiss and Menzel*, 2008), and variations in the crop coefficient k_c might have a 15% sensitivity (*Satti et al.*, 2004).

8.2.5 Water Sources for Irrigation and Return Flow

As the withdrawal of water for irrigation will have different impacts on components of the hydrological cycle, as well as biogeochemical fluxes, depending on the source where it is taken from, it is important to know if the water is supplied by groundwater, locally produced runoff, streamflow, or non-renewable water sources. Although some estimates exists on the global scale, a detailed, consistent inventory of this information is lacking (*Oki and Kanae*, 2006). The fraction of irrigation that is supplied by groundwater varies greatly within regions. U.S. agriculture, for example, relies on 65% groundwater (*Pimentel et al.*, 2004), while groundwater is supplying an estimated 50% to 60% in India (*Singh and Singh*, 2002; *Thenkabail et al.*, 2006), and 40% in China (*Thenkabail et al.*, 2006). *Foster and Chilton* (2003) compiled data on irrigation water use for selected countries and concluded that the contribution of groundwater to irrigation water abstractions is approaching 30% globally. As noted earlier, cases can occur where the demand cannot be met by either locally produced runoff or river corridor discharge, representing mining of fossil groundwater. Recently, *Rost et al.* (2008) suggested that these non-renewable sources supply almost half of the current water used in irrigated areas while an earlier study by *Vörösmarty et al.* (2005) estimated this number to be around 35% to 40%.

The WBM_{plus} estimated volume of water that has to be abstracted from these non-renewable sources is consistent with those estimates; 1,400 km^3a^{-1}, representing almost 40% of the estimated global agricultural water withdrawal need to be withdrawn from non-renewable sources under contemporary conditions. However, these estimates based on the vertical water balance at grid cell level may represent an overestimation as WBM_{plus} does not adequately represent the dynamics of large groundwater systems from which water can be withdrawn in areas far away from the areas where the system is recharged. Figure 8.10 shows the WBM_{plus} estimated contribution of the different water sources to the total irrigation water withdrawal for different design parameters of local irrigation reservoirs. For a medium variant of small reservoir capacity (CCR=5)[1], the estimated contribution of local runoff is 10%, 17% are taken from local groundwater, and 33% are supplied from locally stored runoff in small reservoirs.

[1] This means that the area that is needed to collect runoff for a small reservoir is five times larger than the area that is supplied from that reservoir (see Chapter 7.4.3)

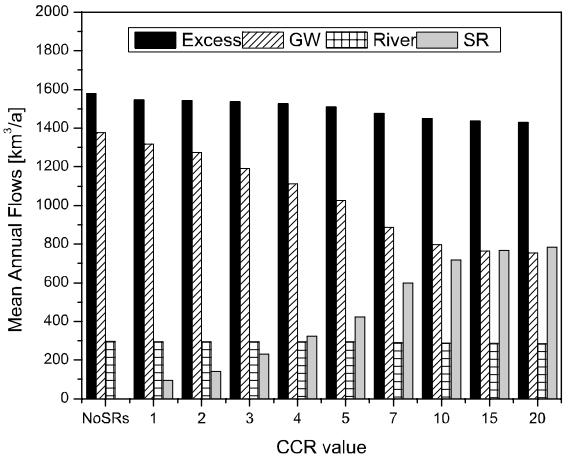

Figure 8.10: WBM_{plus}-estimated water sources for irrigation water demand for varying capacities of small reservoirs (SRs). GW=groundwater.

As described in Chapter 2.5.3, a considerable amount of water abstracted for irrigation purposes percolates through the soil, recharges groundwater and eventually becomes runoff. Owing to the parameterization of paddy rice fields and the percolation from those fields (Chapter 7.3), the return flow is dominated by the percolation from rice fields. Losses due to inefficiencies in the distribution network on non-rice irrigated fields are generally much smaller (assumed to be 10% of the total losses). Globally, the modeled return flow from irrigated areas is around 1,650 km^3a^{-1} under contemporay conditions and using the input data described above, representing 55% of the modeled irrigation water withdrawal. These estimates are consistent with the reported values for return flows discussed in Chapter 7.3.4. At the global scale, a consistent assessment of return flows is not available. By continent, return flow rates are highest in the rice growing regions of Asia. As irrigation water withdrawal in WBM_{plus} is not limited by available water (see Chapter 7.6) and water is supplied from non-renewable sources when it is not locally available, the return flow from irrigated areas can actually increase runoff compared to 'natural' conditions when irrigation water abstractions are not taken into account. The implications of return flows at individual river basins will be demonstrated in Chapter 9.5.

8.3 Discharge

8.3.1 Introduction

After the estimates of irrigation water withdrawal are validated against reported values at country level and uncertainties related to variations in input data and model parameters are quantified, the following section is aimed at validating predictions of discharge that are corrected for interactions with irrigation against measured hydrographs. In this context, the uncertainty related to parameters controlling discharge and uncertainties related to climate drivers will be discussed. The first part of the section will assess the performance of the model globally based on a set of 658 discharge gauging stations. In this context, model

predictions that take into account irrigation and reservoirs are compared with simulations without those effects. Next, the impact of variations in model parameters on discharge simulations are assessed based on Monte Carlo simulations for two selected river basins.

8.3.2 Global Assessments

Previous versions of the WBM/WTM models were validated against discharge records in various geographical regions (e.g. conterminous U.S. (*Vörösmarty et al.*, 1998), Amazon (*Vörösmarty et al.*, 1996) and globally (*Fekete et al.*, 2002)). All previous studies showed that WBM/WTM had little bias over large domains while individual basins could have large discrepancies. For the present study, predicted monthly discharge values for the period 1901 through 2002 were validated against the selected 658[2] GRDC discharge stations (Chapter 5.7.3) that cover 52% of the terrestrial area globally. To quantify the impact of the newly developed modules in WBM_{plus}, simulations where performed under natural conditions (without considering irrigation and reservoirs) and under disturbed conditions (with the irrigation and reservoir modules turned on). Model performance was assessed using the Mean Bias Error (MBE), the Mean Absolute Error (MAE) and d-Statistics (Chapter 6.6). To further assess the impact of irrigation on modeled discharge, these values were computed for basins with irrigation exceeding a given threshold. As the irrigated area for 490 of the 678 basins is less than 1%, the impact of irrigation on discharge will be neglibly small in the majority of basins. The statistics of these measures are summarized in Table 8.4.

Table 8.4: Summary of performance measures for model simulations under pristine and disturbed conditions for all basins and basins that have at least 3% of their area under irrigation. CV = coefficient of variation of monthly discharge

	All Basins (n=658)		Basins with $A_{irr} > 3\%$ (n=110)	
	Pristine	Disturbed	Pristine	Disturbed
MBE (average) [mm]	-0.639	-0.911	-3.449	-4.756
MBE (median) [mm]	0.531	0.270	-1.428	-1.778
CV (modeled) [-]	1.368	1.363	1.113	1.130
CV (observed)[-]	1.121	1.121	1.311	1.310
MAE (average)[mm]	18.68	18.62	14.45	14.29
MAE (median)[mm]	14.91	14.88	10.94	10.38
d-Stat (average)[-]	0.745	0.746	0.691	0.694
d-Stat (median) [-]	0.681	0.682	0.760	0.764

The d-statistics vary between 0.01 and 0.97 with an average of 0.68 (Figure 8.11), the MBE is slightly negative for both pristine and disturbed conditions suggesting that the predicted discharge is underestimated on average. This can partly be explained with biases arising from errors in the precipitation input fields due to gauge undercatch, particularly in high latitude regions (Chapter 5.2.1). The overall results indicate that the model reproduces observed

[2]Selecting only stations with at least 15 years of observation reduced the number from the initial 663 stations

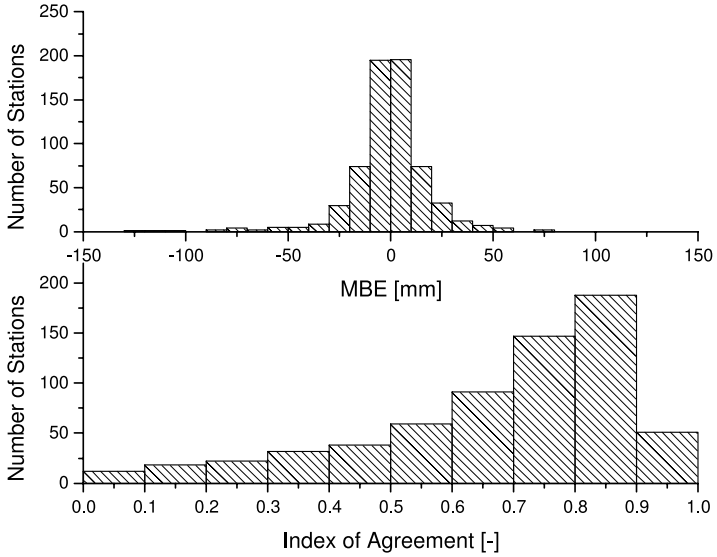

Figure 8.11: Frequency distribution of the mean model bias and the d-statistics for the selected 658 gauging stations with varying periods of observation.

discharge on average reasonably well at large river basins and affirms previous findings regarding the bias of the model. The comparison of model results under natural and disturbed conditions shows a slight improvement of overall model performance when the effects of irrigation and reservoirs are taken into account. For all river basins, the results under disturbed conditions improve d-statistics although the impact is small, owing to the small average fraction of basin area under irrigation (see above).

For basins with more than 3% of their area equipped for irrigation, the improvement in d-statistics is slightly larger but including irrigation in the calculations increases the negative bias in model predictions for those basins (Table 8.4).

As the bias arising from uncertainties in the input data partly cancels out over large domains, the model performance generally increases with basin size (*Fekete et al.*, 2002; *Hunger and Döll*, 2007). This is illustrated in Figure 8.12 where the model performance, MBE and MAE is plotted as a function of catchment size for the selected 658 discharge stations.

Figure 8.14 shows the spatial distribution, magnitude, and sign of the bias for the 658 selected gauging stations. As can be seen, model results are consistently biased low in the northern basis. This underestimation of discharge can be attributed to low biases in CRU precipitation that are caused by gauge undercatch due to snow and biases arising from the distribution of precipitation stations (see Chapter 5.3). For other regions, a distribution of biases is centered around the mean value and does not seem to follow a climatic gradient. Lowest absolute values for the bias can be found in North America, Europe, South Africa, Australia, and parts of South America. As these regions also have the highest density in the precipitation network (see Figure 5.1), the number of precipitation stations upstream of discharge station in each year between 1901 and 2002 was computed and related to the total basin area. The resulting precipitation network density is highest for basins in North

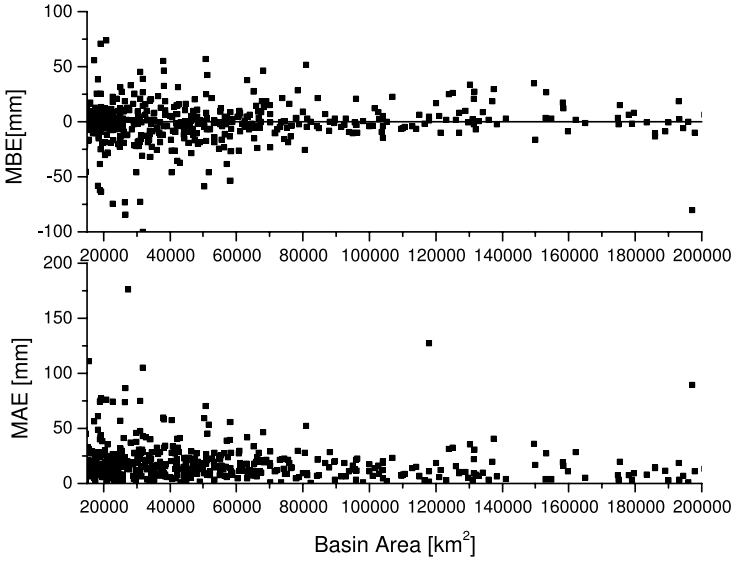

Figure 8.12: Model performance (expressed by the MBE and MAE) as a function of basin size, based on 1901-2002 CRU data

Table 8.5: Meaning, original value, and sampling range of conceptual parameters in the WBM_{plus} model

Parameter	Meaning	Original Value	Unit	Range
α	Drying Function (Eq. 6.3)	5.0	-	2-8
β	Groundwater release (Eq. 6.8)	0.0167	1/T	0.00835- 0.02505
γ	Groundwater partitioning (Eq. 6.8)	0.5	-	0.0-1.0
SF	Snowfall threshold	-1.0	deg C	-2.5-0.5

America, South Africa, and Europe. To test the assumed relationship between the density of the precipitation network and the model performance, the bias has been plotted against the computed precipitation network density for the simulation period (Figure 8.13).

As can be seen, the model bias is lowest in regions with a sparse precipitation network and generally increases with a higher precipitation network density (and thus lower uncertainty in gridded precipitation).

8.3.3 Parameter Uncertainty

To assess the uncertainty of model parameters controlling the formation of runoff and their implications on the predicted model results, the GLUE method discussed in Chapter 6.7.2 was selected. The conceptual parameters controlling the vertical water balance in WBM_{plus} are listed in Table 8.5. The impact of variations of the model parameters α and β within the predefined range on components of the model is qualitatively shown in Figure 8.15.

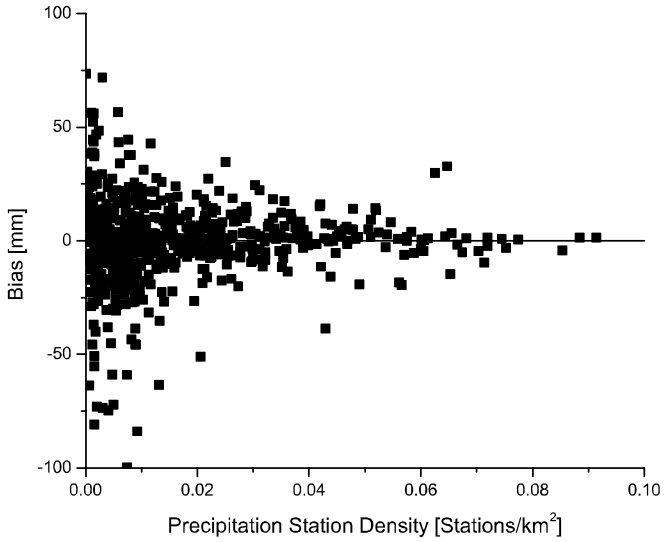

Figure 8.13: Model bias as a function of precipitation network density, computed as a the average number of stations upstream of a discharge gauging station during the period for which discharge data is available

The soil moisture drying function $g(W_w)$ is controlled by the parameter α and reaches its maximum for lower values of relative soil moisture (W_s/W_c) when α increases. The parameter α therefore largely controls the soil water balance of the model and higher values of α lead to higher predictions of actual evapotranspiration and consequently lower runoff. The parameter γ controls the fraction of surplus water that becomes discharge instantaneously and effectively separates the runoff formation in a slow and a fast component. The lower panel qualitatively shows the emptying of the runoff detention pool D_r in periods of no recharge for variations of the model parameter β. Lower values of β lead to a slower release of runoff from the the runoff detention pool. Unlike the parameter α, β controls the temporal dynamics of the runoff detention pool and variations in β will not impact the predicted amount of runoff but the temporal dynamics of active groundwater.

The Monte-Carlo simulations required for the GLUE method have been performed by linearly sampling the parameters within a predefined range around the original values of the parameters (Table 8.5) using a random number generator. While the original value is based on *Vörösmarty et al.* (1998), the range at which the parameters are linearly sampled is based on both the experience from other studies and physically meaningful ranges. The sufficient number of Monte Carlo simulations to be performed for the GLUE analysis is discussed in *Beven* (2006) and generally increases with increasing model complexity. Given the large requirements in terms of computing time and disk space for global simulations[3], model simulations with randomly sampled parameters were performed for two large river basins for the period 1996-1999 and the number of simulations was limited to 4,000. Using the CRU data set and the model configuration described above, the uncertainty was assessed for the

[3] Global simulations require about 16 min per simulation year on a computer system with 2.5 Mhz CPUs and produce about 12 Megabyte of output data per variable per year if monthly values are outputted

Figure 8.14: Bias ($1/n \sum(Modeled - Observed)$) for 658 gauging stations with at least 15 years of observation for simulations under disturbed conditions

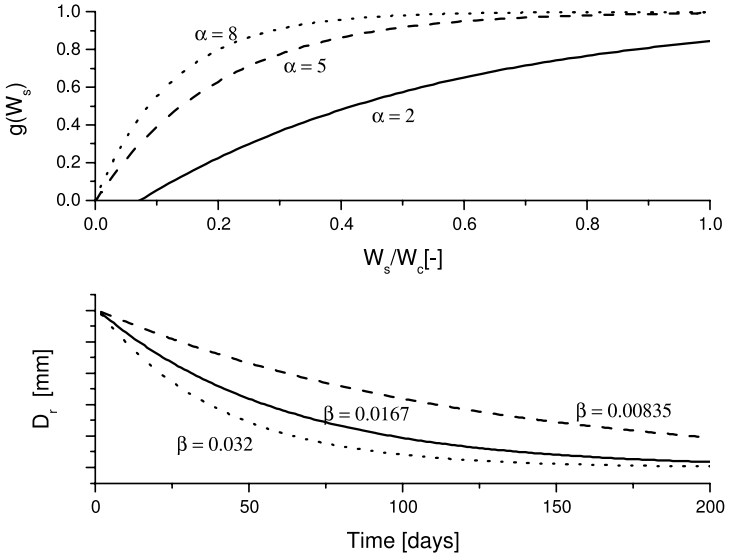

Figure 8.15: Qualitative plots showing the sensitivity of the soil moisture drying function and the runoff pool to the model parameters α and β for extreme values with the sampling range

Danube and Mississippi river basins. The Danube river is about 2,850 km long and its basin covers an area of 788,002 km^2 in 19 countries, making it the most international river basin of the world before it drains into the Black Sea. The Mississippi river that runs from its source at Lake Itasca to the Gulf of Mexico with a total length of 3,870 km has a drainage area of 3,200,000 km^2. As described in Chapter 6.7.2, it is necessary to select acceptable simulations based on some measure of likelihood. If this threshold is based on a fixed value of model performance measures, the number of accepted simulations (and hence the sampled parameter space) will vary for each river basin. Alternatively, the limit of acceptability could be based on a fixed number of simulations out of the total number of simulations. The 1,000 simulations with the highest likelihood (based on the Nash-Sutcliffe efficiency R^2) were therefore selected for both river basins.

Predicted monthly values of discharge for the Mississippi river were compared with observed discharge at the gauging station Vicksburg (A = 2,964,252 km^2). The Nash Sutcliffe efficiency for the 1,000 accepted simulations ranged from 0.63 to 0.75 with a mean value of 0.67. Figure 8.16 shows scatter plots of the likelihood measure R^2 for the model parameters α, β, γ, and SF for the Mississippi river basin. The parameter α shows a moderately identifiable maximum near the original value (5.0). The runoff partitioning parameter γ shows a very clear maximum around the original value of 0.5 whereas the highest likelihood is reached for values of β on the lower end of the sampled range. The snowfall partitioning value SF shows a clearly identifiable pattern at lower values. The highest likelihood of model predictions is achieved for snowfall partitioning values SF of -2.4°, considerable lower than the -1.0° that was used as a threshold for snowmelt in the original version of the model. The parameter β shows a maximum at low values (around 0.00911 1/d), representing a 50% reduction over the value that was initially used. Figure 8.17 shows the the uncertainty range

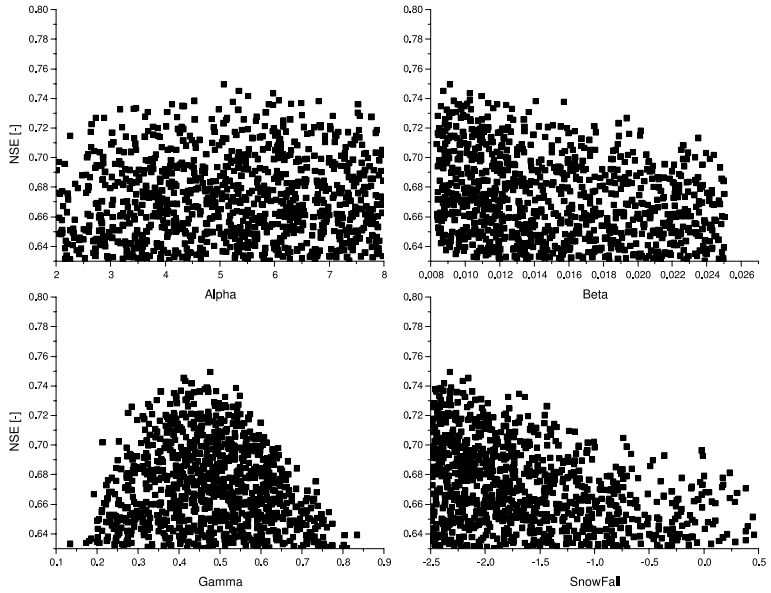

Figure 8.16: GLUE likelihood dotty plots for the model parameters α, β, γ, and the Snowfall threshold for the Mississippi river basin based on 1000 accepted simulations (25% of all simulations)

of the likelihood weighted simulated discharge values for the Mississippi between the 0.05 and the 0.95 percentiles. The mean simulation range is 4,492 m^3s^{-1} and represents 23% of the mean observed discharge during the simulation period (19,530 m^3s^{-1}). The median value of the GLUE simulations underestimates the mean value of the observations by 0.6% on average.

To assess the identifiability of model parameters and the likelihood values as a function of parameter values for a contrasting river basin, the GLUE method was applied for observed monthly discharge at the gauging station Ceatal Izmail, located near the mouth of the Danube river with a catchment area of 788,002 km^2. The model performance, expressed as the Nash-Sutcliffe efficiency R^2 for the 1,000 accepted model simulation (25 % of the total number of simulations) was slightly lower than for the simulations at the Mississippi river basin. R^2 values range from 0.36 to 0.67 with a mean value of 0.49. Figure 8.18 shows the scatterplots for the likelihood of model results as a function of the parameters. With regard to the identifiability of parameters, the results suggest that model predictions are sensitive to the same parameters that have been shown to be important in the Mississippi basin. Discharge simulations are most sensitive to variations in the partitioning parameter γ and the snowfall threshold SF. The range in which the likelihood of the model being a predictor of the system is highest, however, shows significant differences to the optimal range found for the simulations in the Mississippi basin. Whereas SF lies in the same range, α, β, and γ show large deviations (Table 8.6 and Figure 8.18). As the model tends to underestimate discharge in the Danube basin when used with CRU climate drivers (Chapter 9.5.4), optimal values for α are significantly lower, reducing actual evapotranspiration and thereby increasing runoff. The

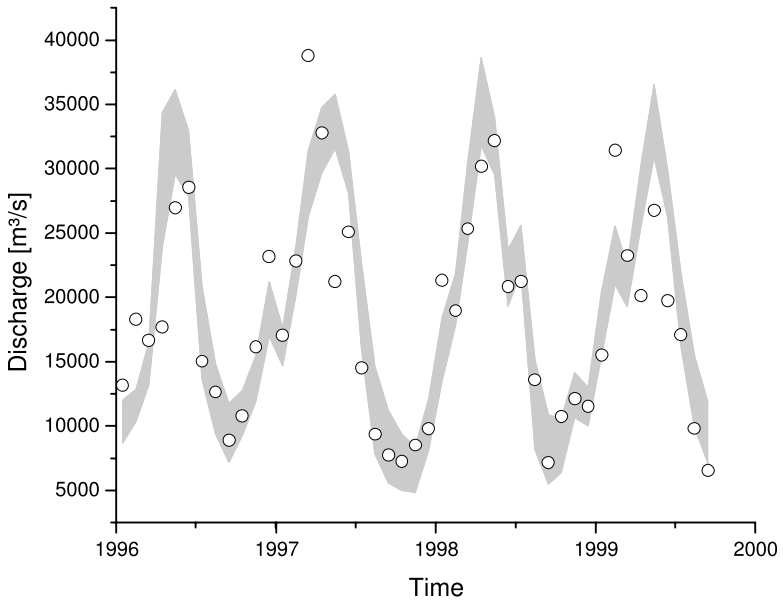

Figure 8.17: GLUE estimated uncertainty in the predicted discharge for the Mississippi river basin based on 1000 selected simulations and observed values (circles)

higher value for γ suggests that the discharge is dominated by slow components (i.e. a larger fraction of runoff fills the runoff detention pool) with a runoff detention time of around 60 days ($\beta = 0.017$) . Uncertainty bands for predicted discharge have been plotted in Figure 8.19 and show considerable ranges and deviations from observed discharge. The average range of the confidence band represents 23% of the observed discharge. On average, the median of the GLUE simulations underestimates the observed discharge in the basin by 8.3%.

Table 8.6: Optimal parameter values based on the Nash-Sutcliffe efficiency R^2 for Mississippi and Danube basin after 4000 simulations

Scenario	α	β	γ	SF	R^2	d	MBE
Danube	2.431	0.01761	0.827	-2.454	0.67	0.90	-5.64
Mississippi	5.071	0.00911	0.476	-2.326	0.75	0.92	-6.56

8.3.4 Uncertainties Arising from Precipitation Data Sets

As described in Chapter 5, considerable differences exist among different global climate data sets. As precipitation is the most important variable for water balance calculations, the uncertainty arising from differences in precipitation data sets will translate to uncertainties in the predicted discharge that might be larger than the uncertainty caused by variations in the parameters alone. The impact of different precipitation data sets was therefore assessed

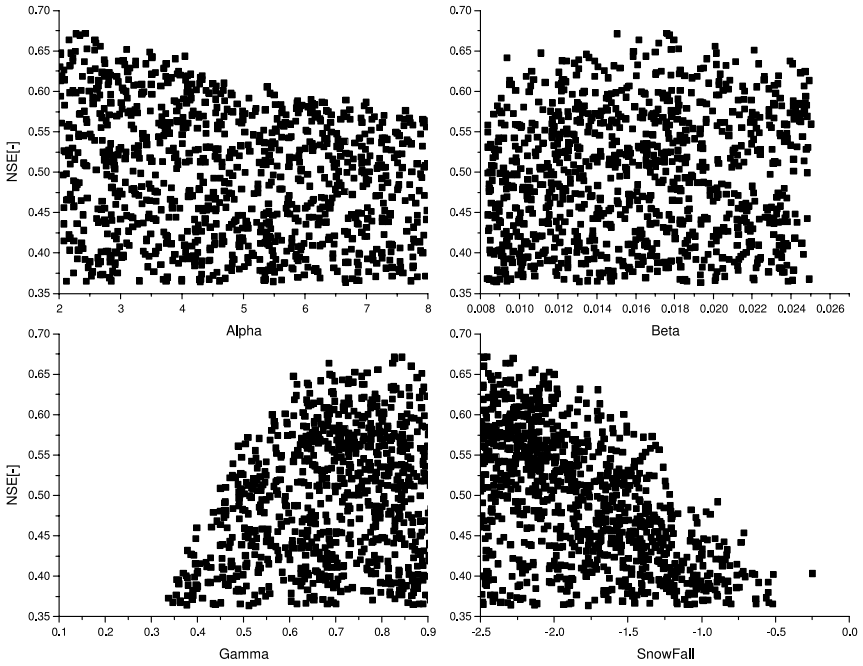

Figure 8.18: GLUE likelihood dotty plots for the model parameters α, β, γ, and the Snowfall threshold for the Danube river basin based on 1000 accepted simulations (25% of all simulations)

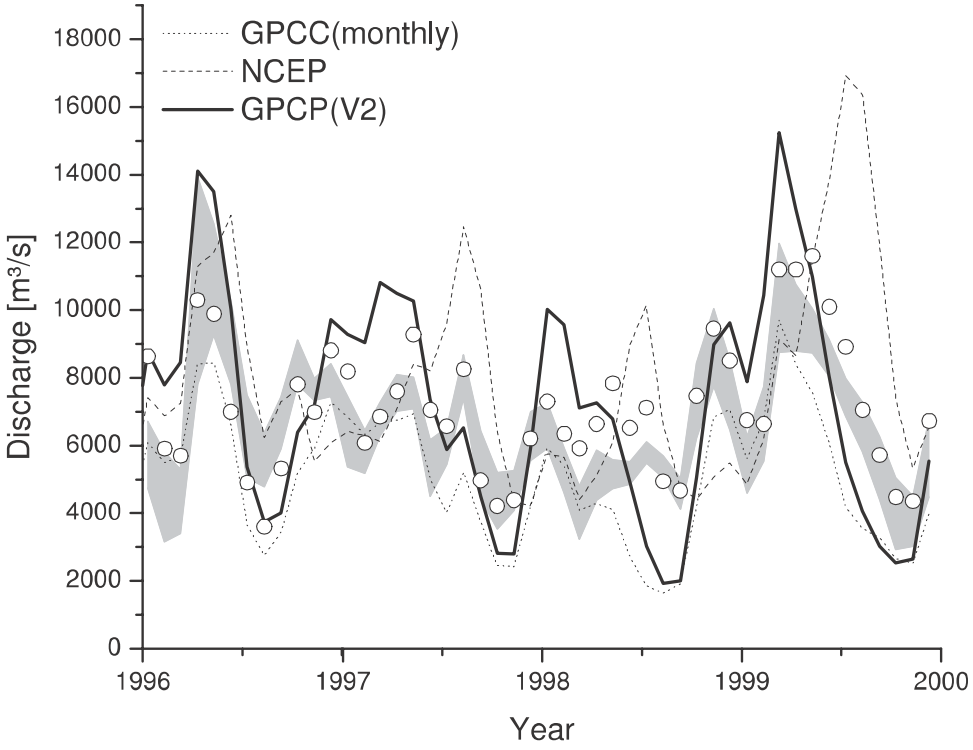

Figure 8.19: GLUE estimated uncertainty in the predicted discharge for the Danube river basin based on 1000 selected simulations (grey), observed values (circles) and model simulations based on different precipitation data sets

for the Danube river basin. Discharge was simulated using three of the global precipitation data sets described in Chapter 5.2, keeping all other input data the same, and applying the 'optimal' parameter set that was found for the CRU simulations. The resulting hydrographs, together with the 90% confidence band derived from CRU simulations is plotted in Figure 8.19. As can be seen, the uncertainty arising from different precipitation data sets are much larger then the uncertainties caused by variations in the model parameters. Whereas discharge simulations based on GPCP and GPCC precipitation data sets show a reasonable agreement with the observed seasonal discharge cycle, the simulations based on NCEP data do not seem to adequately represent the observed variability. The mean discharge for the river basin varies between 5,215 m^3s^{-1} for the GPCC data and 7,776 m^3s^{-1} for the NCEP data.

Table 8.7: Mean values of simulated discharge for the Danube river basin using different precipitation data sets. Observed discharge for the period 1996 to 1999 Q_O = 7,126 m^3s^{-1}

Precipitation data set	CRU	GPCPV2	GPCC	NCEP
Mean Q [m^3s^{-1}]	7,136	7,334	5,215	7,776

8.4 Summary and Conclusions

A comparison of modeled water demand and withdrawal for irrigation purposes with reported national and sub-national statistics and results from other models showed a good agreement between predicted and observed values. The plausibility of the models and its parameters and the impact of variations in parameters on discharge predictions was tested for the Krishna river basin using a Monte Carlo simulation method. The modeled irrigation water withdrawal (and thus the impact on modeled discharge) is largely controlled by the irrigation intensity and irrigation efficiency whereas the parameters controlling the percolation of rice have less impact. At the global scale, the model was found to be most sensitive to the extend of irrigated areas and the fraction of paddy rice in those areas. The sensitivity of the model to variations in climate drivers and irrigated area was assessed by using two different climate reconstructions and two different global maps of irrigated areas and large uncertainties have been revealed. The estimated global withdrawal has a sensitivity of 30% depending on what global data set on irrigation is used and 30% if different climate reconstructions are used, with even larger deviations for individual countries.

Discharge predictions (corrected for the effects of irrigation water withdrawal and return flow) were validated globally against a large set of hydrographs. On average, the model predictions showed a low bias and a reasonable agreement despite large variations at individual river basins. Correcting discharge predictions for irrigation effects slightly improved model results, particularly in basins with considerable fraction of the basin area under irrigation. However, averaged over all gauging stations, the improvement in model performance is small as the impact of irrigation and reservoirs for most basins is small. Model simulations of irrigation water withdrawal and discharge for the Krishna river basin showed that the model is generally capable of predicting the impacts of human interventions on the hydrological

cycle. The comparison of model simulations for pristine and disturbed conditions and observed discharge revealed that structural changes in observed discharge cannot be explained by variations in climate data but by increased evapotranspiration from irrigated areas. These results are in general agreement with previous observations regarding reduced discharge due to increases in irrigation water demand (*Bouwer et al.*, 2006; *Haddeland et al.*, 2006a) and imply that model results and derived indicators can be a useful tool for assessing the impact of changes in climate and irrigation water withdrawal on water resources at the river basin scale. In general, the model performance was found to be related to the density of the precipitation station network (and thus the quality of precipitation data) rather than to a climate gradient.

The impact of variations in the model parameters controlling the formation of runoff was tested for two large river basins. Overall, the results show a reasonable identifiability of parameters and suggest that the model is not over-paramerterized. Model results are sensitive to variations in all parameters and most sensitive to γ and SF and less sensitive to α and β. The performance of WBM_{plus} is therefore largely controlled by the surface runoff partitioning factor γ and the partitioning of precipitation into snow and rainfall. Clearly, the results are strongly dependent on the characteristics of individual river basins and are connected to the hydroclimatic and geomorphological conditions in the basin. These results are consistent with the results presented by *Demaria et al.* (2007) who used Monte Carlo techniques to evaluate parameters in the VIC model for different U.S. watersheds along a hydroclimatic gradient.

Although variations in the model parameters α, β, γ, and SF substantially impact predicted discharge and thereby the likelihood of the model being a predictor of the system, the range of uncertainty caused by parameter variations is small compared to the uncertainty arising from differences in precipitation data sets. This implies that changes in the climate data sets will translate to changes in predicted discharge and that model predictions for different climate data will show the signal of climate drivers regardless of the parameter set and is relevant, for example, when model predictions are used to study the impact of climate change on hydrological cycles. The relative impact of precipitation data sets will be smaller in arid regions where variations in the parameters have a larger impact on the simulated discharge. It is important to note that the empirical constants used to parameterize the flow routing equations (Chapter 7.5) could potentially impact the timing and the shape of the computed discharge. As the uncertainties related to those parameters are considered small compared to the uncertainties associated with the parameters controlling the vertical water balance, they have not been investigated here.

9 Applications

9.1 Introduction

This section is aimed at highlighting applications of the model at larger scales. Applications include simulations to help understand the role of irrigation and reservoirs on water cycles over time, to assess water resources with regard to sustainability and highlight water stress at the river basin scale. It involves a reconstruction of global hydrography for the last century using time varying data sets of irrigated areas and reservoirs and a comparison of those simulations with natural conditions to separate trends in continental and global discharge caused by human interventions and by variations in the climate drivers alone.

The use of model simulations and derived indicators of water stress at river basin scale is demonstrated for three river basins that are heavily affected by the use of irrigation water. After a brief discussion of potential impacts of climate change on irrigation water demand, the implications of climate change on irrigation water demand and water availability will be discussed for the Danube river basin using high-resolution climate predictions from a regional climate model.

9.2 Development of Irrigation Water Demand 1901-2002

The time series of irrigated areas that have been created using the method described in Chapter 4.7.2 were used to estimate the evolution of irrigation water withdrawal over the last century. The cropping pattern (the distribution of different crops) was assumed to be constant over time and CRU climate data was used to simulated irrigation water withdrawal from 1901-2002. The simulated amount of water that needs to be abstracted from groundwater, small reservoirs, and rivers globally based on the time-varying data set of irrigated areas increased from 590 km^3a^{-1} in 1901 to 2,997 km^3a^{-1} for the year 2002. Irrigation water withdrawal in North America ($\sim$6% of the total) increased sharply between 1940 and 1950 (Figure 9.1). With the exception of Europe ($\sim$3% of the global withdrawal), all continents show an upward trend over the last century in irrigation water use reflecting the expansion of irrigated areas but a decrease in growth in the last 20 years of the century. As these simulations are based on the assumption that all irrigation demand is always met, they include a considerable amount of water that is abstracted from non-renewable sources (Chapter 8.2.5). Over the last century, the total accumulated volume of non-renewable water abstractions is 55,639 km^3, representing about half of the total precipitation reaching the Earth's terrestrial surface in one year (*Mitchell and Jones*, 2005). The total water withdrawn from non-renewable water resources represents only about 0.2% the volume of water currently stored in all groundwater stocks, estimated to be $23x10^6$ km^3 (*Oki and Kanae*, 2006).

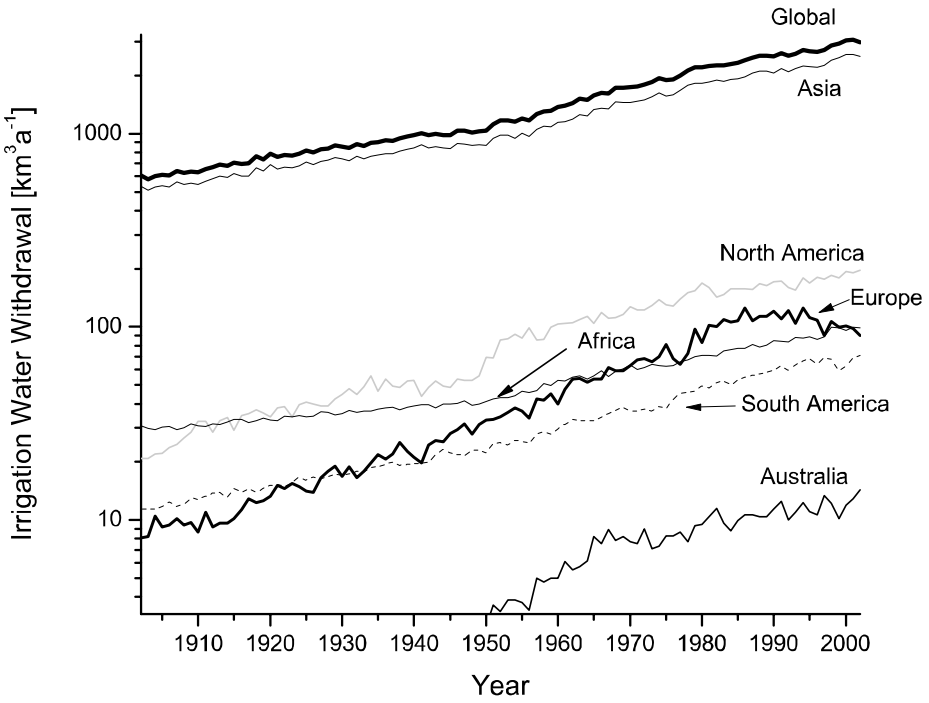

Figure 9.1: Time series of WBM_{plus} modeled irrigation water withdrawal over the last century aggregated by continents using the reconstructed geospatial time series of irrigated areas

9.3 Reconstructing 20th Century Global Hydrography

9.3.1 Introduction

The purpose of this section is to analyze trends in components of the global hydrological cycle in the 20th century and to assess how the estimated changes in irrigation water withdrawal and the construction of reservoirs have impacted the horizontal water balance and the discharge to the oceans. The model simulations in this section were based on the CRU climate data set and the time varying data sets on irrigated areas (Chapter 4.7.2) and reservoirs (Chapter 5.7.4).

9.3.2 Spatial Trends in Hydrological Components

To assess spatial patterns and trends in predicted components of the hydrological cycle over the last century, the trends of the predicted annual values of evapotranspiration and runoff for each grid cell under natural and disturbed conditions were computed. Trends in annual values for each grid cell were tested for significance at the 5% level using t-test statistics.

Under pristine conditions, the spatial distribution of the trend in simulated evapotranspiration over the last century reflects the variations in the temperature and precipitation drivers.

As the temperature shows an upward trend for almost all regions, the trends in evapotranspiration are dominated by increases or decreases in available water and hence by the increases or decreases in precipitation. Increases in evapotranspiration are therefore seen in the mid to high latitude regions, Central Southern Africa, Eastern South America, and Central Australia.

Under disturbed conditions, the expansion of irrigated areas over the last century has significantly increased evapotranspiration in Eastern China, India, Central America, and Central Asia. Figure 9.2 shows significant trends in evapotranspiration under natural and disturbed conditions and the differences between the two. Negative trends in predicted evapotranspiration reflect the changes in precipitation and can be seen in Western and Central Africa, Western South America, and parts of South East China.

Changes in modeled evapotranspiration and trends in the precipitation input data result in increases in the modeled runoff (precipitation - evapotranspiration) in the high latitude regions, Eastern South America, Northern Australia, and mid-latitude North America and runoff decreases in Western Africa, Argentina, Eastern China, and parts of Central Asia. The general pattern of the spatial distribution of runoff trend is consistent with the global distribution of significant trends in observed discharge for the period 1971-1998 compared to 1901 to 1970 (*Milliman et al.*, 2008; *Milly et al.*, 2005) and observed increases in North America (e.g. *Qian et al.* (2007)). Changes in evapotranspiration imposed by the expansion of irrigated areas and increased evapotranspiration translate to significant decreases in the predicted runoff in Eastern China and India. Figure 9.3 shows significant trends (natural, disturbed, and the differences between the two) over the last century. Small negative differences indicate an increase in runoff caused by return flows from irrigated areas that are supplied by non-renewable groundwater resources.

9.3.3 Global Simulations and Discharge to Oceans

The spatial trends in runoff and evapotranspiration described above translate to changes in the predicted terrestrial discharge into the oceans and to endorheic receiving waters (e.g. Aral and Caspian Sea). Based on the basin characteristics given in the STN river network (Chapter 5.7.1), time series of discharge entering the oceans and endorheic basins were calculated and tested for significant trends over the period 1901-2002. Trends were tested at the 5% level.

This section will first discuss the total predicted terrestrial discharge over the last century and then the predicted discharge for individual oceans reflecting the impact of variations in the climate drivers alone and from changes induced by the expansion of irrigated lands and the operation of reservoirs. The results are compared with earlier estimates by *Fekete et al.* (2002) that have been derived by combining modeled runoff with observed discharge at 663 river gauging stations and therefore reflect observations.

The long term mean annual freshwater export from the terrestrial surface of the Earth (taking into account irrigation water abstractions) for the last century is 37,401 km^3a^{-1} and is consistent with earlier estimates (*Dai and Trenberth*, 2002; *Döll et al.*, 2003; *Fekete et al.*, 2002; *Sitch et al.*, 2003). The estimated annual total discharge varies considerably in the last century. Estimated annual values range from 32,783 to 41,725 km^3a^{-1}, a larger range than in

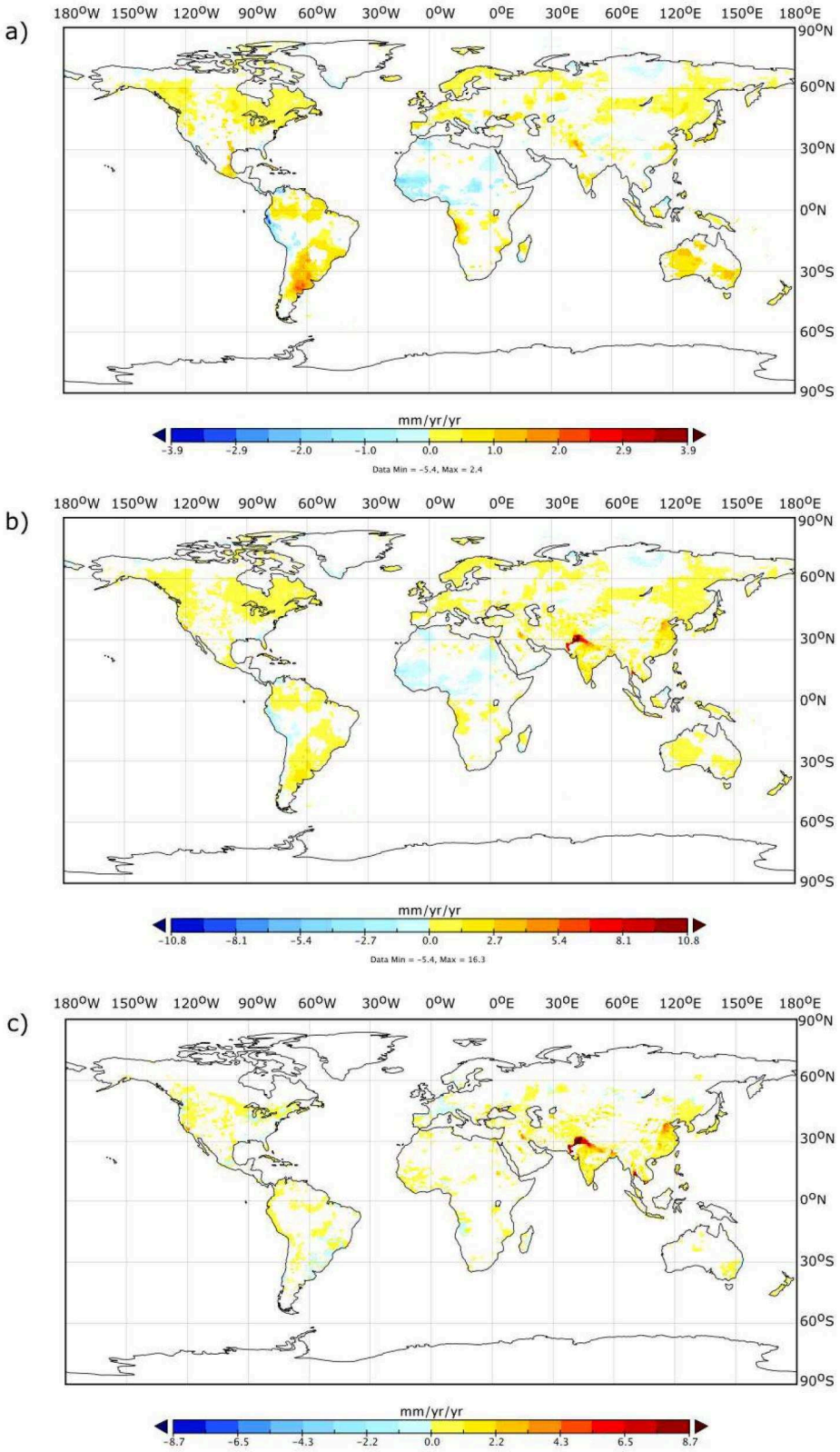

Figure 9.2: Significant trends in evapotranspiration under natural (a), disturbed (b) conditions and the differences between those (c) for the period 1901-2002

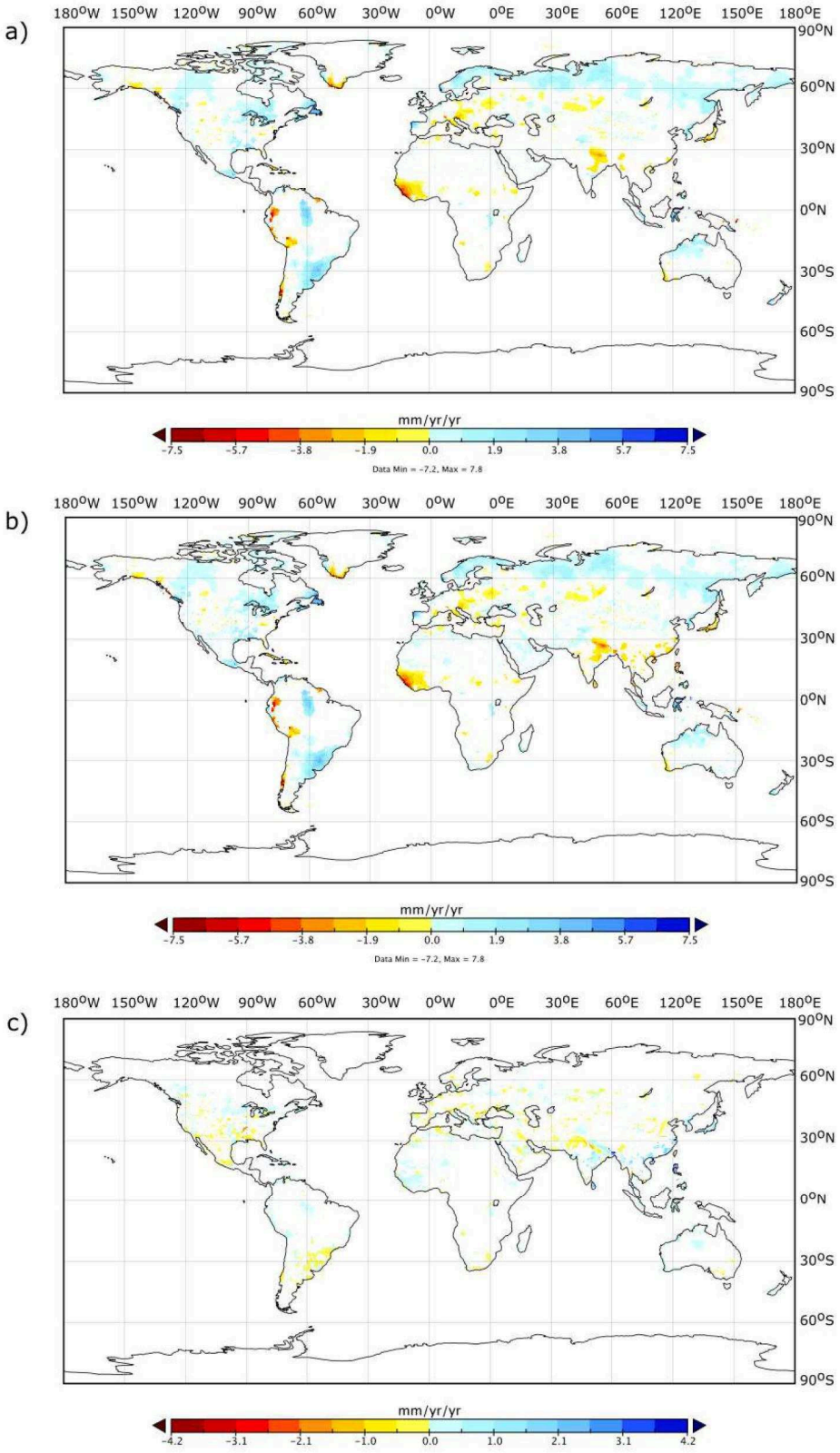

Figure 9.3: Significant trends in runoff under natural (a), disturbed (b) conditions and the differences between those (c) for the period 1901-2002

Table 9.1: Characteristics of endorheic basin and basins draining into the oceans. Irrigated areas and reservoir capacities based on 2002 data. Residence time is computed as total reservoir volume over mean annual discharge; taken from *Fekete et al.* (2002). Basin delineation based on the STN-30 river network. Mediterranean includes Black Sea

Ocean	Area	Res. Cap.	Irr. Area	Irr. Area	Residence Time
	km^2	km^3	km^2	%	*a*
Land	18,743,062	290	271,121	1.45	0.29
Mediteranean	10,678,622	506	233,241	2.18	0.42
Atlantic Ocean	45,729,720	1,904	362,296	0.79	0.1
Indian Ocean	20,688,590	611	927,762	4.48	0.13
Pacific Ocean	19,931,492	742	826,268	4.15	0.07
Arctic Ocean	19,824,778	673	12,472	0.06	0.21
Global	**135,596,264**	**4,726**	**2,633,160**	**1.94**	**0.12**

estimates made by *Shiklomanov and Rodda* (2003). The highest values are simulated during the period 1951-1975 (Table 9.2 and Figure 9.4). The maximum value of annual terrestrial discharge in the last century (41,725 km^3a^{-1}) exceeds the average value by 12%. The minimum annual discharge (in 1992) in the last century is 16% lower than the mean annual value and is related to the substantial decrease in global precipitation following the eruption of Mt. Pinatubo in June 1991 (*Trenberth and Dai*, 2007). Over the entire simulation period, the global discharge increases slightly (11 km^3a^{-1} under natural conditions and 6 km^3a^{-1} when the effects of water abstractions for irrigation are taken into account) but both trends are not significant. The flow alteration imposed by the construction of reservoirs over the last century gradually decreased the variability of the estimated discharge expressed by the coefficient of variation (CV) of monthly discharge values and is discussed in more detail in Chapter 9.4. The increased evapotranspiration over irrigated areas leads to a reduction of terrestrial discharge that is partly offset by the additional water abstracted from groundwater systems that are not connected to the hydrological cycle. Combined, this additional water and increased evapotranspiration leads to a gradual reduction of global discharge ranging from 0.6% at the beginning of the last century to around 2% in 2000.

Despite being insignificant for the total discharge entering the oceans, the hydrologic alterations imposed by the construction of reservoirs and the expansion of irrigated areas may have dramatic effects at the regional scale depending on the degree to which these regions are equipped with irrigated areas and reservoirs. Table 9.1 summarizes the characteristics of basins draining into the oceans and irrigated areas. The combined impact of irrigation water abstractions and reservoirs on time series of discharge entering internally draining basins and the oceans will be discussed in the following section.

Land/Endorheic basins

Major internally draining basins include the Aral Sea drainage basin (A = 1,676,054 km^2 representing 10% of the total area in this category), the basins draining into the Caspian

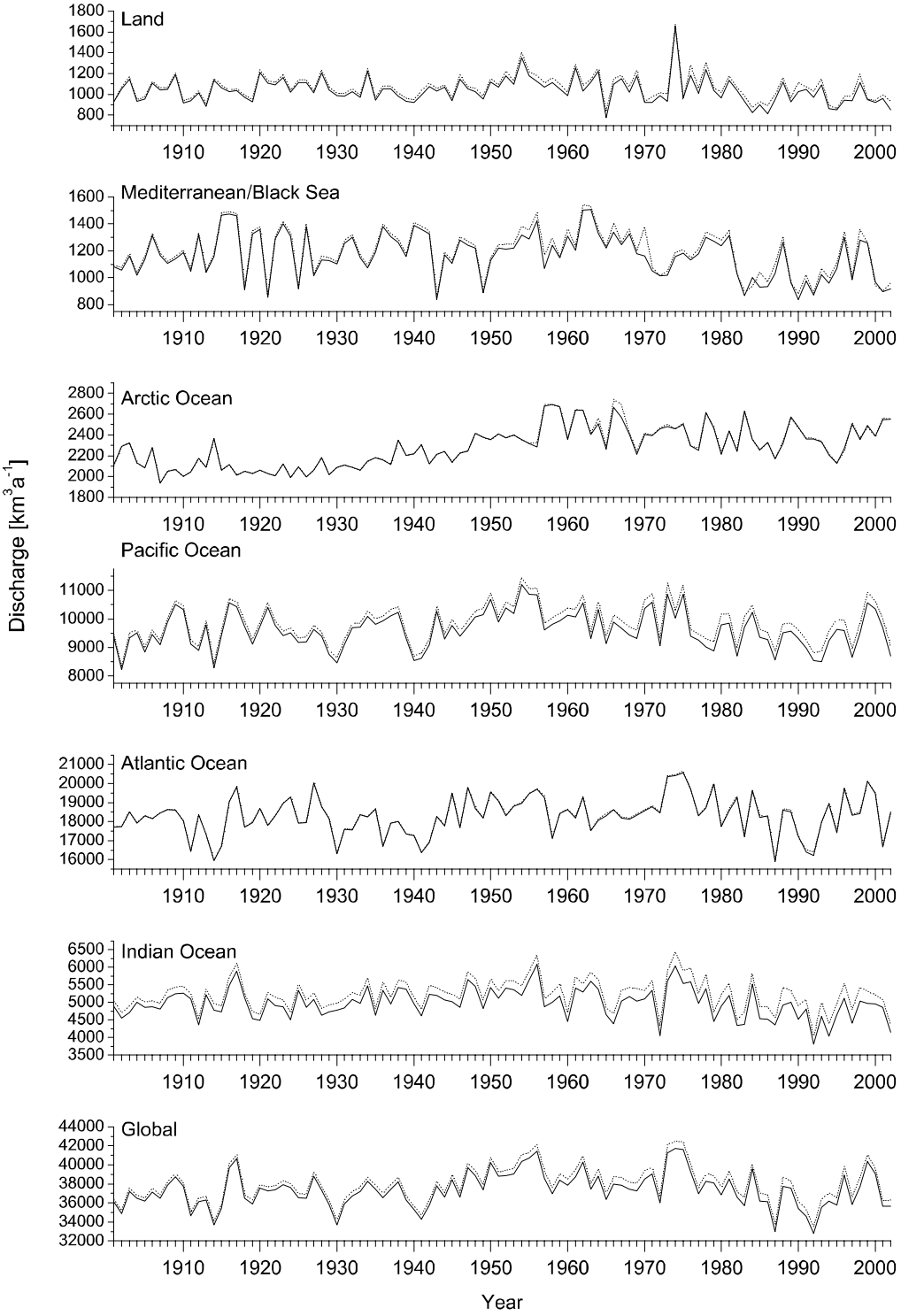

Figure 9.4: Annual time series of modeled discharge to the ocean and to endorheic basins under pristine (dashed line) and disturbed (solid line) conditions 1901-2002

Table 9.2: Components of the hydrological cycle for endorheic basins and basins draining into the Oceans. Fluxes in km^3a^{-1}. Coefficient of variation (CV) calculated for monthly discharge. prist: model run under natural conditions, dist: model results under disturbed conditions (irrigation water abstractions and reservoir operation turned on). P = Precipitation, ET = Evapotranspiration, Q = discharge. MS = Mediterranean Sea, ArO = Arctic Ocean, PO = Pacific Ocean, AO = Atlantic Ocean, IO = Indian Ocean. $\overline{R}$ = modeled long-term mean corrected using observed data (Fekete (2002))

	1901/1925		**1926/1950**		**1951-1975**		**1976-2002**		**1901-2002**		$\overline{R}$
	prist	dist	prist	dist	prist	dist	prist	dist	prist	dist	
Land P	5,799		5,728		5,949		5,917		5,849		
Land ET	4,718	4,764	4,652	4,713	4,793	4,893	4,863	5,012	4,752	4,849	
Land Q	1,060	1,040	1,062	1,033	1,137	1,097	1,032	984	1,072	1,037	993
Land CV	0.51	0.51	0.5	0.49	0.51	0.42	0.52	0.37	0.51	0.45	
MS P	4922		4912		5003		4777		4,901		
MS ET	3,887	3,720	3,688	3,728	3,707	3,765	3,657	3,752	3,684	3742	
MS Q	1,205	1,188	1,213	1,191	1,280	1,236	1,098	1,066	1,197	1,168	1,205
MS CV	0.28	0.28	0.29	0.29	0.27	0.27	0.29	0.34	0.29	0.3	
ArO P	7,613		7,809		8,083		8,018		7884		
ArO ET	4,445	4,446	4,615	4,616	4,561	4,562	4,612	4,614	4,559	4,561	
ArO Q	2,101	2,101	2,185	2,185	2,480	2,462	2,379	2,375	2,288	2,282	3,268
ArO CV	1.03	1.03	0.96	0.96	1.01	0.97	1	0.93	1	0.97	
PO P	21,641		21,857		22,394		21,827		21,928		
PO ET	11,979	12,166	12,086	12,327	12,020	12,388	12,182	12,734	12,069	12,410	
PO Q	9,666	9,518	9,746	9,564	10,357	10,095	9,658	9,350	9,853	9,626	10,476
PO CV	0.19	0.19	0.19	0.19	0.2	0.18	0.19	0.17	0.2	0.18	
AO P	50,215		50,166		51,072		50,931		50,602		
AO ET	32,129	32,153	32,117	32,150	32,275	32,330	32,660	32,742	32,302	32,352	
AO Q	18,106	18,088	18,084	18,060	18,825	18,778	18,344	18,296	18,340	18,305	18,507
AO CV	0.23	0.23	0.24	0.23	0.23	0.22	0.26	0.24	0.24	0.23	
IO P	15,109		15,204		15,579		15,294		15,296		
IO ET	9,925	1,025	9,869	10,292	10,048	10,612	10,193	11,063	10,012	10,566	
IO Q	5,133	4,953	5,274	5,059	5,477	5,196	5,065	4,742	5,234	4,983	4,858
IO CV	0.33	0.3	0.34	0.31	0.33	0.29	0.33	0.3	0.33	0.3	
Global P	**105,298**		**105,675**		**108,081**		**106,764**		**106,461**		
Global ET	**67,083**	**68,274**	**67,027**	**67,826**	**67,404**	**68,550**	**68,167**	**69,917**	**67,378**	**68,480**	
Global Q	**37,271**	**36,888**	**37,564**	**37,092**	**39,556**	**38,864**	**37,576**	**36,813**	**37,984**	**37,401**	**39,307**
Global CV	**0.19**	**0.19**	**0.2**	**0.19**	**0.19**	**0.18**	**0.21**	**0.18**	**0.2**	**0.19**	

Sean (A = 3,202,149 km^2, 17%) and inland basins (A = 13,601,128 km^2, 72%). The largest internally drainining inland basins are the Lake Chad basin, the Great Artesian Basin, Trim basin, and Kerulen basin. Around 1.45% of the area in those basins is equipped for irrigation and the installed reservoir capacity, expressed as the mean residence time (reservoir capacity over mean annual discharge) is 0.29 (under contemporary conditions). The estimated annual discharge from those basins shows considerable variations (between 774 km^3a^{-1} and 1,650 km^3a^{-1} under disturbed conditions) and is 1037 km^3a^{-1} on average (Table 9.2). Discharge in endorheic basins is slightly declining over the entire period, most notably in the last 25 years of the last century. Over the last century, the trend is negative (but insignificant), -0.2 km^3a^{-1} under pristine conditions and -0.5 km^3a^{-1} taking into account the effects of irrigation water withdrawal. The construction of reservoirs has led to a considerable decrease of the variability of monthly flows, most drastically in the period 1975-2002 (Table 9.2).

Mediterranean/Black Sea

The basins draining into the Mediterranean and Black Sea are among the most heavily influenced with regard to the effects of irrigation and reservoirs (Table 9.1). The discharge to the Black Sea is dominated by the Danube (50%), the Dnepr (15%) and the Don (9%). The discharge to the Mediterranean is dominated by the flow of the river Nile contributing more than 53% to the total inflow. Other important rivers include the Po (9%) and the Rhone river (7%). Similar to endorheic basins, basins draining into the Mediterranean are experiencing a decline in discharge in the last 25 years of the last century. Over the entire simulation period, the trend in discharge is -1.2 km^3a^{-1} (significant) under natural and -1.4 km^3a^{-1} (insignificant due to higher variability) under disturbed conditions. It is important to note that the modeled discharge under disturbed conditions can be higher than the estimated discharge under natural conditions in very dry years. This can largely be explained with the inadequate representation of irrigated areas along the Nile river and in the Nile delta and the system of irrigation infrastructure that supplies water from the river; irrigation water in the Nile delta will be assumed to come from unsustainable sources but in reality is supplied from the river through a network of canals.

Atlantic Ocean

About 30% of the terrestrial flow to the Atlantic Ocean is coming from the Amazon river. Other important rivers include the Zaire (9%), Mississippi (4%), and Parana (4%). Given the large volume of discharge entering the Atlantic Ocean, the effect of human interventions on the discharge volume is negligibly small; over the last century, the combined effect of increased evapotranspiration and water withdrawal from non-renewable sources reduces the annual discharge into the Atlantic Ocean by 33 km^3a^{-1} (0.2%). Over the entire simulation period, discharge into the Atlantic Oceans shows and upward (but insignificant) trend of 5.4 km^3a^{-1} and 5.8 km^3a^{-1} under natural and disturbed conditions, respectively.

Indian Ocean

The most important rivers draining into the Indian Ocean are the Ganges (with a flow equivalent to 23% of the total), the Irrawaddy (12%), and the Zambezi (6%). The estimated long-term mean annual discharge entering the Indian Ocean is 4,983 km^3a^{-1} with significant reductions imposed by the expansion of irrigated areas and increased evapotranspiration in basins draining into the Indian Ocean. With 4% of the drainage area being under irrigation, irrigation water abstraction reduces the total flow to the Indian Ocean by almost 5% averaged over the last century with the a reduction reaching the highest values (~7%) in the last 25 years of the 20th century. Under both natural and disturbed conditions, the time series show decreasing but insignificant trends (-0.14 km^3a^{-1} and -2.0 km^3a^{-1}).

Pacific Ocean

Important rivers draining to the Pacific Ocean include the Chang Jiang (9%), the Mekong (4%) and the Amur (3%). Although areas under irrigation represent ~4% of the drainage area (Table 9.1), increased evapotranspiration translates only to a reduction of 341 km^3a^{-1} representing 2.3% of the discharge under pristine conditions (averaged over the entire simulation period). With the expansion of irrigated areas, the reduction of flow gradually increases, with a steep increase in the last half of the last century. The discharge under disturbed conditions is 9,626 km^3a^{-1} on average and varies considerably over the last century. As discharge into the Atlantic, discharge was highest in the 1951-1975 period (~5% higher than averaged over the 20th century. Over the entire simulation period, discharge under natural conditions increased by 2.7 km^3a^{-1} and 0.5 km^3a^{-1} under disturbed conditions, both trends being insignificant.

Arctic Ocean

Flow into the Arctic Ocean is dominated by the Yenisei, Lena, Ob, and Mackenzie river, contributing to more than half of the total flow. Owing to the large volumes of spring discharge that is dominated by snow melt compared to summer flows, the variability of streamflow in basins is higher than for any other ocean (CV for monthly values under pristine conditions is around 1.0 and reduces slightly to around 0.97 when reservoir operation is considered). Reservoirs are responsible for a substantial change in the seasonality of streamflow in Arctic river basins (*Adam et al.*, 2007), and the construction of reservoirs over the last century has gradually led to a slight reduction of the variability of modeled discharge entering the Arctic Ocean (Table 9.2). The coefficient of variation of monthly flow decreased from 1.09 at the beginning of the century to 0.93 during the last 25 years. It is noteworthy that the estimate of the long-term mean annual discharge into the Arctic Ocean (2,282 km^3a^{-1}) is around 30% lower than the 3,268 km^3a^{-1} estimated from gauge corrected runoff fields (*Fekete et al.*, 2002) and the 3,200 km^3a^{-1} estimated based on contemporary discharge records (*Serreze et al.*, 2006). The discrepancy can largely be attributed the huge uncertainties in Arctic hydroclimatological data arising from the sparse network of Arctic climate stations (*Rawlins et al.*, 2006) and gauge under catch, due to the vicinity of gauge locations to highly populated places and the non-representativeness of those gauges of complex topographic features

(*Adam et al.*, 2006). Over the last century, discharge into the Arctic Ocean shows a significant positive trend of 4.2 km^3a^{-1}. This trend is consistent with the annual rate of increase of 2.0 ± 2.7 km^3a^{-1} that has been estimated from observed discharge from the six Eurasian arctic rivers from 1936-1999 (*Peterson et al.*, 2002) and upward trend of 8.2 km^3a^{-1} for the period 1949-2004 that has been found by *Dai et al.* (2009) from a new data set of streamflow records derived from land surface simulations.

9.4 Impact of Reservoirs

The disturbances of the natural water cycle induced by the construction of reservoirs have a number of direct and indirect impacts on the physical, biogeochemical, and geomorphological processes in the river network. Besides a hydrograph distortion, such effects include changes in the sediment trapping efficiency (*Vörösmarty and Sahagian*, 2000), the emission of trace gases from rivers and reservoirs, and others. To illustrate the impact of the construction of reservoirs on discharge, *Vörösmarty et al.* (1997) has introduced the concept of river water aging. The aging of water in its passage to the oceans reflects the impact of reservoirs but must not be confused with the true age of water entering the oceans that can be determined, for example, using tracer hydrological methods. The residence time $\tau[s]$ of water in reservoirs and the river network in each grid cell can be calculated by relating the modeled annual discharge $Q_m[m^3s^{-1}]$ to the river volume $V_{riv}[m^3]$ and reservoir volume $V_{res}[m^3]$ (accumulated downstream using the STN-30 network):

$$\tau_m = \frac{uV_{res} + V_{riv}}{Q_m} \tag{9.1}$$

where u is a utilization factor that relates mean modeled annual storage in each reservoir to the reservoir capacity and V_{riv} is the storage volume in the river, computed as $V_{riv} = Y_m W_m$ (Eq. 7.25 and Eq. 7.24). The computed age varies with the modeled annual discharge and the estimated reservoir storage based on the reservoir operation described in Chapter 7.4. The estimated mean discharge weighted apparent water age globally is 19 days and is consistent with earlier estimates (*Covich*, 1983; *Vörösmarty et al.*, 2000c). The discharge weighted age of water entering the oceans varies considerably between 8 days for basins entering the Pacific Ocean and 39 days for the Mediterranean basins (Table 9.3). Figure 9.5 shows the evolution of the apparent water age for the oceans and the endorheic basins over the last century. Whereas the variations in the apparent water age in the first half of the last century are governed by variations in the computed discharge, the increase in reservoir capacity after the 1950s has drastically altered the discharge regime to the oceans depending on the installed reservoir capacity in relation to discharge (see Table 9.1).

By ocean, the largest changes in the water age are simulated for the Mediterranean Sea basin with the construction of major reservoirs along the Rhone and along the Nile (the largest being the Owen Falls with a capacity of 204 km^3 in 1954). The construction of several reservoirs in basins draining to the Black Sea (along Don and Dnepr river) around the same time has led to a threefold increase of the combined water age for both drainage basins. Similarly, the hydrographs of rivers draining into the Arctic Ocean have significantly been distorted by the operation of reservoirs constructed in the Ob and Yenisei basins starting in the 1950s and 1960s. The increase in the apparent aging in endorheic basins is governed by

Table 9.3: River storage volume, apparent age of water entering the oceans and endorheic basins under pristine and disturbed conditions, and increase in apparent water age. River water age τ for the year 2002

Ocean	V_{riv} $[km^3]$	τ (pristine)$[d]$	τ (disturbed)$[d]$	$\Delta\tau_m$ $[d]$
Pacific	192	8	37	29
Atlantic	1143	22	58	36
Indian	142	11	64	53
Land	50	22	151	129
Mediterranean	105	39	223	184
Arctic	133	23	115	92
Total	**1,765**	**19**	**61**	**42**

the construction of reservoirs along the Volga river, and the rivers draining to the Aral Sea, Syr-Darya and Amu-Darya. Given the low residence in the basins draining into the Atlantic Ocean, the Indian Ocean, and the Pacific Ocean under contemporary conditions (Table 9.1), the increases in the apparent aging in those basins are generally smaller.

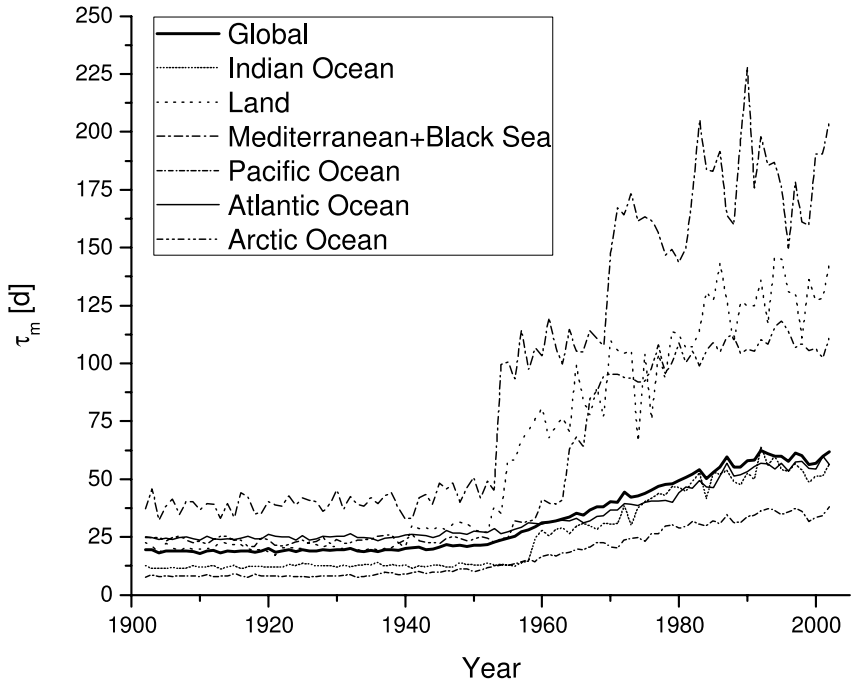

Figure 9.5: Time series of the discharge weighted apparent water age for discharge entering the Oceans and endorheic basins, 1901-2002

9.5 Assessing Unsustainable Abstractions for Selected River Basins

9.5.1 Introduction

This section will discuss water management practices against principles of sustainability and demonstrate the application of the model to highlight water stressed regions resulting from abstraction of water for irrigation purposes. The natural scale at which such assessments have to be carried out is the river basin scale. It is important to note that the results presented below are not calibrated for individual river basins since the focus of macroscale hydrological models is the continental and global discharge and models should generally be applied over those domains without recalibration (see Chapter 6). Before a methodology for assessing water resources and supply is applied to three river basins that are influenced by irrigation water abstractions to a varying degree, it is necessary to briefly review some of the basic concepts of sustainability with regard to water resources management.

Sustainability Concepts

A number of suggestions have been made to adapt the original definition of the sustainability concept[1] of the 1987 Brundtland Report in the water resources context. An adaption of this concept requires that the effects of human activities on the water resources are understood and can be quantified at a reasonable accuracy. A popular concept to assess the sustainability of groundwater abstractions in particular is the concept of *safe yield*[2] that has been developed in the 1920's mainly to preserve the beneficial use of groundwater in the eastern United States as the 'rate of water that can be withdrawn from an aquifer for human use without depleting the supply to such an extent that withdrawal at this rate is no longer economically feasible' (*Custodio*, 2002; *Alley and Leake*, 2004) and was initially primarily based on water quantity assessments. Later, aspects of water quality have been included in this concept before it was broadly defined as 'the amount of water that can be withdrawn from an aquifer annually without producing negative results' (*Alley and Leake*, 2004). Although this concept has been criticized for its vagueness, for neglecting aquifer interactions, long-term effects and environmental impacts, it has been widely used and is still used today. One of the most common misinterpretations resulting directly from this definition is that an aquifer is *safe* if the annual recharge rate exceeds the rate of withdrawal (*Alley and Leake*, 2004). The safe yield concept is further constrained by the perception that the recharge rate is independent of the rate of abstraction and that it has to be known to assess the sustainable pumping rate. *Devlin and Sophocleous* (2005) call this belief the 'Water myth' and show that although the recharge rate is important when considering the sustainability of aquifer systems, it is not *necessary* to estimate sustainable pumping rates. Assessing the sustainability of water resources based on a single year may lead to misinterpretations because withdrawal may exceed the recharge rate in dry years while the aquifer is replenished in wet years. To account for the long-term dynamics of aquifer recharge, *Loaiciaga* (2002) suggested to assess

[1] Sustainable development is defined as *meeting the needs of the present generation without compromising the ability of future generations to meet their demands* (*Bruntland*, 1987)

[2] This concept is sometimes confusingly referred to as sustainable pumping rate

water resources over an 'extended period of time (five or more consecutive years)'. The Environmental Protection Agency (EPA) defines the sustainable abstraction rate as 'the annual quantity of water that can be taken from a source of supply over a period of years without depleting the source beyond its ability to be replenished naturally in wet years' (*Singh and Singh*, 2002). It is important to note that the definitions described above are entirely based on water quantity parameters and ignore water quality and economical considerations. However, aquifers can be economically depleted even before a physical depletion occurs; decreasing water tables render the exploitation of aquifers impossible simply because the pumping and associated energy cost are to high. Large-scale aquifers are economically depleted long before the physical depletion is evident and the economic dimension is therefore central to understanding the meaning of overextraction (*Moench et al.*, 2003). Assessments of water resources systems mentioned above assume that the rate of recharge can be reasonably well quantified. However, the rate of aquifer recharge is difficult to estimate on larger scales and varies generally with land use changes, urbanization processes, changes in surface water regime, lowering the water table of the aquifer system and longer term climatic cycles (*Foster and Chilton*, 2003). Despite recent efforts in mapping and assessment of groundwater resources (*Döll and Fiedler*, 2008; *IGRAC*, 2006; *BGR*, 2006), the global understanding of groundwater resources and their dynamics is very limited (*Foster and Chilton*, 2003) and global data on the source of water for irrigation purposes is not available at the level of detail that is required (Chapter 4.3).

To assess the sustainability of water resources management at the river basin scale, the analysis was carried out using the Water Exploitation Index[3] (WEI) that extends the considerations discussed above to the entire river basin and is simply defined as the water abstractions per year related to the long-term renewable freshwater resources. Although being a very simple indicator, the WEI shows the pressure exerted on water resources and can help identifying regions that are prone to water stress. The European Environmental Agency defines the warning level for the WEI that distinguishes a non-stressed region from a stressed region around 20% and asssumes that severe water stress and unsustainable water use is indicated if the WEI exceeds 40%. *Alcamo et al.* (2000) define 'severe water stress' at WEI levels above 40% and 'very high water stress' over 80% and, based on this levels, estimated that 25% of the Earth are under severe water stress and that this number is expected to further rise due to population growth and an overall increase in irrigated areas. The assessments of water resources in the following section will be based on simulated values of irrigation water withdrawal and discharge.

9.5.2 Aral Sea Basin

The Aral Sea river basin is a landlocked endorheic river basin located in the semi-arid regions of Central Asia and has a catchment area of 1,676,054 km^2. The two main rivers feeding the Aral Sea are the Amu Darya (A = 617,306 km^2) and the Syr Darya (A = 1,058,747 km^2) with a river length of 2,400 km and 2,200 km, respectively. The extensive development of irrigation (most notably cotton) in the two sub basins starting in the 1950's has led to a

[3] Also referred to as Intensity of Water Use (OECD), Withdrawal Ratio or Critical Ratio (CR) (*Alcamo et al.*, 2000)

dramatic reduction of the river flows, subsequently leading to a shrinking of the Aral Sea to about half its size (*Cai et al.*, 2003b), a decline of its water level by about 0.6 ma^{-1} (*Peneva et al.*, 2004), and a reduction of the volume of 90% (*Micklin*, 2006). This reduction in river flow and the environmental consequences caused by pollution related to irrigation are now seen as one of the greatest man-made environmental disasters (*Waltham and Sholji*, 2001) and the basin is a prime example for unsustainable irrigation development (*Cai et al.*, 2003b). It therefore provides a unique opportunity to investigate the basin-wide, long-term effects of irrigation and the operation of reservoirs using the WBM_{plus} macroscale hydrological model.

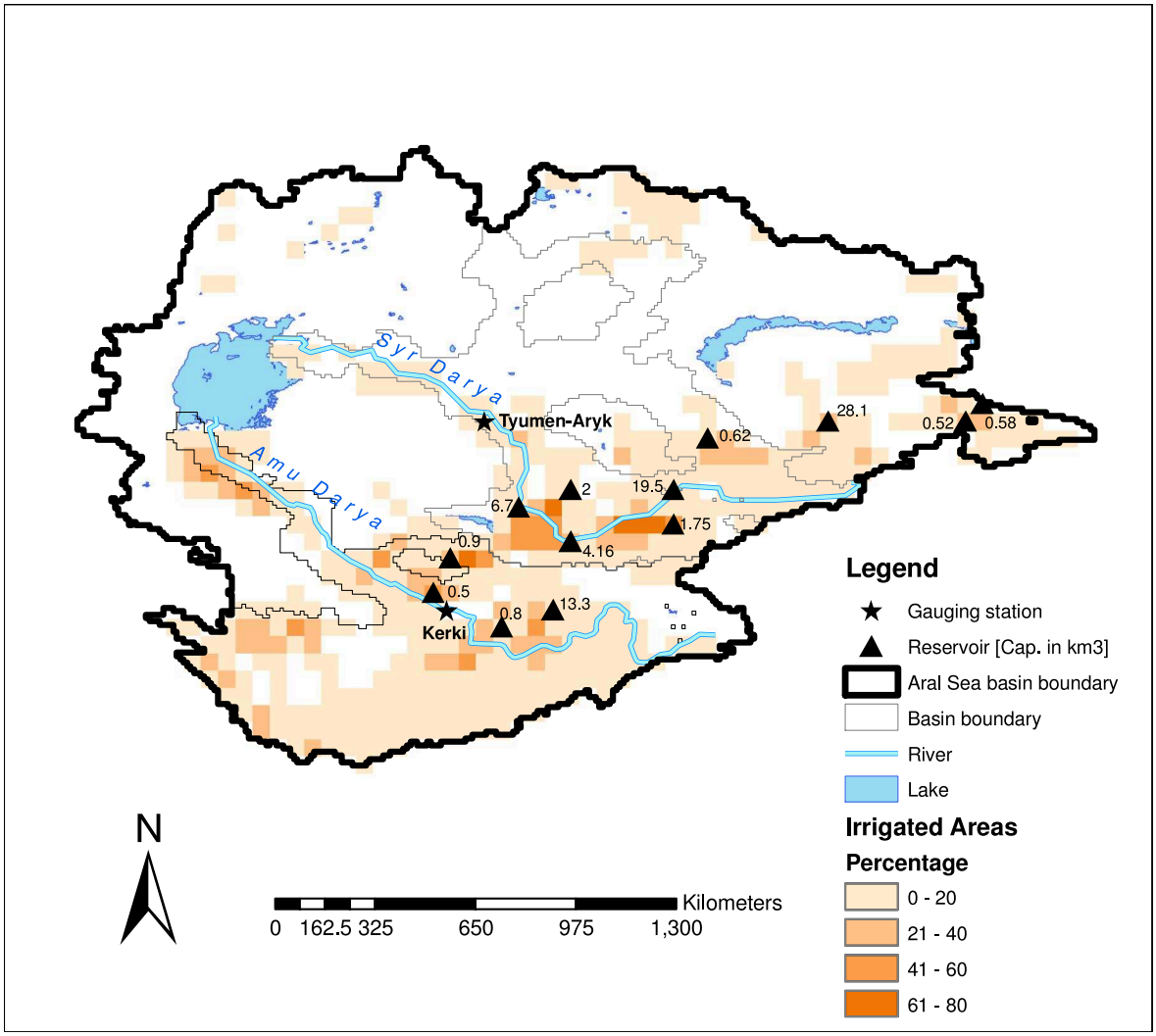

Figure 9.6: Map of the Aral sea basin showing the location of the major reservoirs, irrigated areas, and the gauging stations for which monthly discharge data is available in the GRDC data set. The river basin boundary is based on the STN 30 river network

The climate in the Aral Sea basin is semiarid and extremely continental. Precipitation is concentrated in the winter and spring months and the highest amounts are observed in the mountain regions in the southern part of the basin (*Schiemann et al.*, 2007). Annual precipitation in the basin varies between 246 mm and 856 mm and is 560 mm on average with no

significant trend over the last century. The irrigated area in the basin increased steadily in the last century with a rapid expansion in the 1960's and 1970's. The area equipped for irrigation under contemporary conditions is 3.5 Mha in the Syr Darya sub basin (equivalent to ~3.5% of the basin area), and 5.2 Mha in the Amu Darya sub basin (~8% of the basin area). The development of irrigated areas was accompanied by the construction of water distribution networks and the construction of several major dams. Based on the data set of registered reservoirs (Chapter 5.7.4), the combined storage capacity in the basin is 56 km^3, about 21 km^3 of which were constructed in the Amu Darya basin and 35 km^3 in the Syr Darya basin. The dominant type of irrigation is furrow surface irrigation (*Saiko and Zonn*, 2000). Figure 9.6 shows an overview of the basin, the location of major reservoirs and the distribution of irrigated areas in the basin.

Modeled discharge in the Syr Darya basin and in the Amu Darya basin for the period before 1950, when irrigation was very localized and negligibly small compared to precipitation (*Shibuo et al.*, 2007) is 71 km^3a^{-1} and 39 km^3a^{-1}, close to reported observed values of 72 and 37 km^3a^{-1} (*Cai et al.*, 2003b; *Glantz*, 2005), respectively.

Using the contemporary cropland data set (Chapter 4.8.2), the modeled annual irrigation water withdrawal in the entire basin increased from around 21 km^3a^{-1} at the beginning of the last century (1911/1920) to more than 56 km^3a^{-1} for the period after 1970 (Table 9.4) and is lower than previous estimates based on reported values (*Cai et al.*, 2003b; *FAO*, 1997)[4]. The modeled differences between evapotranspiration under disturbed and natural conditions for the 1991-2002 period are 43 km^3a^{-1} (Table 9.4) and are consistent with the 37 and 50 km^3a^{-1} estimated by *Shibuo et al.* (2007). The underestimation of modeled withdrawals is partly caused by low percentages of cotton in the contemporary distribution of crops. In fact, cotton has been replaced by winter wheat and the percentage of cotton on the total irrigated area has dropped from 45% to 25% after 1990 (*Micklin*, 2006), significantly reducing the water use in irrigation.

To further validate the model, the calculated discharge was compared with monthly observed discharge from the GRDC data sets (Chapter 5.7.3). Observed discharge data for the Syr Darya is available for the gauging Station at Tyumen-Aryk (A = 219,000 km^2) from 1930 to 1986 and for the Amu Darya at Kerki (A = 309,000 km^2) from 1932 to 1989 (Figure 9.6). Under disturbed conditions, the MBE for the stations Tyumen-Aryk and Kerki is 3.2 and 2.2 mm, and the d-Statistics 0.59 and 0.77, respectively. If the model is configured for pristine conditions (i.e. the irrigation and reservoir modules are turned off), the performance at both stations is significantly lower, with MBE values of 5.1 and 3.6 mm and d-Statistics of 0.51 (Tyumen-Aryk) and 0.71 (Kerki). Despite an overestimation of discharge (see discussion below), the modeled results compare reasonably well with the general pattern of observed discharge (Figure 9.7).

Under natural conditions, spring and summer peaks in discharge are grossly overestimated while the 'flattening' of the hydrograph due to the construction of reservoirs and the decrease in discharge due to increased evapotranspiration is captured reasonably well for the stations

[4]FAO (1997) reports a total water withdrawal for the Aral Sea basin in 1980 of 120 km^3a^{-1}, 90% of which are used for agriculture. For the Syr Darya basin alone, *Cai et al.* (2003b) reports *total* withdrawals increasing from 28 km^3a^{-1} in 1961 to 53 km^3a^{-1} in 1990

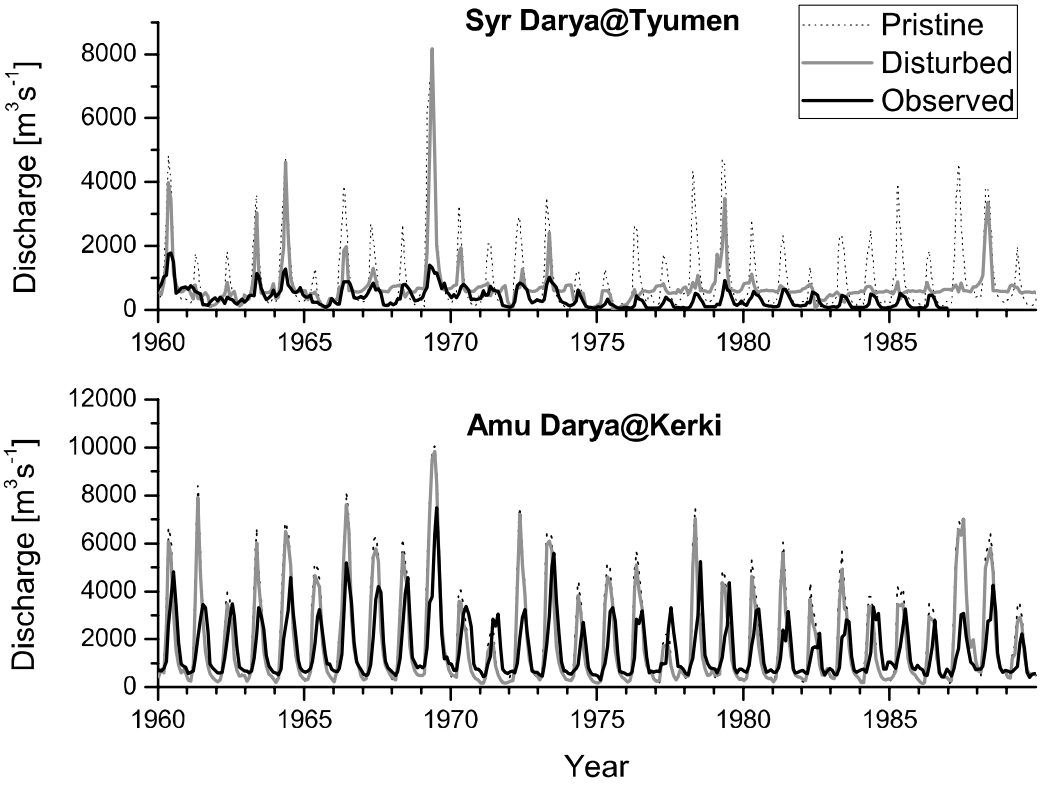

Figure 9.7: Modeled and observed hydrographs for the two rivers feeding the Aral Sea and pristine and disturbed conditions

in the Syr Darya basin and Amu Darya basin. Components of the hydrological cycle for the entire basin for different periods of time are summarized in Table 9.4. Starting from the 1970's, the modeled discharge for both rivers decreases to a total of 104 km^3a^{-1}, despite no decrease in precipitation. This decrease qualitatively reflects the changes in the hydrological cycle due to increased evapotranspiration over irrigated areas but significantly overestimates the flows entering the Aral Sea when compared to reported values. The observed discharge to the Aral Sea for the period 1982-2002 is 12 km^3a^{-1}, 8 km^3a^{-1} of which are coming from the Amu Darya river and 4 km^3a^{-1} from the Syr Darya (*Shibuo et al.*, 2007) while the WBM_{plus} based estimate is 112 km^3a^{-1}.

Table 9.4: WBM_{plus}- modeled components of the hydrological cycle in the Aral Sea basin for different periods of time. P = precipitation, Q = discharge, ET = evapotranspiration, W = withdrawal, prist = natural conditions, dist = disturbed conditions. Fluxes are in km^3a^{-1}, WEI in %

		1911-1920	1921-1930	1931-1940	1941-1950	1951-1960	1961-1970	1971-1980	1981-1990	1991-2002
P	Syr D	285	263	244	255	284	276	253	273	266
	Amu D	188	190	189	199	219	206	181	196	195
	Total	**473**	**453**	**433**	**454**	**503**	**482**	**434**	**469**	**461**
ET	Syr D	216	222	205	212	226	228	214	228	224
prist	Amu D	100	112	118	113	124	121	116	122	119
	Total	**316**	**334**	**323**	**325**	**350**	**349**	**330**	**350**	**343**
ET	Syr D	224	230	214	222	236	239	228	245	241
dist	Amu D	110	123	129	126	139	139	136	146	145
	Total	**334**	**353**	**343**	**348**	**375**	**378**	**364**	**391**	**386**
W	Syr D	10	11	12	14	15	17	29	23	24
	Amu D	11	12	14	16	19	22	24	29	32
	Total	**21**	**23**	**26**	**30**	**34**	**39**	**53**	**52**	**56**
Q	Syr D	33	43	39	45	57	48	41	43	43
prist	Amu D	48	80	71	87	94	86	66	71	67
	Total	**81**	**123**	**110**	**132**	**151**	**134**	**107**	**114**	**110**
Q	Syr D	32	41	37	43	55	46	39	43	43
dist	Amu D	47	79	70	85	92	85	65	70	67
	Total	**79**	**120**	**107**	**128**	**147**	**131**	**104**	**113**	**110**
Excess	Syr D	3	3	4	4	3	5	7	9	11
	Amu D	5	5	5	6	7	9	10	13	15
Total	**Total**	**8**	**8**	**8**	**10**	**10**	**14**	**17**	**22**	**26**
WEI %	Aral Sea	27	19	24	23	23	30	51	46	51

These results suggest that the model is not capable of adequately reproducing the hydrological components in the basin under the impacts of irrigation and can be attributed to three main factors: the underestimation of irrigation water demand, the neglect of inter-basin transfers, and the overestimation of non-sustainable water that partly becomes runoff via return

flow from irrigated areas. Non-agricultural water uses in the basin are less than 8% of the total withdrawal (*Micklin*, 2006). As the consumptive use for water that is used for non-agricultural purposes is typically much smaller than for irrigation, these abstractions can be neglected. As explained earlier, the estimates of irrigation water withdrawal are much lower than reported values and this is due to uncertainties in input data sets. As shown in Chapter 8.2.3, variations in the estimated basin-wide irrigation efficiency drastically impact estimates on irrigation water withdrawal. Similarly, irrigation intensity is not known with certainty and can impact those estimates by around 50%. Secondly, water is transferred out of the Aral sea basin and not taken into account in the model. These inter-basin water transfers out of the basin are significant and an estimated volume of 14 km^3a^{-1} is exported during the period 1983-2002 (*Shibuo et al.*, 2007), mostly through the Karakum canal in the south of the Amu Darya sub basin and other inter-basin transfer projects.

However, even if the model would accurately estimated irrigation water demand and consider inter-basin transfers, simulated discharge values will likely be higher than observations due to the large amount of non-sustainable water abstractions in the basin. This water conceptually represents fossil groundwater that is not connected to the hydrological cycle and increases steadily from around 8 km^3a^{-1} at the beginning of the last century to an average of 26 km^3a^{-1} for the period 1991-2002. As an average of 30% of the withdrawal in the basin returns to rivers and streams, the fossil groundwater abstractions increase discharge compared to natural conditions and partly offset the computed decrease in discharge as a result of increased evapotranspiration induced by irrigation.

The water balance calculations for the Aral Sea basin are further complicated by losses from discharge during the passage of rivers before they reach the Aral Sea that are not accounted for by the model. *Micklin* (2006) estimated these in-stream losses to be around 14% of the total flow. *Nezlin et al.* (2004) estimated that even prior to the development of large scale irrigation, one third of the flow of the Amu Darya is lost by evaporation, transpiration from vegetation along the banks, and bed filtration before the rivers enters the Aral Sea. Similarly, the Syr Darya loses about 50% of its flow during its journey across the Kyzyl-Kum desert. Despite this limitation, model results can qualitatively highlight the pressure on water resources in the basin, for example expressed using the WEI. The increased abstraction for irrigation needs has led to considerable water stress in the basin. Using the WEI as an indicator, the basin has experienced severe water stress starting in the 1970's (Table 9.4). Potential approaches to return to a sustainable use of water resources in the basin must therefore involve a reduction in irrigation water use. As the population in the Aral Sea basin is expected to grow by as much as 35% over the next 30 years (*Cai et al.*, 2003b), a decrease in irrigated areas itself is unlikely. Instead, the water savings would have to come from a shift to crops that have lower water requirements (see above) and improvements in the water distribution and conveyance systems.

9.5.3 Krishna River Basin

The Krishna river basin is the second largest river basin in peninsular India with a catchment area of 258,948 km^2 and is populated by some 70 million people. Like most parts of India, the region experiences a typical Monsoon climate with a distinct rainy season from June through

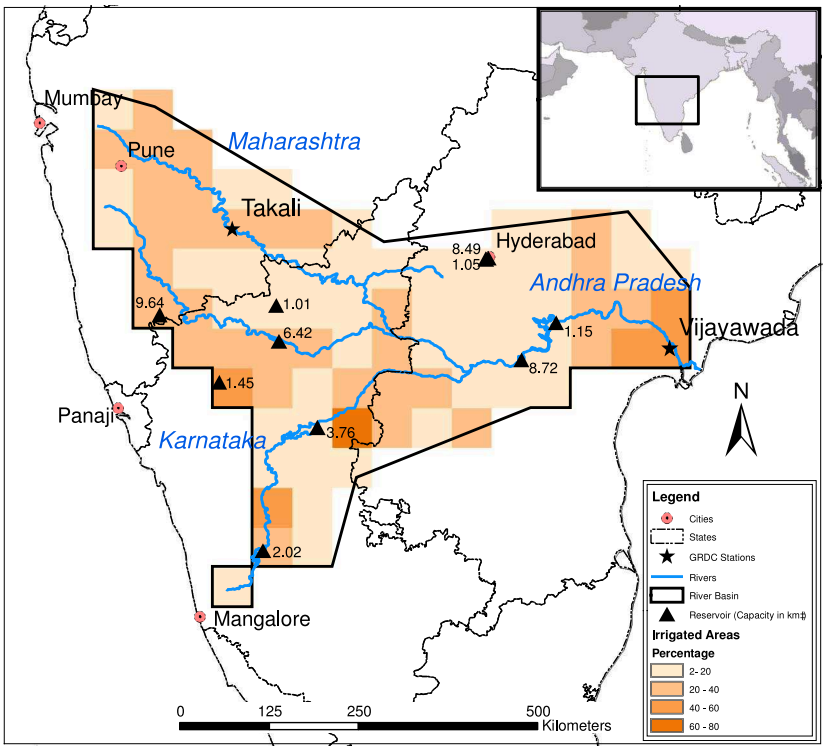

Figure 9.8: Map of the Krishna river basin showing the location of the major reservoirs. The river basin boundary is based on the STN 30 river network

November and thus a high variability in streamflow. The climate is subtropical with most of the rainfall being observed in the mountains of the Western Ghats and arid conditions in the central basin (*Bouwer et al.*, 2008). Average annual precipitation for the last century (based on the CRU data set) varied between 480 mm and 1,112 mm and is 734 mm on average. Over the last century, annual values of precipitation significantly increased by 0.8 mma^{-1}. High variability in streamflow and increasing water use have exerted substantial pressure in the water resources in the basin (*Gaur et al.*, 2007; *Bouwer et al.*, 2006; *Amarasinghe et al.*, 2005; *Jain et al.*, 2005; *Bouwer et al.*, 2003).

The basin has experienced a considerable growth in irrigated areas in the last century, most rapidly after India's independence in 1947. The irrigated area in the basin has increased from just over 9000 ha in 1903 to around around 400,000 in 1984 while the contemporary area equipped for irrigation (according to GMIA) is about 4.4 Mha (Figure 9.9). Irrigated areas include the double cropping of rice and grains, single cropping of sugarcane and areas of supplemental irrigation of cotton, corn, sorghum and others (*Biggs et al.*, 2006). The cropping cycle can be classified into the monsoon season (*Kharif*), from June through October, the post-monsoon season (*Rabi*), from November to March, and the dry season (April-May). As in India in general, practically all irrigated areas are surface-irrigated. Motivated by the need to store water for irrigation purposes, some major infrastructure projects and reservoirs have been constructed since the middle of the 20th century (Figure 9.9). The total contemporary storage capacity of registered reservoirs in the basin is around 42 km^3. An overview of the catchment, the location of large reservoirs and the percentage of irrigated areas is given in Figure 9.8.

The estimated withdrawal of water for irrigation increased from 13 km^3a^{-1} in the beginning of the century to 47 km^3a^{-1} as the mean value for the period 1991-2002. The contemporary estimate is consistent with the 31 km^3a^{-1} consumptive water use that was estimated by *Bouwer et al.* (2006) and an estimated water use for all sectors in the basin of 47 km^3 in 1989 (*Central Water Comission of India*, 1998). To estimate the variability in model results caused by the climate variability alone, additional model simulations were performed under pristine conditions (i.e. neglecting irrigation water abstractions and the operation of reservoirs) and results were compared with observed river discharge. Figure 9.9 shows annual values of modeled and observed discharge under pristine and disturbed conditions for the period 1950-2002 for the station Vijayawada (A = 251,355 km^2) near the mouth of the river. For the period of observation, the model tends to underestimate discharge (MBE = -7.6 *mm* (37% lower than observed discharge) under disturbed conditions and -5.0 *mm* (17% lower) under pristine conditions) but captures the annual and seasonal variations in discharge reasonably well (d-statistics = 0.68 under disturbed conditions and 0.74 under pristine conditions). Table 9.5 summarizes the components of the hydrological cycle in the Krishna basin for the 20th century. The modeled evapotranspiration under disturbed conditions at the end of the last century is about 30 km^3a^{-1} higher than at the beginning of the century. This increase, however, does not translate to an equivalent reduction in discharge because of additional water being added to the system from fossil groundwater that eventually becomes discharge. The modeled amount of water from those sources increased from 5 km^3a^{-1} to an average of 17 km^3a^{-1} for the period 1991-2002. Consistent with the observations, the modeled annual discharge decreases significantly with the expansion of irrigated areas and increased evapotranspiration fluxes. For the last decade of the last century, discharge under disturbed conditions is 12 km^3a^{-1} lower than the estimate under pristine conditions, representing a reduction of nearly 50%, consistent with previous estimates (e.g. *Bouwer et al.* (2006)).

The construction of major reservoirs (most notably the Nagarjunasagar Dam in 1974 with a storage capacity of 11.5 km^3) significantly altered the flow regime of the river by increasing dry season flows (when water is released to augment flow) and decreasing wet season flows (when flows are partly used to fill up reservoirs). While the model captures the reduction of flows during the wet season reasonably well, it tends to overestimate flows during the dry season (Figure 9.9). However, the increasing dry season flows under pristine conditions suggest that the changes are not caused by an inadequate parameterization of reservoir operation but at least partly caused by a change in the rainfall regime in the basin. Increased water abstractions have led to substantial pressure on the existing water resources in the basin. Indicated by the WEI, water stress was apparent from the beginning of the century (Table 9.5). Starting in the 1970s, the annual withdrawals in the basin exceed the runoff indicating severe water stress and leading to a water deficit in the basin that has been previously estimated to be around 6.06 km^3 (*Jain et al.*, 2005).

9.5.4 Danube

While the results for individual river basins presented above were based on data at a spatial resolution of 30 min, this section will demonstrate the application of the model using the STN river network (Chapter 5.7.1) at a resolution of 6 min. CRU climate data, and agricultural

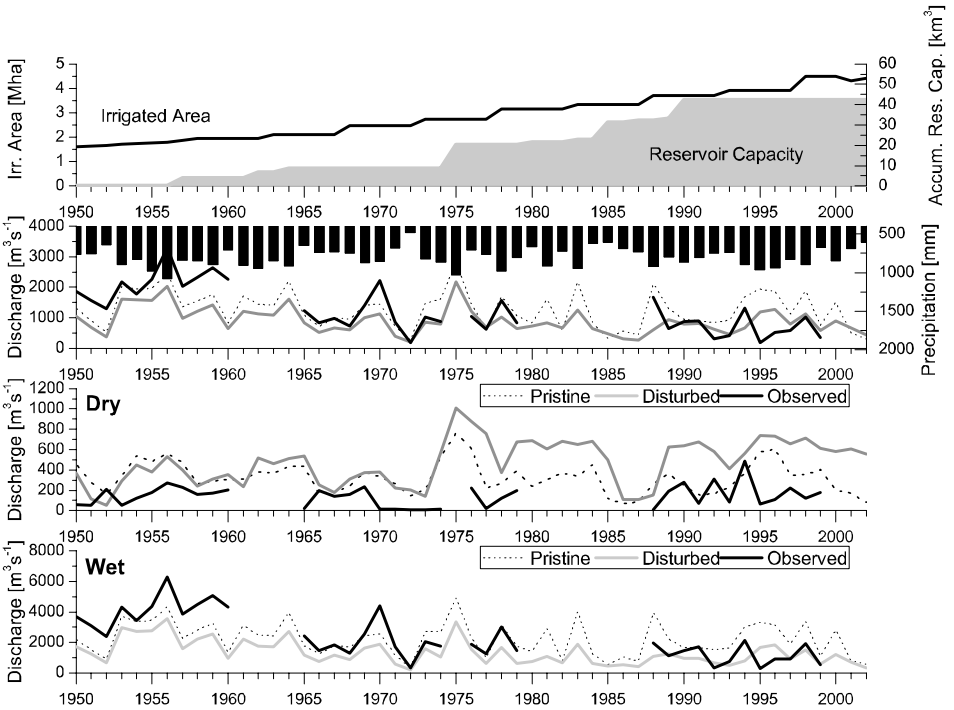

Figure 9.9: Time series of irrigated areas and reservoir capacities for the basin and modeled and observed discharge for the gauging station Vijayawada; annual discharge, dry season flows (December-May), and wet season flows (June-November)

Table 9.5: WBM_{plus}- modeled components of the hydrological cycle in the Krishna basin for different periods of time. P = precipitation, Q = discharge, ET = evapotranspiration, W = withdrawal. Fluxes are in km^3a^{-1}, WEI in %

	1910-1920	1921-1930	1931-1940	1941-1950	1951-1960	1961-1970	1971-1980	1981-1990	1991-2002
P	187	174	199	192	213	206	196	196	202
Q(prist)	36	24	37	38	48	42	39	34	37
Q(dist)	30	19	30	30	38	31	28	21	25
Q(obs)	56	53	56	52	68	23	29	-	21
ET	161	157	172	166	178	180	178	187	195
W	13	15	16	18	20	25	33	40	47
WEI	36	63	43	47	42	60	85	118	127

data sets based on national statistics were regridded to the finer resolution and the original version of the GMIA was aggregated to the STN-6 river network resolution. The results of the model simulation will provide the basis for an assessment of potential climate change impacts on water demand and availability that is discussed later in this Chapter.

The climate in the river basin is strongly influenced by the Atlantic in the upper basin,

whereas the Alps in the west, the Dinaric-Balkan mountain chains in the south and the Carpathian mountain bow in the eastern center provide a significant morphological and climatic barrier (*Lucarini et al.*, 2007). The central and the southern basin are affected by Mediterranean climate. Based on the CRU data set, the annual rainfall in the basin during the period 1961-2002 varies between 611 and 934 mm and is 769 mm on average. Highest rainfall amounts are observed in the mountain chains, while the lowland and the lower basin are generally dry. Figure 9.10 shows an overview of the Danube river basin with the location of major reservoirs and the distribution of irrigated areas. The total area equipped for irrigation under contemporary conditions is 3.58 Mha and represents 4.5% of the total basin area.

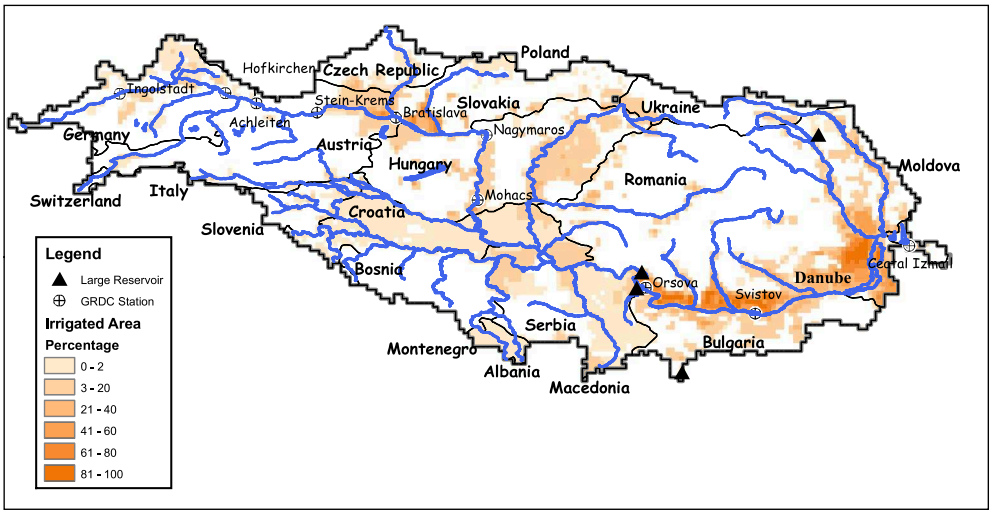

Figure 9.10: Overview of the Danube river basin showing the fraction of irrigated areas and the location of reservoirs.

The estimated average annual water withdrawal increases from around 5 km^3a^{-1} in the 1960's to around 15 km^3a^{-1} under contemporary (1991-2000) conditions (Table 9.6). Most of the water is abstracted in Romania and the estimate for contemporary conditions compares well to the reported water withdrawal from *AQUASTAT* (2008)[5].

As the irrigated areas are concentrated near the lower reaches of the river, the gauging station Ceatal Izmail (A = 788,002 km^2), near the mouth of the Danube was used to compare model predictions with observed discharge. Figure 9.11 shows time series of modeled and observed monthly discharge data for the period 1960-2002 while components of the hydrological cycle for different periods of time are summarized in Table 9.6. Over the entire simulation period, the model tends to slightly underestimate observed discharge in the basin (the predicted

[5]the reported figures for the year 2000 are: 13 km^3 for Romania, 1.9 km^3 for Bulgaria, 2.45 km^3 for Hungary. Abstractions in other countries are insignificant

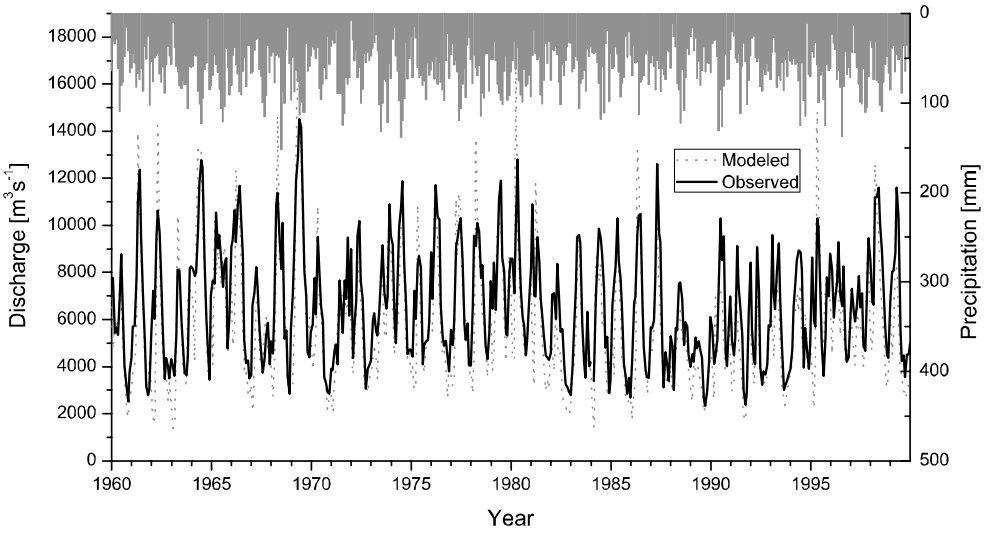

Figure 9.11: Modeled and observed monthly time series of discharge for the gauging station Ceatal Izmail using CRU climate data

values are on average 4.3% lower than the observed values) but is capable of reproducing the variability of observed discharge in the basin reasonably well (Index of agreement = 0.87).

The increased evapotranspiration over irrigated areas, combined with lower discharge has resulted in increasing pressure on water resources in the basin (Table 9.6). Although the estimated withdrawal under contemporary conditions represents ~9% of the computed runoff and indicates no water stress, the WEI has experienced a threefold increase since the beginning of the 1960's. Despite the low WEI, a considerable amount of the estimated irrigation water demand cannot be met by the computed surface water or groundwater resources on a grid-cell basis. The annual amount of non-renewable water resources that needs to be abstracted to satisfy irrigation water demand increased from around 1 km^3a^{-1} in the 1960's to 6 km^3a^{-1} in the last decade of the simulation period, most of which is needed on irrigated areas near the river in the lower reaches of the Danube river.

Implications of Spatial Resolution

As explained in Chapter 7, the calculations of vertical components of the hydrological cycle are generally independent of scale. Neglecting biases arising from interpolation of input data there is no difference in simulated values for different grid cell resolutions. However, the assumptions regarding the water sources for supplying irrigation water demand in a grid cell may lead to different results for different grid resolutions. As water can only be supplied by water stored or flowing in the same grid cell, discharge flowing in a river can supply areas up to a distance of ~50 km (one 30 min grid cell) whereas only areas within a ~5 km range can be supplied from the same river if simulations are based on 6 min resolution. As the the variations imposed by the resolution for the other sources (small reservoirs and groundwater) are generally negligibly small, the differences in river water supply can only be compensated

Table 9.6: WBM_{plus}- modeled components of the hydrological cycle in the Danube basin for different periods of time.Fluxes are in km^3a^{-1}, WEI in %

	1961-1970	1971-1980	1981-1990	1991-2000
Precipitation	618	616	562	595
Evapotranspiration	419	424	416	435
Irrigation withdrawal	4.6	8.5	16.2	15.3
Modeled Q	199	191	162	172
Observed Q	184	183	194	194
WEI	2	4	10	10

by water abstractions from non-sustainable sources. The estimates for non-sustainable water abstractions therefore decrease with coarser resolution. For comparison, simulations for the Danube river where performed with the 30 min river network and keeping all other input data sets. For the entire basin, the simulated amount of river water for irrigation supply is around 40% lower for the 30 min stimulation resolution, ranging from 0.92 km^3a^{-1} for the period 1961-1970 to 5.54 km^3a^{-1} for the period 1991-2000 (Figure 9.12). As water taken from non-sustainable sources partly becomes runoff, the simulated values of runoff might be slightly different depending on the resolution of the model. However, as the WEI relates water abstractions to discharge under natural conditions, the assessments of sustainability of water abstractions will not be dependent on scale.

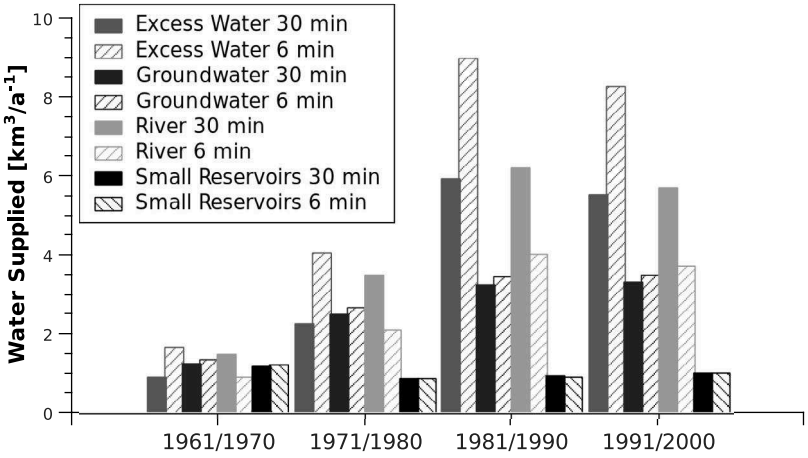

Figure 9.12: Estimated supply of irrigation water from different water sources for different model resolutions for the Danube river basin

9.6 Potential Impacts of Climate Change

9.6.1 Introduction

The potential impacts of global warming on the hydrological cycle, the availability of water resources and their management have been one of the major concerns in the debate about consequences of global warming. Given the important role of agriculture in providing food for a growing population and its dependence on climate drivers and water resources, it is important to assess the impacts of global warming on irrigated agriculture. Climate change may impact the demand and the management practices for irrigation water in two ways. First, the pattern of the availability of water may change so that the water required for irrigation may not be available at the time when it is needed. Secondly, the irrigation water requirements will be affected by changing global climate directly through altering the plants physiological processes and indirectly by changing climate conditions (*Allen et al.*, 1991).

At the crop level, transpiration is controlled by the physiological crop properties responding to global warming: increasing temperatures decrease the stomatal conductance of the crops and thereby lead to a decrease of transpiration (*Betts et al.*, 2007). Higher atmospheric CO_2 concentrations, on the other hand, are generally associated with an increase of plant growth (CO_2 fertilization) and a substantial increase in water use efficiency (expressed as volume of water used per unit of biomass). The overall direct effect on crop transpiration can therefore not yet be quantified due to insufficient knowledge (*Döll*, 2002). With regard to the role of precipitation in partly supplying the crop water demand, the results on the interannual variability of irrigation water demand presented in Chapter 8.2.2 suggest that variability is lowest in regions where irrigation water demand is not strongly supplemented by precipitation and irrigation water demand per unit area is high. Changing precipitation patterns will therefore affect the variability of irrigation water demand in regions with relatively low demand whereas the demand in regions that entirely rely on irrigation water will be controlled by changes in the evapotranspirative demand that are generally smaller. As the predicted irrigation water withdrawal is controlled by the temporal distribution of precipitation in relation to the growing season rather than the annual amount, irrigation water demand may decrease or increase with decreasing annual precipitation and shifts in both the temporal distribution of precipitation and the growing season (*Döll*, 2002). As increasing temperatures are generally associated with longer growing seasons in the temperate zone, additional water demand may be required because multiple (and different) crops can be grown in regions where the crop growth was limited by a short vegetation period.

With regard to the trends in precipitation and the availability of water resources, AOGCM simulation results indicate a wide range of possible trends in different parts of the world. The highest increases in annual precipitation are predicted for the high latitudes which is a very consistent pattern across climate models (*Meehl et al.*, 2007) and consistent with the observed changes in precipitation during the last decades (*Hulme et al.*, 1998). Significant declining trends are observed in Western Africa, Northern Africa, Western South America, and Southern East Asia.

A few studies have investigated the impact of global climate change on the productivity and the water requirements for crops at larger scales. *Izaurralde et al.* (2003) used a modified

version of an agro-ecological model, the EPIC[6] model to assess the impact of climate change on both crop productivity and water requirements for the conterminous United States. The results indicate a wide range of changes in crop yield and water requirements across the United States. While yield increases for irrigated corn were predicted in all regions, the soybean yields are predicted to decrease in the Northern and Southern Plains. These large differences in the simulated results can largely be explained by the differences in predictions of precipitation and temperature across the regions. *Döll* (2002) studied the effects of external climate drivers on irrigation water requirements by using AOGCM outputs to drive a simple irrigation water abstraction model (see Chapter 6.3) and estimated an increase in the net irrigation water demand of 3-5% by the 2020s and up to 15% by the 2070s. However, although mostly consistent over large scales, the results for individual river basins vary with the AOGCM model used and the spatial AOGCM resolution is generally to coarse for most river basin studies (*Lehner et al.*, 2006b). Since the river basin scale is at the focus of such changes, the impact studies should be based on high resolution regional climate models rather then coarse AOGCM data that is not fine enough to adequately reproduce climate conditions at the river basin scale. Considerable progress has recently been made in downscaling the information from the coarser AOGCMs to regional climate models (RCMs) (*Christensen et al.*, 2007) although the atmospheric components of RCMs still face considerable difficulties in reproducing the water balance of large regions (*Lucarini et al.*, 2007). Downscaling can be done statistically (for a comparison of methods, see *Wilby et al.* (1998)) or dynamically where the RCM is nested in the AOGCM and AOGCM output data is used as boundary condition for the RCM and a number of RCMs are now available for many world regions. The following section will exemplarily discuss the implications of modeled future climate predictions on estimates of irrigation water withdrawal and water availability based on the results from a regional climate model for the Danube river basin.

9.6.2 Climate Data

Hollweg et al. (2008) have recently prepared a set of simulations of climate using the Climate version[7] of the Local Model (CLM; *Damrath et al.* (2000)) of the German Weather Service (Deutscher Wetterdienst, DWD) nested in the ECHAM5 AOGCM model (*Roeckner et al.*, 2003).

Model results are available for Europe at a resolution of 0.2° for longitudes between -10.7°E and 36.9°W and latitudes 34.5°N and 69.9°N. The model simulations for 2001-2100 generally show an increase in temperature over the whole domain with larger increases around the Mediterranean and the Alpes region and moderate increases over Central Europe. The annual precipitation totals show a general increase in Northern Europe and a decrease in the Mediterranean. In Central Europe, precipitation is projected to significantly decrease during the summer and increase in winter. The projected increases in mean annual temperatures and the projected changes in mean annual precipitation over the model domain for the

[6] Erosion Productivity Impact Calculator

[7] The Local Model must not be confused with the Community Land Model (CLM) that is a collaborative effort of scientists at NCAR and others and tries to quantify how natural and human changes in vegetation affect climate (http://www.cgd.ucar.edu/tss/clm/)

period 2001-2050 and 2051-2100 are shown in Figure A-1 to A-3 in the Appendix. Simulation results are available for the IPCC scenarios A1b and B1[8] for the period 2001 to 2100. In addition, control runs that reconstruct the 20th century climate based on contemporary conditions are provided for the period 1960-2000. The latter results were compared with simulations based on observed CRU climate data for the period 1961-2000 (Chapter 9.5.4). The projected climate changes in the Danube basin are generally different for the Mediterranean part of the basin where a decrease in average precipitation is projected, and the parts that are under the influence of the Northern European climate system, where an increase in average precipitation is projected (*Lucarini et al.*, 2008). Averaged over the entire basin, the mean annual precipitation shows a slight decrease for the second half of the 21st century (Table 9.7). However, the temporal distribution of precipitation within a year is projected to shift substantially towards more precipitation in the spring and winter months and reduced summer precipitation. Figure 9.13 shows the predicted mean monthly time series of precipitation based on the CLM A1b data for the periods 2001-2050 and 2051-2100, and the relative changes compared to the CLM 20th century simulations. Whereas the predicted decrease in June, July, and August precipitation for the first half of the century are below 10%, the simulated monthly precipitation for June, July and August for the period 2051-2100 is ~30% lower than under contemporary conditions. This sharp decrease in summer precipitation is partly offset by increased precipitation in the rest of the year, most notably in spring precipiation in March and April. It is noteworthy that the simulated annual cycle in contemporary precipitation shows much lower intra annual variability than the observed pattern based on CRU data (upper panel in Figure 9.13). The basin-averaged air temperature for the CLM control run under contemporary conditions compares well with the observed mean temperature based on the CRU data set (Table 9.7). The projected increase for the period 2001/2051 is around 1°C and steadily rises to 3°C for the period 2051/2100. Changes in temperature are highest during the summer and winter months and lowest during the spring (Figure 9.13).

Table 9.7: Basin averaged precipitation (P) and mean air temperature (T) for the Danube basin

	P [mm]	T [°C]
CRU 1960/2000	772	8.84
CLM 1960/2000	742	9.15
CLM A1b 2001/2050	746	10.01
CLM A1b 2051/2100	710	12.23

[8]The A1b scenarios describes a future world with rapid economic growth, a global population peak in the mid-century, the rapid introduction of new and more efficient technologies, and a balanced use of energy from fossil and non-fossil sources. B1 refers to a scenario with rapid changes in economic structures with reduction in material intensity and the introduction of clean technologies. For a complete description of the scenarios see *Barker et al.* (2007)

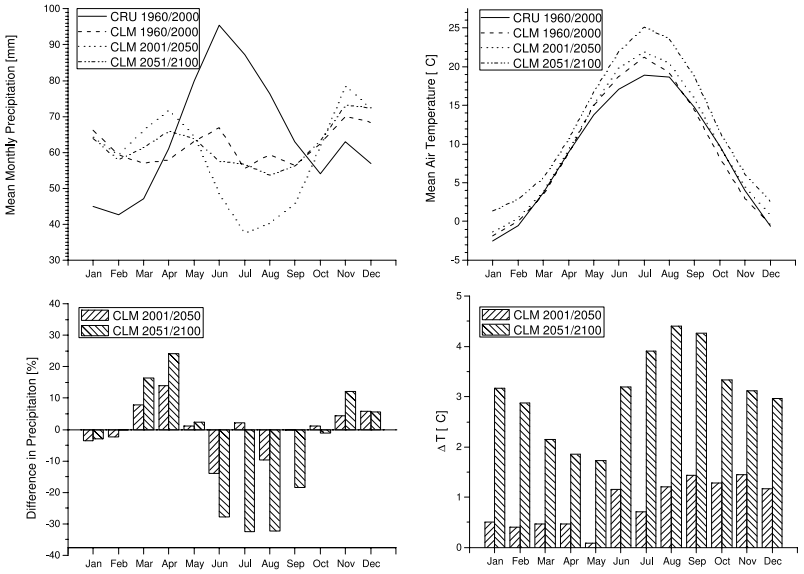

Figure 9.13: Mean monthly values of precipitation and air temperature averaged over the basin and the relative changes compared to the 1960-2000 control run simulations

9.6.3 Changes in Irrigation Water Demand

The projected changes in the magnitude and timing of temperature and precipitation affect the evapotranspirative demand of crops but also change the temporal distribution of precipitation during the growing season. Both of those changes affect the computed irrigation water withdrawal. The annual water withdrawal for irrigation under the A1b scenario is projected to increase to 23.4 km^3a^{-1} for the first half of the century and to more than 29.5 km^3a^{-1} in the second half of the century (Table 9.8), representing an increase of 14 and 43% compared to the mean value computed for the the period 1961-2000 using the CLM control runs. As the impacts of increased atmospheric CO_2 concentrations on plant physiological processes are not considered here, the projected increases are caused by a higher evapotranspirative demand of crops (as a result of higher temperatures) and by the decreases in precipitation during the summer months (described above). Over the course of the year, the largest absolute increases are estimated for July, August, and September, reflecting the projected decrease in precipitation discussed above. In relative terms, these increases are between 5 and 200% higher than the estimated withdrawal under contemporary climate conditions (Figure 9.14). Small relative decreases are simulated for the early summer months where the small increase in precipitation partly offsets the incrased evapotranspirative demand. It is important to note that the modeled irrigation water withdrawal under contemporary conditions using the CLM control runs and assuming constant irrigated areas is substantially higher than the modeled withdrawal using the CRU data. This deviation can largely be explained with the differences in the annual precipitation cycle between modeled and observed precipitation data (Figure 9.13).

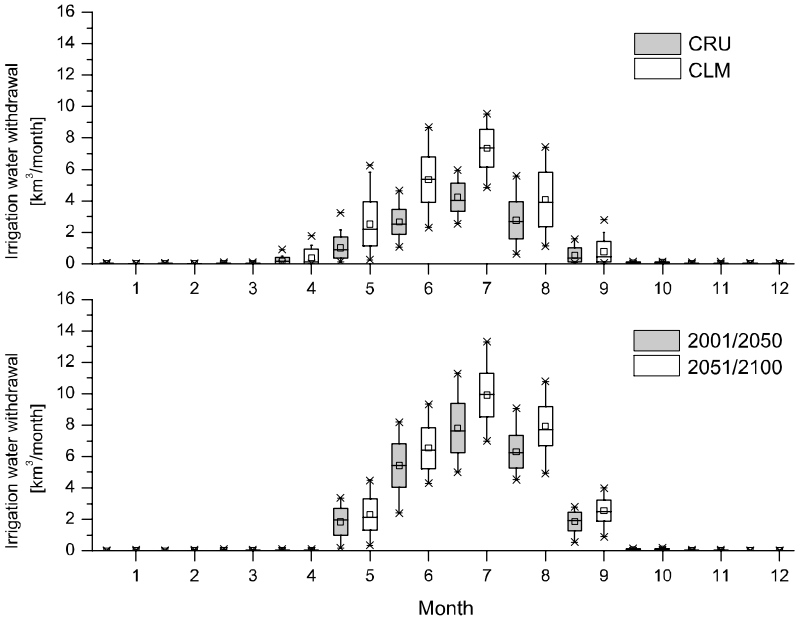

Figure 9.14: Box-Whisker plot of simulated monthly values of irrigation water withdrawal in the Danube basin under contemporary conditions (for CRU and CLM data sets) and under the CLM A1b future climate data. Box indicates starndard deviation, Whisker 10 and 90% percentiles

9.6.4 Changes in Water Availability

To assess the predicted changes in the annual values and in the seasonal pattern of irrigation water withdrawal with regard to available water resources, it is necessary to put those changes into a seasonal water supply context. On an annual basis, the runoff in the basin will not change in the first half of the century but will be substantially (~20%) lower in the period 2051-2100 (Table 9.8). The projected discharge in the basin for the first half of the century is consistent with the results of *Rosenzweig et al.* (2004) who used a number of AOGCMs and found no significant change in runoff in the Danube basin for the first half of the century. Following the changes in the temporal distribution of precipitation, much of the decrease in precipitation will be observed during the summer months. Figure 9.15 shows the long-term monthly mean values of discharge in the Danube basin for contemporary conditions (1960-2000) and for future conditions using the CLM data for the periods 2001-2050 and 2051-2100. The combined effects of higher withdrawal and decreased water resources during the summer months leads to an increased water stress in the basin.

Using the WEI as an indicator to depict water stress based on annual values, the basin could experience higher levels of water stress in the second half of the century when WEI values of up to 20% can be expected (Table 9.8). Given the projected seasonal changes in both water demand and availability, a considerable pressure on water resources is expected during the summer months.

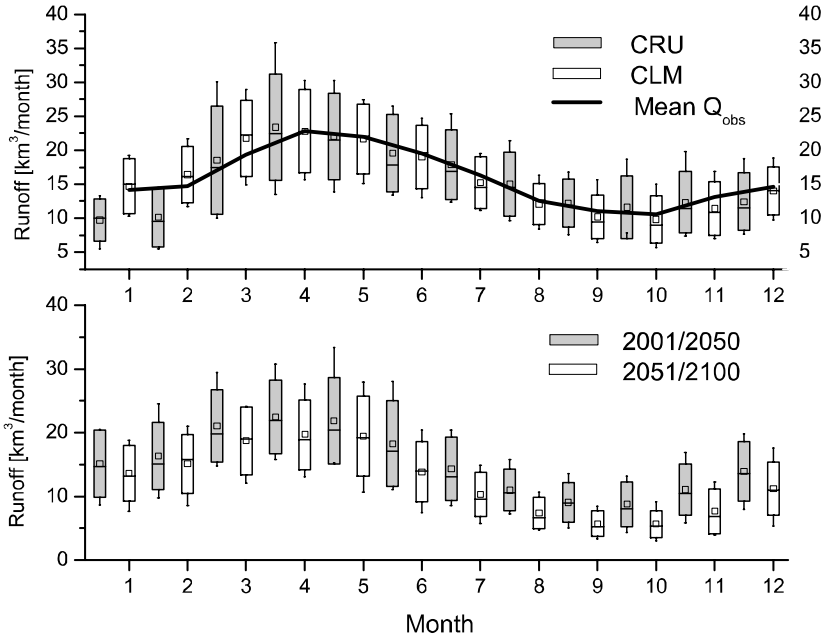

Figure 9.15: Box-Whisker plot of simulated monthly values of discharge in the Danube basin. Upper panel: Long-term mean monthly discharge using the CLM control run (1960-2000) and CRU observed data. Lower panel: Long-term mean monthly discharge under the A1b scenario for the periods 2001-2050 and 2051-2100. Box indicates standard deviation, Whisker 10 and 90% percentiles

Table 9.8: Descriptive statistics for estimated discharge (Q) and irrigation water withdrawal (W) in the Danube basin using CRU and CLM data. CV=Coefficient of variation, P25=25% percentile, P75=75% percentile. Q and W in km^3a^{-1}, WEI in %. Irrigation water withdrawal under contemporary conditions for constant irrigated areas

	CRU 1960-2000		CLM C20 1960-2000		CLM A1b 2001-2050		CLM A1b 2051-2100	
	W	Q	W	Q	W	Q	W	Q
Mean	11.5	188.9	20.5	184.9	23.4	183.2	29.5	148.3
Min	7.7	132.3	13.4	110.0	15.3	108.1	23.1	74.2
Max	17.4	275.4	28.2	291.4	29.9	289.4	37.3	216.7
CV	0.19	0.17	0.15	0.20	0.13	0.23	0.11	0.23
P25	9.6	170.1	18.1	160.2	20.9	153.9	26.5	122.6
P75	13.1	207.9	22.8	205.9	25.4	207.8	32.0	173.3
WEI	6.1		11.1		12.8		19.9	

9.6.5 Summary and Conclusions

The results discussed above suggest that irrigation water demand is increasing substantially due to the effects of climate change on the timing and magnitude of precipitation and higher temperature. At the same time, the available water in the basin sharply decreases. The decrease is most pronounced during low flow periods in the summer months and is generally consistent with the projected increase in the occurrence of severe droughts in areas of south and southern Europe (*Lehner et al.*, 2006b). The combined effect of increasing demand and decreasing supply in the summer months may exert a pressure on local water resources that needs to be taken into account in local and regional water resources planing. As these changes are largely caused by changes in the temporal distribution of precipitation rather than the magnitude of annual values, the results highlight the importance of climate data with a high temporal resolution in climate impact studies. It is important to bear in mind that the results presented above are based on the climate forcings (precipitation and temperature) of one individual regional climate model. However, *Lucarini et al.* (2007) compared several RCMs with regard to the representation of the hydrological cycle in the Danube basin for the period 1961-1990 and found large discrepancies (up to 50%) both for the monthly climatologies and for mean and annual water balances. Although predicted crop water demand is likely to be consistent across climate models (as temperature increases are consistent) the differences in the temporal distribution of precipitation may lead to entirely different results with regard to the supply and demand pattern in the basin. Furthermore, the analysis presented above is based on the assumption that there are no changes in the irrigated areas, the distribution of major crops, and the intensity and efficiency of irrigation water use. Whereas the assumption of little changes in the irrigated areas in Europe is reasonable (*Lehner et al.*, 2006b), variations in the cropping pattern, and water management practices can substantially impact the predictions as well.

10 Summary and Conclusions

10.1 Summary of Results

To investigate the role of irrigation water abstractions and reservoir operation on continental and global water cycles, a macroscale model was developed that explicitly accounts for those human interventions. The development of the new model, WBM_{plus}, was governed by the availability of global data sets for irrigated areas, reservoirs, and related geospatial data sets, both based on statistical data and remotely sensed products. WBM_{plus} simulates the interaction of irrigated areas with non-irrigated areas by explicitly accounting for water withdrawal and return flow from irrigated areas. It is implemented in a modeling framework and can operate with a wide range of geospatial data sets at different resolutions, ranging from one hundred meters to 30 min grid cell size. Based on contemporary data sets of irrigated areas, the modeled volume of water that needs to be abstracted from surface water and groundwater to meet the irrigation water needs was estimated to be around 3000 km^3a^{-1} globally. A comparison of modeled irrigation water withdrawal with reported values from national statistics and other studies showed a reasonable agreement despite differences in some countries. Globally, the model was validated for discharge against observed monthly discharge from a set of 658 discharge stations covering about 50% of the global land mass and showed very little bias suggesting that the model is capable of reproducing long-term continental discharge reasonably well.

Based on time-varying geospatial data sets on irrigated areas and reservoirs that were created from statistical data, the model was used to reconstruct the global hydrography of the last century and to separate trends caused by the climate signal alone and trends caused by human interventions in the hydrological cycle. Over the last century, significant trends in the vertical components of the hydrological cycle suggest increased evapotranspiration with the expansion of irrigated areas. Despite being highly significant in some regions, these changes did not translate to substantial changes or significant trends in the discharge to the oceans over the last 100 years. Furthermore, dramatic reductions in flow imposed by increased evapotranspiration due to the expansion of irrigated areas in individual river basins did not lead to variation in the annual flows entering the oceans. Rather, this variation is governed by variations in the climate forcings over the last century, which is consistent with findings of *Dai et al.* (2009) and *Milliman et al.* (2008). At the global scale, the model did not simulate a significant increase in terrestrial discharge entering the oceans, contradicting the hypothesis of increasing global runoff as a result of global warming (*Labat et al.*, 2004). With the exception of the Arctic Ocean, trends in modeled time series of accumulated streamflow entering the Oceans and endorheic basins over the last century were insignificant, which is also consistent with previous reports (*Dai et al.*, 2009; *Milliman et al.*, 2008). Globally, the most

significant alteration of the hydrological cycle is not induced by the changes in the vertical components but by the distortion of river flow caused by large reservoirs.

The construction of large reservoirs over the last century has gradually but significantly altered the seasonality of streamflow and the dynamics of horizontal water transport in the network of rivers. The construction of reservoirs has led to a threefold increase in the apparent age of water in the horizontal network of rivers globally and even higher increases for individual oceans. These alterations have a number of effects on biogeochemical processes, the transport of sediments, and the cycling of nutrients (*Vörösmarty et al.*, 2003; *Soumis et al.*, 2004; *Seitzinger et al.*, 2002). The model was used to identify river basins under water stress based on simulated irrigation water withdrawal and simulated discharge. Future climate data from a regional climate model was used to assess the impacts of climate change on both irrigation water demand and water supply at the river basin scale. Despite quantitative deviations of model predictions from observed and reported values, the results suggest that the model adequately represents human interventions in the hydrological cycle and that simulations can be used to assess water resources and water demand at large scales. The climate impact assessment showed that future water stress is caused by shifts in the temporal distribution of rainfall rather than by changes in the annual amount. Those variations lead to an increase in irrigation water demand and a decrease in available water resources at the same time and may pose substantial challenges for local water management policies.

The uncertainty in model predictions caused by uncertainties in the input data and the model itself was assessed using a sensitivity analysis for agricultural data sets and Monte-Carlo simulations to estimate the uncertainty in predicted discharge caused by parameter uncertainty and input data. Using two different data sets showing the extent of irrigated areas, results show large uncertainties leading to variations in estimated irrigation water demand of $\pm$ 50% for some countries and $\pm$ 30% for global estimates. Rice paddies have the largest hydrological impact of all irrigated crop types, so uncertainties associated with their distribution and parameterization substantially impacted model results. An analysis of the model parameters and the ability to identify them using the GLUE approach was evaluated on two contrasting river basins (the Mississippi and the Danube river basin). This analysis revealed a wide range of optimal parameter values for individual river basins and a dependence of those parameters on hydroclimatic and geomorphological properties in the basin. To put the estimated uncertainties of discharge predictions into perspective, discharge was simulated using different global precipitation data sets. Variations in the precipitation signal have a much larger impact on simulated discharge than parameter variations.

10.2 Limitations and Uncertainties

The simulation of components of the hydrological cycle under natural and disturbed conditions was limited by a number of uncertainties in the input data as well as structural deficiencies related to the model itself. Data related to agriculture is not often available as explicit geospatial data set and must be taken from national statistics with a resolution much larger than the resolution required for macroscale hydrological models. The uncertainty analysis revealed substantial uncertainties in the spatial distribution of irrigated areas and the cropping intensity globally. Although the application of the model in a heavily irrigated river

basin showed results consistent with observations, predictions of irrigation water demand were found to be highly sensitive to variations in parameters related to the irrigation that are currently available only as country-scale estimates, although the consistency of the results with observations suggests appropriate model assumptions. Furthermore, the time series of irrigated areas created using national statistics do not reflect spatial differences in the dynamics of irrigation expansion within individual countries.

With regard to the distortion of hydrographs due to the operation of reservoirs, the results are limited by the incomplete global repository of registered reservoirs (*Vörösmarty and Sahagian*, 2000). Although the data set of large reservoirs represents an estimated 55% of the total storage volume of impoundments formed by dams over 15 m, river flow is significantly impacted by the operation of smaller reservoirs that are not accounted for in the model but collectively have a significant impact on river flow and sediment retention (*Vörösmarty et al.*, 2003). Furthermore, the current repository of reservoirs provides little information on the purpose of the reservoir and its operation policy which can strongly impact the effect of reservoirs on hydrograph distortion.

The application of the model in selected river basins highlighted some structural problems in the model that limit the application of the model for assessing water availability and demand with regard to sustainability criteria. First and foremost, the estimates on non-sustainable water resources are highly uncertain and limited by the lack of an adequate representation of groundwater that is a general problem of macroscale hydrological models (*Lettenmaier*, 2001). Related to this problem is a structural issue with the model assumptions regarding the supply of irrigation water in a given grid cell; the estimated demand can only be met by abstracting water from stocks or discharge in the same cell. If demand exceeds supply, water is applied under the assumption that it taken from fossil sources. This can lead to an increase of simulated discharge when the effects of irrigation water abstraction are taken into account when part of this water returns from irrigated areas and eventually becomes runoff. This is a widely observed and well-documented phenomenon, in particular in arid regions (e. g. *Abderrahman* (2005); *Al-Weshah* (2000); *Wheida and Verhoeven* (2006)). For example, based on incomplete regional statistics, *Margat et al.* (2006) estimate that the current exploitation of groundwater mining in Northern Africa is around 27 km^3a^{-1}. However, the WBM_{plus} estimated amount of non-sustainable water may be overestimated in some regions of the world. In reality, water demand could be met from horizontally flowing groundwater that does not originate in the same grid cell, from water from neighboring cells that is transported in canals, from reservoirs that are not represented in the model as well as from non-conventional water sources (desalination, waste water re-use, etc.). All of these factors are difficult if not impossible to explicitly consider in macroscale hydrological models that are applied over large spatial domains. As could be shown in Chapter 9.5.4. the simulated values of the amount of water that cannot be met by local resources are dependent on the spatial resolution of the model and will be larger at higher resolutions as the area that can be supplied from one river is smaller. These limitations have to be kept in mind when assessing non-sustainable water abstractions with a macroscale modeling approach such as the one presented here.

With regard to hydrological predictions in general, other studies suggest that the performance of macroscale models can greatly be improved especially during low flow periods if wetlands

and lakes are adequately represented (*Kaspar*, 2004). The hydrology of wetlands and lakes is not explicitly modeled in the current implementation of WBM_{plus}.

It is also important to note that the estimated changes in the magnitude and timing of hydrological components in natural and disturbed model simulations were based soley on climate forcings (precipitation and air temperature), water management practices related to irrigated areas, and the operation of reservoirs. Interactions of atmospheric CO_2 concentration and the hydrological cycle via reduced transpiration and increased runoff (*Betts et al.*, 2007) have not been accounted for. Furthermore, the effects of land use changes (most notably deforestation) have not been included. Such changes have been shown to have significant impacts on the hydrological cycle (*Gordon et al.*, 2005; *Haddeland et al.*, 2007; *Piao et al.*, 2007) and have been linked to increased runoff globally (*Piao et al.*, 2007) at the same order of magnitude as the changes imposed by increased evapotranspiration in irrigated areas (*Gordon et al.*, 2005). Separating the natural and anthropogenic effects of changes in the hydrological cycle is extremely difficult, and the simple method presented here ignores the interrelated links among climate, atmosphere, soil, and vegetation dynamics. For example, it is possible that irrigated areas deliver an additional amount of precipitation (*Moore and Rojstaczer*, 2001, 2002) so that the observed rainfall records already contain an anthropogenic signal. In addition, the analysis is solely based on atmospheric forcings and their effects on runoff and does not consider the potential contribution of melting of permafrost areas and glaciers. Although adding a substantial uncertainty to the model predictions, the limitations discussed so far are small compared to the uncertainties related to global climate data, especially in precipitation data sets. The significance of uncertainties in precipitation on a global-scale water balance context has been shown by *Fekete et al.* (2004). Uncertainties in the precipitation data sets typically translate to higher relative errors in runoff in semiarid regions and the use of different precipitation data sets may therefore lead to different spatial and temporal trends in the hydrological variables.

10.3 Research Needs

To understand the limitations mentioned above, there are several avenues for future research to help understanding the role of human interventions in the continental and global hydrological cycles. The sensitivity analysis revealed that the uncertainties in irrigation water use are related to the input data while uncertainties due to the model parameters are very small. The horizontal flow of water outside the river network is currently not considered in macroscale hydrological models but could help in understanding the role of both renewable and fossil groundwater in supplying water required for irrigation.

To achieve a comprehensive picture of the impact of water abstractions from rivers, aquifers, and lakes, a consistent, systematic, and spatially explicit representation (preferably at high resolution) of irrigated areas is needed. Given the large water demand of paddy rice fields and their implications for water and nutrient cycling, a comprehensive inventory of those areas is critically needed. Remote sensing provides a powerful set of products that can potentially be used to analyze and track agricultural activities over time. Approaches based on remotely sensed and national census data could support the development of such databases (*Xiao et al.*, 2005, 2006; *Frolking et al.*, 2006).

The uncertainties related to the location and hydrological properties of reservoirs will gradually be reduced with the development of more accurate, consistent and comprehensive global inventories of dams and reservoirs in combination with high resolution global river networks that are just beginning to emerge (*Lehner et al.*, 2008).

In addition to higher-resolution input data sets, the model needs to include a better representation of the dynamics of groundwater flow and its interfaces to river discharge. This would help to understand the role of 'loosing streams' in the complex interactions of surface water and groundwater and the role of groundwater in providing water needed for human water use.

The export of water from one basin to another is another important human intervention in the hydrological cycle that needs to be represented in macroscale hydrological models but will remain a challenging task as long as consistent and systemic inventories of interbasin transfers are not available at the global scale. As the uncertainty analysis showed, model predictions are sensitive to conceptual parameters so that spatial variations of those parameters could help improve the model performance. Ideally, the regionalization of those parameters could be associated with physical catchment characteristics (*Hundecha and Bardossy*, 2004). The biggest uncertainty in macroscale hydrological model predictions however, is caused by uncertainties in the climate drivers and significant improvements in model predictions can only be expected if estimates in precipitation data sets are improved. The use of precipitation data sets that are (partly) based on satellite observations such as the Tropical Rainfall Measuring Mission (TRMM), the Global Precipitation Climatology Project 1 degree daily data set (GPCP (*Huffman et al.*, 2001)), and the GPCP Version 2 product (*Adler et al.*, 2003) is limited by the relatively short period of observation but could help reducing the uncertainty in model input data.

Despite those limitation and uncertainties, the results contribute to the understanding of the role of irrigation and reservoirs on global and continental water cycles and can provide information to the improvement of general circulation models with regard to the representation of those human interventions. Furthermore, the results indicate important directions for future research that help minimizing the uncertainties in simulations and for achieving a more comprehensive picture of the role of human interventions in the water cycle.

Bibliography

Abderrahman, W. A. (2005), Groundwater management for sustainable development of urban and rural areas in extremely arid regions: A case study, *International Journal of Water Resources Development*, *21*, 403–412.

Adam, J. C., E. A. Clark, D. P. Lettenmaier, and E. F. Wood (2006), Correction of global precipitation products for orographic effects, *Journal of Climate*, *19*(1), doi: 10.1175/JCLI3604.1.

Adam, J. C., I. Haddeland, F. Su, and D. P. Lettenmaier (2007), Simulation of reservoir influences on annual and seasonal streamflow changes for the Lena, Yenisei and Ob rivers, *Journal of Geophysical Research*, *112*, D24,114.

Adler, R. F., et al. (2003), The version 2 global precipitation climatology poject (GPCP) monthly precipitation analysis (1979-present), *Journal of Hydrometeorology*, *4*, 1147–1167.

Al-Weshah, R. A. (2000), Optimal use of irrigation water in the jordan valley: A case study, *Water Resources Management*, *14*, 327–338.

Alcamo, J., T. Henrichs, and T. Rösch (2000), World water in 2025- global modelling and scenario analysis for the world comission on water for the 21st century, *Tech. rep.*, Center for Environmental Research University of Kassel, Germany.

Alcamo, J., P. Döll, T. Henrichs, F. Kaspar, B. Lehner, T. Rösch, and S. Siebert (2003a), Development and testing the WaterGAP 2 global model of water use and availability, *Hydrological Sciences Journal*, *48*, 317–337.

Alcamo, J., P. Döll, T. Henrichs, F. Kaspar, B. Lehner, T. Rösch, and S. Siebert (2003b), Global estimates of water withdrawals and availability under current and future 'business-as-usual' conditions, *Hydrological Sciences*, *48*, 339–348.

Allen, R., F. Gichuki, and C. Rosenzweig (1991), CO_2-induced climatic changes and irrigation-water requirements, *Journal of Water Resources Planning and Mangement*, *117*(2), 157–178.

Allen, R. G., L. S. Pereira, D. Raes, and M. Smith. (1998), Crop evapotranspiration: guidelines for computing crop water requirements., *Tech. rep.*, Food and Agricultural Organization of the United Nations (FAO).

Alley, W. M., and S. A. Leake (2004), The journey from safe yield to sustainability, *Ground Water*, *42*(1), 12–6.

Amarasinghe, U. A., B. R. Sharma, N. Aloysius, C. Scott, V. Smakhtin, and C. de Fraiture (2005), Spatial variation in water supply and demand across river basins of India, *Tech. rep.*, International Water Management Institute (IWMI).

Anbumozhi, V., K. Matsumoto, and E. Yamaji (2001), Torwards improved performance of irrigation tanks in semi-arid regions of India: modernization opportunities and challanges, *Irrigation and Drainage Systems*, *15*, 293–309.

AQUASTAT, F. (2008), FAOs global information system of water and agriculture, http://www.fao.org/ag/agl/aglw/aquastat/dbase/index.stm.

Arnell, N. W. (1999), A simple water balance model for the simulation of streamflow over a large geographic domain, *Journal of Hydrology*, *217*, 314–335, doi:10.1016/S0022-1694(99)00023-2.

Arnold, J. G., and C. O. Stockle (1991), Simulation of supplemental irrigation from on-farm ponds, *Journal of Irrigation and Drainage Engineering*, *117*, 408–424.

Arora, V. K., and G. J. Boer (2001), Effects of simulated climate change on the hydrology of major river basins, *Journal of Geophysical Research*, *106*(D4), 3335–3348.

Barker, T., et al. (2007), Technical summary, in *Mitigation. Contribution of Working Group III to the Fourth Assessment Report of the Intergovernmental Panel on Climate Change*, Cambridge University Press.

Batjes, N. H. (2002), Global data set of derived soil properties, 0.5-degree grid (ISRIC-WISE), available online (www.daac.ornl.gov).

Baumgartner, A., and E. Reichel (1975), *The world water balance*, Elsevier.

Bazzaz, F., and W. Sombroek (1996), *Global climate change and agricultural production. Direct and indirect effects of changing hydrological, pedological and plant physiological processes*, Wiley and Sons.

Bergström, S. (1995), The HBV model, in *Computer models of watershed hydrology*, edited by V. Singh, W. R. Publications.

Betts, R. A., et al. (2007), Projected increase in continental runoff due to plant responses to increasing carbon dioxide, *Nature*, *448*, 1037–1041.

Beven, K. (2006), A manifesto for the equifinality thesis, *Journal of Hydrology*, *320*, 18–36.

Beven, K., and A. Binley (1992), The future of distributed models: model calibration and uncertainty prediction, *Hydrological Processes*, *6*, 279–298.

BGR (2006), Bundesanstalt für Geowissenschaften - global map of hydrogeological conditions.

Biggs, T. W., P. S. Thenkabail, M. K. Gumman, C. A. Scott, G. R. Parthasaradhi, and H. Turral (2006), Irrigated area mapping in a heterogeneous landscape using MODIS time-series, ground truth, and census data, Krishna basin, India, *International Journal of Remote Sensing*, *27*(19), 4245–4266.

Black, J. N. (1956), The distribution of solar radiation over the Earth's surface, *Wind and Solar Energy Procedings of the New Dehli Symposium*, *1*, 138–140.

Boers, T. M., and J. Benasher (1982), A review of rainwater harvesting, *Agricultural Water Management*, *5*(2), 145–158.

Bouwer, L., J. Aerts, P. Droogers, and A. Dolman (2006), Detecting the long-term impacts from climate variability and increasing consumption on runoff in the Krishna river basin (India), *Hydrology and Earth Sytem Science*, *10*, 703–713.

Bouwer, L. M., J. H. Aerts, and E. van Grol (2003), STREAM Krishna report 2003, *Tech. rep.*, International Water Management Institute.

Bouwer, L. M., T. W. Biggs, , and J. C. J. H. Aerts (2008), Estimates of spatial variation in evaporation using satellite-derived surface temperature and a water balance model, *Hydrological Processes*, *22*, 670–682.

Brass, C., and A. H. Schumann (2003), Planning of operation for multipurpose reservoirs to enhance their reliability under changing conditions, *Proceedings of the 3rd International Conference on Water Resources and Environment Research, Dresden*.

Bronstert, A., J. Carrera, G. Leavesley, and N. Mölders (2005), Scale issues, in *Coupled models for the hydrological cycle: Integrating atmosphere, biosphere and pedosphere*, edited by A. Bronstert, P. Kabat, J. Carrera, and S. Lütkemeier, Springer Berlin.

Brouwer, C., K. Prins, and M. Heibloem (1989), Irrigation water management: Irrigation scheduling; training manual no. 4, *Tech. rep.*, FAO, Rome, Italy.

Bruins, H. J., M. Evenari, and U. Nessler (1986), Rainwater-harvesting agriculture for food production in arid zones: the challenge of the African famine, *Applied Geography*, *6*, 13–32.

Bruntland, G. (1987), *Our common future: the World Comission on Environment and Development*, Oxford University Press.

Brutsaert, W. (1982), *Evaporation into the atmosphere: Theory, history, and applications*, Kluwer Academic Publishers.

Cai, X., and M. W. Rosegrant (2002), Global water demand and supply projections, part 1. A modelling approach, *Water International*, *27*(2), 159–169.

Cai, X., M. W. Rosegrant, and C. Ringler (2003a), Physical and economic efficiency of water use in the river basin: Implications for efficient water management, *Water Resources Research*, *39*, 1–1– 1–12, doi:10.1029/2001WR000748.

Cai, X., D. C. McKinney, and M. W. Rosegrant (2003b), Sustainability analysis for irrigation water management in the Aral Sea region, *Agricultural Systems*, *76*, 1043–1066.

Campbell, J. B. (2002), *Introduction to Remote Sensing*, third ed., Taylor and Francis, London and New York.

Cardille, J. A., J. A. Foley, and M. Costa (2002), Characterizing patterns of agricultural land use in Amazonia by merging satellite classifications and census data, *Global Biogeochemical Cycles*, *16*(3), 18,1–18,12.

Carrera, J., and L. Bastidas (2005), Parametrisation of complex hydrological systems, in *Coupled models for the hydrological cycle: Integrating atmosphere, biosphere and pedosphere*, edited by A. Bronstert, P. Kabat, J. Carrera, and S. Lütkemeier, Springer.

Castellvi, F., I. Mormeneo, and P. Perez (2004), Generation of daily amounts of precipiation from standard climatic data: a case study for Argentina, *Journal of Hydrology*, *289*, 286–302.

Central Water Comission of India (1998), Water and related statistics.

Chen, S.-K., and C. W. Liu (2002), Analysis of water movement in paddy rice fields. (i) experimental studies, *Journal of Hydrology*, *260*, 206–215.

Chmielewski, F.-M. (2003), Phenology and agriculture, *Tech. Rep. 12*, Humboldt-Universität zu Berlin, Institut für Pflanzenbauwissenschaften.

Christensen, J. H., et al. (2007), Regional climate projections, in *Climate Change 2007: The Physical Science Basis. Contribution of Working Group I to the Fourth Assessment Report of the Intergovernmental Panel on Climate*, Cambridge University Press.

Christiaens, K., and J. Feyen (2002), Use of sensitivity and uncertainty measures in distributed hydrological modeling with an application to the MIKE SHE model, *Water Resources Research*, *38*(9), 1169.

Covich, A. P. (1983), Water and ecosystems, in *Water in crisis*, edited by P. H. Gleick, Oxford Univ. Press.

Critchley, W., K. Siebert, and C. Chapman (1991), Water harvesting. a manual for the design and construction of water harvesting schemes, *Tech. rep.*, FAO, Rome.

Custodio, E. (2002), Aquifer overexploitation: what does it mean?, *Hydrogeology Journal*, *10*, 254–277.

Dai, A., and K. E. Trenberth (2002), Estimates of freshwater discharge from continents: latitudinal and seasonal variations, *Journal of Hydrometeorology*, *3*, 660–687.

Dai, A., T. Qian, and K. E. Trenberth (2009), Changes in continental freshwater discharge 1949-2004, *Journal of Climate*, *22*(10), 2773–2792.

Damrath, U., G. Doms, D. Frühwald, E. Heise, B. Richter, and J. Steppeler (2000), Operational quantitative precipitation forecasting at the German weather service, *Journal of Hydrolgy*, *239*, 260–285.

de Rosnay, P., J. Polcher, K. Laval, and M. Sabre (2003), Integrated parameterization of irrigation in the land surface model ORCHIDEE. validation over the Indian peninsula, *Geophysical Research Letters*, *30*(19), 2–1 –2–4, doi:10.1029/2003GL018024.

DeFries, R., and J. Townshend (1994), NDVI-derived land cover classifications at a global scale, *International Journal of Remote Sensing*, *15*, 3567–3586.

Demaria, E. M., B. Nijssen, and T. Wagener (2007), Monte carlo sensitivity analysis of land surface parameters using the Variable Infiltration Capacity model, *Journal of Geophyical Research*, *112*, D11,113.

Devlin, J. F., and M. Sophocleous (2005), The persistence of the water budget myth and its relationship to sustainability, *Hydrogeology Journal*, *13*, 549–554.

Dewandel, B., J.-M. Gandolfi, D. de Condappa, and S. Ahmed (2007), An efficient methodology for estimating irrigation return flow coefficients of irrigated crops at watershed and seasonal scale, *Hydrological Processes*, *22*, 1700–1712.

Dickinson, R. E., et al. (2002), How can we advance our weather and climate model as a community?, *Bulletin of the American Meteorological Society*, *83*(3), 431–434.

Dingman, L. S. (2007), Analytical derivation of at-a-station hydraulic geometry relations, *Journal of Hydrology*, *334*(1-2), 17–27, doi:10.1016/j.jhydrol.2006.09.021.

Döll, P. (2002), Impact of climate change and variability on irrigation requirements: a global perspective, *Climatic Change*, *54*, 269–293.

Döll, P., and K. Fiedler (2008), Global-scale model of groundwater recharge, *Hydrology and Earth System Science*, *12*, 863–885.

Döll, P., and B. Lehner (2002), Validation of a new global 30-min drainage direction map, *Journal of Hydrology*, *258*, 214–231.

Döll, P., and S. Siebert (2000), A digital global map of irrigated areas, *ICID Journal*, *49*(2), 55–66.

Döll, P., and S. Siebert (2002), Global modelling of irrigation water requirements, *Water Resources Research*, *38*(4), 8,2–8,10, doi:10.1029/2001WR000355.

Döll, P., F. Kaspar, and B. Lehner (2003), A global hydrological model for deriving water availability indicators: model tuning and validation, *Journal of Hydrology*, *270*, 103–134.

Douglas, E. M., D. Niyogi, S. Frolking, J. Yelrupruti, R. Pielke Sr, N. Niyogi, C. J. Vörösmarty, and U. Mohanty (2006), Changes in moisture and energy fluxes due to agricultural land use and irrigation in the Indian monsoon belt, *Geophysical Research Letters*, *33*, L14,403, doi:10.1029/2006GL026550.

Downing, J. A., et al. (2006), The global abundance and size distribution of lakes, ponds, and impoundments, *Limnology and Oceananography*, *51*(5), 2388–2397.

Eagleson, P. S. (1986), The emerge of global-scale hydrology, *Water Resources Research*, *22*(9), 6S–14S.

Falkenmark, M., and J. Rockström (2006), The new blue and green water paradigm: Breaking new ground for water resources planning and management, *Journal of Water Resources Planning and Management*, *132*(3), 129–132.

Falkenmark, M., W. Klohn, J. Lundqvist, S. Postel, R. Rockström, D. Seckler, H. Shuval, and J. Wallace (1998), Water scarcity as a key factor behind global food insecurity: round table discussion, *Ambio*, *27*(2), 148–154.

FAO (1997), Irrigation in the countries of the former Soviet Union in figures, *Water report no. 15*, FAO.

FAO (2003), Digital soil map of the world and derived soil properties version 3.6, CD ROM.

FAOSTAT (2008), Statistical database of FAO, available online: http://faostat.fao.org/.

Faures, J.-M., J. Hoogeveen, and J. Bruinsma (2003), The FAO irrigated area forecast for 2030, *Tech. rep.*, FAO, Rome, Italy.

Feddes, R. (1995), Remote sensing- inverse modelling approach to determine large scale effective soil hydraulic properties in soil-vegetation-atmosphere systems, in *Space and time scale variability and interdependencies in hydrological processes*, Cambridge University Press.

Federer, C. A., C. J. Vörösmarty, and B. Fekete (1996), Intercomparison of methods for potential evapotranspiration in regional or global water balance models, *Water Resources Research*, *32*, 2315–2321.

Federer, C. A., C. J. Vörösmarty, and B. Fekete (2003), Sensitivity of annual evaporation to soil and root properties in two models of contrasting complexity, *Journal of Hydrometeorology*, *4*, 1276–1290.

Fekete, B. M., C. J. Vörösmarty, and R. B. Lammers (2001), Scaling gridded river networks for macroscale hydrology: Development, analysis and control of error, *Water Resources Research*, *3*(77), 1955–1967.

Fekete, B. M., C. J. Vörörsmarty, and W. Grabs (2002), High-resolution fields of global runoff by combining observed river discharge and simulated water balances, *Global Biogechemical Cycles*, *16*(3), 15–1–15–10, doi:10.1029/1999GB001254.

Fekete, B. M., C. J. Vörösmarty, J. O. Roads, and C. J. Willmott (2004), Uncertainties in precipitation and their impacts on runoff estimates, *Journal of Climate*, *17*, 294–304.

Fensholt, R. (2004), Earth observation of vegetation status in the Sahelian and Sudanian West Afria: comparison of Terra MODIS and NOAA AVHRR satellite data, *International Journal of Remote Sensing*, *25*, 1641–1659.

Fischer, G., H. van Velthuizen, M. Sha, and F. Nachtergaele (2002), *Global Agro-ecological Assessment for Agriculture in the 21st Century: Methodology and Results*, IIASA Research Report, International Institute for Applied Systems Analysis, Laxenburg, Austria.

Foley, J. A., et al. (2005), Global consequences of land use, *Science*, *309*, 570–574.

Foster, S. S. D., and P. J. Chilton (2003), Groundwater: the processes and global significance of aquifer degradation, *Philosophical Transactions of the Royal Society B*, *358*, 1957–1972, doi:10.1098/rstb.2003.1380.

Freydank, K., and S. Siebert (2008), Towards mapping the extent of irrigation in the last century: time series of irrigated area per country, *Frankfurt Hydrology Paper 08*, Institute of Physical Geography, University of Frankfurt, Frankfurt am Main, Germany.

Friend, A. (1998), Parameterisation of a global daily weather generator for terrestrial ecosystem modeling, *Ecological Modeling*, *109*, 121–140.

Froking, S., J. Qiu, S. Boles, X. Xiao, J. Liu, Y. Zhuang, C. Li, and X. Qin (2002), Combining remote sensing and ground census data to develop new maps of the distribution of rice agriculture in China, *Global Biogeochemical Cycles*, *16*(4), 38,1–38,10.

Frolking, S., T. Frolking, X. Xiao, S. Boles, and T. Milliman (2005), A generalized methodology for incorporating remote sensing data into mapping agricultural land use and management at sub-national scales including a case study of combining census data and remote sensing data to map cropping intensity in vietnam, *Report prepared for the FAO AGLL*, Institute for the Study of Earth, Oceans, & Space.

Frolking, S., J. B. Yeluripati, and E. Douglas (2006), New district-level maps of rice cropping in India: a foundation for scientific input into policy assessment, *Food Crops Research*, *98*((2-3)), doi:10.1016/j.fcr.2006.01.004.

Galy-Lacaux, C., R. Delmas, G. Kouadio, S. Richard, and P. Gosse (1999), Long-term greenhouse gas emissions from hydroelectric reservoirs in tropical forest regions, *Global Biogeochemical Cycles*, *13*(2), 503–518.

Gattke, C. (2006), Modellvergleiche zur Untersuchung struktureller Unsicherheiten- Anwendung objektorientierter Methoden in der hydrologischen Modellierung, Ph.D. thesis, Ruhr Universität Bochum, Germany.

Gaur, A., P. G. MCCornick, H. Turral, and S. Acharya (2007), Implications of drought and water regulation in the Krishna basin, India, *Water Reources Development*, *23*(4), 583–594.

Geng, S., F. W. T. P. de Fries, and I. Supit (1986), A simple method for generating daily rainfall data, *Agricultural and Forest Meteorology*, *36*, 363–376.

Georgiou, P., D. Papamichail, and S. Vougioukas (2006), Optimal irrigation reservoir operation and simultaneous multi-crop cultivation area selection using simulated annealing, *Irrigation and Drainage*, *55*(2), 129–144.

Glantz, M. (2005), Water, climate, and development issues in the Amu Darya basin, *Mitigation and Adaptation Strategies for Global Change*, *10*(1), 22–50.

Gleick, P. H. (2003), Water use, *Annual Review of Environmental Resources*, *28*, 275–314, doi:10.1146/annurev.energy.28.040202.122849.

Gollehon, N., and W. Quinby (2000), Irrigation in the American west: area, water and economic activity, *Water Resources Development*, *16*(2), 187–195.

Gordon, L. J., W. Steffen, B. F. Jönsson, C. Folke, M. Falkenmark, and A. Johannssen (2005), Human modifications of global water vapor flows from the land surface, *Proceedings of the National Academy of Science*, *102*(21), 7612–7617, doi:10.1073 pnas.0500208102.

Green, P., C. J. Vörösmarty, M. Meybeck, J. Galloway, B. J. Peterson, and E. W. Boyer (2004), Pre-industrial and contemporary fluxes of nitrogen through rivers: a global assessment based on topology, *Biogeochemistry*, *68*, 71–105.

Gregorio, A. D., and L. J. M. Jansen (2000), *Land cover classification system (LCCS): Classification concepts and user manual*, FAO Rome.

Groten, S., and R. Ocatre (2002), Monitoring the length of the growing season with NOAA, *International Journal of Remote Sensing*, *23*(14), 2797–2815.

Guera, L., S. I. Bhuiyan, T. Tuong, and R. Barker (1998), Producing more rice with less water from irrigation systems, *Tech. Rep. 29*, International Rice Research Institute, Manila, Phillippines.

Gunnel, Y., and A. Krishnamurthy (2003), Past and present status of runoff harvesting systems in dryland peninsular india: A critical review, *Ambio*, *32*(4), 320–324.

Haddeland, I., D. P. Lettenmaier, and T. Skaugen (2006a), Effects of irrigation on the water and energy balances of the Colorado and Mekong river basins, *Journal of Hydrology*, *324*, 210–223, doi:10.1016/j.jhydrol.2005.09.028.

Haddeland, I., T. Skaugen, and D. P. Lettenmaier (2006b), Anthropogenic impacts on continental surface water fluxes, *Geophysical Research Letters*, *33*(8), L08,406, doi: 10.1029/2006GL026047.

Haddeland, I., T. Skaugen, and D. P. Lettenmaier (2007), Hydrologic effects of land and water management in North America and Asia: 1700-1992, *Hydrology and Earth System Science*, *11*, 1035–1045.

Hafeez, M. M. (2003), Water accounting and productivity at different spatial scales in a rice irrigation system: A remote sensing approach, Ph.D. thesis, Center for Development Research, University of Bonn.

Hamon, W. R. (1963), Computation of direct runoff amounts from storm rainfall, *Int. Assoc. Sci. Hydrol. Publ.*, *63*, 52–62.

Hanasaki, N., S. Kanae, and T. Oki (2006), A reservoir operation scheme for global river routing models, *Journal of Hydrology*, *327*(1-2), 22–41, doi: 10.1016/j.jhydrol.2005.11.011.

Hanasaki, N., S. Kanae, T. Oki, and N. Shirakawa (2008), An integrated model for the assessment of global water resources: Part 2: Applicatios and assessments:, *Hydrology and Earth System Sciences*, *12*, 1007–1025.

Hansen, J. W., and A. Ines (2005), Stochastic disaggregation of monthly rainfall data for crop simulation studies, *Agricultural and Forest Meteorology*, *131*, 233–246.

Hansen, M., R. DeFries, J. Townshend, and R. Sohlberg (2000), Global land cover classification at 1km resolution using a decision tree classifier, *International Journal of Remote Sensing*, *21*, 1331–1365.

Hargreaves, G. H., and G. P. Merkley (1998), *Irrigation Fundamentals*, Water Resources Publications.

Hartkamp, A. D., J. W. White, W. A. H. Rossing, M. K. van Ittersum, E. J. Bakker, and R. Rabbinge (2004), Regional application of a cropping systems simulation model: crop residue retention in maize production systems of Jalisco, Mexico, *Agricultural Systems*, *82*(2), 117–138.

Hartley, A., J.-F.Pekel, M.Ledwith, J.-L.Champeaux, E. Badts, and S.A.Bartalev (2006), Glc2000 database, *Tech. rep.*, European Commision Joint Research Centre.

Harvey, L. D. D. (2000), Upscaling in global change research, *Climatic Change*, *44*, 225–263.

Hillen, D. (1980), *Introduction to soil physics*, Academic Press, London, UK.

Hollweg, H.-D., et al. (2008), Ensemble simulations over Europe with the regional climate model CLM forced with IPCC AR4 global scenarios, *Tech. rep.*, Max-Planck Institut für Meteorologie Hamburg.

Huang, M., and X. Liang (2006), On the assessment of the impact of reducing parameters and identification of parameters for hydrologic model with applications to ungauged basins, *Journal of Hydrology*, *320*, 37–61.

Huffman, G. J., R. F. Adler, M. Morrissey, D. T. Bolvin, S. Curtis, R. Joyce, B. McGavock, and J. Susskind (2001), Global precipitation at one-degree daily resolution from multi-satellite observations, *Journal of Hydrometeorology*, *2*, 36–50.

Hulme, M., T. J. Osborn, and T. C. Johns (1998), Precipitation sensitivity to global warming: comparison of observations with HadCM2 simulations, *Geophyical Research Letters*, *25*(17), 3379–3382.

Hundecha, Y., and A. Bardossy (2004), Modeling of the effect of land use changes on the runoff generation of a river basin through parameter regionalization of a watershed model, *Journal of Hydrology*, *292*(1-4), 281–295.

Hunger, M., and P. Döll (2007), Value of river discharge data for global-scale hydrological modeling, *Hydrology and Earth System Science*, *4*, 4125–4173.

ICOLD (2003), *World Register of Dams*, International Comission on Large Dams ICOLD.

IGRAC (2006), International Groundwater Resources Assessment Centre, http:/igrac.nitg.tno.nl/homepage.

Israelsen, O. W., and V. Hansen (1962), *Irrigation Principles and Practices*, 3rd edition ed., John Wiley and Sons.

Izaurralde, R. C., N. J. Rosenberg, R. A. Brown, and A. M. Thomson (2003), Integrated assessment of Hadley Center (HadCM2) climate-change impacts on agricultural productivity and irrigation water supply in the conterminous United States part ii. regional agricultural production in 2030 and 2095, *Agricultural and Forest Meteorology*, *117*, 97–122.

Jain, S., N. Reddy, and U. Chaube (2005), Analysis of a large inter-basin water transfer system in India, *Hydrological Sciences Journal*, *50*(1), 125–137.

Kahinda, J. M. M., J. Rockström, A. E. Taigbenu, and J. Dimes (2008), Rainwater harvesting to enhance water productivity of rainfed agriculture in semi-arid Zimababwe, *Physics and Chemistry of the Earth*, *32*, 1068–1073.

Kalnay, E., et al. (1996), The NCEP/NCAR 40-year reanalysis project, *Bulletin of the American Meteorological Society*, *77*(3), 437–471.

Kaspar, F. (2004), Entwicklung und Unsicherheitsanalyse eines globalen hydrologischen Models, Ph.D. thesis, Universität Kassel.

Keller, A., J. Keller, and D. Seckler (1996), Integrated water resource systems: Theory and policy implications, Research Report No. 3. International Irrigation Management Institute, Colombo Sri Lanka.

Kendy, E., and J. D. Bredehoeft (2006), Transient effects of groundwater pumping and surface-water-irrigation returns on streamflow, *Water Resources Research*, *42*, W08,415, doi:10.1029/2005WR004792.

Kendy, E., P. Gerard-Marchant, M. T.Walter, Y.Zhang, C. Liu, and T. S. Steenhuis (2003), A soil-water-balance approach to quantify groundwater recharge from irrigated cropland in the North China Plain, *Hydrological Processes*, *17*, 2011–2031.

Kendy, E., Y. Zhang, C. Li, J. Wang, and T. S. Steenhuis (2004), Groundwater recharge from irrigated cropland in the north china plain: case study of Luancheng County, Hebei province, 1949-2000, *Hydrological Processes*, *18*(12), 2289–2302.

Kim, H. K., T. I. Jang, S. Im, and S. W. Park (2009), Estimation of irrigation return flow from paddy fields considering the soil moisture, *Agricultural Water Management*, *96*, 875–882.

Kite, G. W. (1995), Scaling of input data for macroscale hydrologic modeling, *Water Resources Research*, *31*(3), 1769–2781, doi:10.1029/95WR02102.

Klêmes, V. (1986), Operational testing of hydrological simulation models., *Hydrological Sciences Journal*, *31*(1), 13–24.

Knighton, D. (1998), *Fluvial Processes*, Hodder Arnold.

Kramer, H. J. (2002), *Observation of the Earth and its Environment- Survey of Missions and Sensors*, vol. 4, Springer Berlin.

Krause, P., D. P. Boyle, and F. Bäse (2005), Comparison of different efficiency criteria for hydrological model assessment, *Advances in Geoscience*, *5*, 89–97.

Kueppers, L. M., M. A. Snyder, and L. C. Sloan (2007), Irrigation cooling effect: regional climate forcing by land-use change, *Geophysical Research Letters*, *34*, L03,703, doi:10.1029/2006/GL028679.

Labat, D., Y. Godderis, J. L. Probst, and J. L. Guyot (2004), Evidence for global runoff increase related to climate warming, *Advances in Water Resources*, *27*(6), 631–642.

Leff, B., N. Ramankutty, and J. A. Foley (2004), Geographic distribution of major crops across the World, *Global Biogeochemical Cycles*, *18*(GB1009), doi: 10.1029/2003GB002108.

Lehner, B., K. Verdin, and A. Jarvis (2006a), HydroSHEDS technical documentation, *Tech. rep.*, World Wildlife Fund, Washington DC.

Lehner, B., P. Döll, J. Alcamo, T. Henrichs, and F. Kaspar (2006b), Estimating the impact of global change on flood and drought risks in Europe: A continental, integrated analysis, *Climatic Change*, *75*(3), 273–299.

Lehner, B., K. Verdin, and A. Jarvis (2008), New global hydrography derived from spaceborne elevation data, *EOS Transactions*, *89*(10), 93–94.

Lettenmaier, D. P. (2001), Macroscale hydrology: Challanges and opportunities, in *Present and future of modeling global environmental change: toward integrated modeling*, edited by T. Matsuno and H. Kida, pp. 111–136, TERRAPUB.

Li, C., J. J. Qiu, S. Frolking, X. Xiao, W. Salas, B. Moore, S. Boles, Y. Huang, and R. Sass (2002), Reduced methane emissions from large-scale changes in water management of China's rice paddies during 1998-2000, *Geophysical Research Letters*, *29*(20), doi:10.1029/2002GL015370.

Li, K. Y., M. T. Coe, and N. Ramankutty (2005), Investigation of hydrological variability in West Africa using land surface models, *Journal of Climate*, *18*(16), 3173– 3189.

Liang, X., D. P. Lettenmaier, E. F. Wood, and S. J. Burges (1994), A simple hydrologically based model of land surface water and energy fluxes for general circulation models, *Journal of Geophysical Research*, *99*(D7), 13,415–14,428.

Liang, X., D. P. Lettenmaier, and E. F. Wood (1996), One-dimensional statistical dynamics representation of subgrid spatial variability of precipitation in the two-layer Variable Infiltration Capacity model, *Journal of Geophysical Research*, *101*(D 16), 21,403–21,422.

Lillesand, T. M., R. W. Kiefer, and J. W. Chipman (2003), *Remote Sensing and Image Interpretation*, Wiley.

Loaiciaga, H. A. (2002), Sustainable ground-water exploitation, *International Geology Review*, *44*, 1115–1121(7).

Loveland, T., and A. Belaward (1997), The IFBP-DIS global 1 km land cover data set, DISCover: First results, *International Journal of Remote Sensing*, *18*(5), 3289–3295.

Lucarini, V., R. Danihik, and I. Kriegerova (2007), Does the Danube exist? Versions of reality given by various regional climate models and climatological data sets, *Journal of Geophysical Research*, *112*, D13,103, doi:10.1029/2006JD008360.

Lucarini, V., R. Danihlik, I. Kriegerova, and A. Speranza (2008), Hydrological cycle in the Danube basin in present-day and XXII century simulations by IPCCAR4 global climate models, *Journal of Geophyical Research*, *113*, D09,107.

Maclean, J. L., D. C. Dawe, B. Hardz, and G. P. Hettel (2002), *Rice Almanac*, CAB Publishing.

Mantovan, P., and E. Todini (2006), Hydrological forecasting uncertainty assessment: incoherence of the GLUE methodology, *Journal of Hydrology*, *330*, 368–381.

Margat, J., S. Foster, and A. Droubi (2006), Groundwater resources - a guidebook of socially-sustainable managment for water-policy makers, in *Groundwater resources - a guidebook of socially-sustainable managment for water-policy makers*, edited by S. Foster and D. P. Loucks, UNESCO.

Martinez-Alvarez, V., M. M. Gonzalez-Real, A. Baille, J. F. M. Valero, and B. B. Gallego Elvira (2008), Regional assessment of evaporation from agricultural irrigation reservoirs in a semiarid climate, *Agricultural Water Management*, *95*(9), 1056–1066.

Maselli, F., and F. Rembold (2001), Analysis of GAC NDVI data for cropland identification and yield forecasting in Mediterranean African countries, *Photogrammetric Engineering and Remote Sensing*, *67*(5), 593–602.

McCarthy, G.-T. (1938), The unit hydrograph and flood routing, *Conference North Atlantic Division, US Army Corporation of Engineers*.

McCuen, R. H. (2003), *Modeling Hydrologic Change: statistical methods*, Lewis Publishers.

Meehl, G. A., et al. (2007), Global climate projections, in *Climate Change 2007: The Physical Science Basis. Contribution of Working Group I to the Fourth Assessment Report of the Intergovernmental Panel on Climate Change*, edited by S. Solomon, D. Qin, M. Manning, Z. Chen, M. Marquis, K. b. Averyt, M. Tignor, and H. L. Hiller, Cambridge University Press.

Meybeck, M. (2003), Global analysis of river systems: from Earth system controls to Anthropocene syndromes, *Philos Trans R Soc Lond B Biol Sci.*, *358*, 1935–1955, doi: 10.1098/rstb.2003.1379.

Mialhe, F., Y. Gunnel, and C. Mering (2008), Synoptic assessment of water resource variability in reservoirs by remote sensing: General approach and application to the runoff harvesting systems of south india, *Water Resources Research*, *44*(5), W05,411.

Micklin, P. (2006), The Aral Sea disaster, *Annual Review of Earth and Planetary Science*, *35*, 47–72.

Milliman, J. D., K. L. Farnsworth, P. D. Jones, K. H. Xu, and L. C. Smith (2008), Climatic and anthropogenic factors affecting river discharge to the global ocean, 1951-2000, *Global and Planetary Change*, *62*, 187–195.

Milly, P. C. D., K. A. Dunne, and A. V. Veccchia (2005), Global pattern of trends in streamflow and water availability in a changing climate, *Nature*, *437*, 347–350, doi: 10.1038/nature04312.

Mitchell, T. D., and P. D. Jones (2005), An improved method of constructing a database of monthly climate observations and associated high-resolution grids, *International Journal of Climatology*, *25*(6), 693–712, doi:10.1002/joc.1181.

Moench, M., J. Burke, and Y. Moench (2003), *Rethinking the approach to groundwater and food security*, Water Report, 24 ed., Food and Agriculture Organization (FAO) of the United Nations.

Mölders, N. (2005), Feedbacks at the hydrometeorological interface, in *Coupled models for the hydrological cycle: Integrating atmosphere, biosphere and pedosphere*, edited by A. Bronstert, P. Kabat, J. Carrera, and S. Lütkemeier, Springer Berlin.

Monfreda, C., N. Ramankutty, and J. A. Foley (2008), Farming the planet: 2. geographic distribution of crop areas, yields, physiological types, and net primary production in the year 2000, *Global Biogeochemical Cycles*, *22*, GB1022, doi:10.1029/2007GB002947.

Moore, N., and S. Rojstaczer (2001), Irrigation-induced rainfall and the Great Plains, *Journal of Applied Meteorology*, *40*(8), 1297–1309.

Moore, N., and S. Rojstaczer (2002), Irrigation's influence on precipitation: Texas High Plains, U.S.A., *Geophyical Research Letters*, *29*(16).

Nagy, I., K. Asante-Duah, and I. Zsuffa (2002), *Hydrological dimensioning and operation of dams*, Kluwer Academic Publishers.

Nash, J., and J. V. Sutcliffe (1970), River flow forecasting through conceptual models. Part I-A discussion of principles, *Journal of Hydrology*, *10*(3), 282–290.

New, M., M. Hume, and P. Jones (1999), Representing twentieth century space-time climate variability; i: Development of 1960-90 mean monthly terrestrial climatology, *Journal of Climate*, *12*, 829–856.

New, M., M. Hume, and P. Jones (2000), Representing twentieth century space-time climate variability; ii: Development of 1901-1996 monthly grids of terrestrial surface climate, *Journal of Climate*, *13*, 2217–2238.

New, M., D. Lister, M. Hulme, and I. Makin (2002), A high-resolution data set of surface climate over global land areas, *Climate Research*, *21*, 1–25.

Nezlin, N. P., A. G. Kostianoya, and S. A. Lebedevc (2004), Interannual variations of the discharge of Amu Darya and Syr Darya estimated from global atmospheric precipitation, *Journal of Marine Systems*, *47*(1-4), 67–75.

Nickum, J. E. (2003), Irrigated area figures and bureaucratic construction of knowledge: the case of China, *Water Resources Development*, *19*(2), 249–262, doi: 10.1080/0790062032000089347.

Nijssen, B., D. P. Lettenmaier, X. Liang, S. W. Wetzel, and E. F. Wood (1997), Streamflow simulation for continental-scale river basins, *Water Resources Research*, *33,4*, 711–724.

Nilsson, C., C. A. Reidy, M. Dynesius, and C. Revenga (2005), Fragmentation and flow regulation of the world's large river systems, *Science*, *308*, 405–408.

O'Callaghan, J. F., and D. M. Mark (1984), The extraction of drainage networks from digital elevation data, *Computer Vision, Graphics, and Image Process*, *28*(3), 323–344.

Oki, T., and S. Kanae (2006), Global hydrological cycles and world water resources, *Science*, *313*(5790), 1069–1072.

Oki, T., and Y. Sud (1998), Design of total runoff integrating pathways (TRIP)- a global river channel network, *Earth Interactions*, *2*, 2–36.

Oki, T., Y. Agata, S. Kanae, T. Saruhashi, D. Yang, and K. Musiake (2001), Global assessment of current water resources using total runoff integrating pathways, *Hydrological Sciences Journal*, *46*, 983–995.

Olivera, F., M. S. Lear, J. S. Famiglietti, and K. Asante (2002), Extracting low-resolution river networks from high-resolution digital elevation data, *Water Resources Research*, *38*(11), 1231.

Oudin, L., F. Hervieu, c. Michel, C. Perrin, V. Andréassian, F. Anctil, and C. Loumagne (2005), Which potential evapotranspiration input for a lumped rainfall-runoff model ? part 2-towards a simple and efficient potential evapotranspiration model for rainfall-runoff modelling, *Journal of Hydrology*, *303*, 290–306.

Ozdogan, M., and G. Gutman (2008), A new methodology to map irrigated areas using multi-temporal MODIS and ancillary data: An application example in the continental US, *Remote Sensing of Environment*, *112*, 3520–3537.

Peneva, E., E. Stanev, S. Stanychni, A. Salokhiddinov, and G. Stulina (2004), The recent evolution of the Aral Sea level and water properties: analysis of satellite, gauge and hydrometeorological data, *Journal of Marine Systems*, *47*, 11–24.

Penuelas, J., and I. Filella (2001), Phenology: Responses to a warming world, *Science*, *294*(5543), 793–795, doi:10.1126/science.1066860.

Perrin, C., C. Michel, and V. Andreassian (2001), Does a large number of parameters enhance model performance ? Comparative assessment of common catchment model structures on 429 catchments, *Journal of Hydrology*, *242*, 275–301.

Perry, C. J. (1999), The IMWI water resources paradigm- defintions and implications, *Agricultural Water Management*, *40*, 45–50.

Peterson, B. J., R. M. Holmes, J. W. McClelland, C. J. Vörösmarty, R. B. Lammers, A. I. Shiklomanov, I. A. Shiklomanov, and S. Rahmstorf (2002), Increasing river discharge to the Arctic Ocean, *Science*, *298*(5601), 5172–5173.

Piao, S., P. Friedlingstein, P. Ciais, N. D. Noblet-Ducoudre, D. Labat, and S. Zaehle (2007), Changes in climate and land use have a larger direct impact than rising CO_2 on global river runoff trends, *PNAS*, *104*(39), 15,242–15,247.

Pimentel, D., et al. (2004), Water resources: Agricultural and environmental issues, *BioScience*, *54*(10), 909–918.

Pitman, A. J. (2003), The evolution of, and revolution in, land surface schemes designed for climate models, *International Journal of Climatology*, *23*(5), 479–510.

Ponce, V. M., and V. Yevjevich (1978), The Muskingum-Cunge method with variable parameters, *ASCE J. Hydraul. Div.*, *104*, 1663–1669.

Postel, S. (1997), *Last Oasis-Facing Water Scarcity*, Worldwatch Environmental Alert Series, second ed., W.W. Norton and Company, New York, London.

Postel, S. (1998), Water for food:will there be enough in 2025?, *BioScience*, *48*(8), 629–637.

Postel, S. (1999), *Pillar of sand- can the irrigation miracle last?*, Worldwatch Series, W.W. Norton and Company.

Qadir, M., B. R. Sharma, A. Bruggeman, R. Choukr-Allah, and F. Karajeh (2007), Non-conventional water resources and opportunities for water augmentation to achieve food security in water scarce countries, *Agricultural Water Management*, *87*(1), 2–22.

Qian, T., A. Da, and K. E. Trenberth (2007), Hydroclimatic trends in the Mississippi river basin from 1948 to 2004, *Journal of Climate*, *20*, 4599–4613.

Ramankutty, N., and J. Foley (1998), Characterizing patterns of global land use: An analysis of global croplands data, *Global Biogechemical Cycles*, *12*(4), 667–685.

Ramankutty, N., A. T. Evan, C. Monfredo, and J. A. Foley (2008), Farming the planet: 1. geographic distribution of global agricultural lands in the year 2000, *Global Biogeochemical Cycles*, *22*, GB1003, doi:10.1029/2007GB002952.

Rawlins, M. A., R. B. Lammers, S. Frolking, B. M. Fekete, and C. J. Vörörsmarty (2002), Simulating pan-arctic runoff with a macro-scale terrestrial water balance model, *Hydrological Processes*, *17*, 2521–2539.

Rawlins, M. A., C. J. Willmott, A. Shiklomanov, E. Linder, S. Frolking, R. B. Lammers, and C. J. Vörösmarty (2006), Evaluation of trends in derived snowfall and rainfall across Eurasia and linkages with discharge to the Arctic Ocean, *Geophysical Research Letters*, *33*(7), L07,403.

Replogle, J. A., A. Clemmens, and M. Jensen (1996), Irrigation systems, in *Water Resources Handbook*, edited by L. Mays, 1 ed., chap. 22, MacGraw-Hill.

Richardson, C. (1981), Stochastic simulation of daily precipitation, temperature, and solar radiation, *Water Resources Research*, *17*(1), 182–190.

Rockström, J. (1999), On-farm green water estimates as a tool for increased food production in water scarce regions, *Physics and Chemistry of the Earth Part B-Hydrology Oceans and Atmosphere*, *27*(11-22), 949–959.

Roeckner, E., et al. (2003), The atmosphere general circulation model ECHAM5, *Report 349*, Max-Planck-Institut für Meteorologie.

Rosenzweig, C., K. M. Strzepek, D. C. Major, A. Iglesia, D. N. Yates, A. Mccluskey, and D. Hillel (2004), Water resources for agriculture in a changing climate: international case studies, *Global Environmental Change*, *14*, 345–360.

Rost, S., D. Gerten, A. Bondeau, W. Lucht, J. Rohwer, and S. Schaphof (2008), Agricultural green and blue water consumption and its influence on the global water system, *Water Resources Research*, *44*(9), W09,405.

Rudolf, B., H. Hauschild, W. Rueth, and U. Schneider (1994), Terrestrial precipitation analysis: operational method and required density of point measurements, in *Global Precipitations and Climate Change*, *NATO ASI Series*, vol. I, 26, edited by M. Desbois and F. Desalmond, pp. 173–186, Springer Verlag.

Rushton, K. (1997), Recharge from permanent water bodies, in *Recharge of Phreatic aquifers in (semi-) arid areas*, edited by I. Simmers, Balkema, Rotterdam.

Saiko, T. S., and I. S. Zonn (2000), Irrigation expansion and dynamics of desertification in the Circum-Aral region of Central Asia, *Applied Geography*, *20*, 349–367.

Satti, S. R., J. M. Jakobs, and S. Irmak (2004), Agricultural water management in a humid region: sensitivity to climate, soil and crop parameters, *Agricultural Water Management*, *70*, 51–65.

Schiemann, R., M. G. Glazirina, and C. Schär (2007), On the relationship between the Indian summer monsoon and river flow in the Aral Sea basin, *Geophyical Research Letters*, *34*, L05,706.

Seitzinger, S. P., R. V. Styles, E. W. Boyer, R. B. Alexander, G. Billen, R. Howarth, B. Mayer, and N. van Breemen (2002), Nitrogen retention in rivers: model development and application to watersheds in the northeastern USA, *Biogeochemistry*, *57*, 199–237.

Serreze, M. C., et al. (2006), The large-scale freshwater cycle of the Arctic, *Journal of Geophysical Research-Oceans*, *111*, C11,010.

Shah, T., O. Singh, and A. Mukherji (2006), Some aspects of South Asia's groundwater irrigation economy: analyses from a survey in India, Pakistan, Nepal Terai and Bangladesh, *Hydrogeology Journal*, *14*, 286–309.

Sharma, K. P., C. J. Vörösmarty, and B. Moore (2000), Sensitivity of the Himalyan hydrology to land-use and climate changes, *Climatic Change*, *47*(1-2), 117–139.

Shibuo, Y., J. Jarsjö, and G. Destouni (2007), Hydrological responses to climate change and irrigation in the Aral Sea drainage basin, *Geophysical Reserach Letters*, *34*, L21,406, doi:10.1029/2007GL031465.

Shiklomanov, I., and J. Rodda (2003), *World Water Resources at the Beginning of the Twenty-First Century*, Cambridge University Press.

Shuttleworth, W. J. (1992), Evaporation, in *Handbook of Hydrology*, edited by D. R. Maidment, McGraw-Hill Inc.

Siebert, S., and P. Döll (2007), Irrigation water use -a global perspective, in *Global Change: enough water for all?*, pp. 104–107, Universität Hamburg/GEO.

Siebert, S., P. Döll, J. Hoogeveen, J.-M. Faures, K. Frenken, and S. Feick (2005), Development and validation of the global map of irrigated areas, *Hydrology and Earth Systems Sciences*, *9*, 535–547.

Simmers, I. (1997), Groundwater recharge principles, problems and developments, in *Recharge of Phreatice aquifers in (semi-) arid areas*, edited by I. Simmers, Balkema, Rotterdam.

Singh, D. K., and A. K. Singh (2002), Groundwater situation in India: Problems and perspective, *Water Resources Development*, *18*, 562–580.

Sitch, S., et al. (2003), Evaluation of ecosystem dynamics, plant geography and terrestrial carbon cycling in the LPJ dynamic global vegetation model, *Global Change Biology*, *9*(2), 161–185.

Soumis, N., E. Duchemin, R. Canuel, and M. Lucotte (2004), Greenhouse gas emissions from reservoirs in the western United States, *Global Biogeochemical Cycles*, *18*, GB3022, doi:10.1029/2003GB002197.

Srikanthan, R., and T. A. McMahon (2001), Stochastic generation of annual, monthly and daily climate data: a review, *Hydrology and Earth System Sciences*, *5*(4), 653–670.

Srivastava, R. C. (2001), Methodology for design of water harvesting system for high rainfall areas, *Agricultural Water Management*, *47*, 37–53.

St.Louis, V., C. A. Kelly, E. Duchemin, J. W. M. Rudd, and D. M. Rosenberg (2000), Reservoir surfaces as sources of greenhouse gases to the atmosphere: A global estimate, *BioScience*, *50*(9), 766–775.

Suyker, A. E., and S. B. Verma (2009), Evapotranspiration of irrigated and rainfed maize-soybean cropping systems, *Agricultural and Forest Meteorology*, *149*, 443–452.

Syvitski, J. P., C. J. Vörösmarty, A. J. Kettner, and P. Green (2005), Impact of humans on the flux of terrestrial sediment to the global coastal ocean, *Science*, *308*(5270), 376–380.

Tabbla, D., B. Bouman, S. Bhuiyan, E. Sibayan, and M. Sattar (2002), On-farm strategies for reducing water inputs in irrigated rice; case studies in the philippines, *Agricultural Water Management*, *56*, 93–112.

Tan, G., and R. Shibasaki (2003), Global estimation of crop productivity and the impacts of global warmng by GIS and EPIC integration, *Ecological Modelling*, *168*, 357–370.

Tanji, K. K., and N. C. Kielen (2002), Agricultural drainage water management in arid and semi-arid areas, FAO Irrigaiton and Drainage Paper No. 61.

Thenkabail, P. S., M. Schull, and H. Turall (2005), Ganges and Indus river basin land use/land cover LULC and irrigated area mapping using continous stream of MODIS data, *Remote Sensing of Environment*, *95*(3), 317–341.

Thenkabail, P. S., et al. (2006), An irrigated area map of the World (1999) derived from remote sensing, *Tech. rep.*, International Water Management Institute (IWMI).

Tian, X., A. Dai, D. Yang, and Z. Xie (2007), Effects of precipitation-bias correction on surface hydrology over northern latitudes, *Journal of Geophysical Research Letters*, *112*, D14,101, doi:10.1029/2007JD008420.

Tilman, D., K. G. Cassmann, P. A. Matson, R. Naylor, and S. Polasky (2002), Agricultural sustainability and intensive production practices, *Nature*, *418*(6898), 671–677.

Ting, C.-S., I. Tsou, and J.-H. Lu (2005), A study on the estimation of groundwater recharge by agriculture irrigation, *Irrigation and Drainage*, *54*, 339–351.

Trenberth, K. E., and A. Dai (2007), Effects of Mount Pinatubo volcanic eruption on the hydrological cycle as an analog of geoengineering, *Geophyical Research Letters*, *34*(15), L15,702.

Tuong, T., and S. I. Bhuiyan (1999), Increasing water-use efficiency in rice production: farm-level perspectives, *Agricultural Water Management*, *40*, 117–122.

Uhlenbrock, S. (2005), Von der Abflussbildungsprozessforschung zur prozessorientieren Modellierung- ein Review, *Hydologie und Wasserwirtschaft*, *49*(1), 13–24.

USDA (2002), United States Department of Agriculture- agricultural census 2002, available at www.agcensus.usda.gov/.

Vijayalakshmib, S. M. D. (2009), Prediction of irrigation return flows through a hierarchical modeling approach, *Agricultural Water Management*, *96*, 233–246.

Vörösmarty, C. J., C. A. Federer, and A. L. Schloss (1998), Potential evaporation functions compared on US watersheds: Implications for global-scale water balance and terrestrial ecosystem modeling, *Journal of Hydrology*, *207*, 147–169, doi:10.1016/S0022-1694(98)00109-7.

Vörösmarty, C. J. (1991), Models of macro-scale hydrology for use in gobal change research: Tests on two tropical river systems, Ph.D. thesis, University of New Hampshire.

Vörösmarty, C. J., and D. Sahagian (2000), Anthropogenic disturbance of the terrestrial water cycle, *BioScience*, *50*(9), 753–765.

Vörösmarty, C. J., C. J. Willmott, B. Choudhury, A. Schloss, T. Stearns, S. Robeson, and T. Dorman (1996), Analyzing the discharge regime of a large tropical river through remote sensing, ground-based climatic data, and modeling, *Water Resources Research*, *32*, 3137–3150.

Vörösmarty, C. J., K. P. Sharma, B. M. Fekete, A. H. Copeland, J. Holden, J. Marble, and J. A. Lough. (1997), The storage and aging of continental runoff in large reservoir systems of the world, *Ambio*, *26*(4), 210–219.

Vörösmarty, C. J., B. M. Fekete, M. Meybeck, and R. B. Lammers (2000a), Global system of rivers: its role in organizing continental land mass and defining land-to-ocean linkages, *Global Biogeochemical Cycles*, *39*, 169–190, doi:10.1016/S0921-8181(03)00023-7.

Vörösmarty, C. J., B. M. Fekete, M. Meybeck, and R. B. Lammers (2000b), A simulated topological network representing the global system of rivers at 30-minute spatial resolution (STN-30), *Global Biogeochemical Cycles*, *14*, 599–621.

Vörösmarty, C. J., B. M. Fekete, M. Meybeck, and R. B. Lammers (2000c), Geomorphometric attributes of the global system of rivers at 30-minute spatial resolution (STN-30), *Journal of Hydrology*, *237*, 17–39.

Vörösmarty, C. J., P. Green, J. Salisbury, and R. B. Lammers (2000d), Global water resources: vulnerability from climate change and population growth, *Science*, *289*.

Vörösmarty, C. J., M. Meybeck, B. M. Fekete, K. Sharma, P. Green, and J. Syvitski (2003), Anthropogenic sediment retention: Major global-scale impact from the population of registered impoundments, *Global and Planetary Change*, *39*, 169–190, doi:10.1016/S0921-8181(03)00023-7.

Vörösmarty, C. J., C. Leveque, C. R. (Convening Lead Authors), C. Caudill, J. Chilton, E. M. Douglas, M. Meybeck, and D. Prager (2005), Chapter 7: Fresh water ecosystems, in *Millennium Ecosystem Assessment Volume 1: Conditions and Trends Working Group Report*, chap. 7, Island Press.

Vrugt, J. A., H. V. Gupta, W. Bouten, and S. Sorooshian (2003), A Suffled Complex Evolution Metropolis algorithm for optimization and uncertainty assessment of hydrologic model parameters, *Water Resources Research*, *39*(8), 1201.

Wagener, T., N. McIntyre, M. J. Lees, H. S. Wheater, and H. V. Gupta (2003), Torwards reduced uncertainty in conceptual rainfall-runoff model: dynamic identifiability analysis, *Hydrological Processes*, *17*, 455–476.

Wagener, T., H. S. Wheather, and H. V. Gupta (2004), *Rainfall-Runoff Modelling in Gauged and Ungauged Catchments*, Imperial College Press.

Wallace, J. (2000), Increasing agricultural water use efficiency to meet future food production, *Agriculture, Ecosystems and Environment*, (105-119).

Waltham, T., and I. Sholji (2001), The demise of the Aral Sea - an environmental disaster, *Geology Today*, *17*(6), 218–228, doi:10.1046/j.0266-6979.2001.00319.x.

Weiss, M., and L. Menzel (2008), A global comparison of four potential evapotranspiration equations and their relevance to stream flow modelling in semi-arid environments, *Advances in Geoscience*, *18*, 15–23.

Wheida, E., and R. Verhoeven (2006), Review and assessment of water resources in libya, *Water International*, *31*, 295–309.

Wilby, R. L., T. M. L. Wigley, C. Conway, P. D. Jones, B. C. Hewitson, J. Main, and D. S. Wilks (1998), Statistical downscaling of general circulation model output: a comparison of methods, *Water Resources Research*, *34*(11), 2995–3008.

Willmott, C. J. (1981), On the validation of models, *Physical Geography*, *1*, 184–194.

Willmott, C. J., and K. Matsuura (2005), Advantages of the mean absolute error (MAE) over the root mean square error (RMSE) in assessing average model performance, *Climate Research*, *30*(1), 79–82.

Willmott, C. J., C. N. Rowe, and Y. Mintze (1985), Climatology of the terrestrial seasonal water cycle, *Journal of Climatology*, *43*, 495–511, doi:10.1002/joc.3370050602.

Wollheim, W. M., C. J. Vörörsmarty, A. F. Bouwman, J. Harrison, E. Linder, B. J. Peterson, P. A. Green, S. Seitzinger, and J. P. M. Syvitski (2008), Global N removal by freshwater aquatic systems using a spatially distributed, within basin approach, *Global Biogechemical Cycles*, *22*, GB2026, doi:10.1029/2007GB002963.

Wood, E. F., D. Lettenmaier, X. Liang, B. Nijssen, and S. Wetzel (1997), Hydrological modeling of continental scale basins, *Annu. Rev. Earth Planet. Sci.*, *25*, 279–300.

Wood, S., K. Sebastian, and S. Scherr (2000), Pilot analysis of global ecosystems- agroecosystems, available at: http://wri.org/wr3000.

World Water Assessment Programme (2002), Water for people, water for life, The United Nations World Water Development Report.

WRI (1998), *Environmental change and Human health*, Oxford University Press.

Xiao, X., S. Boles, J. Liu, D. Zhuang, S. Frolking, C. Li, W. Salas, and B. Moore III (2005), Mapping paddy rice agriculture in southern China using multi-temporal MODIS images, *Remote Sensing of Environment*, *95*, 480–492.

Xiao, X., S. Boles, S. Frolking, C. Li, J. Y. Babu, W. Salas, and B. Moore III (2006), Mapping paddy rice agriculture in South and Southeast Asia using multi-temporal MODIS images, *Remote Sensing of Environment*, *100*, 95–113, doi:10.1016/j.rse.2004.12.009.

Xie, P., J. E. Janowiak, P. A. Arkin, R. F. Adler, A. Gruber, R. Ferraro, G. Huffman, and S. Curtis (2003), GPCP pentad precipitation analysis: An experimental dataset based on gauge observations and satellite estimates, *Journal of Climate*, *16*, 2197–2214.

Xu, C.-Y. (1999), Climate change and hydrologic models: A review of existing gaps and recent research developments, *Water Resources Management*, *13*, 369–382.

Zhang, X. Y., M. A. Friedl, C. B. Schaaf, A. Strahler, J. C. F. Hodges, F. Gao, B. C. Reed, and A. Huete (2003), Monitoring vegetation phenology using MODIS, *Remote Sensing of Environment*, *84*(3), 471–475.

Appendix

Penman Monteith Equation

The Penman-Monteith method to compute evapotranspiration is based on both an energy balance of the surface and empirical relationships describing the diffusion of energy from the surface. It is therefore known as a combination equation which is given by (*Allen et al.*, 1998):

$$\lambda ET = \frac{\Delta (R_n - G) + \rho_a c_p \frac{e_s - e_a}{r_a}}{\Delta + \gamma \left(1 + \frac{r_s}{r_a}\right)} \tag{A-1}$$

where

ET	$[mmd^{-1}]$	=	potential evapotranspiration
λ	$[MJkg^{-1}]$	=	latent heat of vaporization = 2.45
R_n	$[MJm^{-2}d^{-1}]$	=	net radiation, Eq. A-15
G	$[MJm^{-2}d^{-1}]$	=	soil heat flux density, A-16
e_s	$[kPa]$	=	saturation vapor pressure, Eq. A-18
e_a	$[kPa]$	=	actual vapor pressure
$e_s - e_a$	$[kPa]$	=	saturation vapor pressure deficit
ρ_a	$[Mgm^{-3}]$	=	mean air density at constant pressure
c_p	$[Jkg^{-1}K^{-1}]$	=	heat capacity of the air = 1005
Δ	$[kPa°C^{-1}]$	=	slope of the vapor pressure curve, Eq. A-8
γ	$[kPa°C^{-1}]$	=	psychrometric constant , Eq. A-6
r_s	$[sm^{-1}]$	=	surface or canopy resistance, Eq. A-3
r_a	$[sm^{-1}]$	=	aerodynamic resistance, Eq. A-2

The aerodynamic resistance r_a controls the transfer of heat and water from the evaporating surface to the air and is calculated as (*Allen et al.*, 1998; *Brutsaert*, 1982):

$$r_a = \frac{\ln\left[\frac{z_m - d}{z_{om}}\right] - \ln\left[\frac{z_h - d}{z_{oh}}\right]}{k^2 u_z} \tag{A-2}$$

where

r_a	$[sm^{-1}]$	=	aerodynamic resistance
z_m	$[m]$	=	height of wind measurements

z_h	$[m]$	=	height of humidity measurements
d	$[m]$	=	zero plane displacement height, Eq. A-4 and Eq. A-5
z_{om}	$[m]$	=	roughness length governing momentum transfer
z_{oh}	$[m]$	=	roughness length governing transfer of heat and vapor
k	$[-]$	=	von Karman's constant = 0.41
u_z	$[ms^{-1}]$	=	wind speed at height z

The bulk or surface resistance r_s describes the resistance of vapor flow though the vegetation and evaporating soil surface and can be approximated using the following approximation (*Allen et al.*, 1998):

$$r_s = \frac{r_l}{LAI_a} \tag{A-3}$$

where $r_l[sm^{-1}]$ is the stomatal resistance of the well-illuminated leaf and $LAI_a[m^2\ m^{-2}]$ is the active (sunlit) leaf area index and describes the fraction of the leaf that actively contributes to the transfer of heat and vapor. LAI_a depends on the type of vegetation and varies with time relative to the maximum leaf area index L_p. The stomatal resistance *rl* represents the average resistance of an individual leaf and is a function of climate, crop type, and water availability. The zero plane displacement height can be computed as (*Federer et al.*, 1996)

$$d = \frac{h - z_{oh}}{0.3} \tag{A-4}$$

for $L_p >= 4$ and as

$$d = 1.1h\ ln(1 + (2(L_p + S_p))^{0.25}) \tag{A-5}$$

for $L_p < 4$. $S_p[m^2 m^{-2}]$ is the projected stem area index that is dependent on the type of vegetation. Atmospheric parameters in Eq. 5.6 are calculated as follows:

The psychrometric constant γ can be expressed as

$$\gamma = \frac{c_P P}{\varepsilon\lambda} \cdot 10^{-3} = 0.00163\frac{P}{\lambda} \tag{A-6}$$

where

P	$[kPa]$	=	atmospheric pressure (Eq. A-7)
λ	$[MJkg^{-1}]$	=	latent heat of vaporization
c_P	$[MJkg^{-1}°C^{-1}]$	=	specific heat of moist air = $1.01310^{-3} MJkg^{-1}°C^{-1}$
ε	$[-]$	=	ratio molecular weight of water vapour/dry air = 0.622

The atmospheric pressure P [kPa] as a function of elevation z [m] (assuming ideal gas law and 20°C for a standard atmosphere) can be expressed as

$$P = 101.3\left(\frac{293 - 0.0065z}{293}\right)^{5.26} \tag{A-7}$$

The slope of the saturation vapor pressure curve $\Delta[kPa°C^{-1}]$ is a function of mean temperature $T_m[°C]$:

$$\Delta = \frac{4098\left[0.6108 \cdot \exp\left(\frac{17.27T_m}{T_m+237.3}\right)\right]}{(T_m+237.3)^2} \tag{A-8}$$

The solar radiation received at the top of the earth's atmosphere on a horizontal surface (extraterrestrial radiation) R_a is a function of latitude, date and time of the day:

$$R_a = \frac{24\,(60)}{\pi} G_{SC} d_r \left[\omega_s \sin\varphi \sin\delta + \cos\varphi \cos\delta \sin\omega_s\right] \tag{A-9}$$

where

R_a	$[MJm^{-2}d^{-1}]$	=	extraterrestrial radiation
G_sc	$[MJm^{-2}min^{-1}]$	=	solar constant (0.0820)
d_r	$[-]$	=	inverse relative distance Earth-Sun (Eq. A-10)
ω_s	$[rad]$	=	sunset hour angle (Eq. A-12)
ϕ	$[rad]$	=	latitude
δ	$[rad]$	=	solar declination (Eq. A-11)

Inverse relative distance Earth-Sun d_r and solar declination δ are expressed as a function of date:

$$d_r = 1 + 0.033\cos\left(\frac{2\pi}{365}J\right) \tag{A-10}$$

$$\delta = 0.409\sin\left(\frac{2\pi}{365}J - 1.39\right) \tag{A-11}$$

where J is the number of the day in the year (Julian Day) between 1 (1 January) and 365 or 366 (31 December). The sunset hour angle ω_s is given by:

$$\omega_s = \arccos\left[-\tan\varphi \tan\delta\right] \tag{A-12}$$

The daylight hours N are given by:

$$N = \frac{24}{\pi}\omega_s \tag{A-13}$$

The net longwave radiation R_{nl} is proportional to the absolute temperature of the surface T raised to the power of four and is expressed by the Stefan-Boltzmann law (corrected for humidity and cloudiness):

$$R_{nl} = \frac{\sigma T_{\max,K}^4 + \sigma T_{\min,K}^4}{2}\left(0.34 - 0.14\sqrt{e_a}\right)\left(1.35\frac{R_s}{R_{so}} - 0.35\right) \tag{A-14}$$

where $T_{min,K}$ and $T_{max,K}$ represent the minimum and maximum Temperatures [K], R_s/R_{so} is the relative shortwave radiation (limited to 1.0). Net radiation R_n is the difference between the incoming net shortwave radiation R_{ns} and the outgoing net longwave radiation R_{nl}

$$R_n = R_{ns} - R_{nl} \tag{A-15}$$

To consider the soil heat flux G in Eq. 5.6 complex models are required that calculate the soil heat flux based on the mineral composition and the water content of the soil. However, as G is usually small compared to R_n, particularly when the soil is covered with vegetation, it is ignored if daily time steps are used:

$$G \approx 0 \tag{A-16}$$

Saturation vapor pressure e_s is a function of the mean air temperature T and can be expressed as

$$e_s(T) = 0.6108 \exp\left(\frac{17.27T}{T+237.3}\right) \tag{A-17}$$

Due to the non-linearity of the above equation, the mean saturation vapor pressure should be computed from mean values of the saturation vapor pressure for minimum and maximum temperatures T_{max} and T_{min} for the same period:

$$e_s = \frac{e_s(T_{\max}) + e_s(T_{\min})}{2} \tag{A-18}$$

The solar radiation R_s can be calculated using a simplified version of the Angstrom formula:

$$R_s = \left(0.25 + 0.5\frac{n}{N}\right) R_a \tag{A-19}$$

If cloud cover is used instead of sunshine duration, the solar radiation is calculated as (*Black*, 1956):

$$R_s = 0.803 - 0.340C - 0.458C^2 \tag{A-20}$$

where C is the unitless cloud cover fraction. The clear-sky solar Radiation R_{so} that is required for computing the net longwave radiation (Eq. A-14):

$$R_{so} = 0.75 + 2 \cdot 10^{-5} z R_a \tag{A-21}$$

where $z[m]$ is the elevation of the station above sea level. Net shortwave radiation R_{ns} is the balance between incoming and reflected solar radiation as a function of the Albedo α:

$$R_{ns} = (1 - \alpha) R_s \tag{A-22}$$

A number of empirical relationships have been established to estimate the vegetation-dependent parameters in the above described equations for a number of vegetation classes. *Federer et al.* (1996) list such parameters for a set of typical vegetation cover types.

Table A-1: Root length for different land cover type from *Federer et al.* (2003)

Cover type	Root length [*mm*]
Boreal evergreen forest	2100
Temperate evergreen forest	3100
Tropical evergreen forest	3500
Temperate deciduous forest	3000
Tropical deciduous forest	2900
Tropical savannah	1000
Sclerophyllous shrub	3400
Temperate grassland	1000
Cultivated	110
Tundra	860
Short evergreen grass	1000
Warm Desert	280

Table A-2: Crops considered as major crops by *Leff et al.* (2004) and assumed crop coefficients k_c [-], length of development stages L[d] and rooting depth [m] from *Allen et al.* (1998)

Name	kc_{ini}	kc_{mid}	kc_{end}	L_{Ini}	L_{Dev}	L_{mid}	L_{late}	RootingDepth
Barley	0.3	1.15	0.25	15	30	40	20	1.25
Maize	0.3	1.2	0.6	25	30	40	30	1.1
Millet	0.3	1	0.3	15	27	40	27	1.5
Rice	1.05	1.2	0.8	30	30	70	30	0.75
Rye	0.95	1.05	1	20	30	60	40	0.8
Sorghum	0.3	1.05	0.8	20	35	45	30	1.5
Wheat	0.5	1.15	0.3	20	25	60	30	1.5
Cassava	0.3	0.9	0.3	20	40	90	30	0.7
Potato	0.5	1.15	0.75	20	40	50	30	0.5
Sugarbeet	0.35	1.2	0.7	20	40	50	30	0.9
Sugarcane	0.4	1.25	0.75	35	60	180	100	1.5
Pulses	0.4	1.15	0.55	20	40	50	30	0.8
Soybean	0.4	1.15	0.5	20	40	50	30	0.8
Groundnuts	0.4	1.15	0.6	20	40	50	30	0.7
Rapeseed	0.35	1.07	0.35	20	40	50	30	1.25
Sunflower	0.35	1.07	0.35	20	40	50	30	1.21
Oilpalm	0.35	1.15	0.35	20	40	50	30	1.5
Cotton	0.35	1.17	0.6	20	40	50	30	1.35
Others	0.35	1.15	0.6	20	40	50	30	1.0

Table A-3: Estimated Irrigation Efficiencies (*Döll and Siebert*, 2002)

Region	Efficiency
Canada	0.7
United States	0.6
Mittelamerika	0.45
South America	0.45
North Africa	0.7
West Africa	0.45
East Africa	0.55
South Africa	0.55
OECD (Europe North)	0.5
OECD (Europe South)	0.6
Eastern Europe	0.5
Baltic States, Belarus	0.6
Rest of former	0.6
South Asia	0.4
Oceania	0.7
Japan	0.35

Table A-4: Characteristics of reservoirs with observed operational data. Reservoir purposes based on ICOLD data (H = hydropower, I = Irrigation, C = Flood control, S = Water Supply, N = Navigation, O = Others). β = Residence time. Data were provided by N. Hansaki, Natl. Inst. for Environmental Studies (Japan)

Reservoir Name	County	Basin	C [km^3]	Q[m^3/s]	β[a]	From	To	Purpose
Akosombo	Ghana	Volta	150	1278.29	3.72	1900	1998	H
American Falls	USA	Columbia	2.06	206.42	0.32	1978	1995	IHR
Bhumibol	Thailand	Chao Phraya	13.46	163.22	2.61	1980	1996	IHCS
Big Bend	USA	Mississippi	2.13	728.9	0.09	1970	2000	CHINR
Buford	USA	Apalachicola	2.36	55.99	1.34	1900	2004	CHR
Canyon Ferry	USA	Mississippi	2.4	156.14	0.49	1971	2000	HCISR
Dworshak	USA	Columbia	4.28	152.01	0.89	1974	1996	CHRSF
E. B. Campbell	Canada	Nelson	2.2	387.05	0.18	1993	2002	H
Flaming Forge	USA	Colorado	4.67	66.91	2.21	1971	2000	HCSR
Fort Preck	USA	Mississippi	22.12	306.38	2.29	1970	2000	CHIN
Fort Randall	USA	Mississippi	5.7	754.19	0.24	1970	2000	CHNR
Garrison	USA	Mississippi	22.82	678.27	1.07	1970	2000	CHIR
Glen Canyon	USA	Colorado	33.3	463.35	2.28	1971	2000	HIRX
Grand Coulee	USA	Columbia	11.79	2993.49	0.12	1978	1990	IC
Grand Rapids	Canada	Nelson	9.64	491.82	0.62	1987	1996	H
Hungy Horse	USA	Columbia	4.28	106.16	1.28	1970	2000	IHC
Intern. Amistat	USA	Rio Grande	3.41	81.12	1.33	1900	2000	IHCS
Intern. Falcon	USA	Rio Grande	3.41	103.52	1.04	1977	2002	IHCS
Jenpeg	Canada	Nelson	31.79	1816.56	0.55	1987	1996	CH
Kettle Rapids	Canada	Nelson	2.53	2795.7	0.03	1987	1996	H
Libby	USA	Columbia	7.17	299.04	0.76	1975	1990	HCR
Missi Falls	Canada	Nelson	28.37	784.35	1.15	1987	1997	H
Navajo	USA	Colorado	2.11	40.69	1.64	1971	2000	IR
Ohahe	USA	Mississippi	27.43	974.07	0.89	1970	2000	CHIN
Oroville	USA	Sacramento	4.36	189.21	0.73	1995	2004	SCIHR
Palisades	USA	Columbia	1.73	192.98	0.28	1970	2000	IHCRF
Sirikit	Thailand	Chao Phraya	10.55	166.42	2.01	1980	1996	IHC
Trinity	USA	Klamath	3.02	54.78	1.75	1970	2000	IHCR
Yellowtail	USA	Mississippi	0.02	98.64	0.01	1970	2000	R

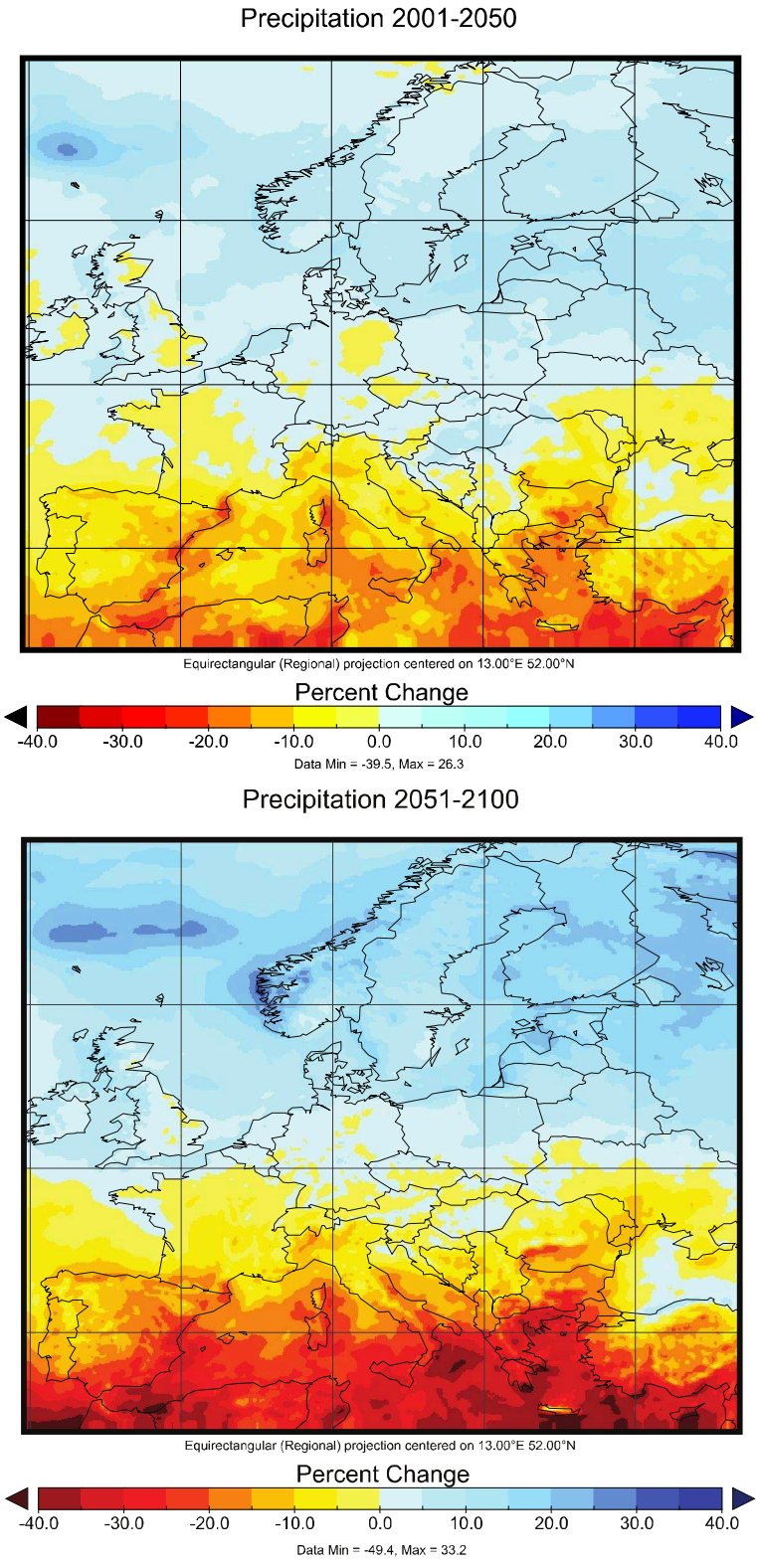

Figure A-1: Relative changes in annual precipitation in the CLM model domain (Sres A1b scenario), compared to the 1960/2000 control runs

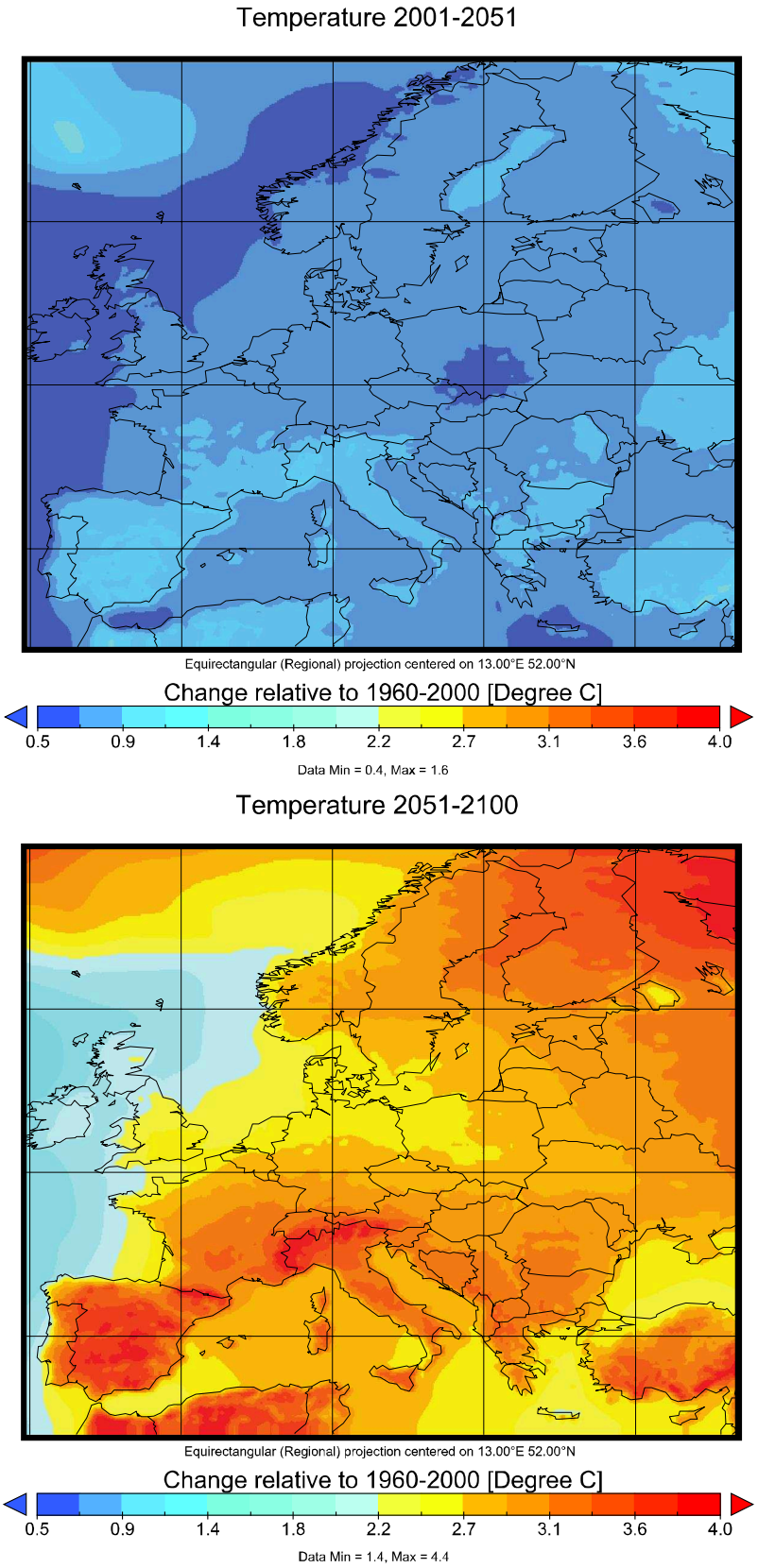

Figure A-2: Projected changes in the mean annual air temperature (2m) from the CLM data set in Europe for the A1b emission scenario, compared to the 1960-2000 Control Runs[°C]

Bisher erschienene Hefte der Schriftenreihe HYDROLOGIE / WASSERWIRTSCHAFT

Heft	Jahr	Autor und Titel
1	1983	**Klatt, Peter** Vorhersage von Hochwasser aus radargemessenem und prognostiziertem Niederschlag
2	1983	**Scheider, Klaus** Modell zur gleichzeitigen Erzeugung von Tagesabflussdaten an mehreren Stellen eines Einzugsgebietes
3	1984	**Strübing, Gert** Satellitendaten als Basis der Bestimmung von monatlichen Abflüssen für wasserwirtschaftliche Planungen
4	1986	**Harboe, Ricardo** Optimaler Betrieb wasserwirtschaftlicher Verbundsysteme mit Speichern und anderen Anlagen
5	1986	**Tegtmeier, Ulrike** Wasserwirtschaftliche Projektbewertung – Methoden und Anwendungsbeispiele
6	1987	**Richter, Karl Gerd** Vergleichende hydrologische Untersuchungen des Hochwasserablaufes in Testeinzugsgebieten mit unterschiedlicher Bebauungsdichte
7	1989	**Salas, Edgar** Anwendung der Bayesschen Theorie auf wasserwirtschaftliche Planungen mit hydrologischen Datenreihen
8	1990	**Vogt, Roland** Stauraumverlandung – Naturmessung und Computersimulation
9	1992	**Tiedt, Michael** Freizeitnutzung als Komponente der Wasserwirtschaftlichen Projektbewertung
10	1993	**Gyau-Boakye, Philip** Filling Gaps in Hydrological Runoff Data Series in West-Africa Ergänzung lückenhafter Abflussreihen in West-Afrika
11	1993	**Schumann, Andreas H.** Der Einfluss von Veränderungen der Umweltbedingungen und sozio-ökonomischer Faktoren auf Hydrologie und Wasserwirtschaft
12	1993	**Fett, Werner** Die Nutzung räumlich hoch aufgelöster Gebietsinformationen für die Simulation von Hochwasserganglinien in humiden Mittelgebirgslandschaften

Heft	Jahr	Autor und Titel
13	1994	**Papadakis, Ioannis** Berechnung historischer Abflüsse mit Hilfe multispektraler und multitemporaler digitaler Satellitenbilder
14	1995	**Schultz, G.A. (Hrsg.)** Verfügbarkeit von Wasser Beiträge zur 8. wissenschaftlichen Tagung des DVWK vom 22.-23.03.1995 an der Ruhr-Universität Bochum
15	1996	**Su, Zhongbo** Remote Sensing Applied to Hydrology: The Sauer River Basin Study Fernerkundung angewandt in der Hydrologie: Die Sauer-Einzugsgebiets-Studie
16	1997	**Wolbring, Frank** Wissensbasierte Methoden für den Betrieb von Talsperren
17	1998	**Hornbogen, Martin** Die Planung von Wasserversorgungssystemen auf der Basis des Nachhaltigkeitsprinzips
18	2002	**Schumann, Andreas H. (Hrsg.)** Proceedings Workshop HydroGIS NRW 2002 23.05.2002 Ruhr-Universität Bochum
19	2003	**Quirmbach, Markus** Nutzung von Wetterradardaten für Niederschlags- und Abflussvorhersagen in urbanen Einzugsgebieten
20	2006	**Brass, Carsten** Betriebsoptimierung von Talsperrensystemen mittels Stochastisch Dynamischer Programmierung (SDP) unter Berücksichtigung veränderlicher Ziele und Randbedingungen
21	2006	**Dietrich, Jörg** Entwicklung einer Methodik zur systemanalytischen Unterstützung adaptierbarer Entscheidungsprozesse bei der integrierten Flussgebietsbewirtschaftung
22	2006	**Gattke, Christian** Modellvergleiche zur Untersuchung struktureller Unsicherheiten – Anwendung objektorientierter Methoden in der hydrologischen Modellierung
23	2009	**Schumann, Andreas H. (Hrsg.)** Verbundvorhaben Entwicklung integrativer Lösungen für das operationelle Hochwassermanagement am Beispiel der Mulde – Abschlussbericht

Heft	Jahr	Autor und Titel
24	2009	**Schumann, Andreas H. (Hrsg.)** Integrative Nutzung des technischen Hochwasserrückhalts in Poldern und Talsperren am Beispiel des Flussgebiets der Unstrut
25	2009	**Klein, Bastian** Ermittlung von Ganglinien für die risikoorientierte Hochwasser-bemessung von Talsperren
26	2010	**Wisser, Dominik** Modeling of Irrigation and Reservoirs in Regional and Global Water Cycles

Lehrstuhl für Hydrologie, Wasserwirtschaft und Umwelttechnik
Ruhr-Universität Bochum, 2010

Universitätsstraße 150, 44780 Bochum
Tel. +49 (0234) 32 - 24693, Fax. - 14153

ISSN 0949-5975